Origin and fate of branched tetraether lipids in river drainage systems

Implications for the use of the MBT/CBT proxy as a continental palaeothermometer in marine sedimentary records

Claudia Irene Zell

Printed by Wöhrmann Print Service, Zutphen.
Cover picture Amazon River by Jung-Hyun Kim
Cover design by Santiago Pérez Gallardo

Origin and fate of branched tetraether lipids in river drainage systems

Implications for the use of the MBT/CBT proxy as a continental palaeothermometer in marine sedimentary records

De herkomst en het lot van vertakten tetraether lipiden in riviersystemen

Implicaties voor het gebruik van de MBT/CBT proxy als continentale palaeothermometer in mariene sedimenten (met een samenvatting in het Nederlands)

Herkunft und Schicksal von verzweigten tetraether lipiden in Flusssystemen

Implikationen für den Gebrauch des MBT/CBT poxie als kontinentales Paleothermomether in marinen Sedimenten (mit einer Zusammenfassung auf Deutsch)

Origem e destino de lipídeos tetraéter ramificados em bacias de drenagem

Implicações para o uso do indicador MBT/CBT como paleotermômetro continental em testemunhos marinhos(com um sumário em Português)

Proefschrift

ter verkrijging van de graad van doctor aan de Universiteit Utrecht op gezag van de rector magnificus, prof. dr. G.J. van der Zwaan, ingevolge het besluit van het college voor promoties in het openbaar te verdedigen op maandag 14 april 2014 des ochtends te 12.45 uur

door

Claudia Irene Zell

geboren op 27 Maart 1985 te Keulen, Duitsland

Promotor: Prof. dr. ir. J.S. Sinninghe Damsté

Co-promotor: Dr. J.-H. Kim

"All religions, arts and sciences are branches of the same tree. All these aspirations are directed toward ennobling man's life, lifting it from the sphere of mere physical existence and leading the individual towards freedom."

-Albert Einstein-

For everyone who has taught me
throughout my life.

Contents

Chapter 1

Introduction

1.1. CLIMATE CHANGE AND THE RECONSTRUCTION OF PAST CLIMATE

The anthropogenic era is generally thought to have started at 1800 A.D. (Crutzen and Stoermer, 2000). During this era, human activities (burning of fossil fuel, industrialization and deforestation) altered the chemical composition of the atmosphere through the build-up of greenhouse gases, primarily carbon dioxide (CO_2). CO_2 concentrations have increased by 40 % since pre-industrial times (IPCC, 2013). Simultaneously, a global temperature increase has been observed, especially fast in the last three decades, which have been successively warmer than any preceding decade since 1850. The awareness of the impact of mankind on climate has increased our interest in understanding the climate of our planet. This knowledge will help us to make predictions about how future climate change might influence human society. In order to make predictions about the future climate we do not only need to understand the present climate, but also the climate of the past. For example, during the Paleocene-Eocene Thermal Maximum (PETM, ~56 Ma), CO_2 concentrations massively increased in the atmosphere (Zachos et al., 2008). The CO_2 increase led to a warming of 4-9°C of the continents and deep and surface ocean waters (e.g. Kennett and Stott, 1991; Tripati, 2005; Wing, 2005; Sluijs et al., 2006; Weijers et al., 2007b) and many further responses of the environment such as sea level rise (Sluijs et al., 2006), changes of the ocean circulation (Nunes and Norris, 2006), and acidification of the sea water (Zachos, 2005). The data achieved by climate reconstructions of the past can be used to validate climate models, which are aimed to predict futures climate changes.

To better assess anthropogenic impact on post-industrial climate, it requires intimate knowledge on amplitude and rapidness in the natural variations of temperature and other temperature-related environmental properties in the ocean, over the continents, and in the cryosphere. However, the time series of direct temperature measurements are too short and fall within the period of suggested strong human impact on natural conditions: global-scale temperature observations only began in the mid-19th century (IPCC, 2013). For reconstruction of temperature and other environmental variables beyond the instrumental period so-called proxies are used (Jones et al., 1998). Proxies are biogenic components which have a close relationship to environmental parameters, providing measurable descriptors of key climatic and environmental (but unobservable) variables such as temperature, salinity, nutrient content, oxygen content, CO_2 concentration, wind speed, and productivity (Wefer et al., 1999). The proxies can be applied to lake and marine sediments, ice cores, tree rings, and corals (e.g. Bradley and Jones, 1993; Jones et al., 1998; Mann et al., 1998; Ruddiman, 2008) and consequently can provide information about climate variations in the past. It is recommendable to apply multiple proxies to reconstruct the paleoclimate changes, because every proxy has its advantages and disadvantages. This is also the reason why climate proxies need to be further developed and vali-

dated.

A range of tools and analytical techniques exist to extract sea surface temperature (SST) information from marine sediments. For the SST reconstructions chemical properties of calcareous skeletons (e.g. foraminifera and corals) are frequently used. SSTs can be reconstructed, for example, using the oxygen isotope composition of these shells ($\delta^{18}O$), since the $\delta^{18}O$ of water depends on temperature (Urey, 1947; Epstein et al., 1953). Furthermore, trace elements in the calcareous shells have been used. It is found that the Mg/Ca ratio in the shells increases with increasing temperature (e.g. Nürnberg et al., 1996; Elderfield and Ganssen, 2000) and that the Sr/Ca ratio has an inverse correlation with the sea water temperature (Weber, 1973; de Villiers et al., 1994). The isotopic and trace elemental inorganic proxies are based on thermodynamically different behavior of isotopes and trace elements during the calcification of foraminifera which is primarily a function of temperature. Many approaches are used to investigate the impact of factors other than temperature (so-called "vital effects") on the reliability of inorganic sea water temperature proxies using culture studies, plankton tows, sediment traps and sediment core-top studies (e.g. Spero et al., 1999). They, generally, show that calibrations of inorganic proxies are different for different species (Elderfield et al., 2000; Rosenthal et al., 2000) and other factors also influence the partitioning of stable isotopes and trace elements such as pH, salinity and the calcifying organism itself (e.g. Arbuszewski et al., 2010). In addition, inorganic proxies require knowledge on the original composition of the sea water especially on longer geological time scales (see Lea, 2003 and references therein).

Besides inorganic chemical proxies organic compounds can be used to reconstruct the past SSTs. Since lipids are well preserved in sediments, they are especially suitable as biomarker molecules. A prime example is the $U^{K'}_{37}$ proxy, which is based on the degree of unsaturation of long-chain, unsaturated ketones (alkanones). They are produced by a limited number of haptophyte algal species within the order Isochrysidales (Medlin et al., 2008), notably Emiliania huxleyi and Gephryocapsa oceanica in the open ocean (Volkman et al., 1980; Marlowe et al., 1984), and Isochrysis galbana (Marlowe et al., 1984; Versteegh et al., 2001) and Chrysotila lamellosa (Volkman et al., 1995, 1980; Conte et al., 1998; Rontani et al., 2004) in coastal regions. A study of a marine sediment core showed that the ratio of the di-($C_{37:2}$), tri-($C_{37:3}$), and tetra-unsaturated ($C_{37:4}$) alkenones ($U^{K'}_{37}$ index) was sensitive to paleotemperature fluctuations in the late Pleistocene (Brassell et al., 1986). Subsequently, Prahl and Wakeham (1987) proposed a modified version ($U^{K'}_{37}$ index) of this index, which excluded the $C_{37:4}$ alkenone because this component was usually not abundant in marine sediments and sediment traps. The quantitative calibration of the $U^{K'}_{37}$ index to temperature was based on culture studies of E. huxleyi (Prahl and Wakeham, 1987; Prahl et al., 1988) and global core-top studies (e.g. Müller et al., 1998; Conte et al.,

2006). Another well-established proxy is based on the varying number of cyclopentane moieties in isoprenoid glycerol dialkyl glycerol tetraethers (GDGTs), the TEX_{86} proxy (TetraEther indeX of tetraethers consisting of 86 carbon atoms; Schouten et al., 2002). These lipids are biosynthesized by Thaumarchaeota, formerly known as Group I Crenarchaeota (Spang et al., 2010), which occur ubiquitously in the marine water column and are one of the dominant prokaryotes in today's oceans (Karner et al., 2001). Thaumarchaeota biosynthesize different types of isoprenoid GDGTs containing 0 to 3 cyclopentane moieties (GDGT-0 to GDGT-3) and crenarchaeol which, in addition to 4 cyclopentane moieties, has a cyclohexane ring (Schouten et al., 2000; Sinninghe Damsté et al., 2002). The regio-isomer of crenarchaeol is also always present in small quantities. From culture studies of the membrane composition of hyperthermophilic archaea it is known that the relative number of cyclopentane moieties increases with growth temperature (Gliozzi et al., 1983; Uda et al., 2001). An initial mesocosm study has shown that Thaumarchaeota use the same mechanism, i.e. higher temperatures result in an increase in the relative amounts of GDGTs with 2 or more cyclopentane moieties (Wuchter et al., 2004). Hence, by measuring the relative amounts of isoprenoid GDGTs present in marine sediments the temperature at which Thaumarchaeota were living when they produced their membranes can be reconstructed (Schouten et al., 2002). Afterwards, the initial proxy has been slightly modified as TEX_{86}^{H}, i.e. defined as the logarithmic function of TEX_{86}, for (sub)tropical oceans and greenhouse periods and TEX_{86}^{L}, a modified version of TEX_{86} with a logarithmic function, which does not include the crenarchaeol regio-isomer, for (sub) polar oceans (Kim et al., 2010a). More recently, the long chain diol index (LDI) was proposed as a new paleothermometer. It is based on the relative abundance of C_{28} 1,13- and C_{30} 1,13- and 1,15-diols, which shows a strong linear correlation with the annual mean SST (Rampen et al., 2012). So far the source organism of the long chain diols is not yet well established (Rampen et al., 2012), but C_{30} 1,13- and 1,15-diols have been found in eustigmatophyte algae (e.g. Volkman et al., 1992).

Compared to the marine temperature proxies, few temperature proxies exist to reconstruct continental air temperatures. Commonly used proxies for continental air temperature reconstruction are, for example based on tree rings (Robinson et al., 1990), fossilized leafs (proportion of toothed and untoothed leafs) (Bailey and Sinnott, 1915; Wolfe, 1971; Greenwood et al., 2004;) and pollen (Colinvaux et al., 1996). However, these plant-based proxies can be influenced by precipitation changes (Adams and Kolb, 2004), extinction of species (Jordan, 1997), or changes in the CO_2 concentration (Street-Perrott et al., 1997). In addition, $\delta_{18}O$ values are widely applied to reconstruct past continental temperature from ice cores (e.g. Jouzel et al., 1987), in carbonates and silicates in lake sediment (Leng and Marshall, 2004), speleothems (McDermott, 2004) and animal bones (Fricke et al., 1998; Kohn and Law, 2006). A disadvantage of the $\delta_{18}O$ method is that it is also influenced by the source

water oxygen composition (Jouzel et al., 1997). Continental temperature can also be reconstructed with the TEX_{86} proxy, when applied to lake sediments (e.g. Powers et al., 2004, 2005, 2010; Blaga et al., 2009). A relatively new proxy for the reconstruction of continental mean annual air temperature (MAAT) is the methylation of branched tetraethers (MBT)/cyclization of branched tetraethers (CBT) proxy. This proxy is like the TEX_{86} proxy based on membrane spanning lipids, but instead of isoprenoid GDGTs it is based on branched GDGTs (brGDGTs). In the following sections, the MBT/CBT proxy is introduced in more detail.

1.2. DISCOVERY OF BRGDGTS AND THEIR ORIGIN

BrGDGTs were detected with a novel HPLC-MS technique, which was originally developed to analyze isoprenoid GDGTs (Hopmans et al., 2000). The brGDGTs that were discovered first, were brGDGT Ia (see Fig. 1.1A for structures) and brGDGT IIa. Their structures were identified by NMR spectroscopy after their isolation from a Dutch peat (Sinninghe Damsté et al., 2000). Subsequently, Weijers et al. (2006) identified brGDGT IIb, which contained a cyclopentane moiety, and its structure was also confirmed by two dimensional NMR spectroscopy after isolation. Other brGDGTs (Ib, Ic, IIc, IIIa, IIIb, and IIIc) were assigned by LC-MS analysis (Schouten et al., 2000) (Fig. 1.1A). Most recently, De Jonge et al. (2013) have reported that the hexamethylated brGDGTs without cyclopentane moieties in a Siberian peat were comprised of at least four structural isomers (1-4; Fig. 1.1B), whilst the pentamethylated brGDGT were comprised of two structural isomers (5-6; Fig. 1.1B).

BrGDGTs occur in high concentrations in soil and peat (Weijers et al., 2006a; Weijers et al., 2007b). Initially it was thought that the brGDGTs in the aquatic environment were derived from soil erosion, but recently indications have been found that they can also be produced in aquatic settings such as lakes (Sinninghe Damsté et al., 2009; Tierney and Russell 2009; Tierney et al., 2010, 2012; Bechtel et al., 2010; Loomis et al., 2011). Further it was suggested that they might be produced in rivers (e.g. Zhu et al., 2011; Yang et al., 2013), and the marine environnent (Peterse et al., 2009a; Zhu et al., 2011; Hu et al., 2012; Strong et al., 2012).

The source organism of brGDGTs remains uncertain. Their chemical structure reveals that they are of bacterial rather than of archaeal origin, because the alkyl chain with the basic structure of 13,16-dimethyloctacosane is more typical for a bacterial membrane lipid (Langworthy et al., 1983; Sinninghe Damsté et al., 2011) as all archaeal GDGTs have isoprenoid carbon skeletons. In addition, the stereochemistry of the glycerol unit in brGDGTs (Weijers et al., 2006a) is inverse to that of archaea (Koga et al., 1998). Due to the high abundance of brGDGTs in peat bogs, it has been suggested that the brGDGT producing bacteria are living in anaerobic conditions (Weijers et al., 2006a; Liu et al., 2010; Peterse et al., 2011a) and according to their stable carbon isotopic composition they are heterotrophs (Pancost and Sinninghe

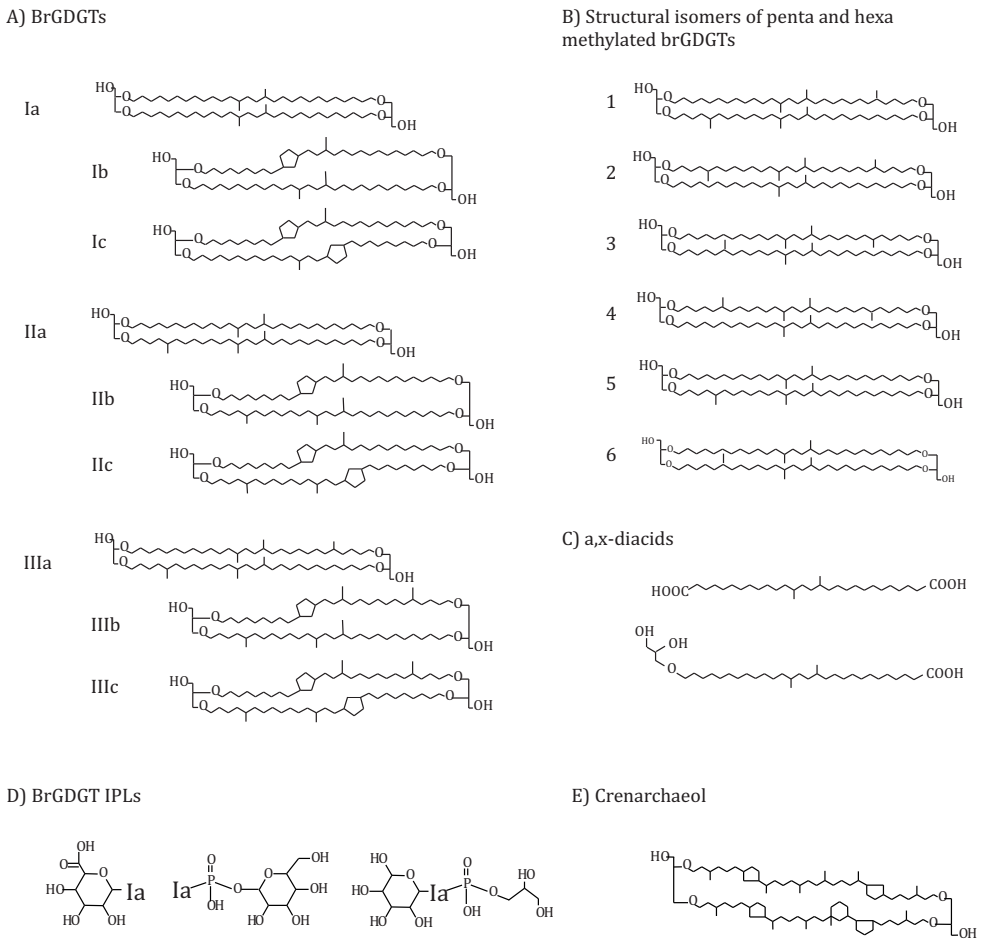

Fig. 1.1 Molecular structures of brGDGTs (Schouten et al., 2000; Sinninghe Damsté et al., 2000; Weijers et al., 2006a)(A), newly discovered brGDGT (De Jonge et al., 2013) (B), a,x-diacids found in Acidobacterial cultures (Sinninghe Damsté et al., 2011) (C), IPL head groups of brGDGT Ia (Liu et al., 2010; Peterse et al., 2011a) (D).

Damsté, 2003; Oppermann et al., 2010; Weijers et al., 2010; Ayari et al., 2013). It was also suggested that they belong to the Acidobacteria because higher brGDGT amounts were found in acidic environment, which are characterized by a high abundance of Acidobacteria (Jones et al., 2009; Weijers et al., 2009a; Peterse et al., 2010). When acidobacterial cultures (n=7) were analyzed for the presence of brGDGTs, it was found that they contained the basic building block of brGDGTs, i.e. a,x-diacids with a 13,16-dimethyloctacosane skeleton (Fig. 1.1C) and two species contained brGDGT Ia (Sinninghe Damsté et al., 2011). Acidobacteria are thus a potential source of brGDGTs, but not all of the known brGDGTs have yet been found in the Acidobacteria cultures, which indicates that they might also be produced by other bacteria.

The brGDGTs in the environment are often present as core lipids, but in liv-

ing cells the membrane lipids are likely present as intact polar lipids (IPLs). This means that they consist of the core lipid with an attached polar head groups. Upon cell death the IPLs degrade relatively fast (White et al., 1979; Harvey et al., 1986; Logemann et al., 2011; Lengger et al., 2012b). If brGDGTs are still found in the form of IPLs, this indicates that the brGDGTs were recently produced. The polar head groups of brGDGTs that were identified so far, on the basis of mass spectroscopy (MS) were glucose and glucoronyl head groups (Liu et al., 2010). In addition, Peterse et al. (2011a) detected brGDGTs with phosphoglycerol and phosphohexose groups (Fig. 1.1D). The exact structures of all of the above described intact polar brGDGTs are still tentative, since no rigorous NMR or synthesis studies have been carried out. Most likely more head groups exist that have not been described yet. Typically IPLs with phospho head groups are the least stable IPL (Logemann et al., 2011; Lengger et al., 2012b; Yang et al., 2013). Hence, when IPLs with phospho head groups are detected, this is a strong indication for recent brGDGT production in the environment from which the sample was taken.

1.3. ENVIRONMENTAL CONTROLS ON THE BRGDGT DISTRIBUTION

Weijers et al. (2007b) demonstrated that the distribution of the brGDGTs varied in different environments (Fig. 1.2). Following this initial discovery, the distribution of brGDGTs was analyzed in an extensive soil sample set. It was found that the number of methyl groups of the alkyl chains of the branched GDGTs correlated inversely with the MAAT and soil pH, while the number of cyclopentane moieties correlated inversely with the soil pH. Based on this observation, the MBT and CBT proxies were defined as follows:

$$MBT = ([Ia]+[Ib]+[Ic])/([Ia]+[Ib]+[Ic]+[IIa]+[IIb]+[IIc]+[IIIa]+[IIIb]+[IIIc]) \quad (1)$$

$$CBT = -\log(([Ib]+[IIb])/([Ia]+[IIa])) \quad (2)$$

To be able to reconstruct the paleotemperature and soil pH from the MBT and CBT the following calibrations were proposed based on a global soil sample set (n=114) (Fig. 1.3) as follows:

$$CBT = 3.33 - 0.38 \times pH \ (r^2 = 0.70) \quad (3)$$

$$MBT = 0.122 + 0.187 \times CBT + 0.020 \times MAT \ (r^2 = 0.77) \quad (4)$$

The root mean square error (RMSE) for soil pH and MAAT estimates were 0.7 and 4.8°C, respectively.

Several field studies were carried out to study the relationship of the brGDGT

distribution with environmental MAAT and soil pH. Peterse et al. (2009b) examined the brGDGTs in geothermally heated soil, with a large soil temperature gradient (>20°C) over a short distance (<5 m). They confirmed the dependence of the MBT on soil temperature. Furthermore, brGDGT distributions were analyzed in soils covering altitude transects, on various mountains (Sinninghe Damsté et al., 2008; Peterse et al., 2009c; Ernst et al., 2013; Liu et al., 2013) and in soils with artificially altered pH (Peterse et al., 2010). All studies showed similar relationships as the global calibration. However, they were not exactly equal to the global calibration. This could be because the global calibration is based on MAAT and not on soil temperatures. Hence, in general the use of absolute values of the reconstructed temperatures is not recommendable. However, it should be considered that the error in calibration is systematic and that the error in comparing MAAT estimates within a single record is likely to be lower (cf. Tierney et al., 2010). Regional calibrations might give more accurate estimates than the global calibration of Weijers et al. (2007c). A regional calibration was made for example for a soil sample set from the Amazon basin (n=22) (Bendle et al., 2010) as follows:

$$CBT = 4.2313 - 0.5782 \times pH \quad (r^2 = 0.75) \qquad (5)$$

$$MBT = 0.187 + 0.0829 \times CBT + 0.0250 \times MAT \quad (r^2 = 0.91) \qquad (6)$$

As brGDGTs are also produced in lakes (see 1.2.), a global calibrations for the use of the MBT/CBT in lake sediments was proposed by Pearson et al. (2011) and regional lake calibrations were made for the East African lakes (Tierney et al., 2010), Asian lakes (Sun et al., 2011) and New Zealand lakes (Zink et al., 2010). Recently, the global soil calibration was re-examined using a larger soil data set (n=176). It was found that brGDGTs-IIIa and -IIIb could be removed from the definition of the MBT, because they frequently did not occur in soils and thus did not improve the paleoreconstructions. Hence, it was suggested to use the MBT' instead of the MBT (Peterse et al., 2012) (Fig. 1.4) as follows:

$$MBT' = ([Ia]+[Ib]+[Ic])/([Ia]+[Ib]+[Ic]+[IIa]+[IIb]+[IIc]+[III]) \qquad (7)$$

$$pH = 7.90 - 1.97 \times CBT \quad (r^2 = 0.70, RMSE = 0.8) \qquad (8)$$

$$MAAT = 0.81 - 5.67 \times CBT + 31.0 \times MBT' \quad (r^2 = 0.59, RMSE = 5.0°C) \qquad (9)$$

Besides the use of brGDGTs in the MBT/CBT (or MBT'/CBT) proxy, brGDGTs are used in combination with the isoprenoid GDGT, crenarchaeol (Fig. 1.1E) in the branched vs. isoprenoid tetraether (BIT) index (Hopmans et al., 2004) to trace soil

organic carbon (OC) from land to aquatic environments (marine and lacustrine):

$$\text{BIT index}=([\text{Ia}]+[\text{IIa}]+[\text{IIIa}])/([\text{Ia}]+[\text{IIa}]+[\text{IIIa}]+[\text{crenarchaeol}]) \quad (10)$$

This proxy is based on the assumption that brGDGTs occur in soils and crenarchaeol in aquatic environments, leading to a BIT index close to 1 in the terrestrial environment and close to 0 in the aquatic environment. In general the BIT index has been shown to indicate a good trend from river to ocean (Herfort et al., 2006; Kim et al., 2006, 2007, 2010b). However, crenarchaeol also occurs ubiquitously in soil, a few soils even have BIT values <0.5 (e.g. Weijers et al., 2006a; Walsh et al., 2008). Especially in alkaline soils crenarchaeol concentrations are higher, leading to lower BIT values (Weijers et al., 2007c; Kim et al., 2010b; Yang et al., 2011; Xie et al., 2012). In addition brGDGTs are produced, albeit in minor amount in marine (e.g. Peterse et al., 2009a) and estuary (Zhang et al., 2012) sediments, but generally the BIT index in marine environment remains below <0.15. In marine environments the BIT can also be influenced by the fluctuations of crenarchaeol concentrations (e.g. Castañeda et al., 2010; Schmidt et al., 2010; Fietz et al., 2011; Smith et al., 2012). Furthermore, Huguet et al. (2008) showed in turbidite sediments that the BIT increased under long term exposure to oxygen. Hence the BIT index may not be applied as a quantitative measure of soil organic matter in marine sediments, but it may still indicate relative fluctuations of soil organic matter input (Ménot et al., 2006; Sluijs et al., 2008).

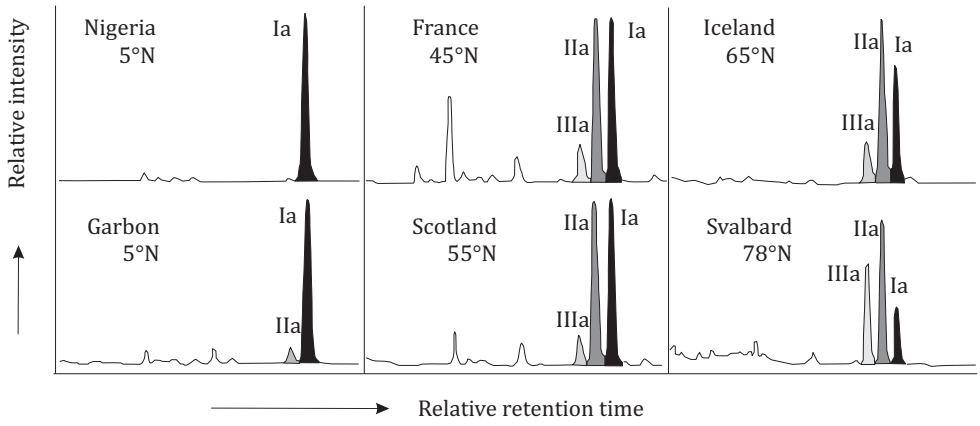

Fig. 1.2 HPLC-MS base peak chromatograms showing the variation of the brGDGT distribution found in different soils (from Weijers et al., 2007c). Roman numerals refer to the structures in Fig. 1A.

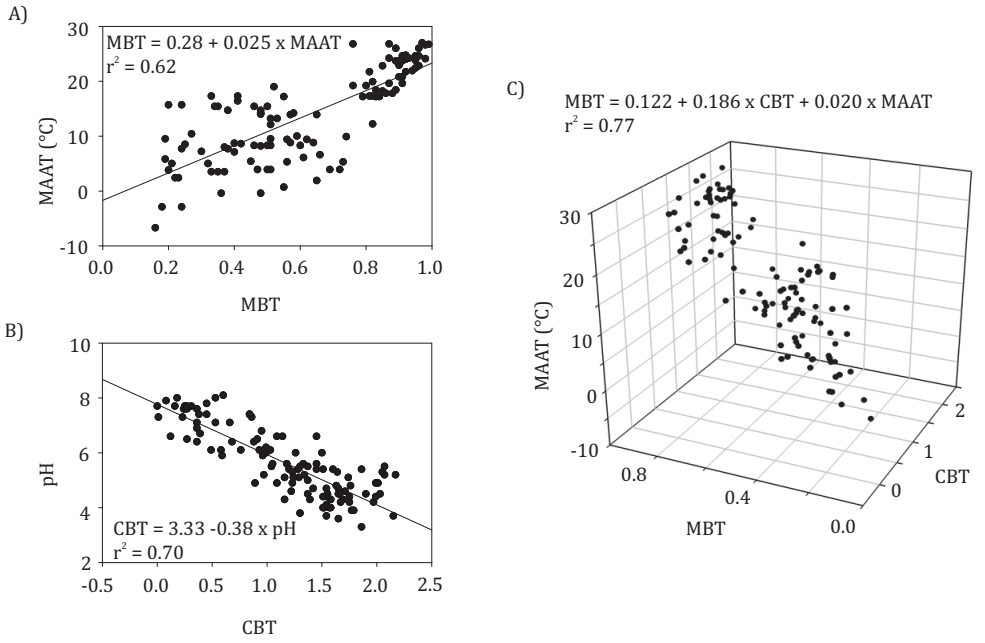

Fig. 1.3 Relationship between the MBT index and MAT (A), the CBT index and pH (B), and the 3D calibration plot of the MBT and CBT indices with MAT (c) for the global soil calibration set (from Weijers et al., 2007c)

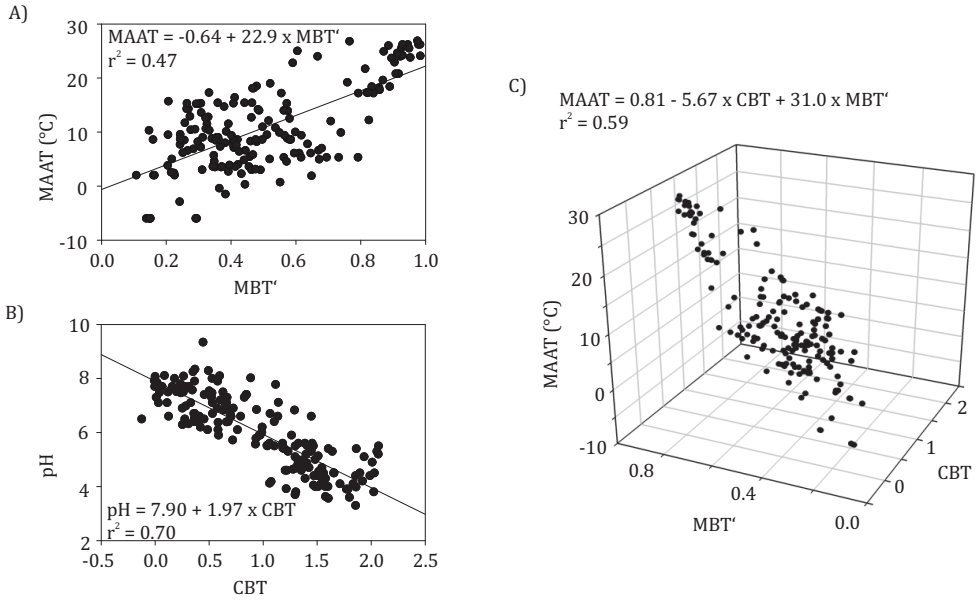

Fig. 1.4 Relationship between the MBT' index and MAT (A), the CBT index and pH (B), and the 3D calibration plot of the MBT' and CBT indices with MAT (C) for the new global soil calibration set (from Peterse et al., 2012).

1.4. APPLICATIONS OF BRGDGTS AS ENVIRONMENTAL PROXIES

Weijers et al. (2007a) showed that in marine sediments, which receive substantial amounts of soil organic matter (such as those from the Congo Fan), the MBT/CBT proxy can be used to reconstruct environmental conditions of the river catchment area. The temperature record reconstructed with the MBT/CBT matched well with known global climate changes and revealed a MAAT for the Last Glacial Maximum ca. 4.5˚C colder than at present. In addition, the soil pH record showed that during wet conditions, soil pH dropped, likely due to soil leaching of basic ions. A similar study was carried out by Bendle et al. (2010) on a sediment core taken close to the Amazon fan. However, in contrast to the findings of Weijers et al. (2007a) the reconstructed MAAT decreased from the glacial period (19.6-23.4°C) to the mid Holocene (10°C), and then increased over the remainder of the Holocene to 17.4°C. It was postulated that an increased brGDGT contribution from the Andean region was responsible for the observed decrease of the reconstructed MAAT during the Holocene (Bendle et al., 2010). From this result it was concluded that a change in the source area of the brGDGTs can have a major impact on the MBT/CBT record. Furthermore soil brGDGTs might be pre-aged when they arrive in the marine sediment (Smittenberg et al., 2005), which could complicate the use of the MBT/CBT in marine settings. Nevertheless, the MBT/CBT has been successfully used to reconstruct temperatures from cores taken in the Arctic region and Greenland (Schouten et al., 2008b; Rueda et al., 2009; Pross et al., 2012).

In addition, the MBT/CBT proxy in ancient sediments can be affected by diagenesis and maturity. The distribution of brGDGTs in an artificial maturation experiment showed that the MBT index had a slight tendency to decrease during artificial maturation, while the CBT index clearly increased with maturity (Schouten et al., 2013b). The impact of (oxic) degradation on the MBT/CBT proxy, specifically during erosion and transport of soil to the marine environment, has not been established, to the best of our knowledge. However, in a small lake in the USA variations in the distribution of brGDGTs were observed, impacting on MBT/CBT values between sediments deposited under oxic and anoxic conditions, respectively. However, this was attributed to different producers of the brGDGTs in the lake sediments (Tierney et al., 2012).

In the terrestrial environment brGDGT-derived proxies have been applied in climate archives like peat, ancient coal and loess (Ballantyne et al., 2010; Hren et al., 2010; Peterse et al., 2011b; Weijers et al., 2011b; Zhou et al., 2011; Gao et al., 2012). However not in all cases the reconstructed temperatures were realistic and thus might have been influenced by other environmental factors rather than pH and temperature. The MBT/CBT was also used on stalagmites, but the MBT/CBT values were different to those of overlying soil (Yang et al., 2011). Furthermore, brGDGT-derived proxies have been used in lake sediments. Since strong influence of in-situ

produced brGDGTs occurs in many lakes, the application of the global soil correlation for the MBT/CBT proxy often led too low reconstructed temperatures (Blaga et al., 2010; Tierney et al., 2010; Zink et al., 2010), while in lakes which were dominated by brGDGTs from soil erosion the global soil correlation for the MBT/CBT proxy could be used (Niemann et al., 2012).

1.5. OBJECTIVE AND OUTLINE OF THIS THESIS

This thesis is focused on the validation of the MBT/CBT (or MBT'/CBT) in marine sediment records that are influenced by rivers. Therefore, a detailed study of the brGDGTs in two different river systems was carried out (Amazon and Tagus River). In order to understand the origin of brGDGTs in the drainage basin, soils and river suspended particulate matter (SPM) were analyzed. In this way, the source of brGDGTs and the role of in-situ production of brGDGTs in the river could be assessed. Subsequently, the transport of brGDGTs from the rivers to the marine environment was examined by analyzing marine SPM and surface sediment and comparing the brGDGT distributions with those of soil and riverine SPM. Here the aim was to constrain the influence of brGDGT distribution coming from the rivers by marine in-situ production and degradation.

Chapters 2-5 present a detailed study of the brGDGTs in the Amazon River basin. The Amazon River is the world's largest river with a drainage basin area of 6.1 x 106 km^2 covering about 40 % of South America (Goulding et al., 2003). Most of its basin is located in the tropical rain forest. The Amazon River flows along the equator. Therefore, there is no big temperature difference in the drainage basin, only between the mountainous and lowland areas. In **Chaper 2** the BIT index, the C:N ratio and $\delta^{13}C_{OC}$ data were used to understand which role soil OC plays in the whole pool of terrestrial OC that is transported by the Amazon River. It was found that the high mountainous Andes were not a major source of brGDGTs in the Amazon River, as suggested previously. In **Chapter 3** the brGDGTs in Amazon basin soils were analyzed and shown to be remarkably similar over a large area of the basin. Furthermore, the brGDGT distribution and concentration (CL and IPL-derived) in soils were compared to those in the river, in tributaries and in floodplain lakes. The difference in the brGDGT distribution of the soils and the river indicated production of brGDGTs in the river itself. As a follow-up of this finding, **Chapter 4** compared the brGDGTs in the Amazon River in four different seasons (low water, rising water, high water and falling water). It was found that the difference between the seasons could be clearly seen in the brGDGT concentration, distribution and also in the BIT index. The results indicate higher soil input during the high water season. **Chapter 5** focused on the transport of brGDGTs from the Amazon River to the ocean. The delivery of brGDGTs from the river was clearly observed in the marine SPM and surface sediments. However, further away from the river the brGDGT distribution was strongly

influenced by in-situ produced brGDGTs in the marine environment.

The second river system that was studied **(Chapters 6-7)** was the Tagus River of the Iberian Peninsula, which is a much smaller river system than the Amazon River. In addition the climate is different since the Tagus River is located in dry temperate climate. **Chapter 6** focused on the brGDGTs in Tagus basin soils and showed that the MBT'/CBT cannot be used in this region because the brGDGTs distributions were diverse and did not represent the MAAT of the basin. The higher concentration of brGDGTs in the Tagus River compared to surrounding soils, and the difference in the brGDGT distribution indicated in-situ production in the Tagus River. Temperature reconstructions using brGDGTs carried out in the Tagus River might be possible using an aquatic calibration. In the marine environment the input of brGDGTs from the Tagus River can be seen clearly, but indications for marine in-situ production were found as well. The last chapter **Chapter 7** dealt with the BIT index and brGDGT concentrations as an indicator for continental OC input along the Portuguese margin. High brGDGT concentrations close to the rivers indicated the brGDGT input by rivers which was also seen in the BIT, but the BIT was also influenced, to some degree, by variations in the crenarchaeol concentration. Therefore, the brGDGT concentration might give a more straight forward indication of continental OC input than the BIT.

In summary, this thesis shows that it is necessary to perform a study of the river basin before the MBT/CBT can be applied with confidence to marine sediment cores. First to confirm that the MBT/CBT of river basin soils represents the MAAT and soil pH, and second to determine the influence of in-situ brGDGT production in the river and in the marine environment. This has to be checked for each river systems in which the MBT/CBT is supposed to be applied, since major differences were found in different settings.

Part I

The Amazon River and Amazon continental margin

Picture by Jung-Hyun Kim

Chapter 2

Tracing soil organic carbon in the lower Amazon River and its tributaries using GDGT distributions and bulk organic matter properties

Jung-Hyun Kim, Claudia Zell, Patricia Moreira-Turcq, Marcela A.P. Pérez, Gwenaël Abril, Jean-Michel Mortillaro, Johan W.H. Weijers, Tarik Meziane, and Jaap S. Sinninghe Damsté

Geochimica et Cosmochimica Acta 90 (2012) 163–180

Abstract
In order to trace the transport of soil organic carbon (OC) in the lower Amazon basin, we investigated the distributions of crenarchaeol and branched glycerol dialkyl glycerol tetraethers (GDGTs) by analyzing riverbed sediments and river suspended particulate matter (SPM) collected in the Solimões-Amazon River mainstem and its tributaries. The Branched and Isoprenoid Tetraether (BIT) index, a proxy for river-transported soil OC into the ocean, was determined from the distributions of these GDGTs. The GDGT-derived parameters were compared with other bulk geochemical data (i.e. C:N ratio and stable carbon isotopic composition). The GDGT-derived and bulk geochemical data indicate that riverine SPM and riverbed sediments in the lower Amazon River and its tributaries are a mixture of C_3 plant-derived soil OC and aquatic-derived OC. The branched GDGTs in the SPM and riverbed sediments did not predominantly originate from the high Andes soils (>2500 m in altitude) as was suggested previously. However, further constraint on the soil source area of branched GDGTs was hampered due to the deficiency of soil data from the lower montane forest areas in the Andes. Our study also revealed seasonal and interannual variation in GDGT composition as well as soil OC discharge, which was closely related to the hydrological cycle. By way of a simple binary mixing model using the flux-weighted BIT values at Óbidos, the last gauging station in the Amazon River, we estimated that 70–80% of the POC pool in the river was derived of soil OC. However, care should be taken to use the BIT index since it showed a non-conservative behaviour along the river continuum due to the aquatic production of crenarchaeol. Further investigation using a continuous sampling strategy following the full hydrological cycle is required to fully understand how soil-derived GDGT signals are transformed in large tropical river systems through their transport pathway to the ocean.

2.1 INTRODUCTION

As one of the major pathways for the ultimate preservation of terrigenous production, the transfer of organic matter (OM) from land to the ocean via rivers is a key process in the global carbon cycle (Ittekkot and Haake 1990; Degens et al., 1991; Hedges et al., 1992). Hence, the role of rivers in the global carbon cycle is most typically expressed as the fluvial export of total organic carbon (TOC, particulate and dissolved organic carbon; POC and DOC, respectively) from land to the ocean (e.g., Likens et al., 1981). Fluvial transport of TOC represents an estimated flux of 0.4 – 0.6 Pg C yr^{-1} to the global ocean (Schlesinger and Melack, 1981; Spitzy and Ittekkot, 1991; Ludwig et al., 1996; Lal, 2003). Tropical rivers are thought to be responsible for 45–60% of this flux (Meybeck, 1982; Ludwig et al., 1996), and thus form an important link between terrestrial and marine carbon pools (Quay et al., 1992). The Amazon River, the world's largest river by water flow, is responsible for 8–10% of the global terrestrial OC export to the oceans, with DOC (83%) dominating over POC (17%) (Moreira-Turcq et al., 2003).

Most previous studies (Hedges et al., 1986a; Quay et al., 1992; Martinelli et al., 2003), predominantly based on bulk organic parameters such as the C:N ratio and the stable isotopic composition of OC $\delta^{13}C_{OC}$), and lignin composition, indicated that OC in the Amazon River is predominantly soil-derived. These studies have also found particulate organic matter (POM) compositions to be nearly constant over substantial time periods, distances, hydrologic fluctuations, and size fractions (Hedges et al., 1986a; Quay et al., 1992). In contrast, POM in the St Lawrence River (Canada) was dominated by phytoplanktonic material during warm seasons, and terrestrial detritus during colder periods and storm surges (Barth et al., 1998). In the Sanaga River (Cameroon) and Congo River (Central Africa), POM also varied with discharge, with high proportions derived from C_4 plants in savannas during high discharge periods, and high proportions derived from C_3 plants from the riverbanks during low discharge periods (Mariotti et al., 1991; Bird et al., 1998).

Recently, the Branched and Isoprenoid Tetraether (BIT) index (Hopmans et al., 2004) has been developed to trace soil OC in marine environments. This index is based on the relative abundance of non-isoprenoidal, so-called branched, glycerol dialkyl glycerol tetraethers (GDGTs, Sinninghe Damsté et al., 2000) vs. a structurally related isoprenoid GDGT "crenarchaeol" (Sinninghe Damsté et al., 2002). Branched GDGTs are ubiquitous and dominant in peats (Weijers et al., 2004, 2006a) and soils (Kim et al., 2006, 2010; Weijers et al., 2006b, 2007; Huguet et al., 2010), probably derived from anaerobic (Weijers et al., 2006a,b) and heterotrophic (Pancost and Sinninghe Damsté, 2003; Oppermann et al., 2010; Weijers et al., 2010) bacteria. Recent studies indicated that bacteria from the phylum Acidobacteria are a likely source for these branched GDGTs (Weijers et al., 2009a; Sinninghe Damsté et al., 2011). Crenarchaeol is considered to be the specific membrane-spanning lipid of non-extremophilic Thaumarchaeota(Sinninghe Damsté et al., 2002; Schouten et al., 2008a; Pitcher et al., 2011a), formerly known as Group I Crenarchaeota (Spang et al., 2010).

The BIT index has been introduced as a new tool initially for estimating the relative amounts of river-transported terrestrial OC in marine sediments (Hopmans et al., 2004) and later, based on the findings of Weijers et al. (2006b), more specifically as a proxy of river-transported oil OC input (Huguet et al., 2007; Walsh et al., 2008; Kim et al., 2009). Recently, Tierney and Russell (2009) showed that in the Lake Towuti area (Indonesia), the concentrations of branched GDGTs were increased along a soil-riverbed-lake sediment transect. Since their branched GDGT distributions were also significantly different to each other, albeit with high and comparable BIT values, they proposed a potential in-situ production of branched GDGTs in the lake water column and/or water–sediment interface in the river itself in addition to soil erosion. In contrast, Zhu et al. (2011) found that the riverbed sediments from the lower Yangtze River had higher branched GDGT concentrations than the marine sediments from the adjacent East China Sea. This indicated that the branched GDGTs in this river system originated predominantly from soil input. Nonetheless, their branched GDGT distribution patterns did not

reflect fully their distribution in catchment soils. This led to a conclusion that branched GDGTs could have been produced in the Yangtze River channel itself, contributing at least partly to the branched GDGT pool in the riverbed sediments. Several recent studies in lacustrine environments (Sinninghe Damsté et al., 2009; Tierney and Russell, 2009; Bechtel et al., 2010; Blaga et al., 2010; Tierney et al., 2010; Tyler et al., 2010; Zink et al., 2010; Loomis et al., 2011; Sun et al., 2011) also indicated that aquatic production of branched GDGTs is likely.

Few studies in large rivers have been conducted with sufficient temporal and/or spatial coverage for adequate assessment of GDGT composition and discharge related to seasonal hydrological changes. Here, we investigated riverbed sediments and suspended particulate matter (SPM) collected in the Solimões-Amazon River mainstem and its main tributaries (Negro, Madeira, and Tapajós) in periods of high and low water discharge in 2005 and 2009. We determined variations in crenarchaeol and branched GDGT concentrations as well as BIT index. The results were subsequently compared with other commonly used proxies for terrestrial OM input such as C:N ratio and $\delta^{13}C_{OC}$. The aims of this study were (1) to trace the potential compositional alteration of soil OM along the transport pathway and (2) to quantify the relative contribution of soil-derived OC to POC and its discharge to the ocean. Our results provide a qualitative and quantitative assessment of GDGT sources (soil vs. aquatic) and composition in the Amazon River and its tributaries.

2.2 MATERIAL AND METHODS

2.2.1 Study area

The Amazon basin runs about 5000 km from the Atlantic coast to the foot of the Andes (Nores, 2011). The boundary between the lowland Amazonian rain forest and the forest of the eastern slopes of the Andes may be restricted to about 500 m in altitude (Patterson et al., 1998; Nores, 2011). The eastern Andean montane forests may be subdivided into two forest belts: lower montane forests (<2500 m in altitude) and upper montane forests (2500–3500 m in altitude, Young, 1999). Páramo (i.e. high alpine grasslands, bogs, and open meadows) is located in the high elevations between the upper forest line (3000 m in altitude) and the permanent snow line (5000 m in altitude). The Amazon River is formed by the confluence of the Ucayali and Marañon Rivers in Peru (Fig. 2.1A). In Brazil, the main river is referred to as the Solimões River upstream of its confluence with the Negro River. The Amazon River is the world's largest river with a drainage basin area of 6.1 x 106 km^2 covering about 40% of South America (Goulding et al., 2003), and a mean annual discharge of 200,000 $m^3 s^{-1}$ at Óbidos, the most downstream gauging station in the Amazon River (Callède et al., 2000). The Amazon River supplies approximately 20% of the total volume of freshwater entering the ocean (Meade et al., 1985; Molinier et al., 1996). The Amazon River also ranks second in terms

of particle transport with an annual mean sediment discharge of 800–1200 109 kg yr^{-1} at Óbidos (Dunne et al., 1998; Martinez et al., 2009). Riverine transport of OC by the Amazon exports 32.7–34.5 Tg C yr^{-1} to the ocean as measured at the outlet of Óbidos, and thus contributes significantly to the global carbon budget (Moreira-Turcq et al., 2003; Bustillo et al., 2011 and references therein).

Rivers within the Amazon drainage basin are traditionally classified according to their colour (Sioli, 1950). White water rivers (e.g., Sõlimoes and Madeira) have high levels of total suspended solids due to the mechanical erosion of the Andean mountain chain (Gibbs, 1967a; Meade et al., 1985). The black water rivers (e.g., Negro) originate from lowland regions with bleached sandy soil (podzols) and are characterized by low SPM but high concentrations of dissolved humic substances (Mounier et al., 1998). The clear water rivers (e.g., Tapajós) are depleted in both suspended and dissolved material and often characterized by a high phytoplankton production (Junk, 1997).

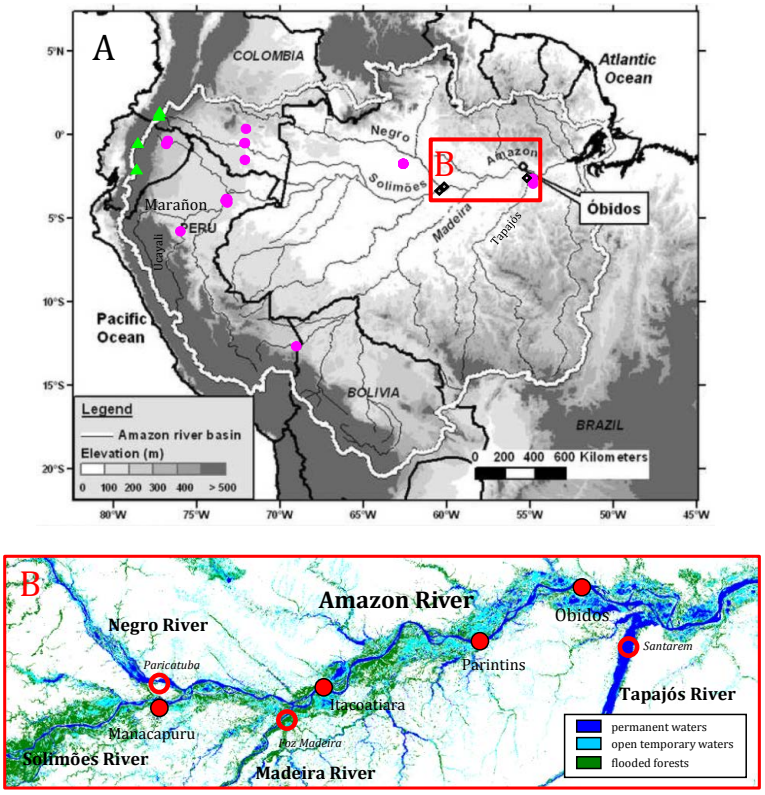

Fig. 2.1 (A) A general map of the Amazon basin (Martinez et al., 2009) showing the study area (red box) with the sample locations of Andes (>500 m in altitude, filled green triangles) and Amazon (<500 m in altitude, filled purple circles) soils and riverbed sediment (black open diamonds) and (B) a detailed lower Amazon basin map (Martinez and Le Toan, 2007) with river SPM sampling sites on the Amazon River (filled red circles) and its tributaries (open red circles).

2.2.2 Hydrological data

The daily water levels recorded at Óbidos (154.080S, 531.1160W) were provided by the Agência Nacional das Águas (ANA). The water level series was described by Callède et al. (2001) and retrieved from the HYBAM project web-site (http://www.mpl.ird.fr/hybam/). Water discharge was measured at selected sampling sites with an Acoustic Doppler Current Profiler (ADCP 600 and 1200 Hz, Work- Horse Rio Grande TMRD Instruments) with a precision better than ±5%. Water discharge was estimated from at least 4 cross-section measurements with an error of about 5%. Discharges in the Amazon River were computed from the rating curve established for the Óbidos stage. This relationship, initially proposed by Jaccon (1987) was improved by Callède et al. (2001) and Filizola and Guyot (2004) using measurements with a 300 and 600 Hz ADCP (WorkHorse Rio Grande TMRD Instruments, Callède et al., 2000).

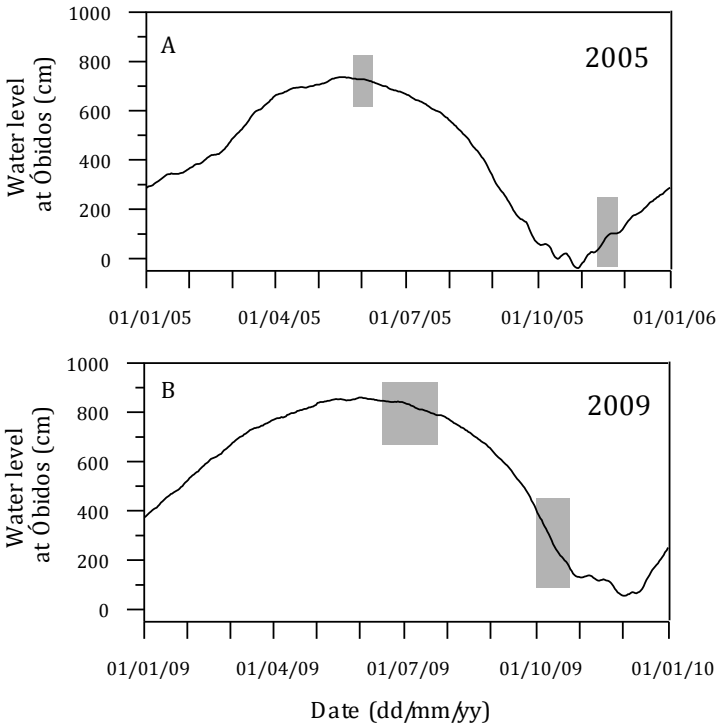

Fig. 2.2 Variations in water level (cm) at Óbidos, which is the last gauging station in the Amazon River. The grey bars indicate the sampling periods.

2.2.3 Sample collection

Riverbed sediment and river SPM sampling sites are shown in Fig. 2.1 (see also Table 2.1). Three surface riverbed sediments were collected using a bottom sediment grab sampler at Paricatuba, Manacapuru, and Óbidos during the December cruise in

2003. River SPM was collected at four mainstem locations (Manacapuru, Itacoatiara, Parintins, Óbidos) on the Solimões-Amazon River and at three of its major tributaries: Negro, Madeira, and Tapajós Rivers (indicated with open circles in Fig. 2.1B). The water regime of the mainstem of the Solimões-Amazon River is characterized by a monomodal hydrogram with high and low water phases, occurring in May–June and in October–November, respectively (Fig. 2.2). Therefore, we collected SPM during high and low water periods in 2005 and in 2009 (Fig. 2.2). Samples were generally collected near the surface. During the 2005 cruises, we also collected SPM along several vertical profiles in the Negro, Solimões, and Amazon Rivers.

All the river SPM samples were collected in a similar way. In brief, about 0.5–5 L of water were collected using a Niskin bottle and filtered onto ashed (450 °C, overnight) and pre-weighed glass fibre filters (Whatman GF-F, 0.7 µm) using a vacuum system, under low pressure. After filtration, the filters were dried either for 24 h at 5 °C or kept frozen on board and freeze-dried after being brought to the lab and then weighed to calculate the concentration of SPM. One part of each filter was used for the elemental and stable isotope analysis. For the GDGT analysis, either the rest of each filter used for the elemental and stable isotope analysis or filters collected separately were used.

2.2.4 Chemical analyses

2.2.4.1 Elemental and stable carbon isotope analysis

TOC (or POC) and total nitrogen (TN) of riverbed sediments and river SPM samples were analyzed using an elemental analyzer C-H-N FISONS NA-2000 at Bondy (France). The average precision on concentration measurements was ±0.1 mg C g^{-1} for TOC and ±0.05 $mg_N g^{-1}$ for TN. The C:N ratio was calculated as TOC:TN for the riverbed sediments and POC:TN for the river SPM samples. The $\delta^{13}C_{OC}$ was analyzed using a Europe Hydra 20–20 mass spectrometer equipped with a continuous flow isotope ratio monitoring (Waterloo University, Canada and University of California, Davis, USA). The $\delta^{13}C_{OC}$ values are reported in the standard delta notation relative to Vienna Pee Dee Belemnite (VPDB) standard. The analytical precision (as standard deviation for repeated measurements of the internal standards) for the measurement was 0.06‰ for $\delta^{13}C_{OC}$.

2.2.4.2 Lipid extraction and purification procedure

All samples were processed at NIOZ (The Netherlands). The riverbed sediments and the freeze-dried filters collected in 2005 were ultrasonically extracted with methanol (MeOH, 3 x), MeOH:dichloromethane (DCM) (1:1 v:v, 3 x), and DCM (3 x). The supernatants were combined, the solvents were removed by rotary evaporation, and the extracts were taken up in DCM and dried under a steady stream of pure N_2.

The freeze-dried filters collected in 2009 were extracted using a modified Bligh and Dyer method (Bligh and Dyer, 1959). Samples were ultrasonically extracted three times for 10 min. using a single-phase solvent mixture of MeOH:DCM:phosphate buffer (8.7 g of K_2HPO_4 in 1 L bidistilled water) 10:5:4 (v:v:v). Upon centrifugation, superna-

tants were collected and combined. DCM and phosphate buffer were added to the combined extracts to create a new volume ratio of 5:5:4 (v:v:v) and obtain phase separation. The extract (DCM phase) containing the GDGTs was separated from the residue (MeOH–phosphate buffer phase)by centrifugation and collected. The residue phase was extracted twice more with DCM and the combined extracts evaporated to near dryness using a rotary evaporator. The extract was passed over a small column plugged with extracted cotton wool to remove any remaining filter particles and then completely dried under N_2.

For the quantification of GDGTs, a C_{46} GDGT internal standard was added to two fractions after the total extracts were separated over a small silica gel (activated overnight) column using n-hexane:ethyl acetate (1:1, v:v) and MeOH,respectively (2009 SPM samples), or to the total extracts before the extracts were separated into two fractions over an Al_2O_3 (activated for 2 h at 150 °C) column using hexane:DCM (9:1, v:v) and DCM:MeOH (1:1, v:v), respectively (all other samples).

A recent study by Lengger et al. (2012b) showed that different extraction and separation techniques for the quantification of core lipid GDGTs gave similar results. Therefore, the two different methods used for quantification of GDGTs in this study provide comparable results.

2.2.4.3 GDGT analysis

The GDGT-containing fractions were analyzed at NIOZ (The Netherlands) for GDGTs according to the procedure described by Schouten et al. (2007) with minor modifications. The fractions were dried down under N_2, re-dissolved by sonication (5 min) in n-hexane:2-propanol (99:1 v:v) solvent mixture in a concentration of ca. 2 mg ml^{-1}, and filtered through 0.45 μm PTFE filters. The samples were analyzed using high performance liquid chromatographyatmospheric pressure positive ion chemical ionization mass spectrometry (HPLC-APCI-MS). GDGTs were detected by selective ion monitoring of their $(M+H)^+$ ions (dwell time 237 ms) and quantification of the GDGT compounds was achieved by integrating the peak areas and using the C_{46} GDGT internal standard according to Huguet et al. (2006). To correct the potential carryover of GDGTs into the MeOH fraction for the SPM samples collected in 2009, the MeOH fractions were also analyzed using the HPLC-APCI-MS. The BIT index was calculated according to Hopmans et al. (2004):

$$\text{BIT index} = ([I] + [II] + [III]) / ([I] + [II] + [III] + [IV]) \quad (1)$$

[I], [II], and [III] are the concentration of branched GDGTs and [IV] the concentration of isoprenoid GDGT crenarchaeol (Appendix 1). The instrumental reproducibility was determined by triplicate measurements of three samples. The average standard deviation of the BIT index was ±0.002. For the concentration of GDGTs, the analytical errors were ±8% for GDGT I, ±8% for GDGT II, ±12% for GDGT III, and ±9% for crenar-

chaeol. Note that only tiny amounts of riverbed sediments and SPM, except for those collected during the low water period in 2009, were available for this study, resulting in low total extract yields. As a consequence, branched GDGTs bearing one or two cyclopentane moieties were below quantification limits. Therefore, we considered only the three major branched GDGT compounds without cyclopentane moieties in this study.

2.2.5 Statistical analysis

A principal component analysis (PCA) was carried out in order to test the statistical difference between GDGT distributions. We used the fractional abundances (f) of crenarchaeol and branched GDGTs acquired from the riverbed sediments and the river SPM samples in the lower Amazon basin as well as those for Andes and lowland Amazon soils (Appendix 2). The Brodgar v.2.5.2 (http://www.brodgar. com) software package was used.

2.3 RESULTS

2.3.1 Hydrological data

During the high and low water sampling periods (Fig. 2.2), the instantaneous water discharge along the mainstem was 125–194 <?> 103 and 60–87 x 10^3 m^3 s^{-1} in 2005 and 161–294 x 10^3 and 67–114 x 10^3 m^3 s^{-1} in 2009, respectively (Table 2.1). During the same periods, the water discharge was 26–46 x 10^3 and 30 x 10^3 m^3 s^{-1} at the Negro River station, while 21–30 x 10^3 and 11– 12 x 10^3 m^3 s^{-1} at the Madeira River station. Unfortunately, water discharge measurements were not carried out at the Negro River sampling site in November 2005 and at the Tapajós River sampling sites in both 2005 and 2009.

2.3.2. Bulk geochemical parameters

2.3.2.1. River SPM

SPM and POC concentrations as well as other geochemical parameters (C:N ratio and $\delta^{13}C_{OC}$) showed little variation with depth for the two stations (Manacapuru and Óbidos) in the Solimões-Amazon River mainstem where this was measured (Fig. 2.3A and C, Table 2.1). In general, no consistent trend with depth was observed in any of the parameters measured. For all investigated stations in the Solimões-Amazon River mainstem, the concentrations of surface SPM were lower at times of relatively high water discharge (Fig. 2.4A) with total SPM concentrations ranging from 23 to 215 mg L^{-1} (Table 2.1). The OC content of SPM was in the range of 1–4 wt.% (Fig. 2.5, Table 2.1) and the POC concentrations varied between 0.8 and 2.3 mg C L^{-1} (Fig. 2.4B). The C:N ratio and the $\delta^{13}C_{OC}$ fluctuated between 7 and 11 and between -35.0‰ and -27.9‰, respectively (Fig. 2.5).

In comparison to the Solimões-Amazon River mainstem, the SPM concentrations were lower in the Negro River, in the range of 4–6 mg L^{-1} (Fig. 2.4A). However, the OC

Table 2.1 Information on the samples and results of bulk OM and GDGT analyses

	Station	Cruise name	Long. (°)	Lat. (°)	Water discharge (10^3 m^3 s^{-1})	Date (mm/yyyy)	Water depth (m)
Riverbed sediment							
Solimões	Manacapuru		-60.553	-3.332		12/2003	Surface
Negro	Paricatuba		-60.263	-3.073		12/2003	Surface
Amazon	Óbidos		-55.302	-1.951		12/2003	Surface
SPM							
Manacapuru			-60.553	-3.332	125	06/2005	Surface
					125	06/2005	7
					125	06/2005	28
					60	11/2005	
					60	11/2005	2
					60	11/2005	8
					60	11/2005	16
					60	11/2005	24
		CBM5			161	06/2009	Surface
		CBM6			67	10/2009	Surface
Negro	Paricatuba		-60.263	-3.073	46	05/2005	Surface
					46	05/2005	10
					46	05/2005	20
					46	05/2005	30
		CBM5			26	06/2009	Surface
		CBM6			30	10/2009	Surface
Madeira	Foz Madeira		-58.79	-3.415	21	06/2005	Surface
					21	06/2005	23
					12	11/2005	Surface
					12	11/2005	3
					12	11/2005	10
		CBM5			30	06/2009	Surface
		CBM6			11	10/2009	Surface
Amazon	Itacoatiara		-58.254	-3.093	90	11/2005	Surface
					90	11/2005	30
					90	11/2005	62
		CBM5			n.d.	06/2009	Surface
		CBM6			111	10/2009	Surface
Amazon	Parintins		-56.757	-2.627	192	06/2005	Surface
					192	11/2005	20
		CBM5			n.d.	07/2009	Surface
		CBM6			n.d.	10/2009	Surface
Amazon	Óbidos		-55.302	-1.951	194	06/2005	Surface
					194	06/2005	15
					194	06/2005	45
					87	11/2005	Surface
					87	11/2005	25
					87	11/2005	50
		CBM5			294	07/2009	Surface
		CBM6			114	10/2009	Surface
Tapajós							
Santarem			-54.431	-2.242	n.d.	06/2005	Surface
					n.d.	08/2206	Surface
					n.d.	11/2005	15
		CBM5			n.d.	07/2009	Surface
		CBM6			n.d.	10/2009	Surface

from riverbed sediments and river SPM samples investigated in this study.

Sample name	SPM (mg L^{-1})	OC (wt.%)	C:N ratio	$d^{13}C_{OC}$ (‰ VPDB)	I (µg g_{OC}^{-1})	II (µg g_{OC-1})	III (µg g_{OC}^{-1})	IV (µg g_{OC}^{-1})	BIT
RB-S4		4	11	-28.2	1	0.3	0.04	0.2	0.89
RB-N1		19	16	-27.6	3	0.2	0.01	0.2	0.93
RB-A1		7	10	-28.8	4	1	0.1	0.3	0.94
RS-S1	113	2	8	-28.6	42	8	1	6	0.9
RS-S2	95	2	7	-28.5	37	7	0.8	5	0.9
RS-S3	121	2	8	-28.4	36	7	0.9	5	0.9
RS-S4	153	1	8	-29.2	50	11	1.5	13	0.83
RS-S5	189	1	7	-29.3	10	3	0.4	3	0.79
RS-S6	146	2	8	-28.9	25	5	0.8	11	0.74
RS-S7	127	2	9	-28.8	34	8	1.1	10	0.81
RS-S8	215	2	9	-28.7	32	7	1	9	0.82
CBM502	41	2	8.23	-35.03	81	16	0	6	0.94
CBM607	74	3	8	-30.2	14	3	0.2	9	0.65
RS-N1	6	15	41	-28.5	34	1	0.1	3	0.92
RS-N2	5	20	30	-29.4	55	2	0.2	5	0.92
RS-N3	6	16	27	-28.8	68	3	0.2	6	0.92
RS-N4	8	16	25	-29	50	2	0.2	4	0.92
CBM514	3	22	11	-31.3	120	9	0.1	11	0.92
CBM601	4	23	11	-31.3	53	4	0.2	6	0.9
RS-M1	53	2	7	-28	29	6	0.6	13	0.73
RS-M2	84	1	7	-27.9	45	9	1	19	0.74
RS-M3	172	1	4	-29.2	39	12	1.5	30	0.63
RS-M4	178	1	5	-29.3	94	29	3.4	51	0.71
RS-M5	309	1	6	-29	27	8	1.1	18	0.67
CBM517	53	2	6	-28.5	165	24	1.4	14	0.93
CBM621	33	2	6	-29.3	25	7	0.5	37	0.46
RS-A6	96	1	9	-28.8	54	13	1.7	17	0.8
RS-A7	107	2	8	-28.9	39	10	1.4	9	0.85
RS-A8	109	2	8	-28.7	28	6	0.8	12	0.74
CBM518	27	4	8	-29.6	152	20	1	11	0.94
CBM622	23	3	8	-29.3	54	10	0.6	65	0.5
RS-A2	34	3	9	-29.5	57	7	0.6	15	0.81
RS-A9	126	1	7	-29.3	46	9	1.1	38	0.6
CBM528	24	3	8	-29.7	74	13	0.6	21	0.8
CBM634	32	3	7	-29.5	32	6	0.5	51	0.42
RS-A3	38	3	11	-28.1	38	6	0.6	12	0.79
RS-A4	97	2	10	-28.1	35	6	0.6	9	0.82
RS-A5	96	2	10	-27.9	40	7	0.7	10	0.83
RS-A10	64	2	8	-29.7	49	15	2.4	6	0.67
RS-A11	75	3	11	-28.4	6	1	0.2	10	0.44
RS-A12	95	2	7	-29.4	18	4	0.6	22	0.51
CBM531	27	3	8	-29.2	78	13	0.5	17	0.84
CBM635	31	3	8	-29.3	22	4	0.4	38	0.41
RS-Ta1	20	32	6	-27.4	4	0.4	0	3	0.59
RS-Ta3	5	14	6	-29.6	10	1	0.1	10	0.52
RS-Ta4	6	10	5	-29.9	18	3	0.2	19	0.53
CBM541	3	15	7	-32.9	57	8	0.4	52	0.56
CBM642	3	22	6	-27.5	9	2	0.2	4	0.74

content of SPM was much higher ranging from 15–23 wt.% (Fig. 2.5, Table 2.1) and consequently the POC concentration, varying between 0.8 and 0.9 mg C L^{-1}, was of the same order of magnitude in the Solimões-Amazon River mainstem (Fig. 2.4B). Except for the extremely high C:N ratio values in the 2005 high water period, in general, the C:N ratio (11) and the $\delta^{13}C_{OC}$ (-31.3‰ to -28.5‰) were comparable to those along the Solimões-Amazon River mainstem (Fig. 2.5). Similar to the water depth profiles of the Solimões-Amazon River mainstem, the water depth profiles of the Madeira River showed no apparent trend with depth for any of the bulk parameters (Fig. 2.3B, Table 2.1). In the Madeira River, the SPM concentrations (Fig. 2.4A) was high during the low water stage (170 mg L^{-1}) compared to the high water period (50 mg L^{-1}) in 2005, but this difference was not apparent in 2009 when only relatively small variations were observed (33–53 mg L^{-1}, Fig. 2.4). The OC content of SPM was between 1 and 2 wt.% (Fig. 2.5, Table 2.1) and the POC concentration between 0.8 and 2.2 mg C L^{-1} (Fig.2.4B), which was comparable to those in the Solimões-Amazon River mainstem. The average values of C:N ratio and $\delta^{13}C_{OC}$ were -5.9‰ and -28.7‰, respectively (Fig. 2.5), similar to those of the Solimões-Amazon River mainstem.

In the Tapajós River, the SPM concentrations were relatively low (i.e. between 3 and 20 mg L^{-1}, Fig. 2.4A) similar to those in the Negro River. The OC content of SPM, ranging from 15–32 wt.% (Fig. 2.5, Table 2.1), was always high in comparison with those in the Solimões-Amazon River mainstem. The POC concentration was much higher during the 2005 high water period (i.e. 6.3 mg C L^{-1}) than the average of other periods (Fig. 2.4B). On average, the C:N ratio was 6.3 and the $\delta^{13}C_{OC}$ -29.4‰ (Fig. 2.5).

2.3.2.2 Riverbed sediments

The TOC content of the riverbed sediments was high (4– 19 wt.%, Table 2.1). The C:N ratio varied between 10 and 16 and the $\delta^{13}C$ value ranged from -28.8‰ to -27.6‰. For the Negro riverbed sediment, the TOC content and the C:N ratio were much higher than for the Amazon River sediments.

2.3.3 GDGT parameters

2.3.3.1 River SPM

Branched GDGTs and crenarchaeol were detected in all river SPM samples and GDGT distributions were dominated by branched GDGT I (Table 2.1). Water depth profiles of GDGT concentrations and BIT values did not show clear trends in the Solimões-Amazon River (Figs. 2.3A and C). Along the Solimões-Amazon River mainstem (Fig. 2.4), the concentrations of branched GDGTs during the high water season in 2005 were lower (50–90 ng L^{-1}) than those during the low water season in 2005 (20–130 ng L^{-1}). In contrast, in 2009, the branched GDGT concentrations were higher during the high water season (70–200 ng L^{-1}) than during the low water season (30–50 ng L^{-1}). The concentrations of crenarchaeol varied between 4 and 18 ng L^{-1} during the high water season and between 8 and 70 ng L^{-1} during the low water season. In general, the crenarchae-

ol concentrations were lower during the high water seasons than during the low water seasons for both 2005 and 2009. It appears that variations in the concentrations of branched GDGTs are larger than those in crenarchaeol along the Solimões-Amazon River mainstem. The BIT index varied between 0.41 and 0.94 with higher values during the high water season than during the low water season. While BIT values during the high water season in 2005 were higher than those from the low water season in 2009. This suggests that interannual variations in the BIT index are higher for the low water seasons than for the high water seasons.

The concentrations of branched GDGTs and crenarchaeol in the Negro River were of the same order of magnitude compared to those in the Solimões-Amazon River mainstem, and varied between 30 and 90 ng L^{-1} and between 2 and 8 ng L^{-1}, respectively (Fig. 2.4). The BIT index was constant at ca. 0.90 and showed no significant difference between the high and low water periods in 2009. Similar to the Solimões-Amazon River mainstem, the concentration profile of GDGTs with water depth did not show clear trends in the Madeira River (Fig. 2.3B). It appears that the Madeira River behaved similar to the Solimões- Amazon River mainstem, showing that the concentrations of both branched GDGTs and crenarchaeol were higher during the low water period (120 and 70 ng L^{-1}, respectively) than during the high water period (30 and 10 ng L^{-1}, respectively) in 2005 (Fig. 2.4). In contrast, the branched GDGT concentrations were elevated during the high water level in 2009, whereas that of crenarchaeol remained similar to that in 2005. The BIT index varied between 0.73 and 0.93.

In the Tapajós River, the concentrations of both branched GDGTs and crenarchaeol obtained from SPM were higher during the high water levels than during the low water levels, ranging from 8 to 30 ng L^{-1} and from 3 to 20 ng L^{-1}, respectively (Fig. 2.4). In general, lower concentrations of the branched GDGTs in the Tapajós River resulted in lower BIT values than in other rivers. However, for the low water season in 2009, the crenarchaeol concentration was lower than that for the low water level in 2005,whilst the branched GDGT concentration was virtually the same. This resulted in an opposite pattern, showing higher BIT value during the low water level than during the high water level in 2009 (Fig. 2.4E).

2.3.3.2 Riverbed sediments

Branched GDGTs and crenarchaeol were detected in all riverbed sediments investigated. Branched GDGT I was the most abundant GDGT (Table 2.1). The summed concentrations of branched GDGTs in riverbed sediments ranged between 2 and 5 μg g_{OC}^{-1}, whilst that of crenarchaeol varied between 0.2 and 0.3 μg g_{OC}^{-1} (Table 2.1). Since the branched GDGTs were much more abundant than crenarchaeol (about one order of magnitude), the resulting BIT values were high (0.91–0.95) close to the terrestrial theoretical end member value of BIT of 1 (Hopmans et al., 2004).

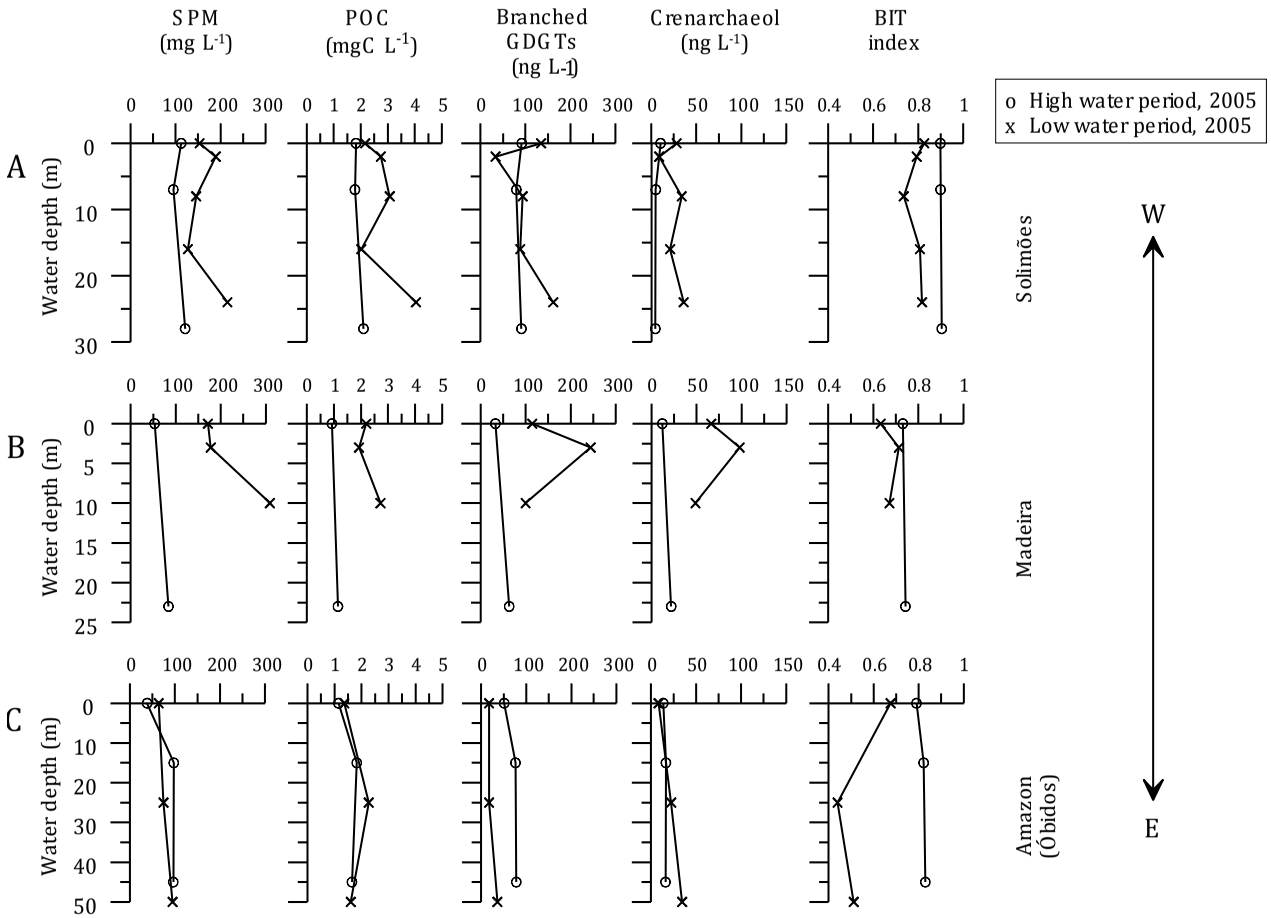

Fig. 2.3 Water depth profiles of SPM (mg L^{-1}), POC concentration ($mg_C L^{-1}$), sum of branched GDGT concentration (ng L^{-1}), crenarchaeol concentration (ng L^{-1}), and BIT index at (A) Manacapuru (Solimões River), (B) Foz Madeira (Madeira River), and (C) Óbidos (Amazon River).

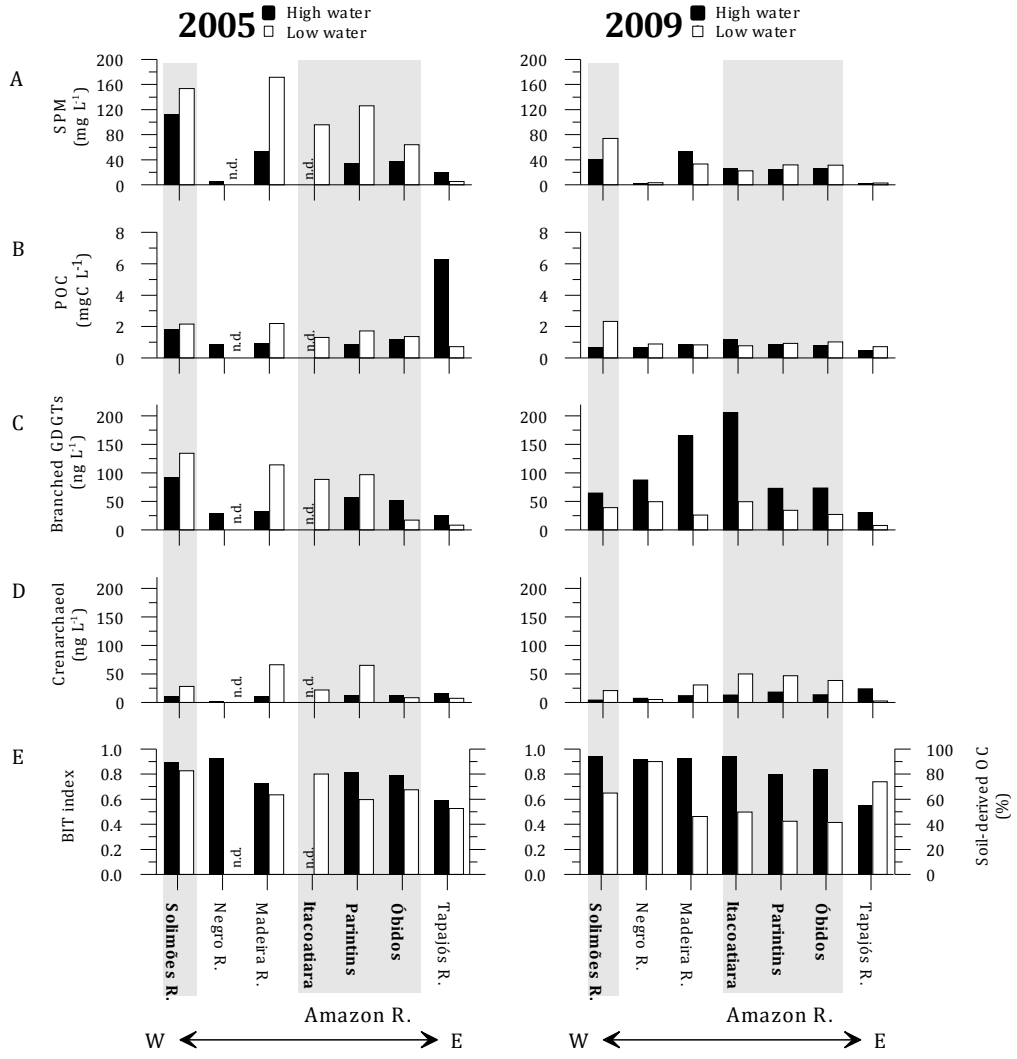

Fig. 2.4 Concentration in near surface water SPM during high and low water stands (black and white bars, respectively) along a W–E transect of stations in the Solimões-Amazon River (in grey areas) and its tributaries: (A) SPM (mg L^{-1}), (B) POC (mg_C L^{-1}), (C) summed branched GDGTs (ng L^{-1}), (D) crenarchaeol (ng L^{-1}), and (E) the BIT index and calculated soil OC percentages. n.d. denotes "not determined".

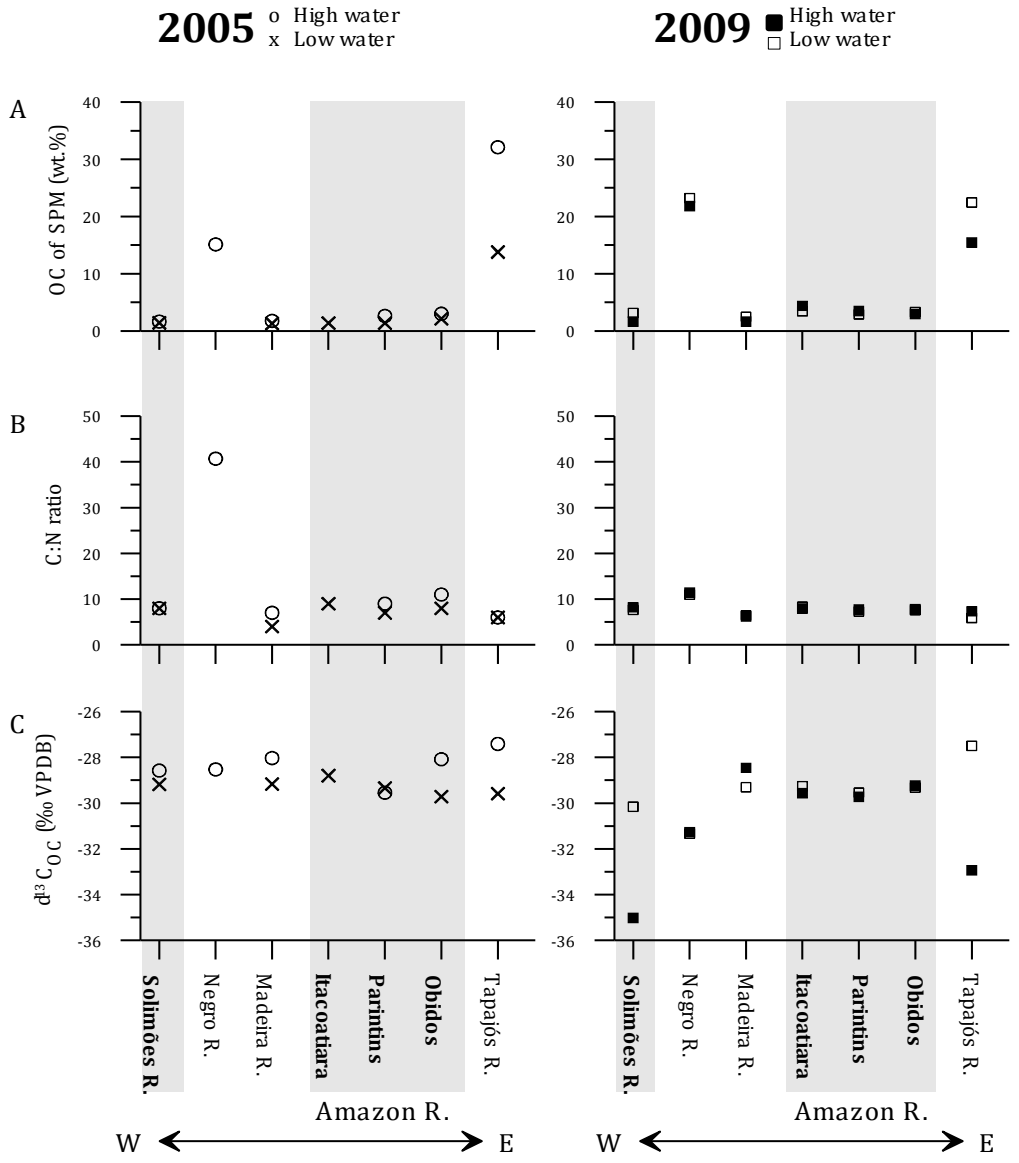

Fig. 2.5 Downriver trends in (A) OC (wt.%), (B) C:N ratio and (C)$\delta^{13}C_{OC}$ (‰ VPDB) of near surface water SPM during high and low water periods along a W–E transect of stations in the Solimões-Amazon River (in grey areas) and its tributaries.

2.4. DISCUSSION

2.4.1. Origin of riverine OM based on bulk geochemical parameters

The C:N ratio and $\delta^{13}C_{OC}$ were used as indicator for the origin of the OM of river SPM and the riverbed sediments. Boundaries for these parameters for major OM sources are illustrated in Fig. 2.6 based on previous studies in the Amazon basin. In the Amazonian forests where most of trees use the Calvin-Benson cycle of carbon fixation (i.e. socalled C_3 plants), $\delta^{13}C_{OC}$ of C_3 plants varies between -27‰ and -35‰ (Hedges et al., 1986a; Martinelli et al., 1994, 2003) and the C:N ratio between 13 and 330 (Hedges et al., 1986a; Martinelli et al., 2003). The $\delta^{13}C_{OC}$ of the surface soil layer under C_3 plant vegetation ranged from -15‰ to -30‰ (Volkoff and Cerri, 1987) with a C:N ratio of 9–28 (Hedges et al., 1986a; Martinelli et al., 2003). On the other hand, the $\delta^{13}C_{OC}$ of C_4 plants (e.g., *Echnochloa polystachya*) was enriched (-9‰ to -16‰) with a C/N ratio of 14–48 (Martinelli et al., 2003; Zocatelli, 2010). Soils under grass (C_4 plant) vegetation were found to have $\delta^{13}C$ values between -12‰ and -16‰ (Hedges et al., 1986a; Martinelli et al., 2003) and C:N ratio of 18–85 (Martinelli et al., 2003). Phytoplankton and periphyton in the Amazon River system are typically depleted in ^{13}C ($\delta^{13}C_{OC}$ -28‰ to -34‰, Araújo-Lima et al., 1986) similar to C_3 land plants ($\delta^{13}C_{OC}$ -27‰ to -35‰, Hedges et al., 1986a; Martinelli et al., 1994, 2003). Although information on the C:N ratio of phytoplankton in the Amazon River system is lacking, the values for the C:N ratio are expected to be close to the range of C:N ratio for freshwater phytoplankton reported in other freshwater systems (4–10, LaZerte, 1983; Lee and Furhman, 1987; Meyers, 1994).

The C:N ratio of SPM samples and riverbed sediments from the white water (Solimões and Amazon) and clear water (Tapajós) rivers was typically <12 and $\delta^{13}C_{OC}$ values were <-27‰ (Fig. 2.6). The typical range of C:N values for world's riverine POM is 10–12 (Meybeck, 1982; Hedges et al., 1986a). Hence, the average C:N ratio of the white and clear water rivers (8 ± 1.5 (mean ± standard deviation (1σ), n = 39) is slightly lower than that of world's riverine POM and the Amazon soil OM. This could be related to the presence of microbial biomass in the river water, which typically has a low C:N ratio, or clay minerals, which can contribute inorganic N lowering C:N ratio (Devol and Hedges, 2001). The SPM and riverbed sediment from the Negro River (black water) collected during the high water period in 2005 differed from the white and clear water rivers as it had a higher C:N ratio (>16; Table 2.1). This suggests that its OM predominantly consists of relatively unaltered vascular plant detritus (Hedges et al., 1986a). Although C_4 aquatic herbaceous macrophytes, such as Paspalum repens and *E. polystachya*, are important for the carbon dynamics in the Amazonian floodplains (e.g., Silva et al., 2009), Hedges et al. (1986a) suggested that only 3% of fine POC in the Solimões-Amazon River mainstem appeared to originate from C_4 plants. This is in good agreement with our $\delta^{13}C$ data, indicating an insignificant input of C_4 grass in riverine SPM. Mostly low C:N ratios and depleted $\delta^{13}C$ values (Fig. 2.6) are indicative of phytoplankton origin, suggesting that aquatic production might be an additional important source to the POC pool of the

Solimões-Amazon River mainstem. Based on fatty acid and stable isotope ($\delta^{13}C_{OC}$ and $\delta^{15}N$) analyses, a recent study (Mortillaro et al., 2011) indeed indicated that cyanobacteria and C_3 aquatic plants were important OM sources in the aquatic system in the lower Amazon basin, particularly during the low water season. Taken together, riverine SPM in the low- er Amazon basin is possibly a mixture of C_3 plant-derived soil OM and aquatic-derived OM.

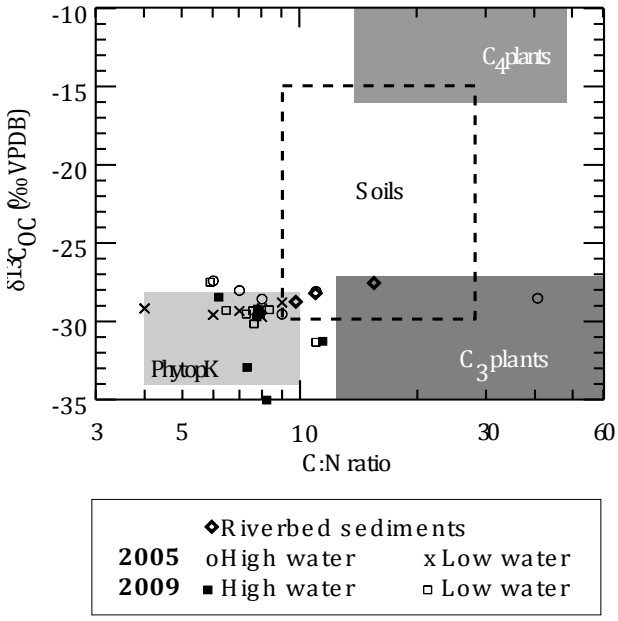

Fig. 2.6 Scatter plot of $\delta^{13}C_{OC}$ (‰ VPDB) vs. the C:N ratio of near surface SPM and riverbed sediments. The boundaries of major OM sources are defined according to Araújo-Lima et al. (1986), Hedges et al. (1986a), Volkoff and Cerri (1987), Martinelli et al. (1994, 2003), Meyers (1994), and Zocatelli (2010). PhytopK indicates phytoplankton.

2.4.2 Sources of branched GDGTs

Branched GDGTs and crenarchaeol were found in all river SPM and riverbed sediments at varying concentrations (Figs. 2.3 and 2.4). The occurrence of branched GDGTs and crenarchaeol has been also reported in SPM of European rivers such as Rhine, Meuse, Niers, and Berkel in the Netherlands (Herfort et al., 2006) as well as Têt and Rhône in France (Kim et al., 2007). The identification of branched GDGTs in the lower Amazon River and its tributaries is consistent with their presence in the Andes and lowland Amazon soils (Bendle et al., 2010; Huguet et al., 2010), and fits the hypothesis that erosion of soil and transport by rivers is an important mechanism for the delivery of branched GDGTs to coastal marine sediments (Hopmans et al., 2004).

To examine the sources of river-transported branched GDGTs, we compared the distribution pattern of the river SPM and the riverbed sediments in the lower Amazon basin with those of the Andes and lowland Amazon soils (Bendle et al., 2010; Huguet et al., 2010; Appendix 2) by performing principal component analysis (PCA) using the fractional abundances (f) of crenarchaeol and branched GDGTs. The PCA biplot of the sample scores and the GDGT loadings (Fig. 2.7A) shows that the first two PCA components (PC1 and PC2) explain 98% of the variation of the GDGT data. On the PC1 axis (ex-

plaining 62% of the variance), GDGT I (r = 0.6) is negatively correlated with GDGT II and GDGT III (r = 0.6 and r = 0.5, respectively). On the PC2 axis (explaining 37% of the variance), crenarchaeol (r = 0.7) is negatively correlated with all branched GDGTs (r = 0.4).

In the PCA, four of the five soils from the high Andes, i.e. from the upper montane forests and páramo vegetation belts (>2500 m in altitude; Appendix 2), cluster as a distinct group in the lower left quadrant of the biplot and are clearly separated from the lowland Amazon soils (<500 m in altitude; Appendix 2) in the lower right quadrant of the biplot. The same pattern is observed in a ternary diagram plotting f(crenarchaeol), f(GDGT I), and f(GDGT II+III) (Fig. 2.7B). The distribution of branched GDGTs in the high Andes soils is different from that in the lowland Amazon soils with roughly equal amounts of branched GDGT I and II (Appendix 2). Changes in the branched GDGT distribution in soils have been attributed to the adaptation of branched-GDGT producing bacteria to temperature for maintaining an acceptable degree of the membrane fluidity at different temperatures by varying the relative abundance of additional methyl groups (Weijers et al., 2007c). Higher proportions of GDGT II (containing five instead of four methyl groups in comparison with GDGT I) in the high Andes soils is thus consistent with the higher altitude and, consequently, lower mean annual air temperature (Bendle et al., 2010). On the other hand, all lowland Amazon soils cluster together (Fig. 2.7) despite their widespread geographical origin (Appendix 2) since variation in the mean annual air temperature is small in the lowland Amazon basin (New et al., 2002).

In general, the river SPM clusters well apart from the high Andes soils (Fig. 2.7), indicating that the branched GDGTs in river SPM did not predominantly originate from the high Andes soils as suggested previously (Bendle et al., 2010). The distribution of branched GDGTs in the riverbed sediments did also not reflect that of the high Andes soils, excluding a predominant Andean source (Fig. 2.7). The branched GDGT distribution in the riverine SPM and the riverbed sediment from the black water (Negro) river, which does not receive any Andes material (Fig. 2.1), resembled the branched GDGT distribution in the lowland Amazon soils to the largest extent. Its score on PC1 (Fig. 2.7B) reflects that the branched GDGT distribution is identical to that of the lowland Amazon soils, suggesting that the branched GDGTs in SPM are predominantly derived from the erosion of lowland soils. The other SPM samples exhibit lower scores on PC1 (Fig. 2.7A), which could mean that soils in the Andes play a more prominent role as a source for the branched GDGTs in SPM. However, the score on PC1 of the clear water SPM from the Tapajós river, which does not contain any Andes material like the black water river (Fig. 2.1), is approximately the same as the average score of all white water SPM samples and clearly distinct from that of the black water SPM and the lowland Amazon soils (Fig. 2.7A). This suggests that, in addition to the soil erosion, aquatic production may contribute at least partly to the riverine branched GDGT pool, and modifies the distribution of branched GDGTs in such a way that it contains higher fractional abundances of GDGT II. Other studies have already suggested that aquatic production of branched GDGTs is probable in river and lacustrine environments (Sinninghe Damsté et al., 2009;

Tierney and Russell, 2009; Bechtel et al., 2010; Blaga et al., 2010; Tierney et al., 2010; Tyler et al., 2010; Zink et al., 2010; Loomis et al., 2011; Sun et al., 2011; Zhu et al., 2011). Our results can thus be explained by a mixed soil-derived/aquatic source for the riverine branched GDGTs. However, it is still difficult to quantitatively disentangle the source (soil vs. aquatic) of branched GDGTs in the Solimões-Amazon mainstem, in part due to the deficiency of soil data from the lower montane forest vegetation belt (500–2500 m in altitude) in the Andes. An extended soil data set with a broader spatial coverage of the Andes as well as the lowland Amazon basin could certainly assist in solving this issue. In addition to the distributional and concentration (which are also lacking for the Amazon River system) data from soils, studies on intact polar lipids, i.e. lipids that still contain a polar head group and presumably are derived from living cells, may shed more light on the source identification of the branched GDGTs along the Solimões-Amazon mainstem.

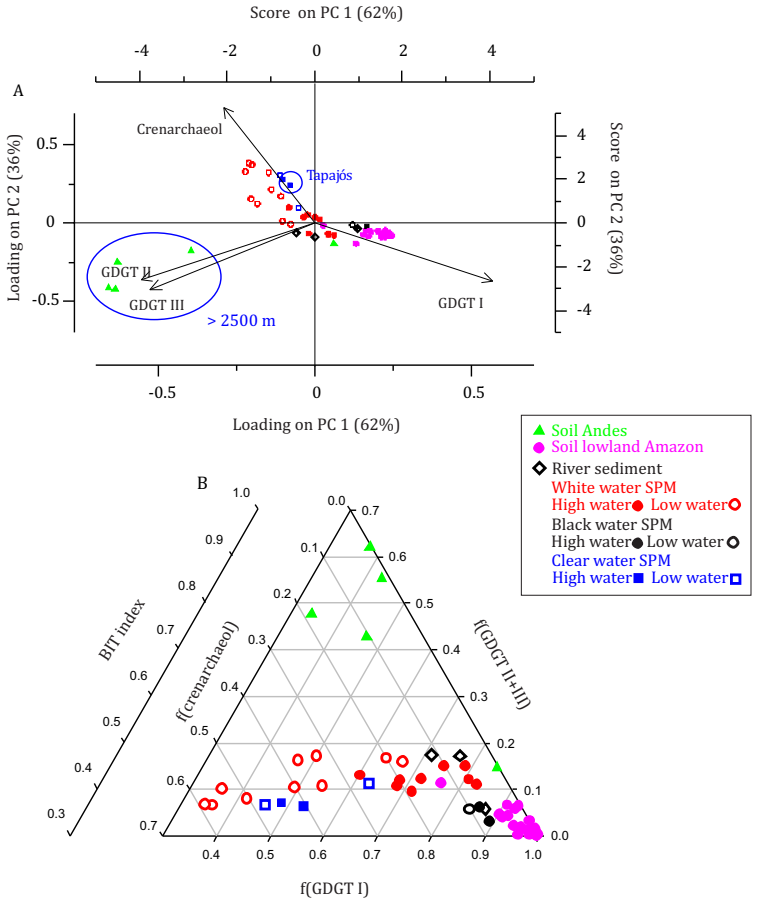

Fig. 2.7 (A) PCA biplot of the sample scores and the GDGT loadings. Symbols and black lines represent scores of the samples and loadings of the response variables (crenarchaeol and three major branched GDGTs), respectively. (B) Ternary diagram showing the relationships of the fractional abundances (f) of crenarchaeol and three major branched GDGTs. Since GDGT II and GDGT III have similar loadings on the PCA biplot, they were combined for construction of the ternary diagram. Note that f(crenarchaeol) is the same as (1-BIT). A BIT axis has therefore been added to the diagram.

2.4.3 Riverine crenarchaeol production: consequences for the BIT index

Due to the presence of crenarchaeol in the Andes and lowland Amazon soils, albeit in relatively low amounts (Appendix 1), the average BIT value (0.97) is slightly lower than the hypothetical terrestrial end-member value of 1(Hopmans et al., 2004). The BIT indices of the riverine SPM revealed large variation in time and space in Amazonian rivers, but is generally (i.e. 0.4–0.9) lower than the BIT values of the Andes and lowland Amazon soils (Figs. 2.4 and 2.7B). This is rather different from the high mountainous, small Têt River (France), where BIT values hardly varied and fitted the average BIT value of soils in the catchment area (Kim et al., 2007, 2010). This indicated that the source of GDGTs to the Têt River remained the same and supported the use of the BIT index as a proxy for soil OM input to aquatic environments (e.g., Hopmans et al., 2004). However, a quite different situation is apparent for the Amazon River system.

The BIT values of the white water river SPM were substantially lower during the low water periods than during the high water periods, whereas this trend was not apparent for the clear and black water SPM (Fig. 2.7B). On the PCA biplot (Fig. 2.7A), most of the white water river SPM collected during the low water periods plots in the upper left quadrant due to its high score on PC2, reflecting the relative abundance of crenarchaeol, clearly distinct from the position of the other SPM samples. Hence, it seems likely that besides minor amount of soil-derived crenarchaeol, aquatic-derived crenarchaeol produced in the river itself and/ or potentially in the floodplain lakes ('várzea') that are part of the Amazone River system is the main source of crenarchaeol for the white water river SPM, predominantly during the low water season. Indeed, there are reports on the presence and growth of Thaumarchaeota, the source organisms for crenarchaeol (e.g., Pitcher et al., 2011a), in rivers (Crump and Baross, 2000; Herfort et al., 2009). Interestingly, the clear water SPM collected during the high water periods also plots in the upper left quadrant of the PCA biplot. This suggests that the aquatic production of crenarchaeol may preferentially occur in settings where both suspended and dissolved material is depleted with a high phytoplankton production. This would be consistent with the physiology of Thaumarchaeota since, as nitrifiers, they would depend on the production of fresh OM from which, upon mineralisation, ammonium is formed.

The BIT index in SPM is significantly correlated with the crenarchaeol concentration normalized on OC ($r^2 = 0.43$, $p < 0.0001$) but, to a much lesser degree, with the branched GDGT normalized on OC ($r^2 = 0.13$, $p = 0.013$). This indicates that variations in the BIT index predominantly reflect variation in riverine crenarchaeol production rather than the soil-derived branched GDGT flux. Similar conclusions have been made in the studies of the Congo Fan (Weijers et al., 2009b) and of African lakes (Tierney et al., 2010). Only when the crenarchaeol concentration is representative for aquatic production in the river, the BIT index reflects the contribution of soil-derived POC in SPM. Taken together with the potential aquatic production of branched GDGTs, care should be taken to use the BIT index as a proxy of river-transported soil OC input. The average BIT value of the riverbed sediments (0.92) is higher than that of SPM (0.73), but somewhat

lower than that of the soils (0.97) considered in this study. This suggests that the riverbed sediments also contain aquatic-derived crenarchaeol in addition to soil-derived crenarchaeol but that during settling of riverine SPM alteration of the GDGT profile takes place, probably by selective degradation of crenarchaeol relative to the branched GDGTs (cf. Huguet et al., 2008). However, this hypothesis should be further explored based on more extensive characterization of GDGT distributions in soils as well as riverbank and riverbed sediments, considering that we investigated only three riverbed sediments in this study.

2.4.4 Variation in discharge of SPM, POC, and GDGTs

The bulk (SPM and POC) and molecular (branched GDGTs and crenarchaeol) concentrations in river water were highly variable among the investigated rivers and seasons (Fig. 2.4). To estimate the impact of tributary input to the Solimões-Amazon River mainstem, we calculated instantaneous fluxes of SPM, POC, crenarchaeol, and branched GDGTs obtained by multiplying the measured water discharge by the corresponding concentration at each station (Fig. 2.8). In general, the SPM and POC discharge was positively related to the water discharge, i.e. high SPM flux at high water discharge and vice versa. Exceptions were at Parintins on the Solimões-Amazon River mainstem and at the station of the Madeira River in 2005, where SPM and POC fluxes were higher during the low water discharge than during the high water discharge. The comparison between the branched GDGT discharge and the water discharge also showed a positive relationship comparable to those observed for SPM and POC. However, the crenarchaeol discharge was lower when the river water discharge was higher, which differs from a previous study carried out in a small, mountainous catchment area, the Têt River system, France (Kim et al., 2007). The Solimões River was always the principal contributor for branched GDGTs to the Amazon River (Fig. 2.8). The inflow of branched GDGTs from the Solimões River and the outflow at Óbidos were virtually the same, except for the 2009 high water season (Fig. 2.8). This suggests that generally the loss of branched GDGTs between the mouth of the Solimões River and the Amazon River at Óbidos by degradation and sedimentation processes was compensated by the supply from the Negro and Madeira Rivers and in-situ production. During the high water period in 2009, however, the branched GDGT discharge at Óbidos was twice as high as at the mouth of the Solimões River. The branched GDGT discharge of the Negro and Madeira Rivers increased two and seven fold, respectively, from the low to high water season but the branched GDGT discharge from these tributaries still accounted only for 34% of the total branched GDGT discharge at Óbidos. Given that the branched GDGT discharge from the Solimões River was 48% of that at Óbidos, there is still a missing source for branched GDGTs, probably in-situ production in rivers and/or floodplain lakes.

In contrast, the crenarchaeol discharge at Óbidos was always substantially higher than that at the mouth of Solimões River, which delivered only 20–50% of the total crenarchaeol pool at Óbidos depending on the season Madeira Rivers could only account for

10–20% of the crenarchaeol discharge at Óbidos. One viable explanation for this missing source is the aquatic production in the river system (see above) and/or the floodplain lakes, contributing 40–60% of the crenarchaeol discharge at Óbidos.

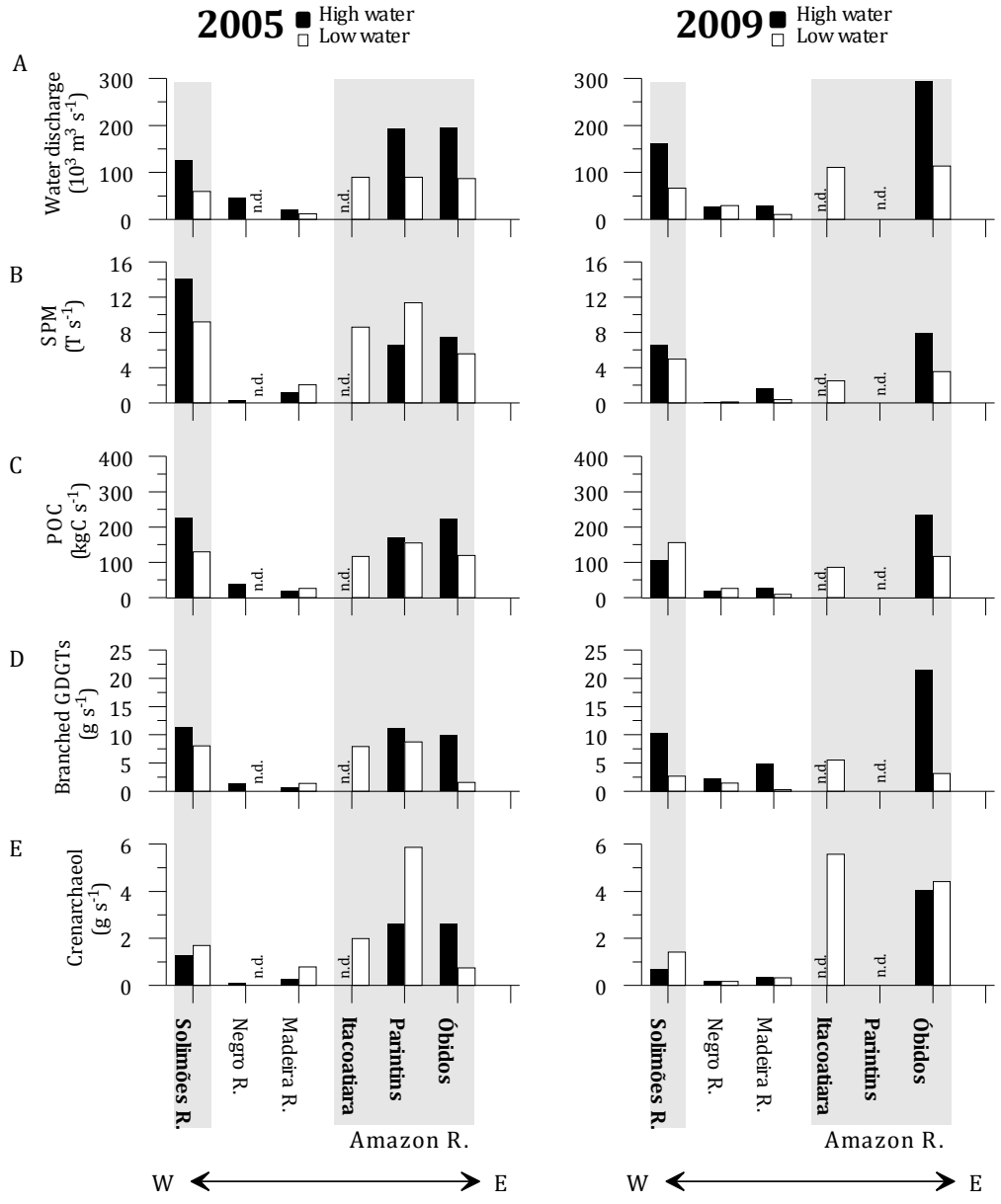

Fig. 2.8 Comparisons of (A) river water discharge (m^3 s^{-1}) with (B) SPM discharge (T s^{-1}, C) POC discharge (kgC s^{-1}), D) branched GDGT discharge (g s^{-1}), and E) crenarchaeol discharge (g s^{-1}) during high and low water periods (black and white bars, respectively) along a W–E transect of stations in the Solimões-Amazon River (in grey areas) and its tributaries. To compare the discharge data between 2005 and 2009, we considered only near surface data in 2005. n.d. denotes "not determined".

2.4.5. Estimation of riverine aquatic and soil OC transport

The BIT values of the Solimões-Amazon River mainstem at Óbidos were variable through time with the mean BIT values of 0.73 for 2005 and 0.63 for 2009. However, the range of the flux-weighted BIT values was smaller with higher values of 0.75 for 2005 and 0.70 for 2009. A binary mixing model based on the BIT index assumes a linear mixing line between the end-members of the BIT index. However, when two end-members with vastly different mass ratio of components are mixed, the resulting mixing line is not linear. Nevertheless, a study in the NW Mediterranean (Kim et al., 2010c) showed that the mass-normalized mixing model resulted in almost identical estimates of soil OC contribution to TOC compared to those based on the BIT values. Hence, we applied a simple binary mixing model based on the flux-weighted BIT values at Óbidos to estimate the portions of aquatic and soil OC to POC as follows:

$$f_{so} = [\text{BITsample}] - [\text{BIT}_{aq}] / [\text{BIT}_{so}] - [\text{BIT}_{aq}] \times 100\% \quad (2)$$

where f_{so} is the soil OC fraction and BITsample is the BIT value of the sample investigated. Thereby, we assumed that soil (BIT_{so}) and aquatic (BIT_{aq}) OC end-members are 0.97 (the average value of soils, Appendix 2) and 0.0, respectively. The estimated contributions of soil OC were 78% for 2005 and 73% for 2009, slightly lower than the previous estimation based on the lignin content in the downstream part of the Amazon River (Hedges et al., 1986a). The annual mean POC discharge at Óbidos is 5.8 ± 0.3 Tg C yr^{-1} (Moreira-Turcq et al., 2003). When conservatively calculating the portion of the soil OC discharge to POC discharge at Óbidos based on the flux-weighted BIT-derived estimations (73–78%), this would account for 4.2–4.5 Tg C yr^{-1}. Given that in-situ production of branched GDGTs in the aquatic system is possible, this estimation should be considered as high-end values of soil OC percentages to POC. Nonetheless, this supports previous studies based on the lignin composition of POC, which suggested that most of POC in the Amazon River was of a refractory nature and the product of extensive soil degradation (Ertel et al., 1986; Hedges et al., 1986a). Intensive degradation processes occurring in soils are the principal factors responsible for the relatively refractory material that composes most of the OC flux in the Amazon River (Hedges et al., 1986a). Ittekkot (1988) estimated that only 15% of the POC in high-sediment loaded rivers was generally potentially labile. Our results suggest that the labile component may be larger (i.e. up to 30%) in the Amazon River, if we assume that aquatic-derived OC is more labile than soil-derived OC. If we consider the aquatic production of branched GDGTs and thus a higher BIT index end-member value for the aquatic source, the relative contribution of soil OC to POC might be even lower. Based on the carbon isotope composition (^{13}C and ^{14}C), it has been reported that bulk OC fractions transported by the Amazonian rivers to the ocean range from tens to thousands of years in age (Hedges et al., 1986b; Raymond and Bauer, 2001; Mayorga et al., 2005). Our study implies that the age of riverine OC can vary significantly depending on the contribution of more labile aquatic-derived OC from

the river to the ocean. This aspect should be addressed in future studies.

2.5 CONCLUSIONS

Bulk geochemical data obtained from the downstream part of the Solimões-Amazon River indicated that in-situ (autochthonous) produced OC in the aquatic system is probably an important source to the riverine POC pool. The BIT values were lower in SPM than in soils, especially during the low water periods, indicating in-situ production of crenarchaeol in the aquatic system. Hence, consistent with bulk geochemical data, the distribution patterns of GDGTs reflected a combined effect of soil- and aquatic-derived OC input to the Solimões-Amazon River mainstem. A variable input of aquatic-produced crenarchaeol to the Solimões-Amazon River mainstem, coupled with hydrological changes, was largely responsible for both seasonal and interannual variations in GDGT composition and for variations in soil OC discharge estimates based on the BIT index. Clearly, future work should also focus on intact polar lipids that presumably are derived from living cells, which will help further to provide more direct evidence of in-situ production of crenarchaeol and branched GDGTs in aquatic settings (river itself and/or floodplain lakes). It should also be noted that care should be taken to use the BIT index for the calculation of the proportion of soil OC to POC, given that the aquatic end-member might be affected by aquatic production of branched GDGTs in the Amazon River system and that the BIT index reflects variations in crenarchaeol concentration rather than soil GDGT flux. Our 'snapshot' SPM samples probably did not capture the complete annual variations in GDGT composition and discharge. Therefore, a continuous sampling approach following the full hydrological cycle is required to constrain the effect of hydrological variations on aquatic production of GDGTs and its influence on the use of BIT index as a proxy to trace soil OC input to the ocean.

Acknowledgements

We would like to thank J. Ossebaar at NIOZ for analytical support. The research leading to these results has received funding from the European Research Council under the European Union's Seventh Framework Programme (FP7/2007-2013)/ERC grant agreement n [226600]. This study was also partly supported by a Marie Curie European Reintegration Grants (ERG) grant to JHK. This work is a part of the CARBAMA project, funded by the ANR, French national agency for research and was conducted within an international cooperation agreement between the CNPq (National Council for Scientific and Technological Development- Brazil) and the IRD (Institute for Research and Development- France). We thank G. Cochonneau and ORG-HYBAM for the water level and river discharge data. We also thank G. Boaventura from the University of Brasilia and P. Seyler from IRD for administrative facilities.

Appendix A. supplementary data

Supplementary data associated with this article can be found, in the online version, at http://dx.doi.org/10.1016/ j.gca.2012.05.014.

Appendix 1

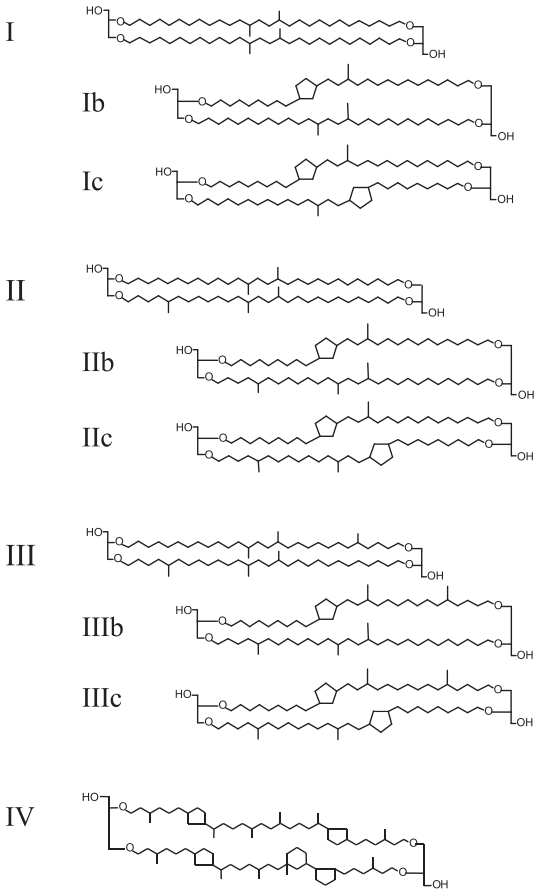

Sample	Location	Sampling depth (cm)	Longitude	Latitude	Altitude (m)	f(I)	f(Ib)	f(Ic)	f(II)	f(IIb)	f(IIc)	f(III)	f(IIIb)	f(IIIc)	f(IV)
Ecuador 3	Ecuador	0-26	-78.6	-0.5	4000	0.34	0.04	0.03	0.45	0.03	0.01	0.10	0.00	0.00	0.00
Ecuador 19	Ecuador	0-50	-78.7	-2.1	2780	0.25	0.10	0.05	0.26	0.10	0.02	0.08	0.01	-	0.13
Colombia 11	Colombia	0-30	-77.4	1.1	3100	0.44	0.04	0.01	0.36	0.01	0.00	0.04	0.00	0.00	0.10
Colombia 12	Colombia	0-30	-77.3	1.3	2350	0.80	0.03	0.01	0.13	0.00	-	0.01	0.01	0.00	0.00
Colombia 14	Colombia	0-30	-77.4	1.2	3810	0.40	0.03	0.01	0.40	0.03	0.00	0.12	0.00	0.00	0.01
Peru 1	Peru	2-15	-73.3	-3.8	150	0.93	0.01	0.04	0.00	0.00	-	-	-	-	0.02
Peru 4	Peru	0-14	-73.3	-3.9	130	0.89	0.02	0.02	0.04	0.00	0.00	0.02	0.00	0.00	0.00
Peru 6	Peru	0-8	-76.1	-5.8	180	0.92	0.01	0.01	0.02	0.00	0.00	0.00	0.00	0.00	0.03
Peru 10	Peru	0-10	-69.1	-12.7	260	0.90	0.01	0.00	0.04	0.00	0.00	0.00	0.00	0.00	0.03
Peru 12	Peru	0-5	-73.3	-4.0	130	0.79	0.11	0.02	0.05	0.01	-	0.00	0.00	-	0.01
Peru 13	Peru	0-15	-73.4	-3.9	130	0.89	0.03	0.05	0.00	-	-	0.00	-	-	0.03
Peru 14	Peru	0-8	-73.4	-3.9	130	0.92	0.02	0.01	0.01	0.00	0.00	0.00	0.00	0.00	0.02
Ecuador 6	Ecuador	0-18	-76.9	-0.5	250	0.84	0.05	0.01	0.06	0.00	-	0.00	0.00	-	0.02
Ecuador 7	Ecuador	0-8	-76.8	-0.3	260	0.85	0.03	0.01	0.04	0.01	0.00	0.00	-	0.00	0.05
Colombia 7	Colombia	0-20	-72.2	-0.5	200	0.93	0.01	0.01	0.02	0.00	0.00	0.00	-	-	0.02
Colombia 9	Colombia	0-10	-72.2	-1.5	290	0.96	0.01	0.01	0.01	0.00	0.00	0.00	0.00	0.00	0.01
Colombia 10	Colombia	0-5	-72.2	-0.5	340	0.97	0.01	0.01	0.00	0.00	-	-	-	-	0.00
Brazil 12	Brazil	0-5	-55.0	-2.6	60	0.53	0.20	0.06	0.07	0.03	0.00	0.01	0.00	0.00	0.09
Brazil 13	Brazil	0-7	-54.9	-2.9	75	0.88	0.02	0.01	0.04	0.00	-	0.00	-	-	0.05
I AEa	Brazil		-62.7	-1.7	100	0.95	0.04	-	0.01	-	-		-	-	-
II A12a	Brazil		-62.7	-1.7	100	0.91	0.01	0.07	0.02	-	-	-	-	-	-
II Bhsa	Brazil		-62.7	-1.7	100	0.83	0.06	0.08	0.03	-	-	-	-	-	-
II Bha	Brazil		-62.7	-1.7	100	0.87	0.03	0.07	0.03	-	-	-	-	-	0.00
III A12a	Brazil		-62.7	-1.7	100	0.86	0.06	0.07	0.01	-	-	-	-	-	-

aThe data are from Huguet et al. (2010).

-: below quantification limits.

Picture by Elena Marin Cadaval

Chapter 3

Disentangling the origins of branched tetraether lipids and crenarchaeol in the lower Amazon River: Implications for GDGT-based proxies

Claudia Zell, Jung-Hyun Kim, Patricia Moreira-Turcq, Gwenaël Abril, Ellen C. Hopmans, Marie-Paule Bonnet, Rodrigo Lima Sobrinho, and Jaap S. Sinninghe Damsté

Published in Limnol. Oceanogr., 58(1), 2013, 343–353
doi:10.4319/lo.2013.58.1.0343

Abstract

To trace the origin of branched glycerol dialkyl glycerol tetraethers (brGDGTs), their distribution in soils and suspended particulate matter (SPM) of Amazonian rivers and floodplain lakes (várzeas) was studied. Differences in distribution between river SPM and surrounding (lowland) soils suggests an additional brGDGT source to eroded soils in the lowland drainage basin. Erosion of high Andean soils (above 2500 m in altitude) has no major influence because its brGDGT distribution differs substantially from that in river SPM. Furthermore, SPM in the Tapajós River, a tributary that does not derive from the Andes, has a virtually identical brGDGT distribution to that of the Amazon main stem. The higher proportion of phospholipid-derived brGDGTs in river SPM compared to soils indicates that in situ production in the Amazon is an additional source for riverine brGDGTs. This affects the methylation and cyclization index of brGDGTs (MBT-CBT), resulting in slightly lower MBT-CBT–derived temperatures and slightly higher CBT-derived pH values, i.e., between the pH of the basin soil and that of the river. Since the difference between MBT-CBT–derived temperatures of Amazon River SPM and the surrounding soils is relatively small (2 °C) compared to other aquatic systems (for lakes a difference of , 10 °C has been observed), it might still be possible to trace large climate changes in the Amazon basin with the MBT-CBT using river fan cores. However, variations in in situ production of brGDGTs in the Amazon River over time and space have to be evaluated in the future. Likewise, in situ production may affect the application of the MBT-CBT paleothermometer in other river systems. Our results also show that crenarchaeol is primarily produced in the Amazon River and that its varying production influences the branched vs. isoprenoid tetraether (BIT) index. This indicates that the BIT index not only represents the input of soil organic carbon to the river but is also affected by in situ production of brGDGTs and crenarchaeol.

3.1 INTRODUCTION

Branched glycerol dialkyl glycerol tetraethers (brGDGTs; Fig. 3.1) are bacterial membrane lipids that occur in soil worldwide (Weijers et al. 2006b, 2007b). Nine different brGDGTs, with and without rings, have been identified (Structures I–IIIc; Fig. 3.1). Some acidobacterial species produce specific brGDGTs but probably do not represent the only biological source (Weijers et al. 2009a; Sinninghe Damsté et al. 2011). The distribution of brGDGTs, expressed by their degree of methylation (methylation index of branched tetraether; MBT) and cyclization (cyclization index of branched tetraethers; CBT), in soil correlates with mean annual air temperature (MAAT) and soil pH (Weijers et al. 2007c). It was assumed that brGDGTs are mainly produced on land and are washed into small streams and rivers by erosion and further transported to the ocean (Hopmans et al. 2004). Subsequent research has indicated that they can be used to trace soil organic carbon (OC) from land to

the ocean (Weijers et al. 2006b; Huguet et al. 2007; Walsh et al. 2008), with the help of the branched vs. isoprenoid tetraethers (BIT) index. The isoprenoid glycerol dialkyl glycerol tetraether (GDGT) used in this index is crenarchaeol, which is the characteristic membrane lipid of Thaumarchaeota (Sinninghe Damsté et al. 2002), formerly known as Crenarchaeota. Crenarchaeol is found in various terrestrial and aquatic systems (Hopmans et al. 2004; Herfort et al. 2006; Weijers et al. 2006b) but typically dominates over brGDGTs in marine systems.

An initial study of Congo Fan deep-sea sediments (Weijers et al. 2007a) revealed that the MBT-CBT paleothermometer showed an integrated temperature signal of the whole drainage basin of the river system. However, various factors could potentially bias the MBT-CBT palaeothermometry. For example, when applying the MBT-CBT paleothermometer to a sedimentary record from the Amazon Fan, Bendle et al. (2010) postulated that an increased brGDGT contribution from the cold Andes region was responsible for the decrease in Holocene reconstructed temperatures. Therefore, it is essential to fully understand the provenance of brGDGTs brought by the river to the sea. In addition, it has recently been suggested that in situ production of brGDGTs in lakes or river channels may influence their distribution (Tierney et al. 2010, 2012; Zhu et al. 2011). This is thought to explain the substantially lower MBT-CBT reconstructed temperatures in lake surface sediments in comparison with the actual temperatures (Tierney et al. 2010). If brGDGTs are produced in situ in freshwater (including river) systems, it may also affect the application of the MBT-CBT palaeothermometer using deep-sea fan sediments and the application of the BIT index as an indicator of riverinetransported soil OC. In order to detect in situ production of brGDGTs the analysis of intact polar lipids (IPLs; Sturt et al. 2004) is deemed to be a useful tool. In living cells brGDGTs are present as IPLs, which are relatively quickly transformed after cell death into ''fossil'' core lipids (CLs) (White et al. 1979; Harvey et al. 1986), which are typically used in the MBT-CBT proxy. Branched and isoprenoid IPL GDGTs have recently been reported in biomass and the environment (Schouten et al. 2008c; Liu et al. 2010; Peterse et al. 2011a).

In this study, we investigated the sources of brGDGTs and crenarchaeol in the lower Amazon basin using both CL and IPL-derived GDGTs. We compared the concentrations and distributions of brGDGTs and crenarchaeol in soils as well as in suspended particulate matter (SPM) of rivers and floodplain lakes (várzeas) along the lower Amazon River (Fig. 3.2) and used IPL-derived brGDGTs and crenarchaeol in soils as well as river and várzeas SPM as an indicator of in situ production. This is the first study that thoroughly tests whether the brGDGT distribution in a river system reflects an integrated signal of the average MAAT and the soil pH of its drainage basin.

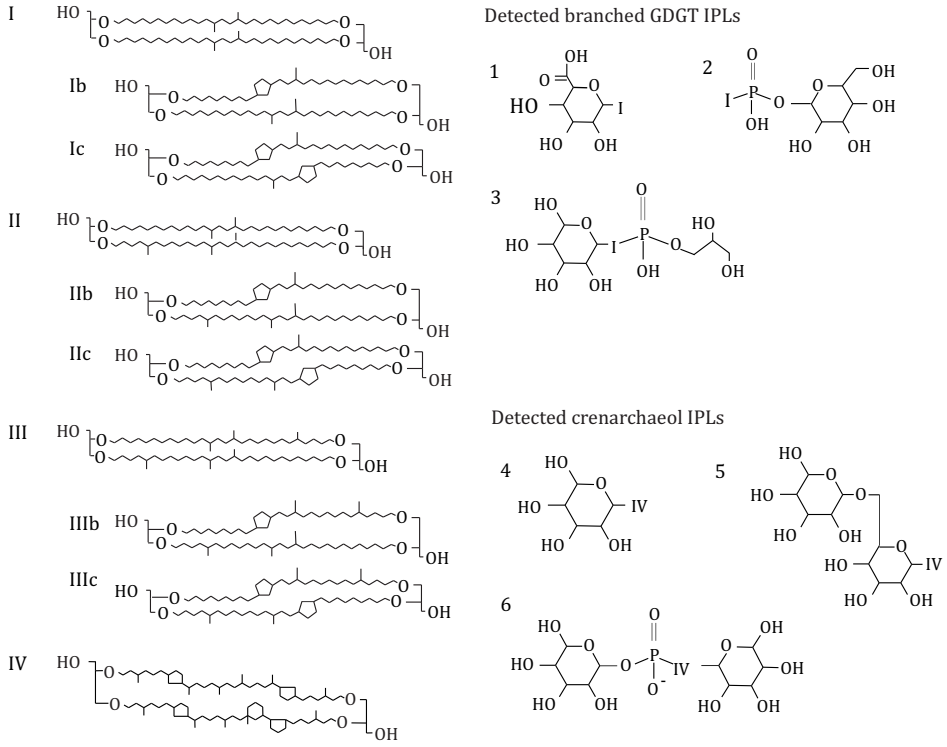

Fig. 3.1 Chemical structures of the brGDGT (I–IIIc) CLs, crenarchaeol CL (IV), and IPLs (1–7). The brGDGT IPLs (with brGDGT I as CL) are glyconyl-brGDGT I (1), phosphohexose-brGDGT I (2), and hexose-phosphoglycerol-brGDGT I (3). The crenarchaeol IPLs are crenarchaeol-monohexose (4), crenarchaeol-dihexose (5), and crearchaeol-hexose-phosphohexose (6).

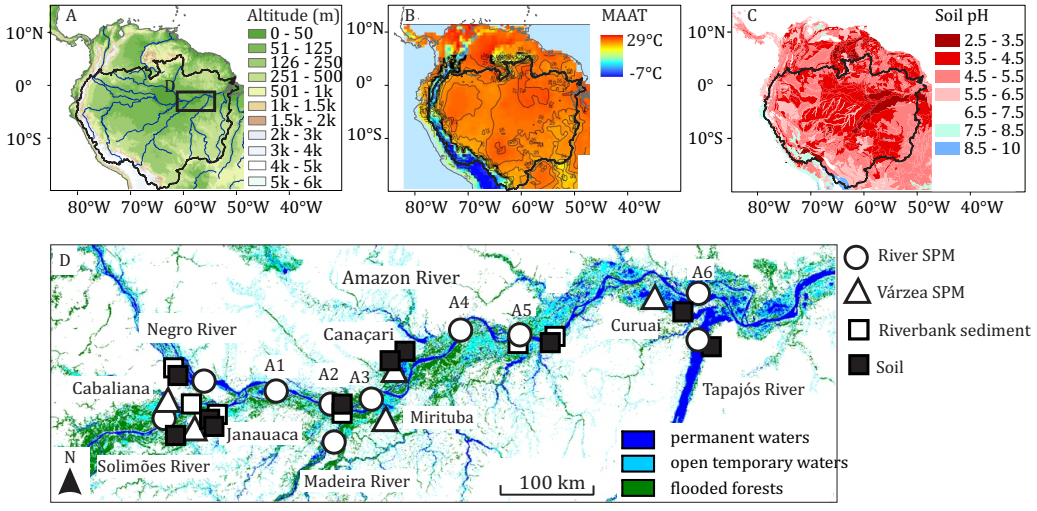

Fig. 3.2 (A) Map of the Amazon basin showing the Amazon watershed (black line) and the sampling area (black square). (B) MAAT in the Amazon basin (redrawn from New et al. 2002). (C) pH of 20 cm top soil in the Amazon basin (redrawn from Batjes 2005). (D) Detailed map (adapted from Martinez and Le Toan 2007) showing sample locations for soil, riverbank sediment, and SPM from rivers and várzeas.

3.2 STUDY AREA

The Amazon River is the largest drainage system in the world in terms of discharge and catchment area. With an area of 6,915,000 km^2, it covers about 40% of the South American continent (Goulding et al. 2003). Due to the equatorial position, temperature in the drainage basin is relatively constant year-round with a MAAT of, 26 °C (Fig. 3.2B; New et al. 2002). Only in the Andes colder temperatures are found, due to their high elevation (Fig. 3.2A). The majority of soils in the lower Amazon basin are Ferralsol and Acrisol, which are both iron-rich, nutrientpoor, and acidic soil types (Quesada et al. 2009). In the Andes, patches of alkaline soils can be found (Fig. 3.2C). The physicochemical characteristics of the Amazonian rivers reflect the soil properties of their drainage region (Konhauser et al. 1994). The biggest tributaries of the Amazon River, i.e., Solimões and Madeira, originate in the Andes. Their headwaters drain the Andean Cordillera with complex and varied lithologies, whereas their lowland portions drain fluvio-lacustrine deposits (Gaillardet et al. 1997). Solimões and Madeira are defined as ''white water'' rivers (Sioli 1984). According to mineralogical and isotopic evidence, the Andes is the source of 82% of the suspended particulate load exported by the Amazon River (Gibbs 1967b). Due to their rich mineral content, the Andean tributaries are important to the productivity of the downstream reaches. Tributaries originating in the lowlands are typically particle and nutrient poor. In this study two tributaries originating in the lowlands were investigated: the Negro River that drains the Guyana shield and Tapajós that drains the Brazilian shield. The Negro River is a ''black water'' river (Sioli 1984). Dissolved humic substances are leaching from podzol found along the Negro River and lead to the typical black color of the water. The Tapajós River is a ''clear water'' river and characterized by a high phytoplankton production (Junk 1997). Its drainage basin has mainly Ferrasol and Acrisol (Quesada et al. 2009). An important part of the Amazon ecosystem are the várzeas, which along the Amazon–Solimões corridor cover an area of, 95,000 km^2 (Melack and Hess 2010). Compared to the main stem, production and decomposition of organic matter is high in várzeas (Junk 1997). These ecosystems are strongly influenced by river dynamics and exchange waters with the main stem almost continuously year-round. During the rainy season (rising and high water) várzeas are flooded by several water types, of which the Amazon main stem has the biggest influence. During the dry season (low water and falling of water) the várzeas export water toward the main stem (Bonnet et al. 2008). Five várzeas were investigated in this study. Two of them are located upstream of Manaus (Cabaliana and Janauaca) and three downstream of Manaus (Mirituba, Canaçari, and Curuai) (the lakes are listed from west to east). These várzeas are predominantly influenced by white waters of the Solimões, Amazon, and Madeira Rivers. The two várzeas located upstream of Manaus are also influenced by their local drainage basin with

water types closer to black or clear waters. Cabaliana is mainly influenced by water from the Solimões River but also by the Manacapuru River (a black water river). Janauaca is comparatively small and influenced by the Solimões River and its local drainage basin. Canaçari is an intermediate as it is also strongly influenced by the Urubu River (a black water river). Marituba is flooded by a mixture of the Amazon River and the Madeira River. Curuai is the biggest várzea explored within this study and is influenced by the Amazon River (Bonnet et al. 2008).While the várzeas upstream of Manaus re surrounded by flooded forests that are relatively untouched by humans, the downstream várzeas are surrounded by cleared areas that are used for larger-scale farming (Fig. 3.2D).

3.3 METHODS

3.3.1 Sample collection

During the CBM6 cruise in October 2009 (low-water season), soil and SPM samples were collected along the Amazon River main stem, four tributaries (Solimões, Negro, Madeira, and Tapajós), and five várzeas (Cabaliana, Janauaca, Marituba, Canaçari, and Curuai) (Fig. 3.2D). Sampling sites are located in a gradient of decreasing flooded forest area and increasing open lake area from Cabaliana on the Solimões River to Santarem at the mouth of the Tapajós River. To determine SPM concentrations, 0.5 liters of water was filtered onto ashed (450 °C, overnight) and pre-weighed glass-fiber filters (Whatman GF-F, 0.7 mm, 47 mm diameter). For the GDGT analysis, about 5 liters of water were separately filtered onto ashed glass-fiber filters (Whatman GF-F, 0.7 mm, 142 mm diameter). The filters and soils were kept frozen onboard and brought to the Royal Netherlands Institute for Sea Research (NIOZ) laboratory, where they were freeze-dried.

3.3.2 Environmental parameters and bulk geochemical analysis

Water pH and temperature were measured in situ with a multiparameter probe (YSIH 6600V2). To determine the pH of the soil samples, a mixture of soil and distilled water 1:3.5 (v:v) was prepared. This mixture was left to settle for 20 min. The pH was measured with a Wissenschaftlich- Technische Werkstätten pH 315i/SET and probe pH Electrode SenTix 41 (pH 0–14, temperature 0–80 °C, stored in 3 mol L^{-1} KCl) at NIOZ. The total organic carbon contents of the freeze-dried and decarbonated soils were analyzed in duplicate with a Thermo-Interscience Flash EA1112 Series Elemental at NIOZ with a precision of 0.2 mg C g^{-1}. Particulate organic carbon content of river and várzea SPM samples was analyzed using an elemental analyzer C–H–N Fisions NA-2000 at Institute for Research and Development–France with a precision of 60.1mg C g^{-1}.

3.3.3 Lipid extraction and fractionation

The freeze-dried samples were extracted with a modified Bligh and Dyer technique (Pitcher et al. 2009). The Bligh and Dyer extracts were fractioned into CLs and IPLs. The separation was carried out on activated silica with n-hexane:ethyl acetate 1:1 (v:v) and methanol as an eluent for CLs for IPLs, respectively (Oba et al. 2006; Pitcher et al. 2009). To each fraction, 0.1 mg C_{46} GDGT internal standard was added (Huguet et al. 2006). Two-thirds of the IPL fraction was hydrolyzed to cleave off polar head groups as described by Weijers et al. (2011). The dichloromethane (DCM) fractions were collected, reduced by rotary evaporation, and dried over a Na_2SO_4 column. CL fractions were separated into polar (DCM:methanol 1:1, v:v) and polar (DCM) fractions over an activated Al_2O_3 column.

3.3.4 Analysis of CL and IPL-derived GDGTs

Before analysis, samples were dissolved in hexane:isopropanol 99: (v:v) and filtered using 0.45 mm polytetrafluoroethylene filters. The CL GDGTs were analyzed using highperformance liquid chromatography–atmospheric pressure positive ion chemical ionization–mass spectrometry in selected ion monitoring mode according to Schouten et al. (2007). Quantification of the GDGT compounds was achieved by comparison of peak areas with that of the C_{46} GDGT internal standard, correcting for the different response factors (Huguet et al. 2006). It was reported by Pitcher et al. (2009) that during the separation of CL and IPL fractions a small amount of the CL GDGTs is carried over into the IPL fraction. Therefore, it was necessary to implement a correction to calculate the amounts of CL GDGTs and IPL-derived GDGTs more accurately as described by Weijers et al. (2011).

3.3.5 Calculation of GDGT-based proxies

The BIT index was calculated according to Hopmans et al. (2004):

$$\text{BIT index} = ([I] + [II] + [III]) / ([I] + [II] + [III] + [V])$$

The roman numerals refer to the GDGTs indicated in Fig. 3.1. I, II, and III are brGDGTs, and IV is the isoprenoid GDGT, crenarchaeol. Additional parameters, degree of cyclization (DC; Sinninghe Damsté et al. 2009), MBT, and CBT (Weijers et al. 2007c), were calculated as follows:

$$DC = ([Ib]+ [IIb])/ ([I] + [Ib] + [II] + [IIb])$$

$$CBT = -\log (([Ib]+ [IIb]) / ([I] + [II]))$$

$$MBT = ([I] + [Ib] + [Ic]) / ([I] + [Ib] + [Ic] + [II] + [IIb] + [IIc] + [III] + [IIIb] + [IIIc])$$

For the calculation of pH and temperature, the regional soil calibration for the Amazon basin was used (Bendle et al. 2010):

$$CBT = 4.2313 - 0.5782 \times pH \quad (r^2 \sim 0.75)$$

$$MBT = 0.1874 + 0.0829 \times CBT + 0.0250 \times MAAT \quad (r^2 \sim 0.91)$$

The analytical errors were determined by duplicate measurements of 11 samples. For the concentration of the sum of brGDGTs, the analytical error was 15% for the CL GDGTs and 13% for the IPL-derived GDGTs. Crenarchaeol concentrations had a standard deviation of 13% (CL) and 16% (IPL-derived). The average standard deviations for the MBT were 0.002 (CL) and 0.019 (IPLderived), for the DC 0.002 (CL) and 0.01 (IPL-derived), for the CBT 0.024 (CL) and 0.063 (IPL-derived), and for the BIT 0.004 (CL) and 0.022 (IPL-derived).

3.3.6 IPL GDGT analysis

Two soil samples (No. 1 and 8), five river SPM samples (Negro, Solimões, Tapajós, Amazon No. 4 and 6), and one várzea SPM sample (Curuai) were analyzed. A selective reaction monitoring (SRM) method according to Peterse et al. (2011a) was used to detect brGDGT IPLs. Crenarchaeol IPLs were detected by high-performance liquid chromatography–electrospray ionization–tandem mass spectrometry using an SRM method (Pitcher et al. 2011b).

3.4 RESULTS

3.4.1 GDGTs in soils and riverbank sediments

All soils (n = 12), which were never inundated by river water (i.e., collected in so-called terra firme), contained crenarchaeol and brGDGTs. The terra firme soils contained, on average, 0.3 - 0.2 mg g_{OC}^{-1} of CL crenarchaeol (average ± standard deviation [1s]). The percentage of IPL-derived crenarchaeol of the total amount of crenarchaeol was, on average, 51% ± 24%. Summed CL brGDGT concentrations were, on average, 21 ± 15 mg g_{OC}^{-1} with 8% ± 6% IPL-derived brGDGTs of the total amount of brGDGTs (Fig. 3.3). The average abundance of brGDGT I was 93% of all CL brGDGTs and 85% of all IPL-derived brGDGTs (Fig. 3.4A,B). The brGDGTs I, Ib, Ic, II, IIb, and III were detected in all soils, whereas brGDGT IIIb and IIIc were not detected and brGDGT IIc was found in only a few soils. The BIT index of the soils was 0.98 ± 0.01 in the CL fractions and 0.8 ± 0.2 in IPL-derived fractions (Fig. 3.3E). Interestingly, the soils showed a difference in CBT and MBT between the CL and IPL-derived fractions. Both CBT and MBT were slightly higher in the CL fractions (Fig. 3.5).

For the riverbank sediments (n = 5), which were underwater during the high-

water seasons, the concentra tions of CL crenarchaeol were, on average, 2.9 ± 2.9 mg g_{OC}^{-1}, an order of magnitude higher than that of the soils. IPL-derived crenarchaeol represented 32% ± 22% of total crenarchaeol. The concentrations of brGDGTs were similar to those of the soils with 45 ± 35 mg g_{OC}^{-1} of which 9% ± 4% were IPL-derived. The average abundance of brGDGT I was lower than in soil, with 77% of all CL brGDGTs and 69% of all IPL-derived brGDGTs. The riverbank sediments showed similar average BIT value as the soils: 0.95 ± 0.03 for the CL GDGTs and 0.80 ± 0.12 for the IPL-derived GDGTs (Fig. 3.3E).

3.4.2 GDGTs in river and várzea SPM

The river SPM (n = 6) contained the highest CL crenarchaeol concentrations with 31 ± 23 mg g_{OC}^{-1}, which is about 100 times higher than in soils (Fig. 3.3C; note the logarithmic scale). The concentration of CL brGDGTs was similar to that of the soils (42 ± 19 mg g_{OC}^{-1}; Fig. 3.3A). The IPL percentages for crenarchaeol and brGDGTs were 23% ± 12% and 11% ± 7%, respectively. The most abundant brGDGT was brGDGT I, but its abundance was lower than in the soils (74% and 69% of all CL and of all IPL-derived brGDGTs, respectively) (Fig. 3.4C,D). The average BIT was 0.60 ± 0.16 in the CL fraction and 0.4 ± 0.2 in the IPL fraction (Fig. 3.3E). In SPM collected from the várzeas (n = 21), the crenarchaeol concentration was higher than that of the soils but 10 times lower compared to that of the river SPM (5 ± 6 mg g_{OC}^{-1}; Fig. 3.3C). The CL brGDGT concentration was similar to that of the soils (22 ± 17 mg g_{OC}^{-1}). The IPL percentage for crenarchaeol and brGDGTs were 25% ± 9% and 13% ± 7%, respectively. As in the soils and river SPM, the most abundant brGDGT was brGDGT I and its average abundance was 78% and 76% of all CL and of all IPL-derived brGDGTs, respectively. Average BIT values were 0.83± 0.13 for the CL fractions and 0.68 ± 0.24 for the IPL-derived fractions.

3.4.3 IPL GDGTs

To obtain more direct evidence for the presence of IPL GDGTs, a selection of samples (n = 8) was analyzed for a number of known IPL GDGTs. The analyzed samples were two soil samples, five river SPM samples (Negro, Solimões, Tapajós, Amazon No. 5 and 6), and one várzea SPM sample (Curuai). Phosphohexose brGDGT I (2; numerals refer to Fig. 3.1) and hexosephosphoglycerol brGDGT I (3) were found in all samples. Glyconyl-brGDGT I (1) was only found in the Amazon 5 SPM sample, probably due to its low concentration. For crenarchaeol-derived IPLs the monohexose (4) and dihexose (5) were found in all samples except in the Tapajo´s River SPM, which lacked the dihexose. Hexose-phosphohexose (6) was detected in all samples except in the Solimões, Amazon 6, and Tapajós SPM.

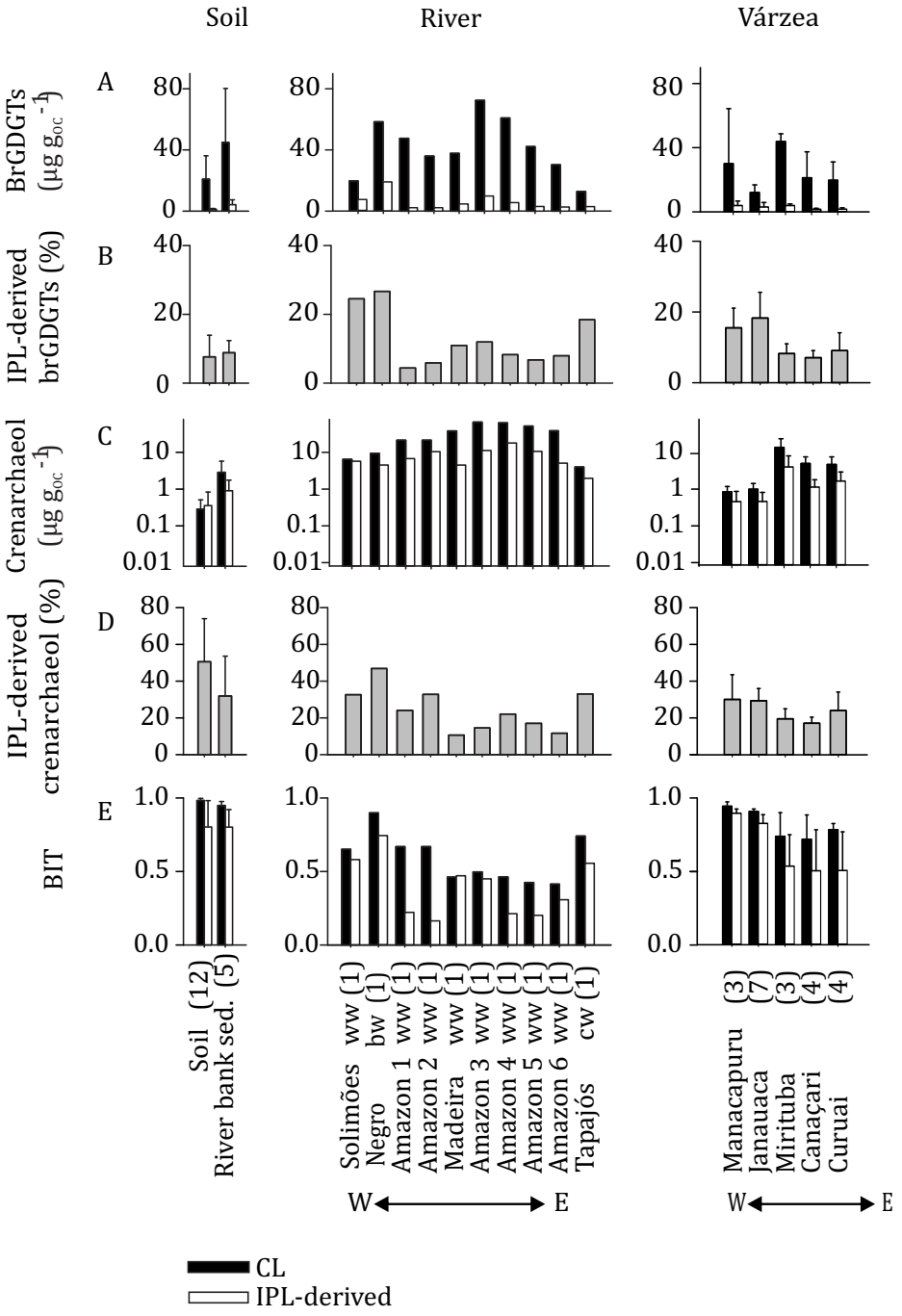

Fig. 3.3 (A) Concentrations of brGDGTs (mg g_{OC}^{-1}), (B) percentage of IPL-derived brGDGTs, (C) concentrations of crenarchaeol (mg g_{OC}^{-1}), (D) percentage of IPL-derived crenarchaeol, and (E) BIT index for soil and SPM from rivers and va´rzeas. The number in brackets relates to the number of samples that were analyzed. Vertical bars indicate the standard deviation (1s). ww 5 white water, bw 5 black water, cw 5 clear water.

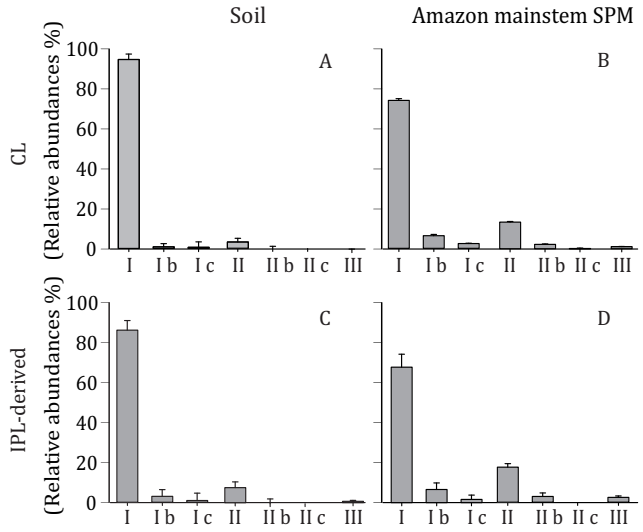

Fig. 3.4 Average CL and IPL-derived brGDGT distributions in 12 soil samples and in six Amazon River SPM samples. Error bars indicate the standard deviation between the measured samples.

3.5 DISCUSSION

3.5.1 Sources of brGDGTs in river SPM

It has been assumed that the majority of brGDGTs are produced in soil and upon erosion of the soil are transported by rivers to the ocean (Hopmans et al. 2004; Weijers et al. 2006b). Our data allow us to critically evaluate this hypothesis. Unlike crenarchaeol (see below), there is no significant difference in OC-normalized concentration of brGDGTSs between soils and SPM in the lower Amazon basin (Fig. 3.3A). This could be in line with the general idea that the majority of brGDGTs in rivers are indeed derived from soil. However, our data also show that the distribution of CL brGDGTs in the lowland soils is different from that in Amazon River SPM, i.e., the abundance of brGDGT I is substantially lower (Fig. 3.4). In addition, the DC of brGDGTs is higher in the Amazon River SPM, whereas theMBT is lower compared to the soils (Fig. 3.6). The higher DC and lower MBT result in higher CBT-derived pH and lower MBT-CBT–derived MAAT values, respectively (Fig. 3.5B,D). Because the Andes air temperature is lower and the soil pH is higher (Fig. 3.2B,C), an influence of brGDGTs originating from Andes soils may explain this, as suggested previously by Bendle et al. (2010). They argued that a major part of the brGDGTs transported by the Amazon River to the Amazon deep-sea fan during the Holocene originated from Andean soils. This was based on the observation that MBT-CBT–reconstructed MAATs for the Holocene were lower than expected for the Amazon lowland.

To evaluate this possibility, a detailed comparison of the brGDGT distribution of river SPM and of soils from the lowland (< 500 m in altitude) and from the high Andes (above 2500 m in altitude) is made (Fig. 3.6). The additional soil data used for this comparison are from Kim et al. (2012). All soils from the lowland showed almost identical distributions even though they are from diverse areas, and they plot

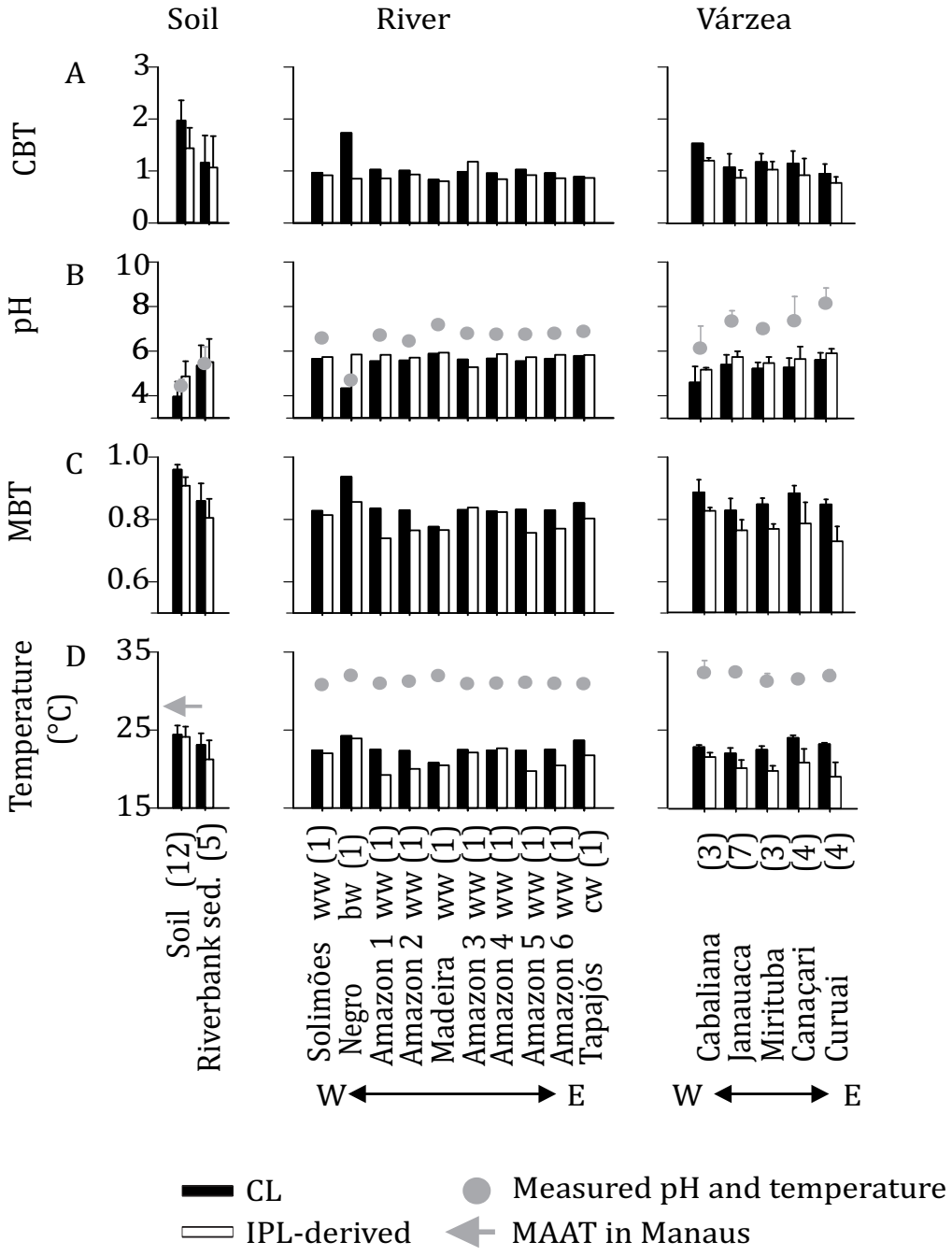

Fig. 3.5 (A) CBT, (B) CBT-derived pH and measured pH, (C) MBT, (D) MBT-CBT–derived MAAT, measured water temperatures, and the MAAT at Manaus. The numbers in brackets relate to the number of samples that were analyzed. Vertical bars indicate the standard deviation (1s). sed. 5 sediment, ww 5 white water, bw 5 black water, cw 5 clear water.

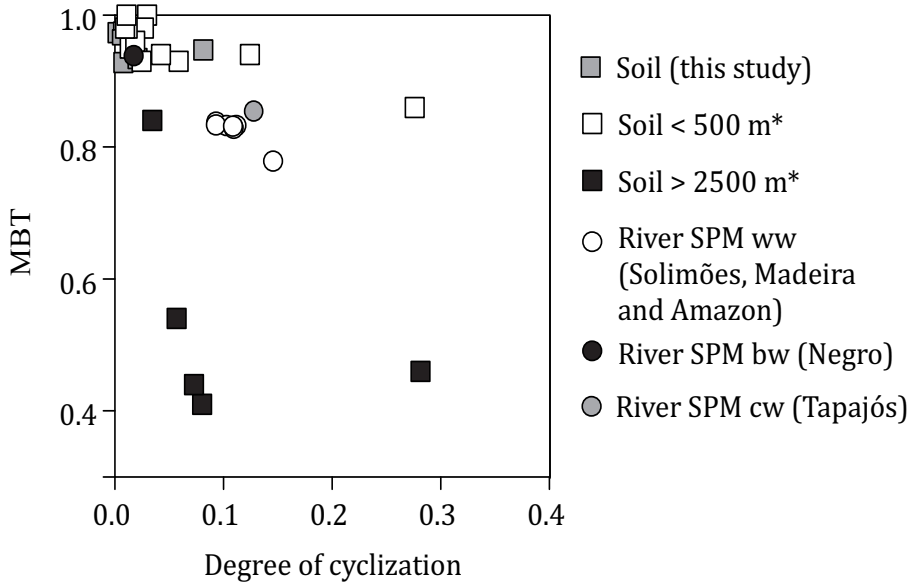

Fig. 3.6 Cross plot to compare the DC and MBT of CL brGDGTs from lowland and high Andean soil with those of CL brGDGTs in river SPM. The data of soil samples marked with an sterisk are from Kim et al. (2012). ww 5 white water; bw 5 black water; cw 5 clear water.

in the upper left corner of the diagram. Soils from the high Andes (above 2500 m in altitude) possess higher DC and lower MBT values (Fig. 3.6). The difference between the distributions in river SPM and Andes soils is larger than between river SPM and the surrounding soils (Fig. 3.6). This does not exclude an Andean influence on the brGDGT distribution in the lower Amazon SPM, but it reveals that the majority of brGDGTs do not originate from the high Andes. As two of the studied tributaries (Negro and Tapajós) do not originate from the Andes, but from the lowlands, their brGDGT distributions provide interesting hints on the source of brGDGTs in the riverine SPM. The brGDGT distribution in the Negro River resembles that of lowland soils (Fig. 3.7), suggesting that brGDGTs in the black water river are predominantly derived from erosion of the surrounding soil. This is in line with the observation that the Negro River SPM has the highest BIT of all studied rivers, approaching that of soil (Fig. 3.3). The brGDGT distribution in the Tapajós River is similar to what is found in the Amazon main stem and the tributaries from the Andes (Madeira and Solimões) (Fig. 3.6). This indicates that the mismatch in GDGT distributions of the SPM in the white and clear water rivers and the lowland soils is unlikely to be explained by a contribution from Andes soils; there must be an additional source of brGDGTs. This suggests that brGDGTs can also be produced in situ in the river water and that this aquatic production is responsible for changing the distribution of brGDGTs derived from lowland soil.

To further investigate potential in situ production of brGDGTs in the river, IPL-derived brGDGTs were also analyzed and revealed the presence of both phospho- and glycolipids. Although the significance of IPLs as unequivocal markers for living cells is a topic of recent discussion (Lipp and Hinrichs 2009; Schouten et al. 2010; Lengger et al. 2012a), it is known that glycosidic ether lipids degrade more slowly than phospholipids (Harvey et al. 1986; Lengger et al. 2012a). The presence of brGDGTs containing a phospho head group thus suggests that at least part of the PL brGDGTs in riverine SPM was freshly produced. In addition, the percentage of IPL-derived brGDGTs in soils is lower than in river SPM (Fig. 3.3B). Since brGDGT IPLs are produced by active microorganisms and are subsequently transformed into CLs, this seems to be in contradiction with a predominant soil origin of brGDGTs in riverine SPM. The higher percentage of brGDGT IPLs in SPM than in soil thus supports the idea of in situ production in the river water. Furthermore, IPL-derived brGDGT distributions clearly differ between soil and riverine SPM (Fig. 3.7B), with lower MBT and higher DC for riverine SPM, although the differences are slightly less apparent as for CLs (cf. Fig. 3.7A,B).

3.5.2 Sources of brGDGTs in várzea SPM

Both CL and IPLderived brGDGT distributions of the várzea SPM samples have similar MBT and DC values compared to the river SPM samples (Fig. 3.7C,D). This suggests that brGDGTs in the SPM of the várzeas are of similar origin as those in riverine SPM (i.e., mixed origin from lowland soils and in situ production). There are some várzea SPM samples (i.e., from the sites Cabaliana 2, Janauaca 2, and Canaçari 1) that plot in the upper left corner of Fig. 3.7C close to the Negro River SPM and the lowland soils. These várzeas are indeed influenced by input of black water from their local watershed. The black water influence is reflected by the pH, which is lower compared to the other várzea sampling sites. Duncan and Fernandes (2010) defined the pH of black water as 4.5 6 0.9. Hence, only Cabaliana 2, which is substantially influenced by the Manacapuru River, falls into this range. The other two sites have slightly higher pH values but still lower than the other sites in the várzeas. As brGDGTs containing a phospho head group were also detected in várzea SPM, it seems likely that the várzeas are also contributing to the in situ aquatic production of brGDGTs. However, from our data it is difficult to estimate the relative importance of brGDGTs produced in the várzeas compared to the Amazon main stem. More data from different seasons and data from várzea channels connecting the rivers and the várzeas including flux data are required for this.

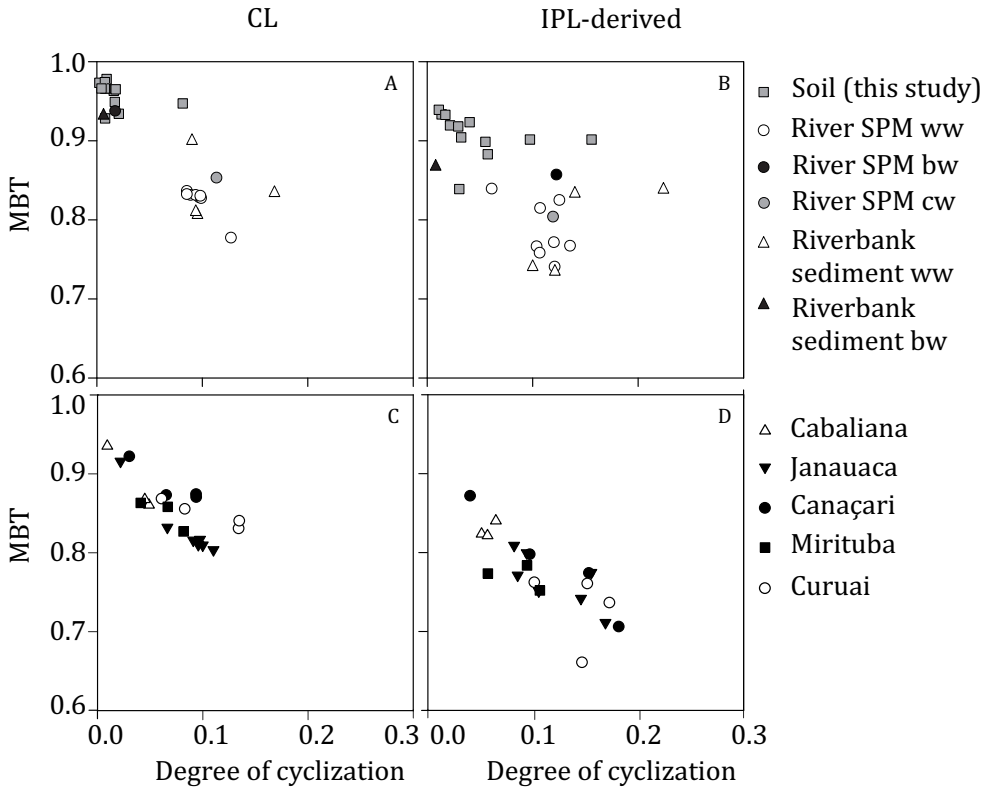

Fig. 3.7 Cross plot to compare the distributions of CL and IPL-derived brGDGTs in the different sample types, using the degree of cyclization (DC) and MBT. (A, B) soil, river SPM, and riverbank samples, and (C, D) va´rzea samples. ww 5 white water; bw 5 black water; cw 5 clear water.

3.5.3 Implications for the MBT-CBT paleothermometer

The CBT-derived pH calculated for our set of lowland soils using the regional Amazon soil calibration by Bendle et al. (2010) and the measured soil pH are comparable (Fig. 3.5B). However, the MBT-CBT–derived temperatures (Fig. 3.5D) were 3 °C colder than the MAAT in Manaus (MAAT measured over the last 100 yr by the World Meteorological Organization at Sta. 823310 is 26.7 °C). The 3 °C difference is within the 5uC calibration error range of the MBT-CBT proxy using the global soil calibration (Weijers et al. 2007c), but since a regional soil calibration was used a lower calibration error would be expected. A possible reason for this cold bias could be that the soils used to make the regional calibration were predominantly taken in the western part of the Amazon basin (Bendle et al. 2010), which might not have been representative of the whole basin.

In the SPM of the Amazon main stem the CBT-derived pH was on average 5.6, which is between the pH of the soils (on average 4.4) and the pH of the river water (on average 6.7). This supports the idea that brGDGTs in the river are a mixture of brGDGTs produced in soil and in the river. The MBT-CBT–derived temperature using SPM was 5 °C lower than the MAAT at Manaus and 2 °C lower than the MBTCBT– re-

constructed temperature of the surrounding lowland soils (24 ± 3°C) (Fig. 3.5D). In comparison with several recent studies on lakes, the difference between MBT-CBT–derived temperatures of Amazon River SPM and the surrounding soils is relatively small. For example, in Sand Pond (U.S.A.), a small kettle pond, the reconstructed MAAT using CL brGDGTs in surface sediments was 12 °C lower than that using soils from the watershed of the lake (Tierney et al. 2012). For Lake Towuti in Indonesia this difference was 10 °C (Tierney and Russell 2009). It was suggested that this difference is due to the fact that the brGDGT-producing microbes in lakes respond differently than those in soils (Tierney et al. 2010). If we assume that brGDGT-producing microbes in the river behave similarly to those in lakes, our results suggest that in the Amazon River the input of brGDGTs from soils is still substantially higher relative to in situ produced brGDGTs.

Our study shows that the MBT-CBT signal in the Amazon River is not substantially influenced by input of brGDGTs from the Andes, nor is it altered by the input of brGDGTs from floodplain lakes. The majority of brGDGTs in the Amazon River most likely originate from erosion of lowland soils, and to a smaller, but uncertain, extent from in situ produced brGDGTs. Application of the MBT-CBT palaeothermometer using cores from the Amazon River fan to trace long-term climatic changes of the Amazon basin may still be possible, if it is assumed that the distribution of brGDGTs produced in the river is also temperature dependent. However, we will first have to examine if in situ production of brGDGTs in the Amazon River varies over time and space. Another major question to be resolved is to what extent in situ production may influence the application of the MBT-CBT paleothermometer in other river systems.

3.5.4 Crenarchaeol production in rivers and várzeas: Implications for the BIT index

Our results show that river and várzea SPM contain about 100 times higher CL and IPLderived crenarchaeol concentrations (normalized to OC) compared to the surrounding soils (Fig. 3.3C). This indicates that crenarchaeol is mainly, but not exclusively produced in the aquatic system. The presence of phospho-IPLs with crenarchaeol as CLs in the SPM confirms in situ production of crenarchaeol in the aquatic system. The crenarchaeol concentration in the Amazon main stem was almost an order of magnitude higher than in the várzeas, with an average of 42 ± 19 mg g_{OC}^{-1} in the Amazon main stem and 5 ± 4 mg g_{OC}^{-1} in the várzeas (Fig. 3.3C). Therefore, it can be concluded that at the time of sampling (low-water season) a substantial amount of crenarchaeol was produced in the river itself. The percentage of IPL for crenarchaeol is higher in soils with an average of 50 % compared to 20–40 % in the SPM (Fig. 3.3B). This may reflect better preservation of the crenarchaeol IPLs in soils and possibly the difference in the suite of crenarchaeol IPLs produced

in these different settings. Tierney et al. (2012) also reported a higher percentage of IPL-derived isoprenoid GDGTs in soils compared to lake sediments.

As observed for the MBT and CBT (or DC) indices, BIT values differ between the CL and IPL-derived fractions with lower values for the IPL-derived fraction (Fig. 3.3E). Because this difference is found in river SPM as well as in the soil samples, it might be due to a lower degradation rate in crenarchaeol IPLs compared to the brGDGTs. However, in river SPM the difference seems to be larger than in soil, which is most likely due to the relatively higher production of crenarchaeol in the Amazon River. Despite the fact that brGDGTs are also produced in the river (which would increase the BIT), the production of crenarchaeol in the river leads to substantially lower BIT values in the river (between 0.41 and 0.67) compared to the surrounding soil (average 0.98). These values represent the lowest BIT values reported for river systems (Herfort et al. 2006; Kim et al. 2007; Zhu et al. 2011). However, the rivers investigated so far are much smaller than the Amazon, and are therefore likely to be much less influenced by in situ production of crenarchaeol. For example, SPM of the Têt River in France has an average BIT value of 0.8. However, locally it has lower BIT values (down to 0.6), which has also been explained by crenarchaeol production in the river (Kim et al. 2007). Our results indicate that within the river the BIT does not solely represent the input of soil OC, but rather reflects the production of crenarchaeol in the rivers and várzeas. The concentration of brGDGTs is likely to be a better indicator for the input of soil OC to the river; however, as shown before, brGDGTs are also partially produced in the river. Consequently, it is of utmost importance to further constrain the effect of aquatic production of GDGTs in the catchment area and its influence on the BIT index in order to use the BIT as a proxy to trace riverine or soil OC input to the ocean.

Acknowledgments

We thank three anonymous reviewers for their constructive comments. The research leading to these results has received funding from the European Research Council (ERC) under the European Union's Seventh Framework Program (FP7/2007–2013) ERC grant agreement [226600]. We thank J. Ossebaar and S. Crayford at Royal Netherlands Institute for Sea Research (NIOZ) for analytical support. This work was carried out in collaboration with the carbon cycle in the Amazon River (CARBAMA) project, funded by the French national research agency (ANR) and was conducted within an international cooperation agreement between the National Council for Scientific and Technological Development–Brazil (CNPq) and the Institute for Research and Development–France (IRD) (490755/ 2008-9) coordinated by G. Boaventura from the University of Brasilia (Brazil) and P. Seyler from the IRD (France).

Picture by Elena Marin Cadaval

Chapter 4

Impact of seasonal hydrological variation on the distributions of tetraether lipids along the Amazon River in the central Amazon basin: implications for the MBT/CBT paleothermometer and the BIT index

Claudia Zell, Jung-Hyun Kim, Gwenaël Abril, Rodrigo Lima Sobrinho, Denise Dorhout, Patricia Moreira-Turcq, and Jaap S. Sinninghe Damsté

published in Frontiers in Microbiology 16August2013
doi:10.3389/fmicb.2013.00228

Abstract
Suspended particulate matter (SPM) was collected along the Amazon River in the central Amazon basin and in three tributaries during the rising water (RW), high water (HW), falling water (FW) and low water (LW) season. Changes in the concentration and the distribution of branched glycerol dialkyl glycerol tetraethers (brGDGTs), i.e., the methylation index of branched tetraethers (MBT) and the cyclization of brGDGTs (CBT), were seen in the Amazon main stem. The highest concentration of core lipid (CL) brGDGTs normalized to particulate organic carbon (POC) was found during the HW season. During the HW season the MBT and CBT in the Amazon main stem was also most similar to that of lowland Amazon (terra firme) soils, indicating that the highest input of soil-derived brGDGTs occurred due to increased water runoff. During the other seasons the MBT and CBT indicated an increased influence of in situ production of brGDGTs even though soils remained the main source of brGDGTs. Our results reveal that the influence of seasonal variation is relatively small, but can be clearly detected. Crenarchaeol was mostly produced in the river. Its concentration was lower during the HW season compared to that of the other seasons. Hence, our study shows the complexity of processes that influence the GDGT distribution during the transport from land to ocean. It emphasizes the importance of a detailed study of a river basin to interpret the MBT/CBT and BIT records for paleo reconstructions in adjacent marine setting.

4.1 INTRODUCTION

Branched glycerol dialkyl glycerol tetraethers (brGDGTs) (Fig 4.1) are membrane-spanning lipids most likely of anaerobic (Weijers et al., 2006a,b) and heterotrophic (Pancost and Sinninghe Damsté, 2003; Oppermann et al., 2010) bacteria that are ubiquitous in peats (Weijers et al., 2006a; Huguet et al., 2010) and soils (Weijers et al., 2007c; Peterse et al., 2012). A study combining brGDGT analysis with molecular ecological techniques of Swedish peat suggested that some Acidobacterial species may produce brGDGTs (Weijers et al., 2009a), which was recently confirmed by the identification of brGDGT-Ia in two acidobacterial cultures (Sinninghe Damsté et al., 2011). However, Acidobacteria so far have only been shown to produce one brGDGT; other bacterial sources of brGDGTs remain possible but are yet unidentified. Crenarchaeol (Fig. 4.1) is a membrane-spanning lipid of Thaumarchaeota, formerly known as Group I Crenarchaeota (Brochier-Armanet et al., 2008; Spang et al., 2010). It is abundant in aquatic environments: oceans (Schouten et al., 2002; Kim et al., 2010a), lakes (Blaga et al., 2009; Sinninghe Damsté et al., 2009; Powers et al., 2010), and rivers (e.g., Herfort et al., 2006; Kim et al., 2007; Zell et al., 2013b), but also occurs in soils (Weijers et al., 2006b).

The brGDGTs were used to define a paleotemperature proxy (i.e., the MBT/CBT proxy), based on the fact that variations in the distributions of brGDGTs with respect

to the number of methyl branches (four–six) and cyclopentane moieties (up to two) in soil (Sinninghe Damsté et al., 2000) correlated with mean annual air temperature (MAAT) and soil pH (Weijers et al., 2007c). The MBT/CBT proxy has been used to reconstruct past MAAT and soil pH changes in diverse settings: lake sediments (Tierney et al., 2010; Tyler et al., 2010; Zink et al., 2010; Fawcett et al., 2011), peat (Ballantyne et al., 2010), loess (Peterse et al., 2011b), and marine sediments in front of rivers (Weijers et al., 2007a; Donders et al., 2009; Rueda et al., 2009; Bendle et al., 2010). The brGDGT and crenarchaeol concentrations are also used to calculate the branched and isoprenoid tetraether (BIT) index, which was defined as a proxy for soil organic carbon input from land to aquatic environments (Hopmans et al., 2004; Herfort et al., 2006; Kim et al., 2006; Blaga et al., 2009). It has been applied to marine and lacustrine sediment cores to reconstruct changes in river runoff and the rainfall amounts in the past (Ménot et al., 2006; Verschuren et al., 2009).

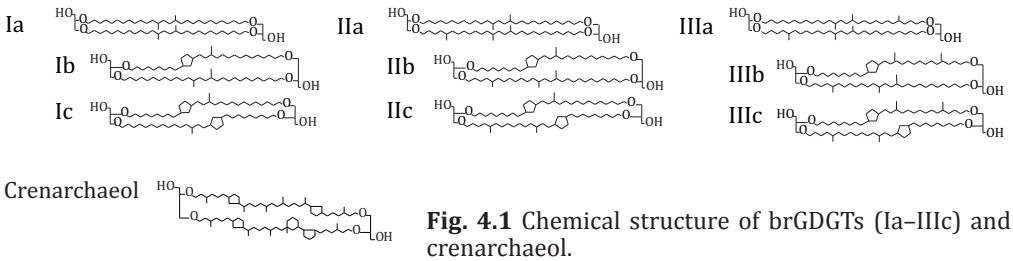

Fig. 4.1 Chemical structure of brGDGTs (Ia–IIIc) and crenarchaeol.

Initially, it was hypothesized that brGDGTs are mainly produced on land, transported to the ocean via rivers by soil erosion, and then deposited in marine sediments (Hopmans et al., 2004). Based on this idea, Weijers et al. (2007b) reconstructed the MAAT and the soil pH of the drainage basin of the Congo River using marine sediments deposited close to the river mouth. However, a recent study in the central Amazon basin showed that the majority of brGDGTs originates from the lowland Amazon soils, but in situ production in the Amazon River itself also influenced, though to a lesser extent, the brGDGT distribution (Zell et al., 2013b). In situ production of brGDGTs was also proposed to occur in the Yangtze River (Zhu et al., 2011; Yang et al., 2013). In addition to the alteration of the brGDGT distribution, the in situ production of brGDGTs can influence the BIT index, which is also influenced by the crenarchaeol production in the river and in soil (Yang et al., 2013; Zell et al., 2013b).

In the present study, we assessed the effects of hydrodynamical variations on the distributions and sources of brGDGTs and crenarchaeol in the central Amazon basin and their implication on the MBT/CBT proxy and the BIT index. Suspended particulate matter (SPM) samples were collected at five stations along the Amazon main stem and three tributaries (Negro, Madeira, and Tapajós) at four different hydrological seasons [rising water (RW), high water (HW), falling water (FW), and low water (LW)]. The concentra-

tion and distribution of brGDGTs of both core lipid (CL) and intact polar lipid (IPL)-derived fractions were investigated. IPL-derived fractions were applied as an indicator of GDGTs derived from more recently-living cells, since IPLs are less stable than CLs (e.g., Harvey et al., 1986).

4.2 STUDY AREA

The Amazon River is formed by the confluence of the Ucayali and Marañon Rivers in Peru and referred to as the Solimões River upstream of its confluence with the Negro River in Brazil. Our study area is located in the downstream section of the Amazon River in Brazil, from the city of Manaus on the Negro River to the city of Santarem at the confluence of the Amazon River with the Tapajós River (Fig. 4.2). The Amazon River is the world's largest river with a drainage basin of 6.1×10^6 km^2, covering about 40% of the South American continent (Goulding et al., 2003). It has a mean annual water discharge of 2×10^5 $m^3 s^{-1}$ (Callède et al., 2000) and an annual mean sediment discharge of 0.8–1.2 × 10^{12} kg $year^{-1}$ (Dunne et al., 1998; Martinez et al., 2009) at Óbidos, the most downstream gauging station in the Amazon River. The Madeira River is the largest tributary of the Amazon River, which originates in the Bolivian Andes and drains the "Planalto Brasileiro" shield and the central plains, while the Negro and Tapajós Rivers originate in the lowland of the Amazon basin. Rivers within the Amazon drainage basin are traditionally classified according to their color (Sioli, 1984): Solimões/Amazon and Madeira (white), Negro (black), and Tapajós (clear).

Wet and dry seasons in the Amazon basin are related with fluctuations in the position of the intertropical convergence zone (Marengo et al., 2001). Precipitation ranges from <2000 mm $year^{-1}$ in the extreme northeastern and southern parts of the basin, and increases to 7000 mm $year^{-1}$ on the east side of the Andes (Salati et al., 1979). The Amazon River is characterized by strong water level changes between the LW (October–November) and HW (May–June) seasons (Fig. 4.3). The water level in the Amazon main stem at Óbidos fluctuates ~10 m during an average year and its water discharge varies by a factor of 2 or 3 (Meade et al., 1979).

4.3 MATERIALS AND METHODS

4.3.1 Sampling

We sampled SPM at five stations along the Amazon main stem (Solimões and Amazon 1–4) and at three tributaries (Negro, Madeira, and Tapajós) (Fig. 4.2; Table 4.1). SPM samples were collected in June–July 2009 (HW), in October 2009 (LW), in August–September 2010 (FW), and in January–February 2011 (RW) (Fig. 4.3). To determine SPM concentrations, 0.5 L of water was filtered onto ashed (450 °C, overnight) and pre-

weighed glass-fiber filters (Whatman GF-F, 0.7 µm, 47 mm diameter). For the GDGT analysis, ~5 L of water were separately filtered onto ashed glass-fiber filters (Whatman GF-F, 0.7 µm, 142 mm diameter). The filters were kept frozen onboard and brought to the Royal Netherlands Institute for Sea Research (NIOZ, The Netherlands) laboratory, where they were freeze-dried.

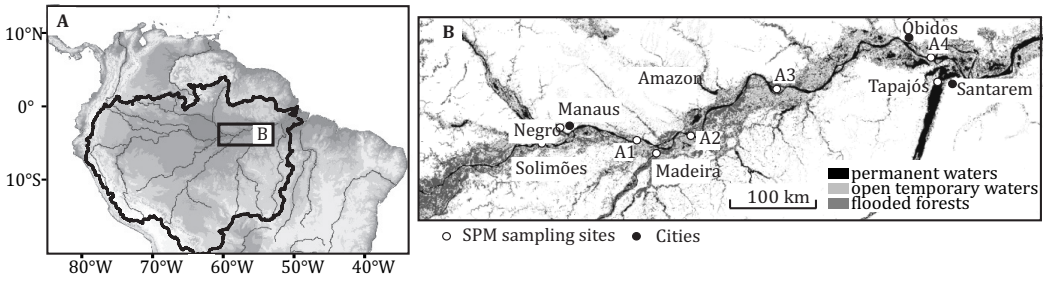

Fig. 4.2 Study area (A) showing the sampling stations along the Amazon main stem an ditstributaries (B). Note that A1–A4 indicate sampling stations Amazon1–4.

4.3.2 Hydrological and environmental parameters and bulk geochemical analysis

The daily relative water level data of the Amazon River recorded at Óbidos (Fig. 4.3) were provided by the Agência Nacional das Águas (ANA, Brazil). Water discharges at three river stations [Solimões, Madeira, and Amazon 4 (Óbidos)] were obtained from the HYBAM observatory program (http://www.ore-hybam. org/) using the site-specific discharge vs. water height relationships. The relationships were established based on the measurements with a 300 and 600 Hz Acoustic Doppler Current Profiler (ADCP, WorkHorse Rio Grande TMRD Instruments, Callède et al., 2000; Filizola and Guyot, 2004) and daily water height observations at each station. Water temperature and pH (Table 4.1) were measured in situ with a multi-parameter probe (YSI 6600 V2). Total organic carbon (TOC) content of river SPM was analyzed using an elemental analyzer C–H–N Fisions NA-2000 at the Institute for Research and Development (IRD, France) with a precision of ± 0.1 mg C g^{-1} and this was used to calculate the particulate organic carbon (POC) concentration.

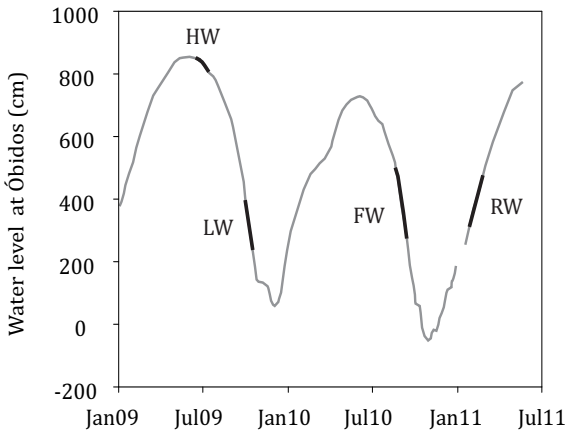

Fig. 4.3 Seasonal water level changes of the Amazon River main stem at the town Óbidos (station Amazon4) (RW, rising water; HW, high water; FW, fallingwater; LW, low water).

4.3.2 Extraction and analysis of GDGTs

Lipid extraction and analyses of CL and IPL-derived GDGTs were carried out using methods as described by Zell et al. (2013b). In brief, the freeze-dried SPM filters were extracted with a modified Bligh and Dyer technique (Pitcher et al., 2009). The extracts were separated into a CL fraction and an IPL fraction on activated silica with n-hexane: ethyl acetate 1:1 (v:v) (CL fraction) and methanol (IPL fraction) as eluents (Oba et al., 2006; Pitcher et al., 2009). For GDGT quantification 0.1 mg C_{46} GDGT internal standard was added into each fraction (Huguet et al., 2006). Part of the IPL fraction was hydrolyzed to obtain IPL-derived CLs (Weijers et al., 2011a). The CL GDGTs were analyzed using high performance liquid chromatography–atmospheric pressure positive ion chemical ionization–mass spectrometry (HPLC-APCI-MS) with an Agilent 1100 series LC/MSD SL and they were separated on an Alltech Prevail Cyano column (150 × 2.1 mm; 3 µm) using the method described by Schouten et al. (2007) and modified by Peterse et al. (2012). The compounds were eluted isocratically with 90% A and 10% B for 5 min at a flow rate of 0.2 ml min^{-1}, and then with a linear gradient to 16% B for 34 min, where A = hexane and B = hexane:isopropanol 9:1 (v:v). The injection volume was 10 µl per sample. Selective ion monitoring of the $[M + H]^+$ of the different brGDGTs and crenarchaeol was used to detect and quantify them. Quantification was achieved by calculating the area of its corresponding peak in the chromatogram and comparing it with the peak area of the internal standard and correcting for the different response factors (cf. Huguet et al., 2006). The analytical error was determined by duplicate measurements of 6 samples. For the concentration of the sum of brGDGTs, the analytical error was 8% for the CL brGDGTs and 6% for the IPL-derived brGDGTs. Crenarchaeol concentrations had a standard deviation of 8% (CL) and 9% (IPL-derived).

4.3.3 Calcualtion of GDGT-based indices

The numerals refer to the GDGTs indicated in Fig. 4.1. The BIT index (Hopmans et al., 2004), the DC (Sinninghe Damsté et al., 2009), and the MBT and CBT indices (Weijers et al., 2007a) were calculated as follows:

$$\text{BIT index} = ([Ia] + [IIa] + [IIIa]) / ([Ia] + [IIa] + [IIIa] + [IV]) \quad (1)$$

$$\text{DC} = ([Ib] + [IIb]) / ([Ia] + [Ib] + [IIa] + [IIb]) \quad (2)$$

$$\text{CBT} = \log ([Ib] + [IIb]) / ([I] + [II]) \quad (3)$$

$$\text{MBT} = ([Ia]+[Ib]+[Ic]) / ([Ia]+[Ib]+[Ic]+[IIa]+[IIb]+[IIc]+[IIIa]+[IIIb]+[IIIc]) \quad (4)$$

The average standard deviations of the MBT was 0.001 (CL) and 0.013 (IPL-derived), for the DC 0.001 (CL) and 0.008 (IPL-derived), for the CBT 0.007 (CL) and 0.036 (IPL-derived), and for the BIT 0.003 (CL) and 0.007 (IPL-derived).For the calculation of

pH and MAAT, the regional soil calibration for the Amazon basin (Bendle et al., 2010) was used:

$$CBT = 4.2313 - 0.5782 \times pH \ (r^2 = 0.75) \quad (5)$$

$$MBT = 0.1874 + 0.0829 \times CBT + 0.0250 \times MAAT \ (r^2 = 091) \quad (6)$$

4.3.3 Statistical analysis

We performed the non-parametric Mann-Whitney U-test which does not meet the normality assumption of the One-Way analysis variance (ANOVA) to evaluate the differences in mean values between two different groups. Groups that showed significant differences ($p < 0.05$) were assigned different letters. The software SPSS 19 was used to perform the statistical tests.

Table 4.1 Sampling stations and environmental data.

Sample name	Sampling station	Sampling date	Latitude	Longitude	Temperature (°C)	pH	SPM (mgL^{-1})	TOC (wt.%)
High water season								
CBM 502	Solimões	20/06/2009	−3.3188	−60.5056	28	6.5	40.6	2
CBM 514	Negro	26/06/2009	−3.0746	−60.2639	29	5	3.1	22
CBM 516	Amazon1	27/06/2009	−3.2412	−58.9916	28	6.4	28.6	4
CBM 517	Madeira	27/06/2009	−3.3935	−58.7775	28	6.2	53.4	2
CBM 518	Amazon2	28/06/2009	−3.2085	−58.3050	28	6.2	27.3	4
CBM 528b	Amazon3	1/7/2009	−2.5073	−57.3078	28	6.3	24.4	3
CBM 531	Amazon4	3/7/2009	−1.9713	−55.4704	29	6.2	26.9	3
CBM 541b	Tapajós	7/7/2009	−2.4745	−55.0157	30	6.4	3	15
Low water season								
CBM 607	Solimões	5/10/2009	−3.3311	−60.5434	31	6.6	74.2	3
CBM 601	Negro	3/10/2009	−3.0727	−60.2627	31	4.7	3.8	23
CBM 620	Amazon1	9/10/2009	−3.2423	−58.9755	31	6.4	40.2	4
CBM 621	Madeira	9/10/2009	−3.4090	−58.7852	32	7.2	33.4	2
CBM 622	Amazon2	10/10/2009	−3.1744	−58.4091	31	6.8	22.6	3
CBM 634	Amazon3	14/10/2009	−2.5423	−57.0267	31	6.8	31.8	3
CBM 635	Amazon4	16/10/2009	−1.9509	−55.4904	21	6.8	31.2	3
CBM 642	Tapajós	20/10/2009	−2.5262	−55.0292	31	6.9	3.2	22
Falling water season								
CBM 706	Solimões	27/08/2010	−3.3255	−60.5528	30	6.9	37.9	2
CBM 701	Negro	25/08/2010	−3.0762	−60.2635	30	5.4	3.1	19
CBM 714	Amazon1	1/9/2010	−3.3110	−58.8621	30	6.7	40.9	3
CBM 715	Madeira	1/9/2010	−3.4071	−58.7894	31	7.3	21.1	3
CBM 722	Amazon2	3/9/2010	−3.1614	−58.3778	30	6.7	31.2	3
CBM 727	Amazon3	6/9/2010	−2.5095	−57.2977	31	6.9	36.7	3
CBM 729	Amazon4	8/9/2010	−1.9468	−55.4990	31	7	25.1	3
CBM 736	Tapajós	12/9/2010	−2.4578	−54.9883	31	6.8	2.7	18
Rising water season								
CBM 805	Solimões	23/01/2011	−3.3254	−60.5533	29	7.1	17.5	1
CBM 801	Negro	21/01/2011	−3.0709	−60.2660	29	4.5	3.8	4
CBM 812a	Amazon1	26/01/2011	−3.3007	−58.8720	29	7	130.9	2
CBM 813a	Madeira	27/01/2011	−3.4090	−58.7869	28	6.4	354	1
CBM 814a	Amazon2	27/01/2011	−3.1678	−58.4211	29	6.8	149.9	1
CBM 822	Amazon3	31/01/2011	−2.5419	−57.0026	29	6.7	127.8	1
CBM 824	Amazon4	1/2/2011	−1.9115	−55.5535	29	6.8	114	1
CBM 830	Tapajós	5/2/2011	−2.5301	−55.0355	28	6.1	9.2	10

4.4 RESULTS

4.4.1 Bulk parameters:SPM and TOC

SPM concentrations varied between 20 and 150 mg L^{-1} in the Amazon main stem (Solimões and Amazon 1–4, Fig. 4.4A). The concentrations were about three times higher during the RW season than during other seasons. The SPM concentrations in the Negro and Tapajós Rivers (on average 3 ± 0.4 and 4.5 ± 3 mg L^{-1} , respectively) were low compared to those of the Madeira River (on average 115.5 ± 156 mg L^{-1}) and the Amazon main stem (Table 4.1).

In contrast, the TOC content of the SPM in the Amazon main stem was lower during the RW season than during other seasons. Overall the TOC content of SPM in the main stem varied between 1 and 4 wt.% (Fig. 4.4B). The TOC content of the SPM was substantially higher in the Negro and Tapajós Rivers (on average 21 and 16 wt.%, respectively) compared to the Madeira River (on average 2 wt.%) and the Amazon main stem (Table 4.1).

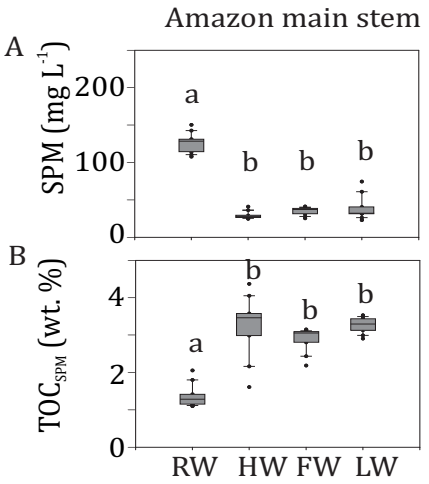

Fig. 4.4 SPM concentration(A) and TOC content of SPM in wt.% (B) in the Amazon mainstem (Solimões and stations Amazon 1–4). Letters indicate statistically significant groups of data($p < 0.05$).

4.4.2 CL and IPL-derived GDGT concentrations

Variations in the concentration of both CL and IPL-derived brGDGTs and crenarchaeol along the Amazon main stem and in the tributaries are shown in Fig. 4.5. CL brGDGT concentrations varied between 13 and 230 µg g_{POC}^{-1} (35–235 ng L^{-1}) along the Amazon main stem. On average, IPL-derived brGDGTs contributed 12% to the total brGDGT pool. The CL crenarchaeol concentrations were lower than those of CL brGDGTs, ranging from 4 to 75 µg g_{POC}^{-1} (5–70 ng L^{-1}) along the Amazon main stem. The percentage of IPL-derived crenarchaeol was on average 36% of the total amount of crenarchaeol, with no significant difference between the seasons. However, in the HW season IPL-derived crenarchaeol could not be detected in all samples (Table 4.2). In order to investigate the

overall hydrological effect on the concentration of brGDGTs and crenarchaeol in the central Amazon basin, the data from the stations in the Amazon main stem are illustrated in box plots, showing the concentrations in the different seasons according to the water level cycle (RW-HW-FW-LW, Fig. 4.6). The box plots show that CL brGDGT concentrations varied over the hydrological cycle. The highest average brGDGT concentration per liter and normalized to POC occurred during the HW season, with the values of 130 ng L^{-1} and 140 μg g_{POC}^{-1}, but was also highly variable along the Amazon River. The lowest average concentrations (40 ng L^{-1} and 40 μg g_{POC}^{-1}) were found during the LW season. CL crenarchaeol concentrations showed a different pattern, with the lowest values (8 ng L^{-1} and 8 μg g_{POC}^{-1}) during the HW season. The tributaries (Negro, Madeira, and Tapajós) showed a similar range of CL brGDGT concentrations as those of the Amazon main stem: 60–140 μg g_{POC}^{-1} (50–90 ng L^{-1}), 40–200 μg g_{POC}^{-1} (30–180 ng L^{-1}), and 10–80 μg g_{POC}^{-1} (9–69 ng L^{-1}), respectively (Fig. 4.5; Table 4.2). The average IPL percentage was 14% in the Negro River, 12% in the Madeira River, and 13% in the Tapajós River. The CL crenarchaeol concentrations in tributaries were 6–10 μg g_{POC}^{-1} (5–8 ng L^{-1}) in the Negro River, 10–60 μg g_{POC}^{-1} (10–40 ng L^{-1}) in the Madeira River, and 4–70 μg g_{POC}^{-1} (3–35 ng L^{-1}) in the Tapajós River (Fig. 4.5; Table 4.2). The average IPL percentages were 35% in the Negro River, 26% in the Madeira River, and 37% in the Tapajós River.

4.4.3 Distribution pattern of CL and IPL-derived GDGTs

The distribution of CL and IPL-derived brGDGTs at all stations showed a strong dominance of brGDGT Ia with a relative abundances of 70 and 80%, respectively. The second most abundant brGDGT was brGDGT IIa (Fig. 4.7). Variations in MBT, DC, and BIT of the CLs and IPL-derived GDGTs from the Amazon main stem are illustrated in box plots, following the water level cycle (Fig. 4.8) and scatter plots (Fig. 4.9). In general, IPL fraction-derived indices are more variable than those of CLs. All the indices varied over the hydrological cycle. The MBT ranged from 0.78 to 0.90 for CL brGDGTs and from 0.71 to 0.90 for IPL-derived brGDGTs, with the highest average value of CL and IPL-derived brGDGTs during the HW season. The DC varied between 0.04 and 0.12 for CL brGDGTs and between 0.05 and 0.14 for the IPL-derived brGDGTs. The lowest average DC value of CL brGDGTs occurred during the HW season. The BIT ranged from 0.41 to 0.97 for CL GDGTs and from 0.16 to 0.91 for IPL-derived GDGTs. The highest average BIT value for the CL fractions (0.92) was found during the HW season, while the lowest average BIT occurred during the LW season (0.52). In the IPL-derived GDGTs a similar pattern was seen but the differences between the seasons were less clear (Fig. 4.8C).

The MBT and DC values in tributaries were 0.77–0.96 and 0.02–0.13 for CL brGDGTs and 0.63–0.93 and 0.02–0.14 for IPL-derived brGDGTs, respectively (Fig. 4.9B; Table 4.3). The CL and IPL-derived BIT values in tributaries were 0.20–0.94 and 0.09–0.94, respectively. The Negro River greatly differed from other tributaries, with higher MBT (on average 0.94) and BIT (on average 0.92) and lower DC (on average 0.02) values during all seasons (Table 4.3).

Table 4.2 GDGTconcentrations.

		CL GDGT µg g_{POC}^{-1}										IPL-derived GDGT µg g_{POC}^{-1}									
Sample name	**Sampling site**	**Ia**	**Ib**	**Ic**	**IIa**	**IIb**	**IIc**	**IIIa**	**IIIb**	**IIIc**	**Cren.**	**Ia**	**Ib**	**Ic**	**IIa**	**IIb**	**IIc**	**IIIa**	**IIIb**	**IIIc**	**Cren.**
CBM502	Solimões	81.4	5.6	1.8	15.8	2.5	-	1.3	-	-	6.3	n.d.	n.d.	n.d.	n.d.	n.d.	n.d.	n.d.	n.d.	n.d.	n.d.
CBM 514	Negro	120.5	2.2	0.9	8.7	0.2	-	0.1	-	-	11.1	n.d.	n.d.	n.d.	n.d.	n.d.	n.d.	n.d.	n.d.	n.d.	n.d.
CBM 516	Amazon 1	198.8	6.3	2.2	18.2	2.7	0.5	2.0	-	-	7.1	6.6	6.3	2.4	12.3	1.7	-	1.2	-	-	2.0
CBM 517	Madeira	164.6	7.8	2.8	23.6	2.8	0.2	1.4	-	-	14.2	n.d.	n.d.	n.d.	n.d.	n.d.	n.d.	n.d.	n.d.	n.d.	n.d.
CBM 518	Amazon 2	153.4	8.9	2.8	19.6	2.8	-	1.0	-	-	9.2	0.5	0.0	0.0	0.0	0.0	-	0.0	-	-	2.0
CBM 528b	Amazon 3	63.2	3.3	1.1	9.9	1.1	0.2	0.6	-	-	7.7	n.d.	n.d.	n.d.	n.d.	n.d.	n.d.	n.d.	n.d.	n.d.	n.d.
CBM 531	Amazon 4	61.3	3.1	1.1	9.0	1.1	0.2	0.5	-	-	11.5	16.7	2.3	0.6	3.9	0.6	-	0.0	-	-	5.6
CBM 541b	Tapajós	51.6	3.0	1.1	7.0	0.9	-	0.4	-	-	34.9	5.0	0.5	0.2	1.1	0.0	-	0.0	-	-	16.8
CBM 607	Solimões	14.2	1.3	0.5	2.7	0.5	-	0.2	-	-	9.1	5.0	0.6	0.2	1.1	0.2	-	0.0	-	-	4.4
CBM 601	Negro	52.8	1.0	0.7	3.5	0.0	-	0.2	-	-	6.4	13.8	1.9	0.5	2.0	0.4	-	0.4	-	-	5.6
CBM 620	Amazon 1	26.7	2.2	0.9	4.7	0.8	0.2	0.5	-	-	20.9	1.5	0.2	0.0	0.4	0.1	-	0.0	-	-	10.2
CBM 621	Madeira	24.8	3.3	1.1	6.7	1.3	-	0.5	-	-	37.3	3.1	0.4	0.1	0.8	0.2	-	0.1	-	-	4.4
CBM 622	Amazon 2	53.5	4.8	1.8	9.8	1.8	-	0.6	-	-	64.8	7.6	0.4	0.2	1.2	0.2	-	0.2	-	-	11.0
CBM 634	Amazon 3	31.5	2.6	0.9	5.5	0.9	0.2	0.5	-	-	50.9	2.0	0.2	0.1	0.5	0.1	-	0.1	-	-	10.4
CBM 635	Amazon 4	22.1	2.2	0.8	4.1	0.7	-	0.4	-	-	37.8	1.6	0.3	0.1	0.5	0.0	-	0.1	-	-	5.0
CBM 642	Tapajós	9.5	1.2	0.3	1.5	0.2	-	0.2	-	-	3.9	1.9	0.3	0.2	0.5	0.1	-	0.0	-	-	1.9
CBM 706	Solimões	77.7	6.6	2.2	15.4	2.7	0.3	1.2	-	-	24.9	6.0	0.5	0.2	1.3	0.1	-	0.1	-	-	3.9
CBM 701	Negro	127.3	1.9	1.0	7.4	0.3	-	0.3	-	-	9.3	6.5	0.2	0.1	0.5	0.0	-	0.0	-	-	1.2
CBM 714	Amazon 1	66.2	5.1	1.8	10.6	2.0	0.2	0.5	-	-	22.9	2.1	0.2	0.1	0.7	0.1	0.2	0.0	-	-	6.4
CBM 715	Madeira	29.2	3.3	1.1	7.0	1.2	-	0.4	-	-	57.4	5.0	0.7	0.2	1.5	0.2	-	0.1	-	-	21.4
CBM 722	Amazon 2	83.5	4.9	1.8	11.2	1.8	0.3	0.6	-	-	25.5	9.7	0.7	0.3	1.8	0.3	-	0.1	-	-	7.0
CBM 727	Amazon 3	61.6	3.5	1.2	8.2	1.3	0.2	0.3	-	-	28.8	3.2	0.2	0.1	0.6	0.1	-	0.0	-	-	5.0
CBM 729	Amazon 4	87.9	5.8	2.1	13.0	2.0	0.3	1.2	-	-	75.1	5.9	0.5	0.2	1.2	0.2	-	0.1	-	-	15.3
CBM 736	Tapajós	15.4	2.0	0.5	2.6	0.3	-	-	-	-	72.8	1.5	0.2	0.1	0.5	0.0	-	0.0	-	-	20.7
CBM 801	Solimões	83.3	9.9	3.3	19.5	4.5	0.6	1.9	-	-	38.7	6.0	0.6	0.2	1.6	0.3	-	0.2	-	-	9.9
CBM 805	Negro	n.d.	n.d.	n.d.	n.d.	n.d.	n.d.	n.d.	n.d.	n.d.	n.d.	n.d.	n.d.	n.d.	n.d.	n.d.	n.d.	n.d.	n.d.	n.d.	n.d.
CBM 812 a	Amazon 1	48.5	5.4	1.9	9.5	2.3	0.4	0.6	-	-	18.6	4.2	0.6	0.1	1.1	0.3	0.1	0.1	-	-	4.2
CBM 813 a	Madeira	28.8	3.0	1.0	7.6	1.4	0.3	0.3	-	-	9.2	1.5	0.2	0.1	0.6	0.1	-	0.0	-	-	2.7
CBM 814 a	Amazon 2	39.9	4.0	1.3	8.8	1.8	0.3	0.4	-	-	16.7	1.5	0.1	0.1	0.5	0.1	-	0.0	-	-	2.6
CBM 822	Amazon 3	53.2	5.2	1.8	11.2	2.4	0.4	0.5	-	-	28.2	2.0	0.1	0.1	0.5	0.1	-	0.1	-	-	5.0
CBM 824	Amazon 4	61.1	5.6	2.0	11.8	2.3	0.4	1.1	-	-	35.0	11.4	0.5	0.2	1.2	0.1	-	0.1	-	-	6.8
CBM 830	Tapajós	66.5	2.9	0.9	6.7	0.7	-	0.2	-	-	3.6	4.8	0.2	0.1	0.7	0.1	-	0.0	-	-	0.6

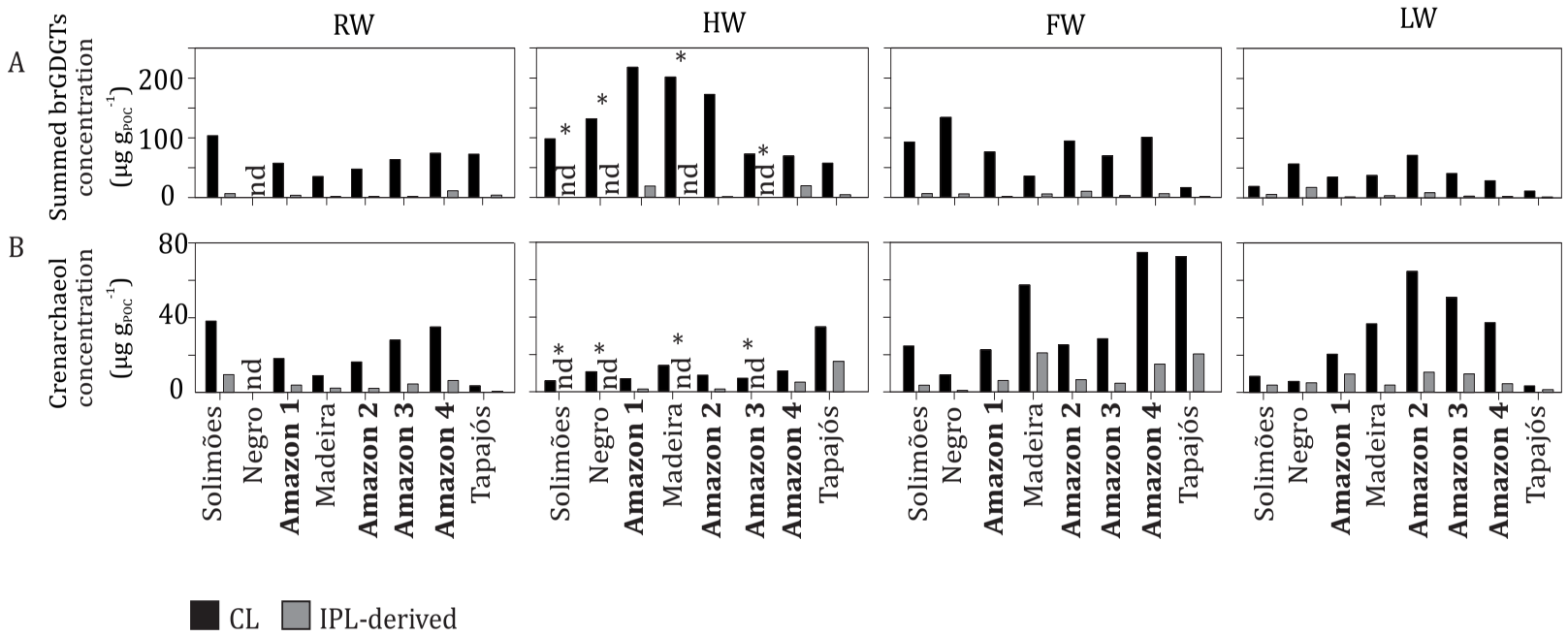

Fig. 4.5 Concentration of CL and IPL-derived summed brGDGTs (A) and crenarchaeol (B) normalized to POC along the Amazon mainstem and its tributaries in the four different seasons (nd, no data; *only the CL fraction was analyzed).

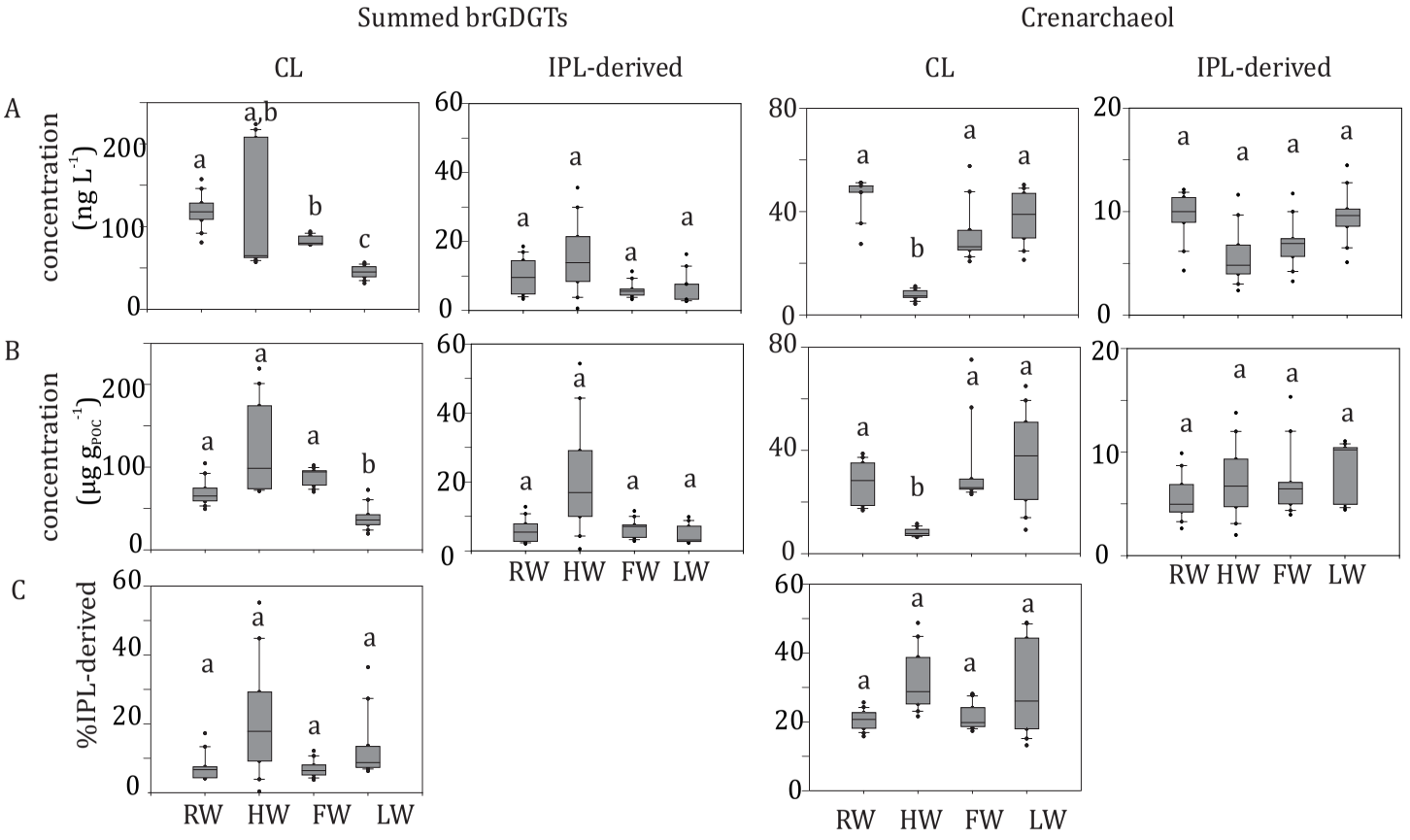

Figure 4.6 Box plots of CL and IPL-derived summed brGDGT and crenarchaeol concentrations per liter (A) and normalized to POC (B) the percentage of IPL-derived brGDGTs and crenarchaeol (C) in the Amazon mainstem (Solimões and stations Amazon1–4) at four different seasons. Letters indicate statistically significant groups of data ($p < 0.05$).

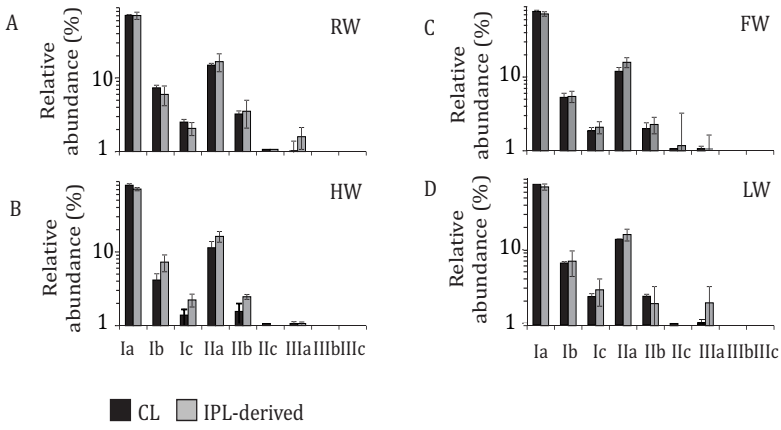

Figure 4.7 Distribution patterns of the average relative abundances of CL and IPL-derived brGDGTs for the Amazon mainstem during (A) RW, (B) HW, (C) FW, and (D) LW seasons. Note that they axes are logarithmic scales.

Table 4.3 BIT, MBT, DC, reconstructed pH and reconstructed MAAT values of all analyzed samples.

	CL					IPL-derived				
Sampling site	**BIT index**	**MBT**	**DC**	**pH***	**MAAT (°C)***	**BIT index**	**MBT**	**DC**	**pH***	**MAAT (°C)***
High water season										
Solimões	0.9	0.82	0.08	5.4	21.7	0.9	0.83	0.08	5.5	22.2
Negro	0.9	0.93	0.02	4.3	24.1	n.d.	n.d.	n.d.	n.d.	n.d.
Amazon 1	1.0	0.90	0.04	4.9	23.9	0.9	n.d.	n.d.	6.7	11.3
Madeira	0.9	0.86	0.05	5.2	22.8	n.d.	n.d.	n.d.	n.d.	n.d.
Amazon 2	0.9	0.88	0.06	5.3	23.7	0.2	n.d.	n.d.	n.d.	n.d.
Amazon 3	0.9	0.85	0.06	5.2	22.5	0.5	0.79	0.09	5.6	20.6
Amazon 4	0.9	0.86	0.06	5.2	22.8	0.8	0.81	0.12	5.8	22.1
Tapajós	0.6	0.87	0.06	5.3	23.4	0.3	0.84	0.08	5.5	22.7
Low water season										
Solimões	0.7	0.83	0.10	5.7	22.4	0.6	0.81	0.11	5.7	22.0
Negro	0.9	0.94	0.02	4.3	24.2	0.7	0.86	0.12	5.8	23.9
Amazon 1	0.6	0.83	0.09	5.6	22.3	0.2	0.76	0.10	5.7	20.0
Madeira	0.5	0.78	0.13	5.9	20.8	0.5	0.77	0.14	5.9	20.5
Amazon 2	0.5	0.83	0.09	5.6	22.5	0.4	0.84	0.06	5.3	22.1
Amazon 3	0.4	0.83	0.09	5.5	22.4	0.2	0.76	0.11	5.7	19.7
Amazon 4	0.4	0.83	0.10	5.7	22.5	0.3	0.77	0.12	5.8	20.5
Tapajós	0.7	0.85	0.11	5.8	23.6	0.6	0.80	0.12	5.8	21.7
Falling water season										
Solimões	0.8	0.82	0.09	5.6	21.8	0.7	0.81	0.08	5.5	21.5
Negro	0.9	0.94	0.02	4.2	24.3	0.9	0.93	0.03	4.7	24.7
Amazon 1	0.8	0.85	0.08	5.5	22.9	0.3	0.71	0.09	5.5	17.4
Madeira	0.4	0.80	0.11	5.8	21.4	0.2	0.76	0.12	5.9	20.1
Amazon 2	0.8	0.87	0.07	5.3	23.4	0.6	0.83	0.08	5.5	22.3
Amazon 3	0.7	0.87	0.06	5.3	23.4	0.4	0.82	0.07	5.4	21.6
Amazon 4	0.6	0.85	0.07	5.4	23.0	0.3	0.81	0.09	5.5	21.6
Tapajós	0.2	0.86	0.11	5.8	23.9	0.1	0.79	0.10	5.7	21.0
Rising water season										
Solimões	0.7	0.78	0.12	5.8	21.1	0.4	0.76	0.11	5.7	19.8
Negro	0.9	0.96	0.02	4.2	24.9	0.9	0.94	0.02	4.5	24.7
Amazon 1	0.8	0.81	0.12	5.8	22.2	0.6	0.75	0.14	6.0	19.9
Madeira	0.8	0.77	0.11	5.7	20.3	0.5	0.69	0.12	5.8	17.2
Amazon 2	0.7	0.80	0.11	5.7	21.4	0.4	0.74	0.10	5.6	19.1
Amazon 3	0.7	0.81	0.11	5.7	21.6	0.3	0.75	0.10	5.6	19.4
Amazon 4	0.7	0.81	0.10	5.7	21.9	0.7	0.90	0.05	5.1	24.1
Tapajós	1.0	0.90	0.05	5.0	24.2	0.9	0.86	0.06	5.2	22.9

*reconstructed

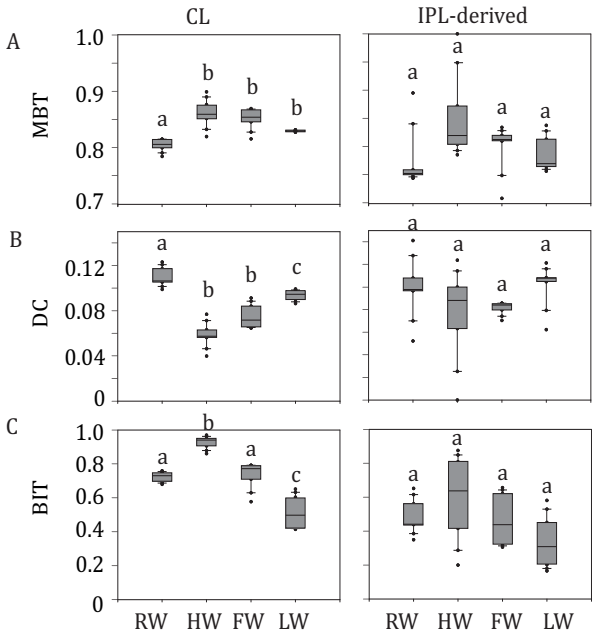

Figure 4.8 Box plots of CL and IPL-derived MBT (A), DC (B), and BIT(C) in the Amazon mainstem (Solimões and stations Amazon1–4) at the four different seasons. Letters indicate statistically significant groups of data ($p < 0.05$).

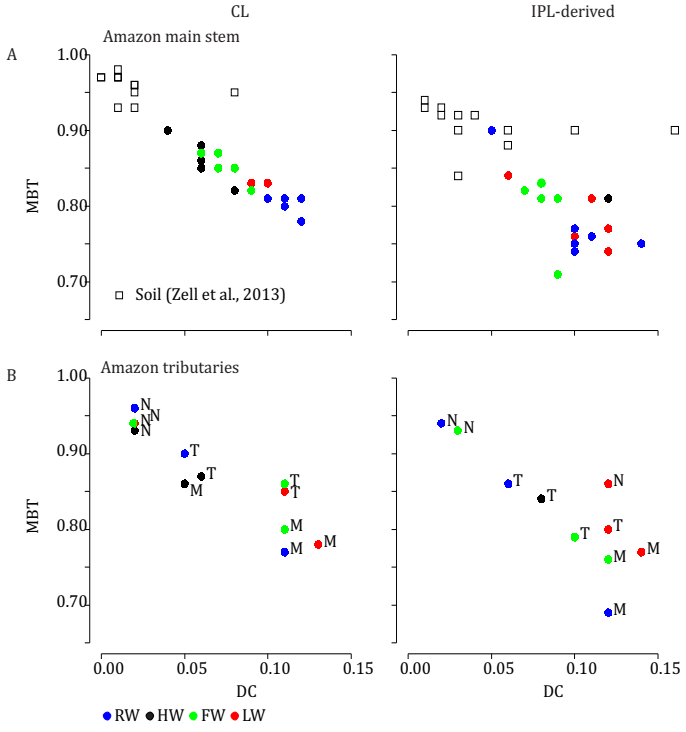

Figure 4.9 Scatter plot of MBT vs. DC of CL and IPL-derived brGDGTs from the Amazon mainstem SPM (Solimões and stations Amazon1–4)(A) and Amazon tributaries (N, Negro; M, Madeira; T, Tapajós)(B).

4.5 DISCUSSION

4.5.1 Seasonal variation in SPM concentration and TOC of SPM

The seasonal pattern of SPM concentration in the Amazon main stem was statistically significant, with the highest concentration during the RW season (Fig. 4.4). The SPM load is controlled by sediment erosion mostly coming from the Andes (Gibbs, 1967a), but also by sediment storage and resuspension (Meade et al., 1985). Similarly, the seasonal pattern of the TOC content of SPM was statistically significant, with the lowest value during the RW season (Fig. 4.4). Our results are in good agreement with the seasonal pattern observed at Óbidos (Amazon 4) between 1999 and 2006 (Moreira-Turcq et al., 2013).

4.5.2 Seasonal variation in brGDGT concentration and source

Both CL brGDGT concentration per liter (ng L^{-1}) and normalized to POC (μg g_{POC}^{-1}) in the Amazon main stem showed a significant seasonal pattern (Fig. 4.6). As observed for the POC contents, the RW and LW seasons differed most significantly. In addition, in contrast to the SPM concentrations and the POC contents, significant differences in concentration (both ng L^{-1} and μg g_{POC}^{-1}) were also observed between the HW and LW seasons as well as between the FW and LW seasons. Interestingly, the seasonal pattern of the CL brGDGT concentrations in μg g_{POC}^{-1} and to a lesser extent in ng L^{-1} was similar to the hydrological pattern of the Amazon main stem. It is noteworthy that CL brGDGT concentrations (normalized on POC) during the HW season were on average higher than in the other seasons but varied along the Amazon River. After the confluence of the tributaries Negro and Madeira Rivers with the Amazon main stem (stations Amazon 1 and 2) the concentrations were substantially higher than in the Solimões (Fig. 4.5). This suggests that a significant amount of brGDGTs was supplied from the Negro and Madeira tributaries to the Amazon main stem. The MBT and the DC for CL fractions in the Amazon main stem also showed clear seasonal patterns (Fig. 4.8A,B). The differences of the CL MBT were only significant between the RW and other seasons as observed for the SPM concentrations and the organic carbon contents. Similar to the CL MBT, the differences of the CL DC were apparent between the RW and other seasons. However, the CL DC during the RW and LW season was also significantly different from those of the HW and FW seasons. The CL MBT and CL DC values of the Amazon main stem SPM during the HW season were most similar to those of lowland Amazon soils (<500 m in altitude) as well as the Negro River (Fig. 4.9). This suggests that there was a higher input of brGDGTs derived from lowland Amazon soils during the HW season. This supports the hypothesis that soils containing brGDGTs are primarily eroded during the periods of high rainfall and surface runoff and that this material is transported by small streams and tributaries to the main river system (cf. Hopmans et al., 2004).

Our previous study of SPM sampled during the LW season (Zell et al., 2013b) dem-

onstrated that in situ production in the Amazon River and its tributaries (Madeira and Tapajós) might be an additional source for riverine brGDGTs, since their brGDGT distributions were substantially different from those of the lowland Amazon soils and the proportion of phospholipid-derived brGDGTs in river SPM were higher than that of the lowland Amazon soils. Our new results covering SPM from all four seasons, showing that both CL and IPL-derived MBT and DC values differed from those of the lowland Amazon soils (Fig. 4.9), are in good agreement with the previous data. The fact that IPL-derived brGDGTs were detected in river SPM in all seasons (Fig. 4.5) further supports the idea that in situ production of brGDGTs occurs in the Amazon River and its tributaries, although it should be stressed that in this study we did not analyze IPL brGDGTs directly (as performed previously; Zell et al., 2013b) and that IPL brGDGTs may also partly derive from preservation of IPL brGDGTs produced in situ in soil. However, the %IPL content for brGDGTs in riverine SPM (11% on average) is higher than that of soils (8%; Zell et al., 2013b), arguing for a contribution of riverine in situ produced IPL brGDGTs to the total pool of IPL brGDGTs. Variations in IPL-derived brGDGTs in the Amazon main stem over the different seasons were insignificant (Fig. 4.6C). Overall, our data suggest that the observed variation in CL MBT and DC in the Amazon main stem (Fig. 4.8, 9A) results from a mixing of soil-derived and in situ produced brGDGTs due to the variation in the contribution of brGDGT supply from the lowland Amazon soils associated with changes in precipitation and run-off and consequently soil erosion. This also holds for the tributaries (Fig. 4.9B), except for the Negro river that is apparently dominated by soil-derived brGDGTs in all seasons.

Notably, the differences of CL MBT and CL DC in the Amazon main stem were most significant between the RW and HW seasons (Fig. 4.8A, B, 4.9A). Accordingly, the CL MBT and CL DC values of SPM during the RW season were most different (i.e., lower and higher, respectively) from those of the lowland Amazon soils (Fig. 4.9A). One possible explanation might be that the relative proportion of riverine in situ produced brGDGTs was largest during the RW season, while the brGDGT contribution from the lowland Amazon soils was dominant during the HW season. This could be quantitatively constrained by a two end-member mixing model, if it would be possible to constrain end-member values for MBT and DC for the in situ produced brGDGTs. However, the end member value of brGDGTs produced in the river could not be determined, because the IPLderived brGDGTs in the river may still contain brGDGTs that are partly derived from soil and are transported to the river unaltered (see above). A further complication is that there might be a brGDGT source in addition to the lowland Amazon soils and riverine in situ production. Our previous studies (Kim et al., 2012; Zell et al., 2013b) showed that erosion of high altitude (>2500 m) Andean soils had no major impact on brGDGT distributions in Amazon River SPM in the central Amazon basin. However, a small influence of Andean soils on brGDGT distributions in the lower Amazon SPM cannot be excluded. It is probable that organic carbon depleted Andean (Batjes and Dijkshoorn, 1999) soils were more strongly eroded from the Amazon and Madeira drainage basins

during the RW season than other seasons which would correspond with the lower TOC content in the SPM during the RW season (Fig. 4.4). To assess this hypothezis, more Andean soils should be investigated in future studies. On the other hand the MBT and DC in the Tapajós River, which does not receive any material from the Andes, was also different to that of soils. Therefore, we conclude that the in situ production of brGDGTs is the main factor that alters brGDGT distribution coming from low land soils. Interestingly a similar study by Yang et al. (2013) showed that there were no seasonal change of the MBT/CBT in the Yangtze River. This might be because there are bigger differences in the MBT/CBT along the Yangtze River and in the drainage basin soils, while the MBT/CBT along the Amazon River and in the Amazon basin soils is more constant, which makes it easier to detect seasonal differences.

4.5.3 Seasonal variation in discharge of brGDGTs: Implications for the MBT/CBT paleothermometer

The water discharge along the Amazon main stem varied during the seasons between 68 and 1.1 × 10^3 m^3 s^{-1} at the Solimões station and between 120 and 2.5 × 10^3 m^3 s^{-1} at the Amazon 4 (Óbidos) station (Fig. 4.10A). During the same periods, the water discharge varied between 5 and 30 × 10^3 m^3 s^{-1} at the Madeira River station. Water discharge data were not available for other river stations. To estimate the impact of the Madeira tributary to the Amazon main stem, we calculated the discharge of SPM, POC, and summed CL brGDGTs, multiplying the water discharge by the corresponding concentration at each station (Fig. 4.10B–D). SPM discharges were highest during the RW season at all stations. Remarkably during the RW season, the SPM discharge of the Madeira exceeded that of the Solimões and contributed a large (>50%) fraction of SPM to the Amazon main stem. The POC discharge of the Madeira tributary was as high as that of the Solimões station during the RW season. However, the discharge of the summed CL brGDGTs to the Amazon main stem of the Madeira tributary was always substantially lower than that at the Solimões station. This illustrates that the importance of a tributary of a river system may vary depending on the geochemical parameter measured.

The brGDGTs discharged in each season in percent of the annual brGDGT discharge varied considerably between the stations. At the Solimões and Amazon-4 stations during the HW season, approximately one third of the annual brGDGT flux was discharged (i.e., 37 and 32%, respectively), whilst at the Madeira River station 61% of the annual brGDGT discharge occurred during the HW season. Overall, the Solimões River accounted for 50–86% of the summed CL brGDGT discharge at the Amazon 4 station and thus was the main contributor for CL brGDGTs to the Amazon River during most of the seasons assuming conservative behavior of CL brGDGTs. The contributions of the Madeira River were higher during the RW and HW seasons (19 and 36%, respectively) and much lower during the FW and LW seasons (1 and 8%, respectively). During the FW season, the contribution of the Solimões River represented only 50% of the brGDGT discharge at the Amazon 4 station. It is unlikely that the tributaries supplied all the CL

brGDGTs since the brGDGT discharge in the Madeira River was low in the FW season (1%, Fig. 4.10D). This indicates that there is an additional source of brGDGTs between the Solimões River station and the Amazon 4 station. Since water from the floodplain lakes runs into the Amazon main stem during the FW season (Bonnet et al., 2008) and also during the sampling of the LW season (cf. Fig. 4.3), brGDGTs are carried in from the floodplain lakes and the surrounding soils. Our previous studies have already indicated that in situ production of brGDGTs occurs in floodplain lakes that are part of the Amazon River system in the central Amazon basin (Kim et al., 2012; Zell et al., 2013b). Hence, it might be possible that floodplain lakes are an additional source of brGDGTs to the Amazon main stem during that the FW season and when the LW season was sampled. This hypothesis needs to be tested in the future.

As discussed in the previous section Seasonal Variation in brGDGT Concentration and Sources, the brGDGT distributions varied in response to the hydrological changes, which led to substantial variation in MBT and DC in the Amazon main stem (Fig. 4.8, 4.9A). To assess a basin-wide integrated signal over time and space, we calculated discharge-weighted average MBT and DC values (Table 4.4).

Overall, the discharge-weighted MBT values were slightly lower than those of the lowland Amazon soils for both CL and IPL-derived fractions, while the discharge-weighted DC values were slightly higher. The reconstructed pH and MAAT values calculated with the regional calibration for Amazon basin soils (Bendle et al., 2010) were 5.5–5.6 and 21.0–22.5 °C for CL fractions. These estimates are different from the pH and MAAT reconstructed from MBT/CBT data of lowland Amazon soils (pH 4.4, MAAT 24 °C) (Zell et al., 2013b) as well as reported soil pH (~4) and MAAT (26 °C) values for the lowland Amazon basin (New et al., 2002; Batjes, 2005). This demonstrates that the in situ production of brGDGTs affects the MBT/CBT paleothermometer in the central Amazon basin. However, compared to the influence of in situ production of brGDGTs in lakes, which results in much larger, differences of reconstructed temperatures compared to those of soils of the surrounding water shed (e.g., Tierney et al., 2010), the influence of in situ production in the Amazon River is relatively minor.

4.5.4 Seasonal variation in crenarchaeol concentrations: Consequences for the BIT index

Our results show that river SPM contained about 40–70 times higher CL and IPL-derived crenarchaeol concentrations compared to the surrounding soils for all four seasons (crenarchaeol concentration in soil = 0.3 μg g_{OC}^{-1}, Zell et al., 2013b). This indicates that crenarchaeol was primarily produced in the aquatic system. The presence of phospho-IPLs with crenarchaeol as CLs in the SPM samples during the LW season further confirmed the aquatic production of crenarchaeol in the Amazon River (Zell et al., 2013b).

The seasonal differences of crenarchaeol concentrations in both ng L^{-1} and μg g_{OC}^{-1} were only statistically significant between the HW and other seasons with sub-

stantially reduced concentrations in the HW season (Fig. 4.6). Similar to brGDGTs, the seasonal pattern in IPL-derived crenarchaeol (%) in the Amazon main stem was statistically insignificant and varied strongly in the HW season, but was on average (28%) higher than that for brGDGTs (12%). This indicates that the production of crenarchaeol in the Amazon River is important.

The BIT index is commonly used to indicate the soil organic carbon input from soil into the ocean (Hopmans et al., 2004), but it might also reflect the soil organic carbon input to the Amazon River. The difference of the CL BIT index was significant between the HW and other seasons (Fig. 4.8C). The IPL-derived BIT in the Amazon main stem showed similar seasonal patterns in comparison to those of the CL fractions, but these differences were insignificant due to the larger scatter. The seasonal pattern of the CL BIT index strongly resembled that of the CL brGDGT concentrations with the highest value during the HW season (Fig. 4.6). The crenarchaeol concentration was significantly reduced during HW, which also led to a higher BIT index. Therefore, variations in the BIT index of river SPM should be interpreted cautiously: they are not only reflecting changes in soil organic matter input, but also changes in the riverine production of brGDGTs and crenarchaeol. Similar results were found in the Yangtze River which had an even bigger seasonal difference of the BIT (0.11–0.93) (Yang et al., 2013).

The CL crenarchaeol discharge (Fig. 4.10E) was lowest during the HW season. The CL crenarchaeol input from the Solimões and Madeira Rivers only accounted for 18–45% and 3–16% of the CL crenarchaeol discharges at the Óbidos station, respectively. The discharge-weighted BIT index revealed a large difference between the Solimões station and the Amazon-4 station (Table 4.4). In general, the BIT index for both CL and IPL-derived fractions at the Amazon-4 station was lower than that at the Solimões station. This would all be consistent with a riverine in situ production of crenarchaeol as the most important. Considering that water and sediment is carried in from the floodplain lakes to the Amazon main stem (e.g., Moreira-Turcq et al., 2013), crenarchaeol produced in the floodplain lakes might also be transported to the Amazon main stem. In addition nutrient discharge from the floodplain lakes could trigger the growth of crenarchaeol in the Amazon main stem. Further investigations are thus required to better constrain how the floodplain lakes influence the crenarchaeol concentration in the Amazon River system. The decrease of the flux weighted BIT index between the Solimões and Amazon-4 station indicates that the BIT index in the Amazon River compared to soil is already lower at our study site and it might decrease even further toward the river mouth. This must be considered when the BIT index is applied in a marine sedimentary record to estimate the soil organic carbon influence from the Amazon basin.

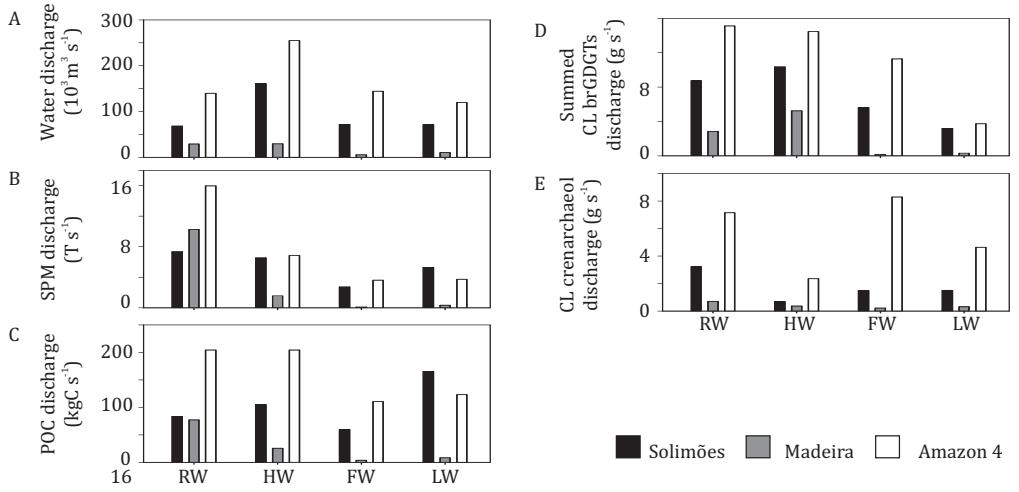

Figure 4.10 Comparisons of (A) river water discharge (10^3 m^3 s^{-1}) with (B) SPM discharge(T s^{-1}), (C) POC discharge (kgC s^{-1}), (D) CL brGDGT discharge(g s^{-1}), and (E) CL crenarchaeol discharge(g s^{-1}) at Solimões, Madeira and Óbidos stations.

Table 4.4 Flux-weighed MBT, DC, BIT, and reconstructed pH and MAAT at Solimões, Madeira, and Amazon4 (Óbidos) stations.

River station	GDGT fraction	MBT	DC	BIT index	Reconstructed pH	Reconstructed MAAT (° C)
Solimões	CL	0.81	0.19	0.80	5.6	22
	IPL-derived	0.83	0.08	0.85	5.4	22
Madeira	CL	0.83	0.08	0.84	5.4	21
	IPL-derived	0.71	0.13	0.41	5.9	18
Amazon 4 (Óbidos)	CL	0.84	0.08	0.66	5.4	23
	IPL-derived	0.84	0.10	0.62	5.6	23

4.6 CONCLUSION

Seasonal changes in the brGDGT concentrations and the MBT and DC indicate changes of the brGDGT source. The main source is Amazon low land soil and to a smaller extent riverine in situ produced brGDGTs. The highest brGDGT concentrations and MBT and DC values that are most similar to those of Amazon low land soils are found during the HW season, indicating that brGDGTs from soils are washed into the river due to high rainfall and surface runoff. During the RW season the highest relative proportion of in situ produced brGDGTs are found. To estimate the proportion of these two sources for the final brGDGT signal, further investigation to determine the end member MBT-DC of in situ produced brGDGTs is needed. The difference between the MBT and DC of brGDGTs derived from soils and the flux weighted MBT and DC values from the Amazon River also leads to a small difference of the reconstructed pH and MAAT of the Amazon River (River pH 5.5–5.6, MAAT 21.0–22.5 °C) and that of Amazon low land soil (pH 4.4, MAAT 24 °C) (Zell et al., 2013b).

Crenarchaeol is mostly produced in the river; only during HW season lower concentrations are found. Changes in both brGDGT and crenarchaeol concentrations are influencing the BIT index. Since the flux weighted BIT value is lower at the Óbidos station compared to the Solimões station, it may decrease even further toward the river mouth, which has to be considered if the BIT is used to reconstruct soil input into the marine environment.

Acknowledgments

The research leading to these results has received funding from the European Research Council (ERC) under the European Union's Seventh Framework Program (FP7/2007-2013) ERC grant agreement [226600]. This work was carried out in collaboration with the carbon cycle in the Amazon river (CARBAMA) project, funded by the French national research agency (ANR) and was conducted within an international cooperation agreement between the National Council for Scientific and Technological Development-Brazil (CNPq) and the Institute for Research and Development-France (IRD) (490755/2008-9). We thank P. Fraizy for all ADCP measurements. Topic organized by Chuanlun Zhang, Eric Boyd, Hailiang Dong, Brian P. Hedlund on Response of microbial ether lipids in the terrestrial critical zone to environmental and climatic changes.

Picture by Enrique Montes

Chapter 5

Sources and distributions of branched and isoprenoid tetraether lipids on the Amazon shelf and fan: implications for the use of GDGT-based proxies in marine sediments

Claudia Zell, Jung-Hyun Kim, David Hollander, Laura Lorenzoni, Paul Baker, Cleverson Guizan Silva, Charles Nittrouer, and Jaap S. Sinninghe Damsté

Submitted to GCA

Abstract

Branched glycerol dialkyl glycerol tetraethers (brGDGTs) in river fan sediments have been used successfully to reconstruct mean annual air temperature (MAAT) and soil pH of the Congo River drainage basin. However, in a previous study of Amazon deep-sea fan sediments the reconstructed MAATs were ca. 10°C colder than the actual MAAT of the Amazon basin. In this study we investigated this apparent offset, by comparing the concentrations and distributions of brGDGTs in Amazon River suspended particulate matter (SPM) and sediments to those in marine SPM and surface sediments. The riverine brGDGT input was evident from the elevated brGDGT concentrations in marine SPM and surface sediments close to the river mouth. The distributions of brGDGTs in marine SPM and sediments varied widely, but generally showed a higher relative abundance of methylated and cyclic brGDGTs than those in the river. Since this difference in brGDGT distribution was also found in intact polar lipid (IPL)-derived brGDGTs, which were more recently produced, the change in the marine brGDGT distribution was most likely due to marine in-situ production. Consequently, the MAATs calculated based on the Methylation of Branched Tetraethers (MBT) and the Cyclisation of Branched Tetraethers (CBT) were lower and the CBT-derived pH values were higher than those of the Amazon basin. However, SPM and sediments from stations close to the river mouth still showed MBT/CBT values that were similar to those of the river. Therefore, we recommend caution when applying the MBT/CBT proxy, it should only be used in sediment cores that were under high river influence. The influence of riverine derived isoprenoid GDGT (isoGDGT) on the isoGDGT-based TEX_{86} temperature proxy was also examined in marine SPM and sediments. An input of riverine isoGDGTs from the Amazon River was apparent, but its influence on the marine TEX_{86} was minor since the TEX_{86} of SPM in the Amazon River was similar to that in the marine SPM and sediments.

5.1 INTRODUCTION

During the last decade, the implementation of high-performance liquid chromatography/mass spectrometry (HPLC/MS) has enabled the detection of structurally diverse intact glycerol dialkyl glycerol tetraethers (GDGTs) (see Schouten et al., 2013b for a review). The most commonly detected tetraether lipids in coastal marine sediments are branched and isoprenoid GDGTs (brGDGTs and isoGDGTs, respectively).

BrGDGTs are membrane-spanning lipids most likely of anaerobic (e.g. Weijers et al., 2006a, b) and heterotrophic (Pancost and Sinninghe Damsté, 2003; Oppermann et al., 2010) bacteria that are ubiquitous in peat (Weijers et al., 2006a) and soil (Weijers et al., 2007c). Recent studies indicate that some acidobacterial species produce brGDGT-Ia (Fig. 5.1) (Weijers et al., 2009a; Sinninghe Damsté et al., 2011), but the producers of other brGDGTs remain unknown. The brGDGTs vary in the degree of methylation (4–6) and may contain up to two cyclopentane moieties formed by internal cyclization (Sinninghe

Damsté et al., 2000; Weijers et al., 2006a) (Fig. 5.1). The distribution of the brGDGTs in soils, as expressed by the degree of methylation (methylation index of branched tetraethers; MBT) and cyclization (cyclization index of branched tetraethers; CBT) of the brGDGTs, correlates with mean annual air temperature (MAAT) and soil pH (Weijers et al., 2007c; Peterse et al., 2012). Hence, the MBT/CBT proxy has been used to reconstruct past environmental and climate changes in diverse settings: marine (e.g. Weijers et al., 2007c; Donders et al., 2009; Rueda et al., 2009; Bendle et al., 2010), and lacustrine (e.g. Tyler et al., 2010; Zink et al., 2010; Fawcett et al., 2011) sediments, peat (Ballantyne et al., 2010), and loess (Peterse et al., 2011b). Weijers et al. (2007a) applied the MBT/CBT proxy in Congo deep-sea fan sediments, assuming that brGDGTs were mainly produced in soils, washed into small streams and rivers by soil erosion, and further transported to the ocean. Since then it has been argued that the MBT/CBT paleothermometer of deep-sea fan sediments reflect an integrated environmental signal of the whole river basin. However, it has also been found that the brGDGT distributions in marine sediments might be altered by in-situ production and degradation processes in the marine environment (Peterse et al., 2009a; Zhu et al., 2011; Hu et al., 2012).

Following the successful use of the MBT/CBT proxy in the Congo deep-sea fan, Bendle et al. (2010) in turn applied it to the Amazon deep-sea fan sediments. In contrast to the findings of Weijers et al. (2007a), the reconstructed MAAT in the Amazon decreased from the glacial period (20-23°C) to the mid-Holocene (~10°C), increasing over the remainder of the Holocene to 17°C. It was postulated that an increased brGDGT contribution from the Andes region was responsible for the observed decrease of the reconstructed MAAT during the Holocene (Bendle et al., 2010). However, subsequent studies (Kim et al., 2012b; Zell et al., 2013b) have shown that the brGDGTs in the river suspended particulate matter (SPM) and riverbed sediments in the central Amazon basin do not predominantly originate from the high Andes soils (>2500 m in altitude). Zell et al. (2013a) found that the MBT/CBT-derived temperature from the lower Amazon River was about 2°C lower than that in surrounding soils. This difference was related to in-situ production in the river, but this can also only partially explain the ~10°C lower estimates of Holocene temperatures in Amazon deep-sea fan sediments (Bendle et al., 2010). This highlights the complex interplay between allochthonous and autochthonous sources of brGDGTs, and consequent impact on the MBT/CBT proxy, which can lead to large underestimations of MAAT (e.g. Tierney et al., 2010, Zink et al., 2010, Sun et al., 2011). Consequently, it is of particular importance to further characterize sources of brGDGTs on the Amazon shelf and deep-sea fan.

IsoGDGTs are membrane-spanning lipids mainly biosynthesized by Thaumarchaeota, formerly known as Group I Crenarchaeota (Brochier-Armanet et al., 2008; Spang et al., 2010). They are abundant in both marine environments (e.g. Schouten et al., 2002; Kim et al., 2010a) and lakes (e.g. Blaga et al., 2009; Sinninghe Damsté et al., 2009; Powers et al., 2010). There occur isoGDGTs containing 0 to 4 cyclopentane moieties, and there is crenarchaeol and its regio-isomer, which in addition to 4 cyclopentane

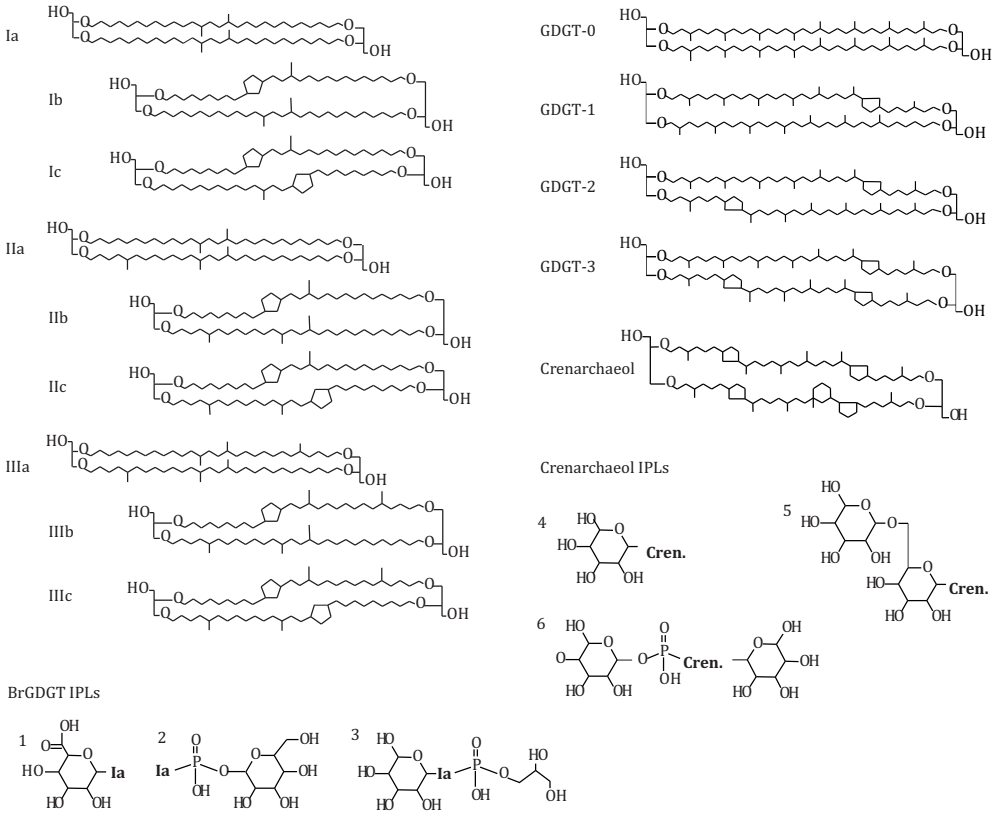

Fig. 5.1 Chemical structures of brGDGTs (Ia- IIIc) and isoGDGTs (1-3 and crenarchaeol) and the detected IPLs of brGDGT Ia and crenarchaeol in this study.

moieties contain a cyclohexane moiety (Schouten et al., 2000, 2008a; Sinninghe Damsté et al., 2002) (Fig. 5.1). Schouten et al. (2002) found that the number of cyclopentane moieties in marine sediments increased with increasing sea surface temperature (SST) and thus introduced the TEX_{86} (TetraEther indeX of tetraethers consisting of 86 carbon atoms) as a SST proxy. More recently, the TEX_{86} was refined as TEX_{86}^{H} for tropical and subtropical oceans (Kim et al., 2010a), and a new water-depth-integrated annual mean temperature calibration (0-200 m water depth) has been introduced (Kim et al., 2012b). Since isoGDGTs also occur in soil (Weijers et al., 2006b) and river SPM (e.g. Herfort et al., 2006; Kim et al., 2007) the distribution of isoGDGTs in marine sediments can be influenced by input of riverine isoGDGTs (Weijers et al., 2006b), presumably affecting the TEX_{86}^{H} proxy inference.

In this study, we compared the concentrations and distributions of brGDGTs and isoGDGTs in the Amazon shelf and deep-sea fan with those in the adjacent terrestrial Amazon basin in order to assess the impact of the brGDGT provenance on the application of the MBT/CBT proxy in this region. To identify the source of the GDGTs, we ex-

amined the presence of reported intact polar lipids (IPLs) of brGDGTs and crenarchaeol (Liu et al., 2010; Pitcher et al., 2010, 2011; Peterse et al., 2011a) as well as the concentrations and distributions of IPL-derived GDGTs as in the approach by Zell et al. (2013b). This study provides new insights on the interpretation of the GDGT-based sedimentary record of the Amazon River deep-sea fan and for other river systems.

5.2 STUDY AREA: THE AMAZON SHELF AND FAN

The Amazon River (Fig. 5.2A) is the largest drainage system in the world in terms of fresh-water discharge (Milliman and Meade, 1983) and catchment area (Goulding et al., 2003). The mean annual water discharge is 2 x 105 m^3 s^{-1} at Óbidos, the most downstream gauging station in the Amazon River (Callède et al., 2000). The Amazon River ranks second globally in terms of suspended sediment particle transport, with an annual mean sediment discharge of 8-12 x 10^{11} kg y^{-1} at Óbidos (Dunne et al., 1998). Once on the Amazon Shelf, the Amazon River plume is advected offshore and transported northwestward along the north Brazilian coast as it is entrained by the North Brazilian Current, covering most of the continental shelf from 1°S to 5°N (Muller-Karger et al., 1988). Average annual water temperature and salinity provides an idea about the extent of the Amazon River plume (Fig. 5.2B-C). Over the shelf, the Amazon freshwater plume is typically 3–10 m thick and between 80-200 km wide (Fig. 5.2C; Lentz and Limeburner, 1995). The Amazon shelf is strongly influenced by tidal currents with an extreme tidal range of 10 m at the mouth of the Amazon River (Gibbs, 1982). The flow of the Amazon River is so large that the estuary effectively extends across the entire inner shelf, in a band within 25 km off the river mouth. The estuarine-like circulation on the shelf allows high-salinity ocean water to penetrate underneath the low-salinity surface plume and prevents most riverine sediments from escaping off the shelf, causing a sediment deposition as a band of highly mobile, inner shelf muds extending 1600 km north-west and 50–150 km across the shelf (Nittrouer and DeMaster, 1986). Thus, the Amazon shelf is an area of active sediment deposition at an estimated rate of ~6 x 10^{11} kg y^{-1} (Kuehl et al., 1986).

The Amazon fan (or Amazon cone) is globally the third largest modern 'mud-rich' deep-sea fan and forms a significant proportion of the continental margin of Brazil (Damuth and Flood, 1985). The Amazon Fan extends downslope from the shelf break for ~700 km and exhibits an elongated radial pattern covering ~3.3 x 10^5 km^2. When sea-level was low during glacial periods, sediment eroded from the continent within the Amazon drainage basin was transported directly to the fan (Damuth and Kumar, 1975). In contrast, when sea-level was high during interglacial periods (such as today), the sediment load from the river was transported in long shore currents to the northwest and deposited on the continental shelf (Milliman et al., 1975; Nittrouer and DeMaster, 1986).

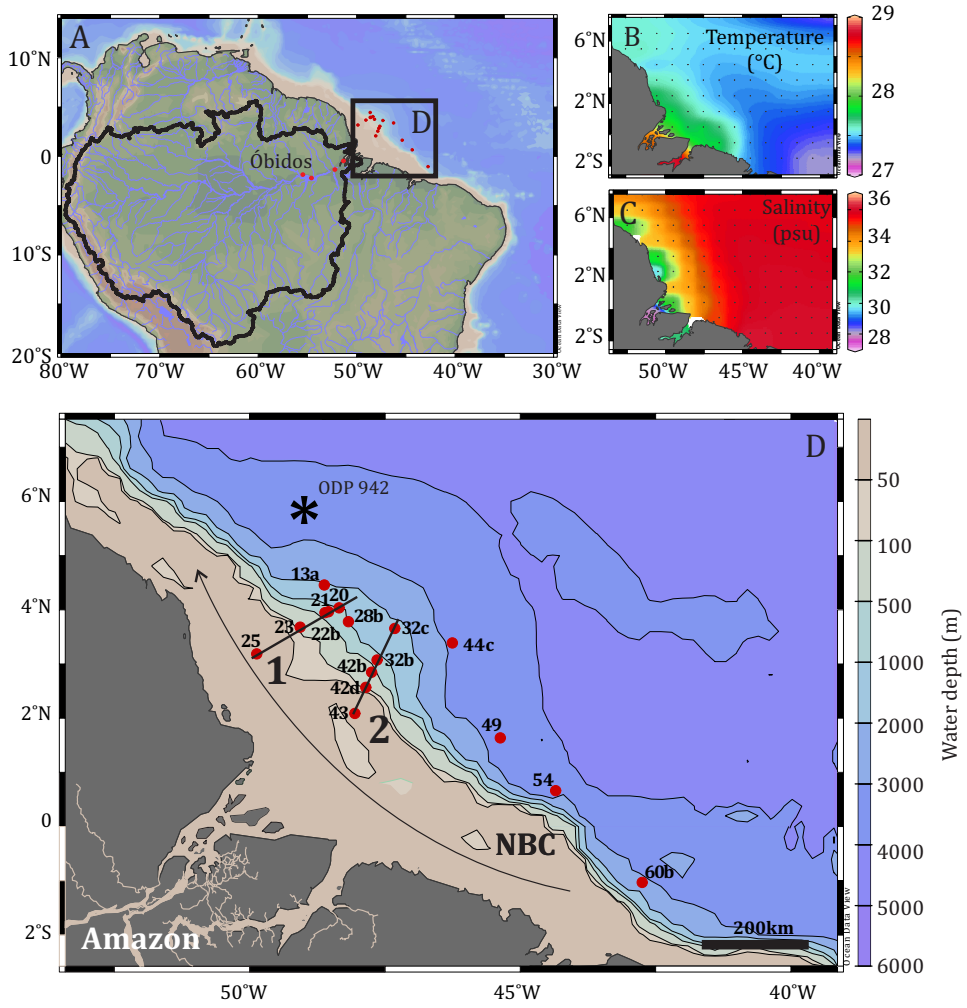

Fig. 5.2 (A) Map of the Amazon basin showing the Amazon watershed (back line) and the sampling stations (red dots). (B) Mean annual SST and (C) mean annual salinity in the western tropical Atlantic from the world ocean atlas 09 (WOA09) data set (Antonov et al., 2010; Locarnini et al., 2010). (D) Detailed view of the marine study area showing the sampling stations and indicating transects 1 and 2. NBC = North Brazilian Current.

5.3 MATERIALS AND METHODS

5.3.1 Sample collection

Marine SPM and surface sediments over the Amazon Shelf and slope were collected on board of the R/V Knorr 197-4 between February and March 2010 (Table 5.1). Sediment was collected at all stations, but SPM was only collected along the sampling stations of the two transects as indicated in Fig. 5.2D. SPM sampling was carried out at two water depths, at the chlorophyll maximum (chl_{max}) and close to the bottom. The

depth of the chl_{max} was determined with a fluorescence detector (Fluorescence, Wetlab ECO-AFL/FL). The water used to determine the SPM concentration and the total organic carbon (TOC) analysis of the SPM was collected with Niskin bottles. Between 1 and 26 L of this water were filtered onto ashed (450°C, overnight) and pre-weighed glass fibre filters (Whatman GF-F, 0.7 µm, 47 mm diameter). For the lipid analysis about 300 L of water were separately filtered onto ashed glass fibre filters with in-situ pumps (Whatman GF-F, 0.7 µm, 142 mm diameter, WTS, McLane Labs, Falmouth, MA). All samples were kept frozen at -20°C and freeze dried before analysis. Sediment cores were collected using a box corer from which the top 1 cm was subsampled.

River SPM was taken at Óbidos, which is the last gauging station in the Amazon River and located 800 km westwards from the Atlantic Ocean just beyond tidal influences. Four SPM samples were collected each of them at a different river water level: rising, high, falling and low water level (Zell et al, 2013b). In addition, three river-bed sediments were collected in 2010; one 26 km downstream from Óbidos and the other two close to the Amazon River mouth (Fig. 5.2A).

5.3.2 Environmental parameter and bulk geochemical analysis

The pH of the sediment samples was measured in a mixture of sediment and distilled water 1:3.5 (v:v). This water and sediment were stirred vigorously and left to settle for 20 min. The pH was measured with a Wissenschaftlich-Technische Werkstätten pH 315i/SET and probe pH-Electrode SenTix 41 (pH 0-14, T 0-80°C, stored in 3 mol L^{-1} KCl) at the Netherlands Institute for Sea Research (NIOZ). Before the pH measurements, the pH analyzer was calibrated with CertiPUR buffer solutions with pH 4.01, 7.00, and 10.00.

All sediment samples were freeze dried and decarbonated (using 2 mol L^{-1} HCl) prior to analyses. The marine SPM filters were also decarbonated using HCl vapor as described by Lorrain et al. (2003). The TOC contents of the marine sediments were analyzed with a Fison NA 1500 Elemental Analyzer at the University of South Florida (USF, USA). The analyses were determined in duplicates and the precision was 0.1 mg OC g^{-1}. Particulate organic carbon (POC) and TOC of Amazon River sediment were analyzed with a Thermo-Scientific Flash 2000 Elemental Analyzer at the NIOZ. The analyses were determined in duplicate and the precision was 0.2 mg OC g^{-1}.

5.3.3 Extraction and analysis of GDGTs

Extraction and analysis of core lipid (CL), IPL-derived GDGTs and IPLs were carried out in the same way as described by Zell et al. 2013b. Briefly, the freeze-dried samples were extracted with a modified Bligh and Dyer technique (Pitcher et al., 2009) and fractioned into CLs and IPLs (Oba et al., 2006; Pitcher et al., 2009). For GDGT quantification, 0.1 mg C_{46} GDGT internal standard was added (Huguet et al., 2006). Part of the IPL fraction was hydrolyzed to obtain IPL-derived CLs (Weijers et al., 2011a). The CL GDGTs were analyzed using high performance liquid chromatography atmospheric pressure

positive ion chemical ionization–mass spectrometry in selected ion monitoring mode (Schouten et al.; 2007).

For the analysis of IPLs in SPM samples and marine sediments four sampling stations (25, 28b, 42d, and 43, see Fig. 5.2D) were chosen. To analyze the brGDGT IPLs a selective reaction monitoring (SRM) method according to Peterse et al. (2011) was used. Crenarchaeol IPLs were detected by high-performance liquid chromatography–electrospray ionization–tandem mass spectrometry using an SRM method (Pitcher et al., 2011a).

5.3.4 Calculation of GDGT-based indices

In the following equations, the numerals refer to the GDGTs indicated in Fig. 5.1. The BIT (Branched and Isoprenoid Tetraether) index (Hopmans et al., 2004), the degree of cyclization (DC, Sinninghe Damsté et al., 2009), and the MBT and CBT values (Weijers et al., 2007c) were calculated as follows:

$$\text{BIT index} = ([Ia]+[IIa]+[IIIa])/([Ia]+[IIa]+[IIIa]+[IV]) \quad (1)$$

$$\text{DC} = ([Ib]+[IIb])/([Ia]+[Ib]+[IIa]+[IIb]) \quad (2)$$

$$\text{CBT} = -\log(([Ib]+[IIb])/([Ia]+[IIa])) \quad (3)$$

$$\text{MBT} = ([Ia]+[Ib]+[Ic])/([Ia]+[Ib]+[Ic]+[IIa]+[IIb]+[IIc]+[IIIa]+[IIIb]+[IIIc]) \quad (4)$$

For the calculation of pH and temperature, the regional soil calibration for the Amazon basin was used (Bendle et al., 2010):

$$\text{CBT} = 4.23 - 0.58 \times \text{pH} \ (r^2 = 0.75, n = 37) \quad (5)$$

$$\text{MBT} = 0.19 + 0.08 \times \text{CBT} + 0.03 \times \text{MAAT} \ (r^2 = 0.91, n = 37) \quad (6)$$

TEX_{86} was calculated according to Schouten et al. (2002). The TEX_{86} values were converted to temperatures using the global core-top calibrations for 0-200 m water depth (Kim et al., 2012b):

$$TEX_{86} = ([GDGT\text{-}2]+[GDGT\text{-}3]+[Cren'])/([GDGT\text{-}1]+[GDGT\text{-}2]+[GDGT\text{-}3]+[Cren']) \quad (7)$$

$$T\ (°C) = 54.7 \times \log(TEX_{86}) + 30.7 \ (r^2 = 0.84, n = 255, p < 0.0001) \quad (8)$$

Table 5.1 Amazon River and marine SPM and sediment samples studied and their general properties.

	Sampling date (dd/mm/yy)	Long.	Lat.	Sampling water depth (m)	Water temperature (°C)	MAAT 0-200 m (°C)[b]	pH	OC (wt. %)
Amazon River SPM								
CBM5 (high water)	03/07/09	55.47	1.97	surface	28.8	-	6.2	3.0
CBM6 (low water)	16/10/09	55.49	1.95	surface	31.0	-	6.8	3.3
CBM7 (falling water)	08/09/10	55.50	1.95	surface	30.5	-	7.0	3.0
CBM8 (rising water)	01/02/11	55.55	1.91	surface	28.7	-	6.8	1.0
Amazon River sediments								
AMAZA 26	-[a]	-54.25	-2.41	-	-	-	-	0.6
AMAZC RO11B	-	-51.01	-0.13	-	-	-	-	0.2
AMAZC RO3	-	-50.80	-0.95	-	-	-	-	0.6
Marine SPM								
13a	23/02/10	-48.61	4.46	1700	4.0	23.1	-	0.5
13a	23/02/10	-48.61	4.46	85	27.2	23.1	-	0.9
20	24/02/10	-48.35	4.04	1000	5.0	23.1	-	2.0
20	24/02/10	-48.35	4.04	75	27.5	23.1	-	5.2
21	25/02/10	-48.54	3.96	700	5.4	23.1	-	0.6
21	25/02/10	-48.54	3.96	85	27.8	23.1	-	6.0
22b	25/02/10	-48.61	3.95	600	5.9	23.1	-	2.8
22b	25/02/10	-48.61	3.95	89	27.7	23.1	-	16.3
23	25/02/10	-49.06	3.68	100	24.0	23.4	-	10.0
23	25/02/10	-49.06	3.68	75	27.9	23.4	-	13.7
25	26/02/10	-49.86	3.19	25	27.5	27.6	-	0.6
25	26/02/10	-49.86	3.19	5	28.7	27.6	-	4.3
28b	27/02/10	-48.17	3.78	990	5.0	23.1	-	0.6
28b	27/02/10	-48.17	3.78	100	27.4	23.1	-	0.5
32b	28/02/10	-47.64	3.07	1777	3.9	23.2	-	0.8
32b	28/02/10	-47.64	3.07	100	26.3	23.2	-	1.4
42b	02/03/10	-47.74	2.85	590	6.2	23.4	-	0.7
42b	02/03/10	-47.74	2.85	90	27.0	23.4	-	1.4
42c/d	03/03/10	-47.85	2.57	200	12.1	23.4	-	2.1
42c/d	03/03/10	-47.85	2.57	60	26.4	23.4	-	0.9
42d	03/03/10	-47.85	2.57	100	24.7	23.4	-	0.2
42d	03/03/10	-47.85	2.57	60	26.9	23.4	-	0.8
43	03/03/10	-48.05	2.09	55	27.5	26.7	-	0.7
43	03/03/10	-48.05	2.09	10	28.3	26.7	-	0.9
Marine surface sediments								
13a	23/02/10	-48.61	4.46	1711	-	23.1	7.9	0.9
20	24/02/10	-48.35	4.04	1088	-	23.1	7.9	1.1
21	25/02/10	-48.54	3.96	738	-	23.1	8.0	1.1
22b	25/02/10	-48.61	3.95	640	-	23.1	8.0	0.7
23	25/02/10	-49.06	3.68	107	-	23.4[c]	8.0	0.6
25	26/02/10	-49.86	3.19	32	-	27.6[c]	8.2	0.7
28b	27/02/10	-48.17	3.78	1014	-	23.1	8.0	1.0
32b (=42a)	28/02/10	-47.64	3.07	1028	-	23.2	7.9	0.7
32c	02/03/10	-47.31	3.65	2079	-	23.4	8.0	1.1
42b	02/03/10	-47.74	2.85	609	-	23.4	8.0	0.8
42d	03/03/10	-47.85	2.57	110	-	23.4[c]	9.0	0.1
43	03/03/10	-48.05	2.09	65	-	26.7[c]	8.9	0.0
44c	04/03/10	-46.25	3.39	3375	-	22.9	7.9	1.1
49	04/03/10	-45.36	1.64	-	-	22.8	8.1	1.4
54	07/03/10	-44.35	0.66	2372	-	23.1	8.1	0.3
60b	10/03/10	-42.74	-1.03	3113	-	23.2	7.9	1.0

[a] '-' = no data available

[b] Data from the world ocean atlas 09 (WOA09) data set (Locarnini et al., 2010)

[c] Depth integrated temperature for 0-100 m water depth

5.4 RESULTS

5.4.1 Amazon River SPM and sediments

The concentrations of brGDGTs in river SPM varied between 30 and 100 μg g_{OC}^{-1} (30 and 100 brGDGT ng L^{-1}) for the CL fraction and between 2 and 16 μg g_{OC}^{-1} (2 and 18 brGDGT ng L^{-1}) for the IPL fraction (Fig. 5.3A-B; Table 5.2). The IPL fraction was on average 12 % of the total amount of brGDGTs. In the river-bed sediments, the concentrations of CL brGDGTs were between 60 and 170 μg g_{OC}^{-1}, while the concentrations of IPL-derived brGDGTs were between 4 and 17 μg g_{OC}^{-1} (Table 5.2), which is on average 7 % of the total amount of brGDGTs . The distribution of brGDGTs in river SPM and sediments were similar (Fig. 5.4A). The most abundant brGDGT in both river SPM and sediments was brGDGT Ia, with an average of 75 % and 72 % of the total CL brGDGTs and the total IPL-derived brGDGTs, respectively. The MBT values of the river SPM and sediments varied between 0.80 and 0.86 in the CL brGDGTs, and between 0.77 and 0.09 in the IPL-derived brGDGTs (Fig. 5.5A). The DC values of river SPM and sediments were 0.06-0.11 in the CL brGDGTs and 0.05-0.13 in the IPL-derived brGDGTs (Fig. 5.5B). The CBT-derived pH of CL brGDGTs varied from 5.3 to 5.7 and from 5.1 to 5.9 in the IPL fraction (Fig. 5.5C). The MBT/CBT-derived MAAT ranged from 21 to 24°C in the CL brGDGTs and from 21 to 24°C in the IPL-derived brGDGTs (Fig. 5.5D).

The concentrations of isoGDGTs of river SPM were 34-99 μg g_{OC}^{-1} (27-76 ng L^{-1}) for the CL fraction and 5-15 μg g_{OC}-1 (4-11 ng L^{-1}) for the IPL fraction (Fig. 5.3C-D, Table 5.2). IPL-derived isoGDGTs represented on average 32 % of the total amount of isoGDGTs. River sediments contained 20-54 μg g_{OC}^{-1} of CL isoGDGTs and 13-30 μg g_{OC}^{-1} of IPL-derived isoGDGTs (Table 5.2). IPL-derived isoGDGTs represented on average 40 % of the total isoGDGTs. In the CL fraction of SPM the most dominant isoGDGT was crenarchaeol (Fig. 5.6A), representing 55 % of all isoGDGTs. In the sediments GDGT-0 was the most common isoGDGT (51 %) (Fig. 5.6A). GDGT-0 was also the most common isoGDGT in the IPL fraction of river SPM and sediments, representing 40 % and 71 % of all isoGDGTs, respectively. This results in a GDGT-0 to crenarchaeol ratio in river SPM and sediments varying between 0.2 and 2.3 in the CL isoGDGTs and between 1.0 and 12.6 in the IPL-derived isoGDGTs (Fig. 5.7A). The TEX_{86} values of CL and IPL-derived isoGDGTs were 0.64-0.74 and 0.66-0.83, respectively (Fig. 5.7B). The TEX_{86}-derived temperatures were 21-30°C for CL isoGDGTs and 29-32°C for IPL-derived isoGDGTs (Fig. 5.7C). The BIT of river SPM was between 0.4 and 0.9 in the CL fraction and between 0.3 and 0.7 in the IPL fraction (Fig. 5.7D), while the river sediments had an average BIT of 0.9 in the CL fraction and of 0.7 in the IPL fraction.

5.4.2 Marine SPM

From the sampling station closest to the river mouth (station 25; Fig. 5.2D), the brGDGT concentration in marine SPM decreased rapidly. In the bottom water SPM of station 25, the concentration of the CL brGDGTs was 28 μg g_{OC}^{-1} (2 μg L^{-1}), while the

concentration of the IPL-derived brGDGTs was 0.1 μg g_{OC}^{-1} (0.3 μg L^{-1}) (Fig. 5.3A-B, Table 5.2), comprising 0.3% of the total brGDGTs. At all other stations, the concentrations of the brGDGTs varied between 0 and 2 μg g_{OC}^{-1} (0-0.02 μg L^{-1}) for the CL fraction and 0 and 1.4 μg g_{OC}^{-1} (0-0.02 μg L^{-1}) for the IPL fraction, which comprised (Figs. 5.3A-B; Table 5.2), on average, 43 % of the total amount of brGDGTs present. As in the river SPM, brGDGT Ia was the most abundant brGDGT in marine SPM (Fig. 5.4B). However, relative abundance of brGDGT Ia in the marine SPM was more variable than in the river, accounting for 30-100 % of the total amount of the detected CL brGDGTs. MBT and DC could not be calculated for some of the SPM samples, as there was not sufficient material to detect all the brGDGTs required to calculate these indexes. This was especially the case for SPM from the chl_{max} (Table 5.2). For the samples in which the MBT and CBT were calculated, the MBT ranged from 0.28 to 0.94 in the CL brGDGTs, and from 0.77 to 0.96 in the IPL-derived brGDGTs (Fig. 5.5A). The DC varied between 0.03 and 0.38 in the CL fraction and between 0.03 and 0.4 in the IPL fraction (Fig. 5.5B). The CBT-derived pH varied from 4.6 to 8.3 in the CL brGDGTs and from 4.6 to 8.4 in the IPL-derived brGDGTs (Fig. 5.5C). The MBT/CBT-derived MAAT ranged from 17 to 28°C in the Cl brGDGTs and from 23 to 29°C in the IPL-derived brGDGTs (Fig. 5.5D).

The concentrations of CL isoGDGTs in marine SPM ranged from 3 to 160 μg g_{OC}^{-1} and those of the IPL-derived isoGDGTs from 1.8 to 82 μg g_{OC}^{-1} (Fig. 5.3C-D, Table 5.2). IPL-derived isoGDGTs comprised on average 34 % of the total amount of isoGDGTs. The concentrations were in the same range as the concentration in the river. However, the concentration per L was about 100 times higher in river SPM than in marine SPM (0.06 to 4 ng L^{-1} for the CL fraction and 0.03 to 1.7 ng L^{-1} for the IPL fraction). In the marine SPM, crenarchaeol was the most abundant isoGDGT (on average 56 % of the total amount of all CL isoGDGTs). The GDGT-0/crenarchaeol ratio varied between 0.1 and 0.6 in the CL fraction. In the IPL fraction, the variation was larger, with values varying between 0.1 and 3.0 (Fig. 5.7A). The TEX_{86} varied from 0.59 to 0.83 in the CL isoGDGTs and from 0.65 to 0.81 in the IPL-derived isoGDGTs (Fig. 5.7B). The TEX_{86}-derived temperatures were 18-26°C for CL isoGDGTs and 20-25°C for IPL-derived isoGDGTs (Fig. 5.7C). The BIT values in marine SPM were in general low with values of 0-0.1 in the CL fraction. Only in the SPM of the bottom water of station 25 the BIT was higher (0.41). The BIT in the IPL fraction varied between 0 and 0.53 (Fig. 5.7D).

5.4.3 Marine sediments

In the marine surface sediments the brGDGT concentrations varied between 2 and 74 μg g_{OC}^{-1} in the CL fraction and between 0.1 and 2.7 μg g_{OC}^{-1} in the IPL fraction (Fig. 5.3A-B, Table 5.2). IPL-derived brGDGTs represented on average 5 % of the total brGDGTs. The highest concentrations were found at stations 25 and 43, the two sampling stations closest to the Amazon River mouth (Fig. 5.2D). Surprisingly, high concentrations were also found at station 54. The distribution of brGDGTs varied widely (Fig. 5.4C); in general GDGT Ia was most abundant, but its relative abundance varied from

11 to 80 % in the CL brGDGTs and from 16 to 36 % in the IPL-derived brGDGTs (Table 5.2). The second most abundant brGDGTs was either IIa or IIIa. The MBT of the core-top sediments varied between 0.48 and 0.85 (CL brGDGTs) and between 0.35 and 0.81 (IPL-derived brGDGTs) (Fig. 5.5A). The DC was between 0.04 and 0.72 (CL brGDGTs) and between 0.13 and 0.55 (IPL-derived brGDGTs) (Fig. 5.5B). The highest values were found at the stations 42d and 43, where higher pH values (~9) were also measured than at other stations (~8) (Table 5.1). The CBT-derived pH varied from 4.9 to 8.0 in the CL brGDGTs and from 6.0 to 7.5 in the IPL-derived brGDGTs (Fig. 5.5C). The MBT/CBT-derived MAAT ranged from 12 to 23°C in the CL brGDGTs and from 6 to 23°C in the IPL-derived brGDGTs (Fig. 5.5D).

IsoGDGT concentrations in the marine surface sediments varied between 32 and 300 μg g_{OC}^{-1} for the CL fraction and between 5 and 65 μg g_{OC}^{-1} for the IPL fraction (Fig. 5.3C-D, Table 5.2). IPL-derived isoGDGTs represented 14 % of the total isoGDGTs. In marine sediments, the most common isoGDGT was also crenarchaeol (e.g. Fig. 5.6B) in both the CL fraction (52 %) and the IPL fraction (39 %). The ratio between crenarchaeol and GDGT-0 varied between 0.13 and 0.76 in the CL GDGTs and between 0.15 and 2.20 in the IPL derived GDGTs (Fig. 5.7A). The TEX_{86} varied between 0.6 and 0.74 in the CL isoGDGTs and between 0.5 and 0.79 in the IPL-derived isoGDGTs (Fig. 5.7B). The TEX_{86}-derived temperatures were 19-24°C for CL isoGDGTs and 14-25°C for IPL-derived isoGDGTs (Fig. 5.7C). Surprisingly, the highest BIT value of the CL GDGTs was found at station 54 with a BIT of 0.78 (0.20 for IPL-derived GDGTs) and not at station 25, which had a BIT of 0.37 (0.11 of IPL-derived isoGDGTs). At all other stations the BIT was lower, varying between 0.06 and 0.12 for CL GDGTs and between 0.01 and 0.07 for IPL-derived GDGTs (Fig. 5.7D).

5.4.4 IPL GDGTs

Chl_{max} and bottom water SPM and marine sediments from four stations (25, 28b, 42d, and 43) were analyzed for intact IPLs. BrGDGTs with polar head-groups were only detected at stations 25 and 42d. The detected brGDGT IPLs were glyconyl-brGDGT I (1, numerals refer to Fig. 5.1), phosphohexose-brGDGT I (2), and hexose-phosphoglycerol-brGDGT I (3). All three brGDGT IPLs were found in the sediment of station 25. In the bottom SPM IPLs 2 and 3 were found, while at the chl_{max} compound 1 was detected. At station 42d the sediment contained compound 2 and 3, while the SPM contained compound 1. Crenarchaeol IPLs were detected in SPM and sediments of all four tested stations. The following crenarchaeol-derived IPLs were detected: crenarchaeol-monohexose (4), crenarchaeol-dihexose (5), and crenarchaeol-hexose-phosphohexose (6). The relative amount of the respective IPLs is reported in Table 5.3.

Table 5.2 Concentrations of brGDGTs and isoGDGTs normalized to OC.

	brGDGTs																		isoGDGTsb											
	CL (μg g_{oc}^{-1})									IPL-derived (μg g_{oc}^{-1})									CL (μg g_{oc}^{-1})						IPL-derived (μg g_{oc}^{-1})					
	Ia	Ib	Ic	IIa	IIb	IIc	IIIa	IIIb	IIIc	Ia	Ib	Ic	IIa	IIb	IIc	IIIa	IIIb	IIIc	0	1	2	3	Cren	Cren'	0	1	2	3	Cren	Cren'
Amazon River SPM																														
CBM5	78.4	4.5	1.6	12.6	1.6	0.2	0.7	0.2	-a	13.8	1.0	0.1	2.6	0.4	-	-	-	-	15.2	2.0	1.8	1.4	12.6	0.3	19.3	2.2	2.0	2.5	6.8	-
CBM6	22.1	2.2	0.8	4.1	0.7	-	0.4	-	-	1.6	0.3	0.1	0.5	-	-	0.1	-	-	7.9	3.5	4.5	4.1	38.7	1.2	5.0	0.9	1.7	2.7	4.7	-
CBM7	82.0	5.3	1.9	11.8	1.8	0.3	1.1	-	-	5.9	0.5	0.2	1.2	0.2	-	0.1	-	-	18.7	6.1	6.4	5.1	62.4	1.2	14.3	2.9	4.1	5.8	14.8	1.7
CBM8	49.6	5.1	1.7	10.7	2.2	0.4	1.0	-	-	11.5	0.6	0.2	1.2	0.2	-	0.1	-	-	11.0	2.8	3.3	2.9	28.6	0.8	8.1	1.4	2.0	2.8	6.7	1.1
Amazon River sediments																														
AMAZA 26	122.5	13.3	4.0	22.6	3.7	0.6	1.2	-	-	3.7	0.4	0.2	0.5	0.1	-	-	-	-	30.1	3.7	3.8	2.9	13.0	0.5	28.1	2.7	2.1	2.3	2.7	0.4
AMAZC RO11B	48.1	4.8	1.7	7.2	1.1	0.2	0.3	-	-	12.3	1.7	0.5	2.5	0.4	0.1	0.1	-	-	8.8	1.3	1.5	1.2	7.0	0.2	8.4	0.8	0.8	1.0	1.8	0.3
AMAZC RO3	72.2	7.9	2.4	13.8	2.4	0.3	0.8	-	-	2.8	0.4	0.1	0.7	0.1	0.0	0.1	-	-	23.6	3.0	3.5	3.2	10.1	0.4	23.3	1.7	1.4	1.6	1.9	0.3
Marine SPM																														
13a bottom	1.0	0.1	-	0.2	0.1	-	0.2	-	-	0.2	0.02	-	0.04	-	-	0.01	-	-	9.9	3.1	3.3	0.5	18.7	1.3	2.6	1.0	1.4	0.2	2.1	0.3
13a chlmax	-	-	-	-	-	-	-	-	-	0.1	-	-	-	-	-	-	-	-	1.3	0.9	2.4	0.9	10.4	0.8	1.2	0.7	1.5	0.8	6.0	0.6
20 bottom	1.0	0.03	0.02	0.1	-	-	0.01	-	-	1.1	0.1	0.03	0.2	-	-	0.1	-	-	4.7	1.8	1.9	0.2	8.9	0.7	2.1	0.5	0.3	-	0.9	0.3
20 chlmax	0.01	-	-	-	-	-	-	-	-	0.1	-	-	-	-	-	-	-	-	0.4	0.3	0.3	0.1	2.3	0.1	0.5	0.3	0.3	0.2	1.4	0.2
21 bottom	0.6	0.1	-	0.1	-	-	0.1	-	-	0.9	0.1	0.1	0.2	-	-	-	-	-	27.4	9.4	10.2	1.0	45.4	3.7	6.3	2.6	4.2	0.1	3.8	1.5
21 chlmax	0.2	0.02	-	0.04	-	-	-	-	-	0.1	-	-	-	-	-	-	-	-	3.9	2.2	2.4	1.1	20.2	1.2	4.7	3.3	3.7	2.2	28.1	2.3
22b bottom	0.04	-	-	-	-	-	0.1	-	-	0.1	-	-	-	-	-	-	-	-	3.1	1.1	1.2	0.1	5.3	0.4	2.0	1.0	1.7	0.05	1.6	-
22b chlmax	0.2	0.02	0.01	0.03	-	-	-	-	-	-	-	-	-	-	-	-	-	-	1.0	0.6	0.6	0.2	5.0	0.3	1.8	1.3	1.6	0.9	9.4	0.9
23 bottom	0.1	0.03	-	-	-	-	0.1	-	-	0.4	-	-	0.1	-	-	-	-	-	14.7	7.4	10.4	5.2	49.7	3.3	15.1	6.0	7.8	4.4	38.2	5.2
23 chlmax	0.02	-	-	-	-	-	-	-	-	0.02	-	-	-	-	-	-	-	-	0.3	0.3	0.5	0.3	2.7	0.1	0.2	0.1	0.2	0.1	1.0	0.1
25 bottom	18.6	3.5	1.6	3.8	0.8	0.2	0.3	-	-	0.02	-	-	-	-	-	-	-	-	7.5	2.8	3.8	2.2	33.1	1.2	5.8	1.5	2.1	1.6	12.0	1.6
25 chlmax	0.7	0.1	0.1	0.2	0.04	-	0.01	-	-	0.1	0.04	0.02	-	-	-	-	-	-	1.6	0.9	1.9	0.6	12.6	0.3	0.5	0.3	0.7	0.3	3.4	-
28b bottom	0.3	0.03	-	0.1	-	-	0.1	-	-	-	-	-	-	-	-	-	-	-	18.2	5.1	5.0	0.8	31.3	2.1	5.8	2.5	4.8	0.01	2.0	1.2
28b chlmax	0.04	-	-	-	-	-	-	-	-	0.1	-	-	-	-	-	-	-	-	4.5	2.4	4.8	2.0	22.7	2.2	8.0	4.4	5.9	2.8	37.1	2.5
32b bottom	0.2	-	-	0.1	-	-	0.3	-	-	0.4	-	-	-	-	-	-	-	-	12.3	4.7	4.6	0.5	22.3	1.7	6.0	3.4	5.9	0.3	5.0	-
32b chlmax	0.02	-	-	-	-	-	-	-	-	0.03	-	-	-	-	-	-	-	-	1.4	0.8	1.1	0.4	6.7	0.4	0.9	0.5	0.5	0.3	3.7	0.3
42b bottom	0.8	0.1	0.03	0.2	0.03	-	0.2	-	-	0.2	-	-	-	-	-	-	-	-	22.7	7.6	8.3	0.8	36.8	3.0	20.2	8.8	13.0	0.5	14.5	5.0
42b chlmax	0.1	-	-	-	-	-	-	-	-	0.1	-	-	-	-	-	-	-	-	1.7	0.8	1.2	0.3	7.2	0.5	1.4	0.8	1.0	0.5	5.8	0.5
42c/d bottom	0.1	-	-	0.03	-	0.04	0.2	-	-	0.1	-	-	-	-	-	-	-	-	10.0	3.7	5.4	0.8	23.4	2.4	7.3	2.8	6.2	0.6	9.4	5.1
42c/d chlmax	0.1	-	-	-	-	-	-	-	-	0.1	-	-	-	-	-	-	-	-	0.9	0.5	0.9	0.4	4.7	0.3	0.4	0.3	0.6	0.2	2.4	0.2
42d bottom	0.1	0.04	-	-	-	-	0.02	-	-	0.04	-	-	-	-	-	-	-	-	12.6	8.1	12.5	8.2	63.7	3.3	7.8	3.7	4.3	2.9	24.6	2.2
42d chlmax	-	-	-	-	-	-	-	-	-	0.03	-	-	-	-	-	-	-	-	0.3	0.2	0.4	0.2	2.1	0.1	0.2	0.1	0.2	0.1	0.8	0.1
43 bottom	0.2	0.2	0.1	0.2	0.1	0.04	0.1	-	-	0.1	0.04	0.03	-	-	-	-	-	-	2.1	1.7	3.2	2.4	24.2	0.7	0.7	0.5	0.7	0.5	3.9	-
43 chlmax	0.4	0.3	0.4	0.2	0.1	0.1	0.2	-	-	0.1	0.04	0.03	-	-	-	-	-	-	6.6	6.0	10.2	7.7	69.8	2.1	1.8	1.1	1.8	1.6	14.4	0.6

Cotinuation of Table 5.2 Concentrations of brGDGTs and isoGDGTs normalized to OC.

	brGDGTs																		isoGDGTsb											
	CL ($\mu g\ g_{oc}^{-1}$)									IPL-derived ($\mu g\ g_{oc}^{-1}$)									CL ($\mu g\ g_{oc}^{-1}$)						IPL-derived ($\mu g\ g_{oc}^{-1}$)					
	Ia	Ib	Ic	IIa	IIb	IIc	IIIa	IIIb	IIIc	Ia	Ib	Ic	IIa	IIb	IIc	IIIa	IIIb	IIIc	0	1	2	3	Cren	Cren'	0	1	2	3	Cren	Cren'
Marine surface sediments																														
13a	3.9	0.4	0.1	0.9	0.4	0.1	0.7	0.1	0.02	0.1	0.02	0.01	0.1	0.03	0.02	0.04	0.01	-	28.7	7.8	8.6	1.5	46.7	4.1	3.4	0.6	0.6	0.2	3.2	0.2
20	2.9	0.2	0.1	0.6	0.2	0.1	0.3	0.1	0.01	0.02	0.01	0.01	0.03	0.02	0.01	0.01	0.01	-	16.4	4.6	4.9	0.8	27.8	2.4	4.7	0.8	0.7	0.2	3.3	0.2
21	2.9	0.2	0.1	0.6	0.2	0.1	0.2	0.02	-	0.1	0.01	-	0.1	0.01	0.01	0.02	-	-	19.6	5.6	6.2	1.0	40.0	2.8	3.5	0.6	0.5	0.2	2.8	0.2
22b	6.0	0.5	0.2	1.3	0.5	0.1	0.4	0.1	-	0.3	0.1	0.02	0.2	0.1	0.03	0.03	-	-	35.1	10.4	11.4	2.0	53.3	5.0	7.9	1.3	1.1	0.3	6.6	0.4
23	3.7	0.3	0.1	1.0	0.2	0.1	1.6	0.1	-	0.3	0.1	0.02	0.1	0.03	-	0.1	0.01	-	43.9	10.9	11.0	1.5	74.6	4.8	8.5	0.8	0.8	0.2	4.9	0.4
25	46.5	9.1	4.3	10.8	2.0	0.4	0.6	0.1	-	1.6	0.3	0.1	0.3	0.1	0.02	0.02	-	-	13.2	4.3	6.2	3.8	56.2	2.4	6.8	1.4	2.2	1.6	15.0	1.4
28b	4.4	0.3	0.1	0.8	0.3	0.1	0.4	-	-	0.2	0.02	0.01	0.04	0.02	-	0.02	-	-	38.7	10.2	11.2	1.6	74.7	5.0	10.8	1.5	1.3	0.3	7.2	0.4
32c	2.3	0.2	0.1	0.5	0.2	0.1	0.5	0.03	0.01	0.1	0.01	0.01	0.1	0.02	-	0.02	-	-	25.7	7.3	8.2	1.2	48.3	3.8	4.3	0.5	0.5	0.1	2.8	0.2
32b	3.1	0.2	0.1	0.6	0.2	0.1	0.4	0.04	-	0.1	0.01	0.01	0.04	0.01	-	0.02	-	-	18.8	4.8	5.3	0.8	37.4	2.4	3.3	0.5	0.4	0.1	2.7	0.2
42b	17.6	1.1	0.4	3.0	0.8	0.2	0.6	0.1	-	0.4	0.1	0.02	0.2	0.1	0.03	0.02	-	-	17.4	4.3	4.6	1.0	35.1	2.2	7.7	1.2	0.8	0.3	5.6	0.3
42d	0.7	1.7	1.4	0.4	1.0	0.2	0.04	-	-	0.1	0.2	0.2	0.04	0.1	-	0.03	-	-	10.5	5.7	7.3	4.2	54.9	2.4	3.6	2.1	3.1	2.1	24.2	-
43	13.7	6.6	6.0	9.0	3.6	1.4	4.0	-	-	1.4	0.2	0.2	0.6	0.2	0.01	0.2	-	-	26.8	15.9	22.8	16.0	211.5	6.7	8.5	3.4	5.1	3.4	42.2	2.5
44c	3.5	0.3	0.1	1.0	0.2	0.1	1.7	0.1	-	0.1	0.02	-	0.1	0.02	0.01	0.1	-	-	37.4	10.0	10.1	1.4	71.3	4.8	6.5	0.7	0.8	0.2	4.6	0.4
49	0.6	0.1	0.02	0.2	0.1	0.02	0.4	0.03	-	0.03	0.01	-	0.01	0.01	-	0.01	-	-	14.6	3.7	3.7	0.5	24.3	1.5	3.9	0.4	0.3	0.1	2.1	0.1
54	61.4	1.9	0.5	8.2	0.9	0.2	1.7	0.2	0.1	0.2	0.03	0.01	0.2	0.1	0.03	0.2	-	-	12.0	2.1	1.9	0.3	15.7	0.8	3.4	0.3	0.2	0.1	1.5	0.1
60b	2.9	0.2	0.1	0.7	0.1	0.1	0.9	0.1	-	0.1	0.01	0.01	0.02	0.02	-	0.02	-	-	28.0	7.3	7.5	1.0	50.6	3.1	7.8	0.9	0.8	0.2	4.1	0.4

a "-" = below detection limit

b isoGDGT 0-3 refere to GDGT-0 to GDGT-3 in Fig. 1

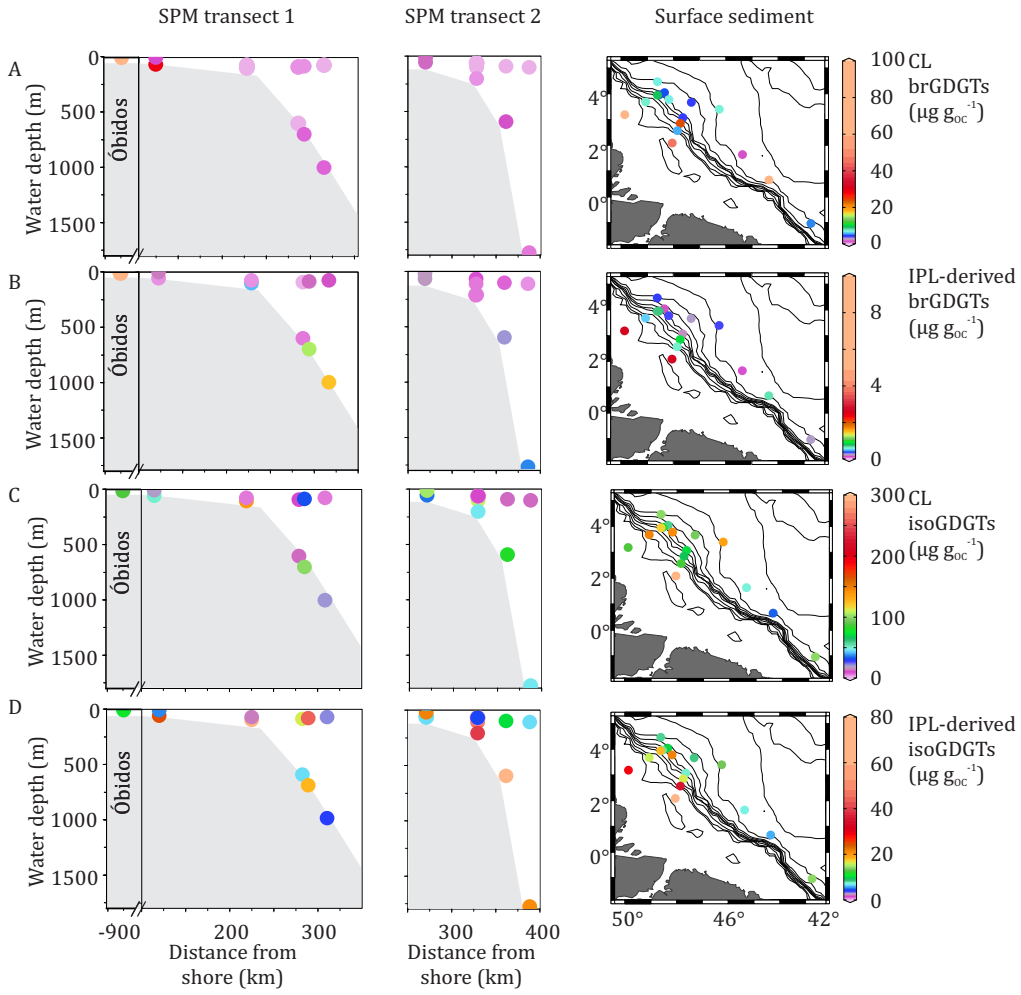

Fig. 5.3 CL and IPL-derived brGDGT concentrations (A, B) and CL and IPL-derived isoGDGT concentrations (C, D) in riverine and marine SPM (transects 1 and 2; see Fig. 2D) and in marine surface sediments.

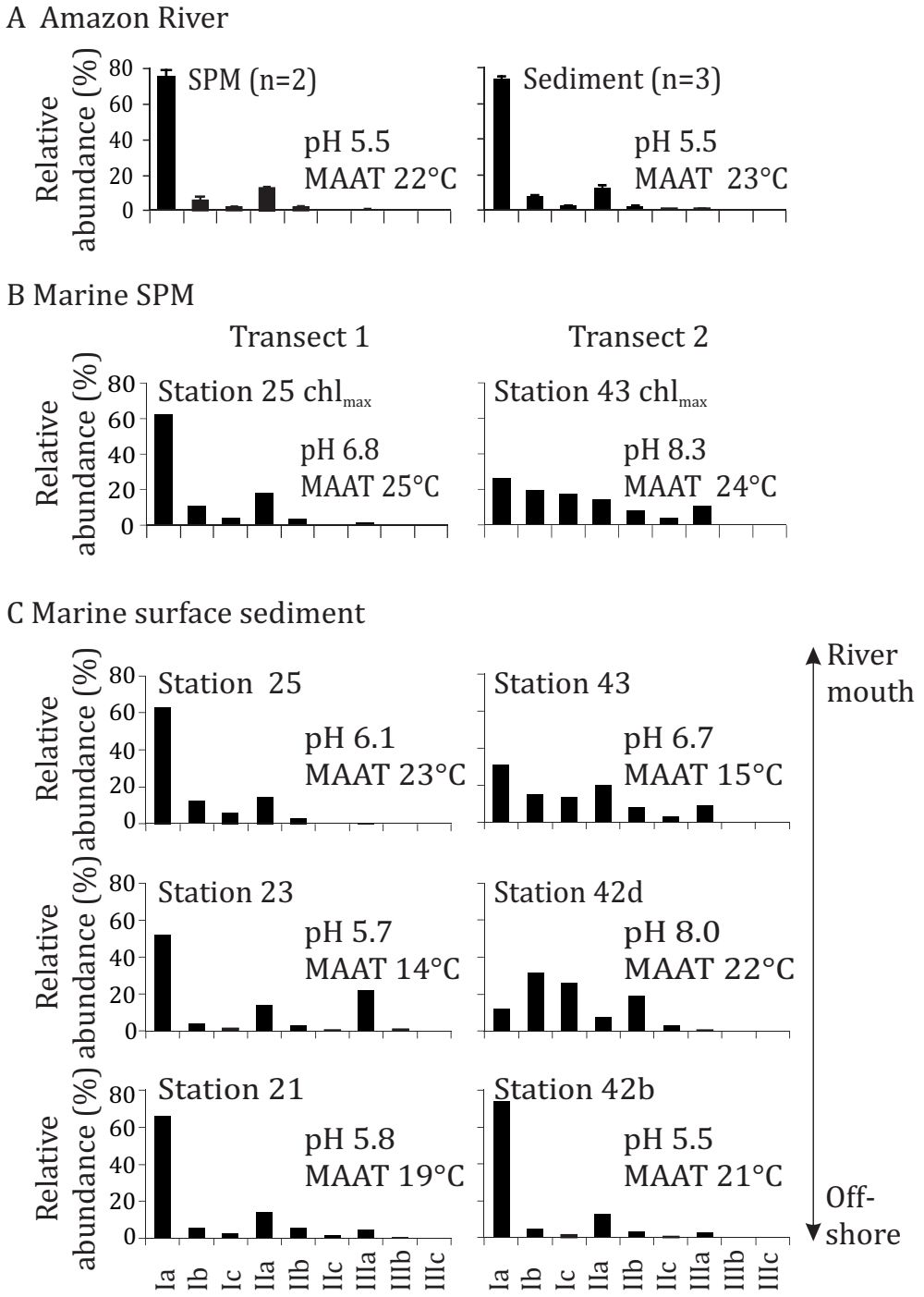

Fig. 5.4 Average CL brGDGT distribution in (A) Amazon River SPM and sediments and in (B) marine SPM and (C) surface sediments from 3 stations closest to the shore from the two studied transects (Fig. 2D). Also indicated are the respective CBT-derived pH and MBT/CBT-derived MAAT values. Vertical bars indicate the standard deviation (1δ).

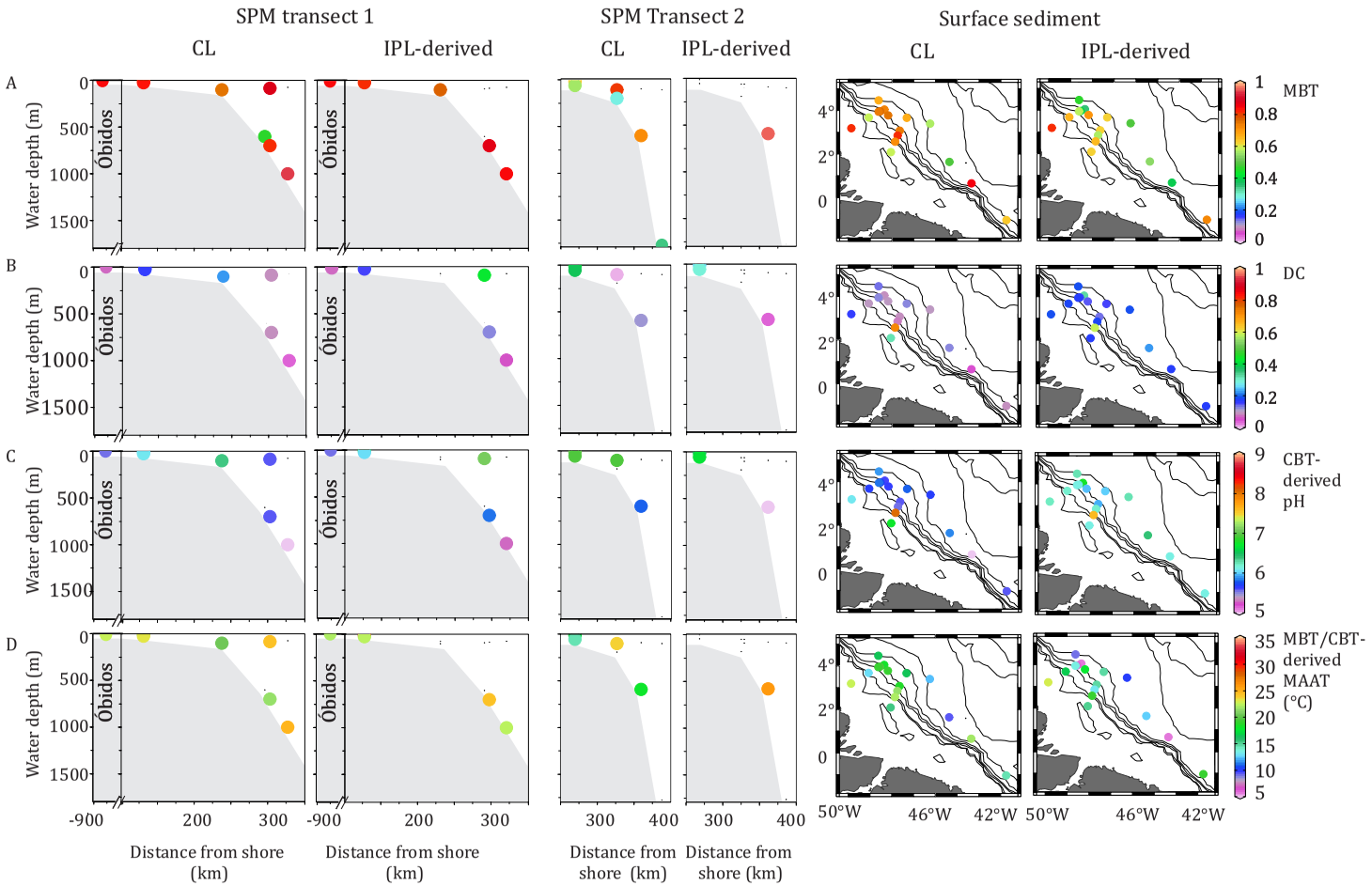

Fig. 5.5 MBT (A), DC (B), and CBT-derived pH (C), and MBT/CBT-derived MAAT values (D) in riverine and marine SPM (transects 1 and 2; Fig. 2D) and in marine surface sediments.

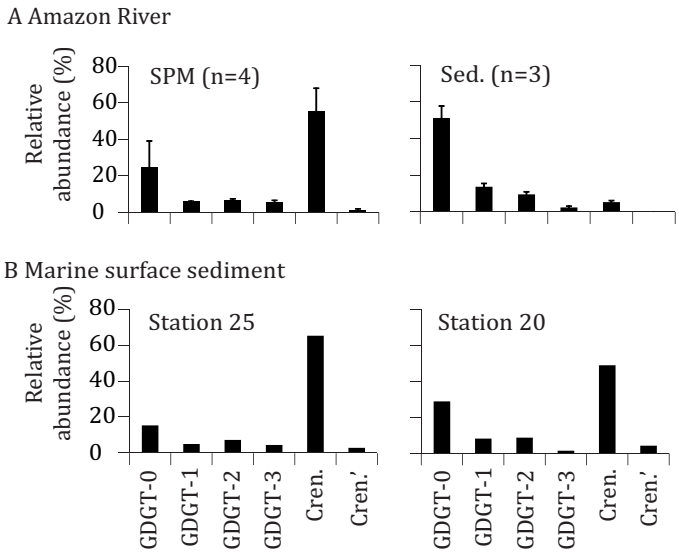

Fig. 5.6 Average CL isoGDGT distribution in (A) Amazon River SPM and sediment, and in two two marine surface sediment (B). Vertical bars indicate the standard deviation (1δ).

5.5 DISCUSSION

5.5.1 Origin of brGDGTs on the Amazon shelf and in the Amazon fan

It has been assumed that the brGDGTs in marine sediments are mainly derived from erosion of soils and are transported through rivers to the coastal marine environment (Weijers et al., 2007a). Hence, it is expected that the highest concentrations of brGDGTs normalized to OC are to be found in the river and close to the river mouth and then should decrease gradually offshore until brGDGTs can no longer be detected (cf. Hopmans et al., 2004). It is also anticipated that the distribution of the nine brGDGTs derived from soil is preserved in coastal marine sediments, without a substantial alteration of the brGDGT distribution (Weijers et al., 2007a). Zell et al. (2013b) examined the distribution of brGDGTs in 'terra firme' soils from the Amazon watershed and compared it against brGDGTs in river SPM. They found that the brGDGT distribution in river SPM was slightly different from that in the lowland soils, most likely due to additional in-situ production of brGDGTs within the Amazon River. In the present study, we concentrate on examining the second step: the delivery of brGDGTs to the ocean by the Amazon River.

The concentrations of the CL brGDGTs normalized to OC in Amazon River SPM and Amazon sediment (Table 5.2) and the distributions of CL brGDGTs in river SPM and sediments were similar (Fig. 5.4A). That the distributions were similar is also apparent from the fact that these samples plot close vicinity to each other in a brGDGT "prov-

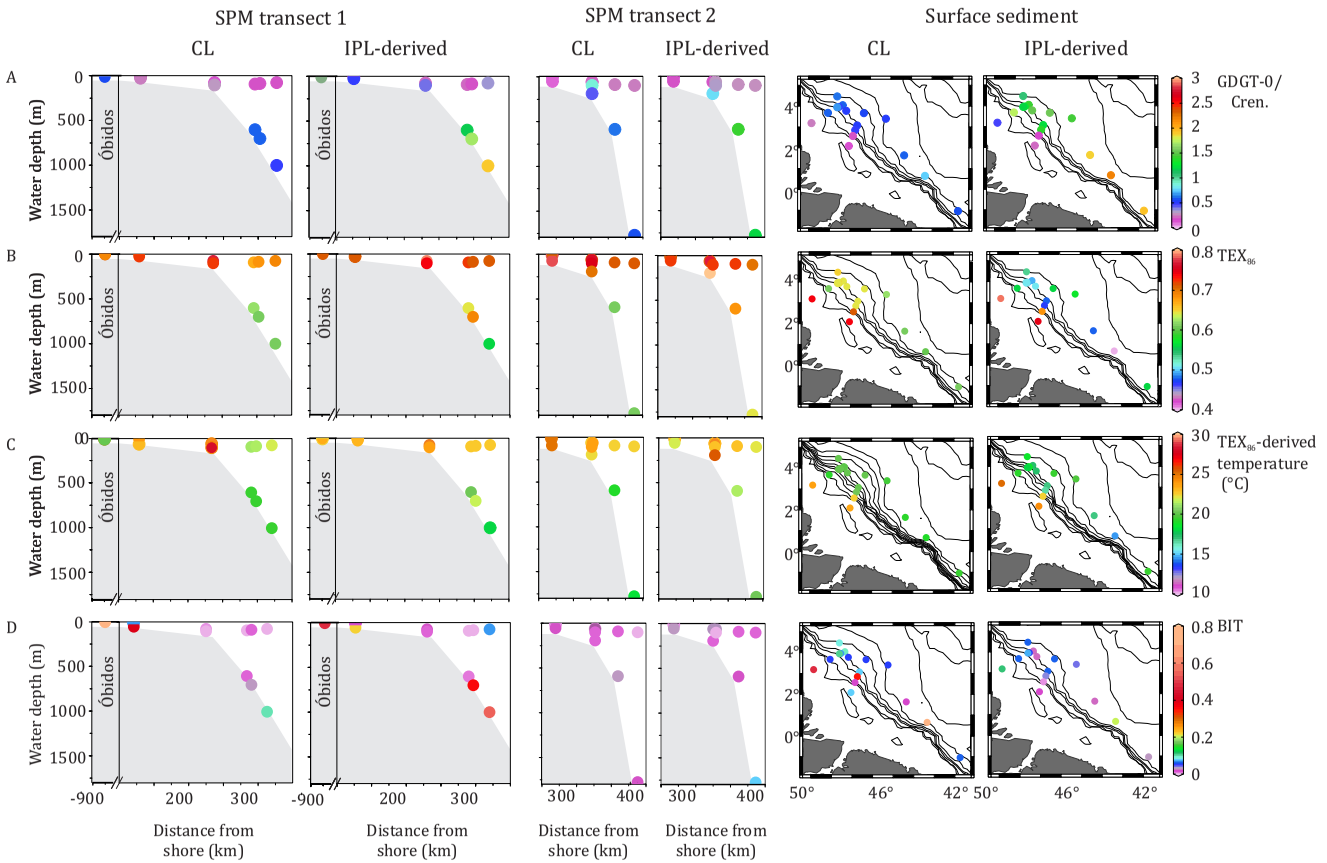

Fig. 5.7 GDGT-0/crenarchaeol ratio (A), TEX_{86} values (B), TEX_{86}-derived temperature (C) , and BIT index values (D) in riverine and marine SPM (transects 1 and 2; Fig. 2D) and in marine surface sediments.

enance plot" (i.e. a plot of DC vs. MBT, Fig. 5.8A; cf. Sinninghe Damsté et al., 2009). The distribution (Fig. 5.8A) and the average percentage of IPL-derived brGDGTs (11 % and 7 %, respectively) were also similar in the Amazon River SPM and sediment. Since the SPM and one riverbed sediment were collected close to the town of Óbidos and the two other riverbed sediments were collected farther downstream (Fig. 5.2A), our results also show that there is no alteration of the brGDGTs between Óbidos and shortly before the river mouth.

On the Amazon shelf, station 25 is the station that was mostly strongly influences by the Amazon River water, because of the NW deflection of the river plume caused by the North Brazilian Current (Fig. 5.2D). The CL brGDGT concentration in the surface waters at station 25 was lower than in the deeper waters (Fig. 5.3A, Table 5.2), but at both depths in station 25 the CL brGDGT distribution was similar to that of Amazon River SPM (Fig. 5.8A). The marine SPM at the other sites had 50 to 1000 times lower CL brGDGT concentrations (normalized to OC) and most of them had a different CL brGDGT distribution than the river SPM (Fig. 5.8A). The MBT of most marine SPM was lower than that in the Amazon River (Fig. 5.8A). The DC of marine SPM was variable but relatively high (>~0.3) at stations 28b, 42d, and 43 (Fig. 5.8A) compared to the other stations. Station 43 is the station of transect 2 which is closest to the shore (Fig. 5.2D), but clearly showed a much higher DC in both chl_{max} and bottom water SPM compared to the DC of CL brGDGTs in the Amazon River (Figs. 5.4, 5.5A-B, 5.8A). Only four SPM samples contained sufficient IPL-derived brGDGTs (stations 13, 20, 21, and 25) to determine the MBT and DC. In contrast to CL brGDGTs, they showed MBT and DC values similar to those found in the Amazon River (Fig. 5.8A).

Similar observations were made for the marine surface sediment; the sediments from the two stations closest to the river mouth (stations 25 and 43; Fig. 5.2D) had high CL brGDGT concentrations normalized to OC compared to those of the other stations (Fig. 5.3A). Of these two stations only the brGDGT distribution at station 25 was similar to that of the Amazon River (Fig. 5.8A). Station 54 also had a surprisingly high CL brGDGT concentration (Fig. 5.3A) and a MBT and DC similar to that of the Amazon River (Fig. 5.8A), even though it is unlikely that it is influenced by the Amazon River since the ocean current flows northwards (Fig. 5.2). We assume that this station receives brGDGTs from the Bacanga River, a river southeast of the Amazon basin, which enters the ocean at the city of São Luis (S 2.5°, W 44.3°) and probably delivers brGDGTs to the ocean with a distribution that is comparable to that found in SPM of the Amazon River. In the other marine sediments the CL brGDGT concentration was lower (Fig. 5.3A) and the distribution of CL brGDGTs varied strongly (Fig. 5.4C), resulting in substantial differences in MBT and DC values (Figs. 5.5A, 5.8A). The sediment of the shelf stations 43 and 42d were special as they exhibited exceptionally high DC values (Fig. 5.8A). Almost all sediments had a lower MBT compared to the Amazon River. The MBT showed a tendency to decrease with increasing water depth (Fig. 5.8B). Changes in DC and MBT were also evident in the IPL-derived brGDGTs. Their DC values were generally slightly higher than those of

the CL brGDGTs (Fig. 5.8A). However, only one of the two stations (i.e. 42d) which were characterized by substantially higher DC values in the CL brGDGTs also showed a higher DC in the IPL-derived GDGTs (Fig. 5.8A). MBT values of IPL-derived brGDGTs were generally lower and more variable. No decrease with water depth was apparent (Fig. 5.8B). A ternary plot showing the relative abundance of the various groups of brGDGTs (Fig. 5.9A) reveals that in most SPM and surface sediments lower MBT values for CL brGDGTs are due to higher relative amounts of II(a-c) and III(a-c). The same can be seen in the IPL-derived brGDGTs (Fig. 5.9B), but in the IPL-derived brGDGTs the fraction of brGDGT II(a-c) varies to a larger extent than the CL brGDGT III(a-c).

Our results show that there are major changes in the brGDGT distribution from the Amazon River to marine SPM and sediment and also within the marine environment. This is most likely caused by selective degradation processes of brGDGTs derived from the terrestrial environment or by in-situ production of brGDGTs in the marine environment, or both. Furthermore, seasonal variations in hydrodynamics in the river catchments (Zell et al., 2013a) or, perhaps, input by eolian transport (Fietz et al., 2013) might play a role in altering the riverine brGDGT signals in marine settings. Intensive degradation of organic compounds take place on the Amazon shelf where it was previously shown that 55-70 % of the POC flux from the Amazon River is decomposed or otherwise lost before being buried in sediments (Aller et al., 1996). Long residence times of organic-rich particulates in deltaic "fluid muds" underlying oxygenated water makes the Amazon shelf region relatively inefficient for organic carbon preservation (Blair and Aller, 2012). Oxic degradation might presumably affect the brGDGTs, but the brGDGT delivered from the river should have been affected in a similar way. Therefore, it seems unlikely that the large differences of the brGDGT distributions between marine surface sediments and SPM can be explained solely by microbial degradation. Hydrodynamic processes in the Amazon Basin slightly altered brGDGT distributions of the Amazon River SPM (Zell et al., 2013a). However, the riverine brGDGT data obtained at the Óbidos station, the last gauging station in the Amazon River, very closely clustered together, separated from those of the most of the marine SPM and sediments. Therefore, it is unlikely that hydrodynamic processes occurred in the Amazon basin are solely responsible for variable distributions of brGDGTs observed in the Amazon shelf and fan. Recently, Fietz et al. (2013) showed that atmospheric dust samples collected off northwest Africa contained brGDGTs and thus an eolian input of brGDGTs might also influence brGDGT signals, especially in remote open ocean settings. However, the eolian input of brGDGTs is also unlikely due to the heterogeneous distribution of brGDGTs observed in coastal marine SPM and sediments in our study area.

In-situ production of brGDGTs in the marine environment is an alternative explanation. Marine in-situ production of brGDGTs has previously been proposed in coastal sediments of Svalbard (Peterse et al., 2009a), in East China Sea shelf sediments (Zhu et al., 2011), and in hydrothermal vents in the south Pacific Ocean (Hu et al., 2012). A higher amount of cyclic brGDGTs, similar to what we observed in SPM and sediment of

the Amazon shelf, was observed in the coastal sediments of Svalbard and East China Sea shelf sediments. However, Zhu et al (2011) reported that the MBT increased from the Yangtze River sediment to coastal sediment, which is opposite the trend we observe for the Amazon system.

In order to investigate whether marine in-situ production causes the difference between the brGDGT distributions in the Amazon River, compared to that in the marine environment, we analyzed IPL-derived brGDGTs. IPL-derived brGDGTs are more labile compared to CL brGDGTs, since the polar head group of IPL brGDGTs is lost relatively fast (within days) after cell death (Harvey et al., 1986, Logemann et al., 2011). Therefore, IPL-derived GDGTs are considered to represent the more recently produced, 'fresher' brGDGTs than CL brGDGTs. The percentage of IPL-derived brGDGTs of the total amount of brGDGTs might indicate where increased production of brGDGTs occurs. In marine SPM, the percentage of IPL-derived brGDGTs was substantially higher (43 %) than that in the river (7 %) and in marine sediments (5 %). This higher percentage in marine SPM might indicate that brGDGTs are at least partially produced in the water column and potentially sink down to the sediments where they are preserved as CLs. However, the MBT and DC values of IPL-derived brGDGTs in marine SPM were similar to those found in the IPL-derived brGDGTs in the Amazon River (Fig. 5.8A), which would suggest that the brGDGTs produced in the marine water column are similar to the brGDGTs in the river and that the different distribution of the CL brGDGTs must derive from another source. However, these results should be interpreted with care, since there were only four SPM samples that contained sufficient amounts of IPL-derived brGDGTs to calculate the MBT and DC. Of the marine sediments, station 42d sediment had the highest percentage of IPL-derived brGDGTs, this was also the only station besides station 25 in which IPLs could be directly detected. The detected IPLs included phospholipids which are known to degrade faster than glycolipids (Harvey et al. 1986; Lengger et al. 2012a), which suggests that at least some of the IPL-derived GDGTs were recently produced. The DC of IPL-derived brGDGTs in marine sediments was slightly higher than that of the Amazon River, except for the sediment of station 42d in which it was much higher (Fig. 5.8A). The higher DC was associated with higher sediment pH at stations 42d and 43 (Table 5.1). This might indicate that the DC of brGDGTs produced in the marine environment, like the DC of soil brGDGTs (Weijers et al., 2007c), is related to the environmental pH. If we assume that this is the case, the brGDGT distributions at stations 42d and 43 would be a strong indication for marine in-situ production at these sites. The CBT-derived pH from station 42d was not as high as the measured pH, but this could be due to a flattening of the CBT-pH relationship at higher pH values as proposed by Xie et al., (2012). In addition, it is probable that the calibrations made for soils are not valid for the marine environment. In previous studies, it has been found that an increase of cyclic brGDGTs may be related with marine in-situ production (Peterse et al., 2009a, Zhu et al., 2011) which might be associated with the fact that the pH in the marine environment is typically higher than that of soil.

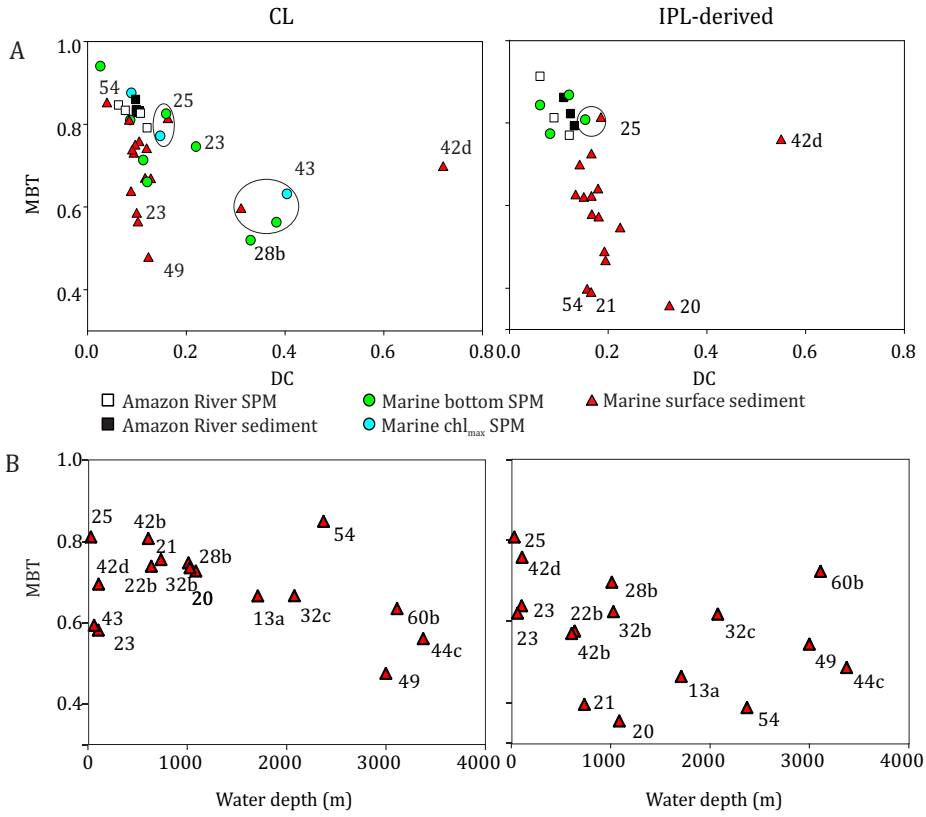

Fig. 5.8 MBT vs. DC cross plot (A) to compare the distributions of CL and IPL-derived brGDGTs of all analyzed riverine and marine SPM and sediment samples and (B) the relationship of MBT with water depth in marine surface sediments.

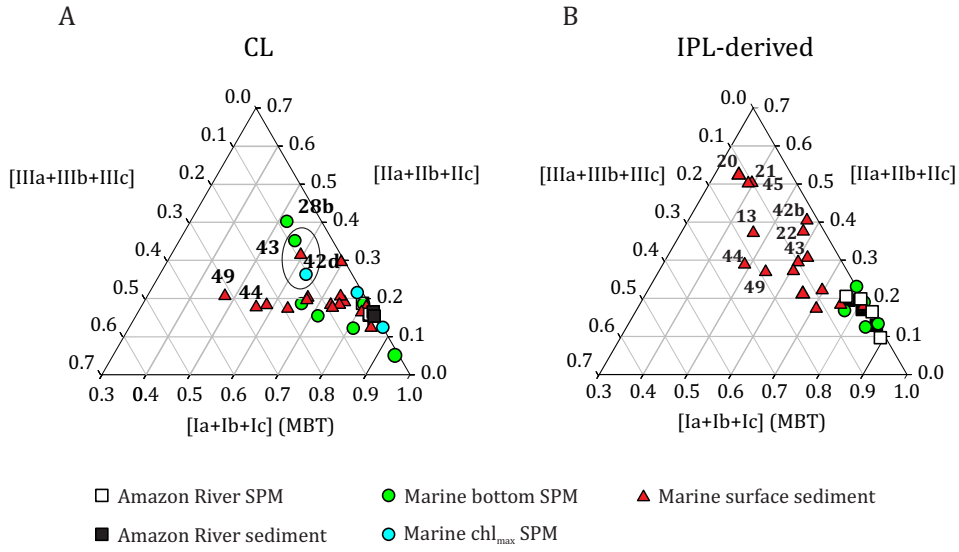

Fig. 5.9 Ternary plot showing the relative amount of the sum of brGDGT I(a-c), II(a-c), and III(a-c) in all analyzed samples for (A) CLs and (B) IPLs.

The MBT of IPL-derived brGDGTs in most marine surface sediments showed reduced values (0.4-0.75) compared to the river signature (0.8-0.9; Fig. 5.8A). In contrast to the CL brGDGTs an apparent decrease of the MBT with water depth cannot be observed in the IPL-derived brGDGTs (Fig. 5.8B). However, in the IPL fraction higher relative amounts of GDGT II(a-c) are evident from the ternary plot (Fig. 5.9B) compared to the CL brGDGTs in marine surface sediments from deep water. This might indicate that the processes that alter the brGDGT distribution in marine settings are more complex and might not only be influenced by in-situ production. Another factor could be that the brGDGT distribution in the IPL-derived brGDGTs is not the same as that of the CL brGDGTs. For example, Lengger et al. (2012a) showed that the TEX_{86} values of different isoGDGT IPLs is different. As some isoGDGT IPLs degrade faster than others, the TEX_{86} of the IPL fraction was consistently higher than that calculated with CL isoGDGTs. We assume that this could also be the case for brGDGTs, leading to a different MBT and DC in IPL-derived brGDGTs, compared to CL brGDGTs.

Overall our results show that brGDGTs are transported from the Amazon River to the ocean. However, only the brGDGT distribution of marine SPM and surface sediments in stations closest to the river source is similar to that in the river. Further away from the river, the brGDGT distribution in marine sediments varies widely. The major reason for this seems to be marine in-situ production of brGDGTs with a variable distribution, which seems to be influenced by the pH and potentially lower temperatures in deeper water. This illustrates that the distribution of brGDGTs produced in the ocean may also correspond to the ambient environment.

5.5.2 Origins of isoGDGTs on the Amazon shelf and in the Amazon fan

Unlike the case of the brGDGTs, the concentration of CL isoGDGTs per g_{OC} in the Amazon River SPM is similar to that in the ocean (Fig. 5.3C), but the concentration per liter was about 10 to 100 times higher in the river (Amazon River SPM on average: 60 µg L^{-1}, marine SPM at station 25: 3 µg L^{-1} and marine SPM at all other stations: 0.5 µg L^{-1}). Similar values have been reported for other river systems, e.g. the Rhine River (Herfort et al., 2006). This indicates that the Amazon River may act as a source of isoGDGTs in the marine environment. To determine if the riverine isoGDGTs influence the isoGDGT distribution in marine SPM and sediments, the GDGT-0/crenarchaeol ratio and the TEX_{86} values were compared (Fig. 5.10). The main difference between Amazon SPM and river-bed sediments was found in the relative amount of GDGT-0 and crenarchaeol. Crenarchaeol is only produced by Thaumarchaeota, while GDGT-0 is produced by many archaea, including Thaumarchaeota. Methanogenic archaea produce predominantly GDGT-0 (e.g. Schouten et al., 2013b). In Thaumarchaeota, the GDGT-0/crenarchaeol ratio is temperature-dependent, and typically varies between 0.2 and 2 (Schouten et al., 2002). It has been proposed for lakes, that if this ratio is >2 it indicates a substantial methanogenic origin of GDGT-0 (Blaga et al., 2009). The values of the CL GDGT-0/crenarchaeol ratio were low (<1.5) in the river SPM, but in two out of three Amazon River

sediments the values were slightly >2 (Fig. 5.10A). In the IPL-derived isoGDGTs from the three river-bed sediments, the GDGT-0/crenarchaeol ratio was even much higher (GDGT-0/crenarchaeol ratio = 5-13, the data are not shown in Fig. 5.10B). It is thus likely that methanogens from anoxic sediments in the Amazon system (Conrad et al. 2010) contribute to the GDGT signal in river sediments. However, these isoGDGTs in river sediments are only to a minor extent contributing to the isoGDGTs transported by the river since GDGT-0/crenarchaeol ratios of SPM for both the IPL and CL fractions are much smaller (Fig. 5.10).

When the GDGT-0/crenarchaeol ratio and TEX_{86} of the river SPM were compared to those of the marine SPM and sediments (Fig. 5.10A), it is observed that the GDGT-0/crenarchaeol ratio was higher in the river. TEX86 values of river SPM and sediment fell between those of marine SPM and sediments, which showed a wider range. CL values of isoGDGTs from the marine samples occurred in two clusters (Fig. 5.10A). The first cluster contained chl_{max} SPM of all stations, as well as bottom SPM and surface sediments of stations 25, 43 and 42d. The second cluster was formed by offshore bottom SPM samples and sediments. IPL-derived isoGDGTs showed more variation in TEX_{86} values but a similar clustering (Fig. 5.10B). The different IPL-derived isoGDGT distributions in offshore chl_{max} SPM compared to offshore bottom SPM and sediment suggests production of isoGDGTs below the chl_{max}. The higher GDGT-0/crenarchaeol ratio and the lower TEX_{86} values in cluster 2 may be explained by an increased contribution of Thaumarchaeota residing in deeper water. The more distinct appearance of this second cluster in IPL-derived isoGDGTs (Fig. 5.10B), supports the idea that isoGDGDTs are indeed produced in-situ below the chl_{max}. This hypothesis is supported by the detection of crenarchaeol-hexose-phosphohexose, which is less stable than the other two crenarchaeol IPLs (Lengger et al., 2012a), in these samples.

5.5.3 Implications for the use of GDGT-based paleoproxies in marine sediments

5.5.3.1 BIT

The flux-weighted value of the BIT index of SPM at Óbidos is 0.67 (Zell et al., 2013a) and the average BIT value of the river-bed sediments is 0.74. This is lower than the BIT index of lowland Amazon soils (0.9 on average), which is attributed to production of crenarchaeol in the Amazon River (Zell et al., 2013a, b). In the marine environment, the highest value of the BIT index was found in surface sediments at station 25 (0.50), at station 42b (0.36) and, surprisingly, also at station 54 (0.78), which is distant from the Amazon River. It is possible that the high concentration of brGDGTs measured at station 54 is due to the influence of the Bacanga River, which has its outflow further to the south. In agreement with this is that the brGDGT distribution observed at this station is similar to that of river SPM (see section 5.1). In all other marine SPM samples and surface sediments, the BIT index was much lower, likely due to the substantially lower brGDGT concentrations (normalized on OC; Fig. 5.3A, Table 5.2). It has been reported for various systems that variations in the BIT index in marine SPM and sediments

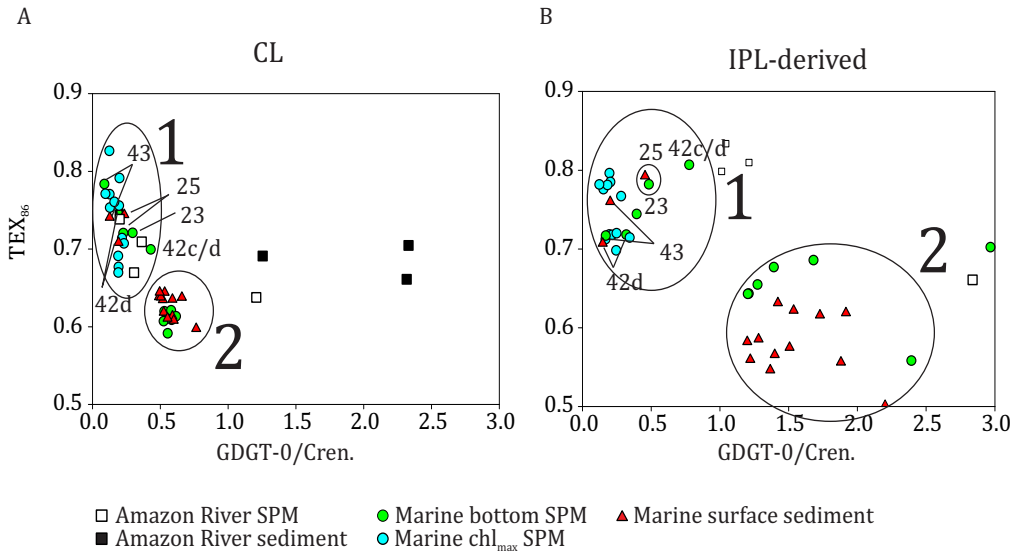

Fig. 5.10 GDGT-0/crenarchaol ratio vs. TEX_{86} cross plot showing the differences in isoGDGT distribution of the different sample types: (A) CL isoGDGTs and (B) IPL-derived isoGDGTs. The data of the Amazon River sediments are not shown in (B) because the GDGT-0/crenarchaeol values were much higher than those of the other samples (GDGT-0/crenarchaeol ratio = 4, 10, and 12, TEX_{86} = 0.70, 0.64, and 0.67, respectively). Clusters 1 and 2 are discussed in the text.

predominantly reflect variations in marine production of crenarchaeol rather than in the delivery of riverine brGDGTs (e.g., Weijers et al., 2009b; Fietz et al., 2011; Smith et al., 2012). However, in the Amazon River fan we generally observe relatively constant crenarchaeol concentrations (Fig. 5.3C, Table 5.2) in combination with sharply declining (with increasing distance from the river mouth) brGDGT concentrations, arguing for a dominant control of the delivery of brGDGTs from the river on the BIT index values. Despite the advocated potential in-situ production of brGDGTs, it is still possible to use the BIT to detect riverine input apparently because the amounts of brGDGTs produced in-situ in the marine environment are substantially lower than that of crenarchaeol.

5.5.3.2 The MBT/CBT paleothermometer

In order to be able to use the MBT/CBT as a continental temperature proxy, it is essential that the brGDGT distribution from soils is not altered during the transport and deposition of marine sediments. However, it has been shown that there is already a difference in the distribution of brGDGTs between Amazon basin soils and Amazon River SPM, due to in-situ production in the river itself (Zell et al., 2013a, b). In the present study we found even more variable brGDGT distributions in marine SPM and surface sediments of the Amazon shelf and fan. Consequently, the MBT/CBT-derived pH and MAAT from the brGDGTs in most of the marine surface sediments using the Amazon soil calibration did not represent those of the Amazon drainage basin. In the marine envi-

ronment, the highest CBT-derived pH (8) was 2.5 pH units higher than that of the Amazon River SPM (pH 5.5), whereas the MBT/CBT-derived MAAT was up to 14ºC colder than that of the Amazon River SPM. However, station 25, which was characterized by the highest OC-normalized brGDGT concentration (and high BIT index; 0.5) provided MBT/CBT-reconstructed MAAT and pH values comparable to the results obtained from the Amazon River watershed (Fig. 5.5D). Hence, it can be concluded that although most of the stations were only weakly influenced by the Amazon River outflow, the stations under high river influence still possess the "continental" Amazon brGDGT distribution. This suggests that the MBT/CBT proxy should only be used to reconstruct paleoenvironmental conditions from sediment cores that are demonstrably strongly influenced by the fluvial inputs of brGDGTs. In general, the BIT index may serve as a good, initial indicator for screening potential sites which are under strong fluvial influences.

Our new data allow us to re-evaluate the results obtained from ODP Site 942 (Bendle et al., 2010), a site that was used to reconstruct the climate of the Amazon basin during the late Quaternary. ODP Site 942 (Fig. 5.2, 5°45′N, 49°6′W, 3346 m water depth) is situated slightly north of the stations of the present study. The MBT/CBT-derived temperature (ca. 17°C) of the surface sediments from their study compares well with the temperatures derived from our surface sediments that were located closest to ODP Site 942 (our sites 13a, 20, and 21; Fig. 5.2D). Their MBT/CBT-derived temperature record showed relatively constant values of around 21°C between 40 and 10.5 ka with a temperature drop just after 10.5 ka to values as low as 10°C. This was followed by a general increase to 17°C in the last 6 ka. The unexpected temperature drop of the early Holocene was explained by an increased input of brGDGTs from Andean soils, which would carry a "low temperature" signal (Bendle et al., 2010). This seems to be a conceivable argument, since ~82 to 95 % of the suspended sediments in the Amazon River is currently derived from the Andes (e.g. Meade, 1994; Wittmann et al., 2011). However, the MBT/CBT-derived temperature from modern Amazon River SPM were higher (22°C) than the temperatures derived from marine surface sediments and the brGDGT distribution from the river did not resemble the brGDGT distribution in the high Andes (Kim et al., 2012b; Zell et al., 2013b). Therefore, a major influence of brGDGTs from the Andean soils can be excluded, both today and presumably during the past. With our detailed data set on surface sediments in this area, we surmise that sea level changes had a significant impact on the MBT/CBT-derived temperature record of ODP Site 942. During a much reduced sea level stand, between 40 and 10.5 ka, river SPM could reach OPD Site 942 more directly than during the sea level high stand of the Holocene when the input of riverine SPM to ODP Site 942 was nil. This undoubtedly led to a much stronger influence of in-situ produced brGDGTs on the MBT/CBT temperature record during the Holocene. This interpretation is supported by the BIT record which showed high values (ca. 0.6) from 40 to 10.5 ka and a subsequent reduction in the Early Holocene. However, the BIT values during the Holocene for this core remain remarkably high (ca. 0.3), indicating that the BIT index should be used with caution as an indicator for the applicability of the terrestrial

MBT/CBT palaeothermometer. In conclusion, in order to reconstruct the MAAT of the Amazon basin during the Holocene, a core site near to the Amazon River mouth, where more riverine terrestrial material is being deposited should be considered.

The comparison of our results with those of similar studies showed that there might be substantial differences between river systems. So far, two other river systems have been studied for the applicability of the MBT/CBT as a paleothermometer in marine sediments, i.e. the Yangtze River and the Pearl River in China (Zhu et al., 2011; Strong et al., 2012; Zhang et al., 2012). In the marine sediments of these river systems, like in the Amazon River system, MBT/CBT-derived MAATs were lower than the actual MAATs of the drainage basins. In addition the cause of lower MBT/CBT-derived MAATs was different in the two Chinese rivers. In front of the Yangtze River, DC values increased, but lower MBT values were not found (Zhu et al., 2011). In the Pearl River, DC and MBT changes between the soil, river and marine sites were not obvious (Strong et al., 2012; Zhang et al., 2012). This suggests that the applicability of the MBT/CBT proxy can vary between different river systems, potentially due to the differences in the sedimentary regimes, hydrodynamics, and degradation loss (Strong et al., 2012), but also differences between the populations of brGDGT producing bacteria. We conclude that it is necessary to investigate recent samples from a river system before applying the MBT/CBT proxy and we suggest caution in the application of the proxy to past periods of low sea level and changing delivery rates of riverine sediments to marine depositional sites.

5.5.3.3 The TEX_{86} paleothermometer

Since the TEX_{86} values for Amazon River SPM and for marine SPM at the chl_{max} and surface sediments were similar, the influence of riverine isoGDGTs on the TEX_{86} could not be detected in our study area. All marine samples (except for station 25) had a BIT value <0.2 and a GDGT-0/crenarchaeol ratio <2. This means that their TEX_{86} values should record the sea temperature of the top 200 m water column (Weijers et al., 2006b; Kim et al., 2012a). TEX_{86}-derived temperatures from the chl_{max} SPM were about 24°C (average water depth chl_{max} = 72 m) compared with the depth-integrated temperature between 0 and 100 m of 27°C (WOA09 data base). Therefore, the TEX_{86}-derived temperatures were ca. 3°C lower than expected; we should note that the temperature reconstructed from the SPM is a snap shot and not the annual mean. However, since the sampling site is close to the equator, no strong seasonal temperature changes are expected. In offshore bottom SPM and sediments, TEX_{86}-derived temperatures were even lower (20°C), possibly due to the influence of isoGDGTs produced below the chl_{max}. This led to TEX_{86}-derived temperatures that were on average 4°C colder than the depth-integrated annual mean temperatures from 0 to 200 m water depth (Table 5.1). The detection of crenarchaeol-hexose-phosphohexose in marine SPM and sediments also indicates that the in-situ production of isoGDGTs in sediments might occur in the Amazon shelf and fan. However, the sedimentary production of isoGDGTs is unlikely to influence the TEX_{86}, because the majority of isoGDGTs is derived from the water column and the isoGDGTs produced in

sediments might be more easily degradable (Lengger et al., 2012a).

5.6 CONCLUSIONS

Our study shows that brGDGTs are primarily transported from the Amazon River to marine sediments. However, brGDGTs are also produced in the marine environment. Hence caution has to be taken when using the MBT/CBT proxy in marine sediments to derive continental paleotemperatures. Only sediments which are under strong river influence should be considered acceptable for this purpose. In-situ production of brGDGTs in the marine environment does not have a strong influence on the BIT, since the concentration of brGDGTs is much lower than that of crenarchaeol. No obvious influence on the TEX_{68} paleothermometer by the riverine isoGDGTs is detected in marine SPM and sediments due to similar TEX_{86} values in the river and marine SPM and sediments.

Acknowledgements

We are grateful for the constructive comments of two anonymous reviewers. We also thank the crew of the R/V Knorr for their great services during the cruise, E. Montes and E. Goddard at the University of South Florida for sampling assistance while on cruise and the carbon analyses, and Dr. E. C. Hopmans and J. Ossebaar for analytical support at NIOZ. The research leading to these results has received funding from the European Research Council under the European Union's Seventh Framework Program (FP7/2007-2013) / ERC grant agreement n° [226600] (to J. S. Sinninghe Damsté) and from NSF-OCE-0823650 (to P. Baker).

Part II

The Tagus River and Portuguese margin

Chapter 6

Transport of branched tetraether lipids from the Tagus River basin to the coastal ocean of the Portuguese margin: Consequences for the interpretation of the MBT'/CBT paleothermometer

C. Zell, J.-H. Kim, M. Balsinha, D. Dorhout, C. Fernandes, M. Baas, and J. S. Sinninghe Damsté

Biogeosciences Discuss., 11, 1–46, 2014
doi:10.5194/bgd-11-1-2014

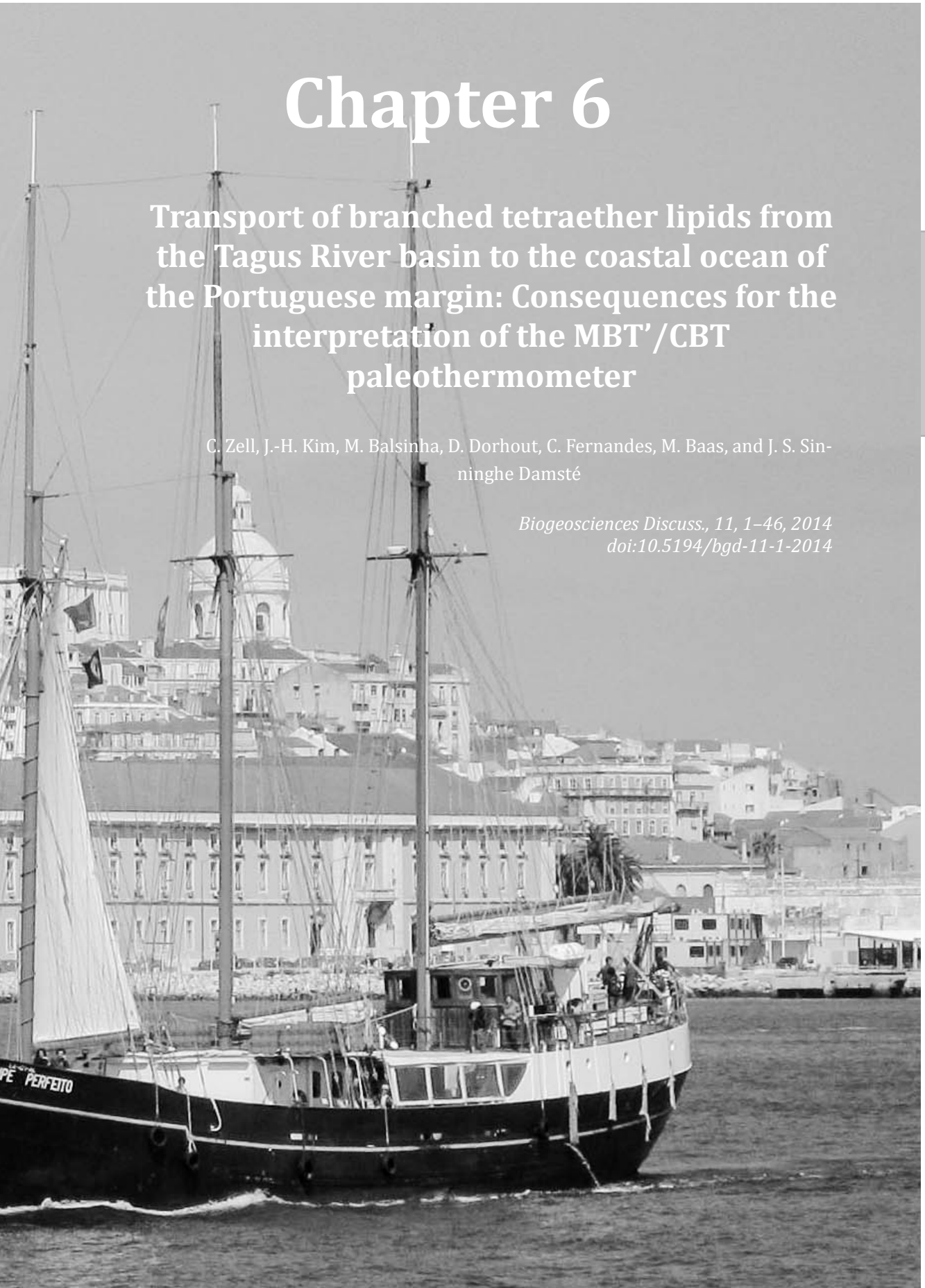

Abstract

Branched glycerol dialkyl glycerol tetraethers (brGDGTs), which are transported from soil to marine sediment by rivers, have been used to reconstruct the mean annual air temperature (MAAT) and soil pH of the drainage basin using the methylation index of branched tetraethers (MBT, recently refined as MBT') and cyclization index of branched tetraethers (CBT) from coastal marine sediment records. In this study we are tracing the brGDGTs from source to sink in the Tagus River basin, the longest river system on the Iberian Peninsula, by determining their concentration and distribution in soils, river suspended particulate matter (SPM), riverbank sediments, marine SPM, and marine surface sediments. The concentrations of brGDGTs in river SPM were substantially higher and their distributions were different compared to those of the drainage basin soils. This indicates that brGDGTs are mainly produced in the river itself. In the marine environment, the brGDGT concentrations rapidly decreased with increasing distance from the Tagus estuary. At the same time, the brGDGT distributions in marine sediments also changed, indicating that marine in-situ production also takes place. These results show that there are various problems that complicate the use of the MBT'/CBT for paleoreconstructions using coastal marine sediments in the vicinity of a river. However, if the majority of brGDGTs are produced in the river, it might be possible to reconstruct the environmental (temperature and pH) conditions of the river water using appropriate aquatic calibrations, provided that marine core locations are chosen in such a way that the brGDGTs in their sediments are predominantly derived from riverine in-situ production.

6.1 INTRODUCTION

Branched glycerol dialkyl glycerol tetraethers (brGDGTs) are membrane-spanning lipids, most likely derived from heterotrophic (Pancost and Sinninghe Damsté, 2003; Oppermann et al., 2010; Weijers et al., 2010) bacteria that occur ubiquitously in peat (e.g. Weijers et al., 2006a) and soil (e.g. Weijers et al., 2007c). The major brGDGTs contain a variety of methyl groups (4–6) and may contain up to two cyclopentane moieties formed by internal cyclization (Sinninghe Damsté et al., 2000; Weijers et al., 2006a). Four of these methyl groups are present in mid-chain positions of the two C28 linear chains of the tetraether structure (Fig. 6.1), whilst the others are present at the C-5 and C-5' positions. Recently, De Jonge et al. (2013) identified four new isomers of the previously described pentamethylated and hexamethylated brGDGTs in a Siberian peat. These isomers are characterized by the presence of methyl groups at the C-6 and C-6' instead of the C-5 and C-5' positions. Concerning the biological origin of the brGDGTs, it has been found so far that brGDGT Ia (see for structures Fig. 6.1) is produced by some species of Acidobacteria (Sinninghe Damsté et al., 2011). However, it remains unclear whether other bacteria are also able to produce brGDGTs.

The distribution of brGDGTs, as expressed by the degree of methylation (methyla-

tion index of branched tetraethers; MBT) and cyclization (cyclization index of branched tetraethers; CBT) of the brGDGTs, in soil correlates with mean annual air temperature (MAAT) and soil pH (Weijers et al., 2007c). The MBT/CBT proxy is one of the few quantitative temperature proxies that have been introduced for terrestrial environments. The MBT/CBT proxy has been used to reconstruct past MAAT changes in diverse settings: marine (e.g. Weijers et al., 2007a; Donders et al., 2009; Rueda et al., 2009; Bendle et al., 2010) and lacustrine (Niemann et al., 2005; Tyler et al., 2010; Zink et al., 2010; Fawcett et al., 2011; D'Anjou et al., 2013) sediments, peat (Ballantyne et al., 2010), and loess deposits (Peterse et al., 2011b; Zech et al., 2012; Jia et al., 2013).

To reconstruct terrestrial climate changes using the MBT/CBT proxy, sediment cores in front of river outflows have been used (e.g. Weijers et al, 2007b). Initially, it was thought that brGDGTs were only produced in soils, washed into rivers by soil erosion, and transported to the marine environment where they are deposited in sediments. Consequently, it was thought that the MBT/CBT records of marine sediment cores would represent an integrated signal of the whole river drainage basin. An initial study that applied the MBT/CBT proxy in Congo deep-sea fan sediments (Weijers et al., 2007a) showed its potential to reconstruct changes of MAAT of the Congo basin over the last glaciation. However, subsequent studies have shown that in-situ production in rivers (Yang et al., 2013; Zell et al., 2013a,b) and in the marine environment (Peterse et al., 2009a; Zhu et al., 2011; Hu et al., 2012; Strong et al., 2012, Zell et al., submitted) may affect the original brGDGT signal of soil and, therefore, complicates the use of the MBT/CBT proxy. Depending on the river systems, it seems that the influence of in-situ production can differ. In addition, other potential factors may hamper the application of the MBT/CBT proxy in coastal sediments. For example, an increased input of brGDGTs from a certain area of the drainage basin could obscure the representativeness of the entire river basin (Bendle et al., 2010; Strong et al., 2012). Therefore, it is of utmost importance to further investigate how different environmental conditions affect the application of the MBT/CBT proxy. Recently, the MBT was adjusted to the MBT', by excluding brGDGT IIIb and IIIc, because they occur less frequently in soil (Peterse et al., 2012). Hereafter, we will therefore use the term of the MBT'/CBT instead of the MBT/CBT.

The relative amount of brGDGTs to the isoprenoid GDGT, crenarchaeol, which is produced predominantly in the marine environment by Thaumarchaeota may indicate a

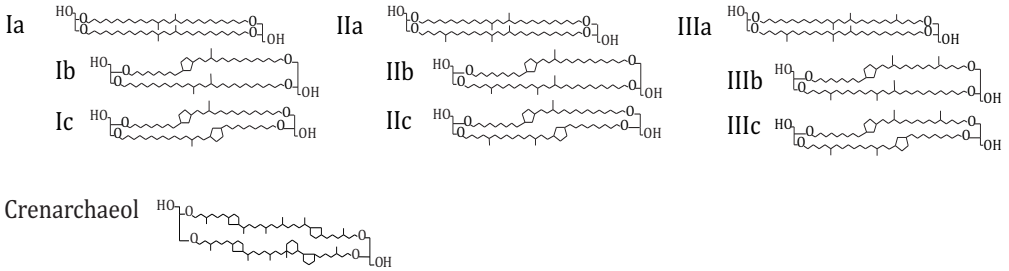

Fig. 6.1 Chemical structure of brGDGTs (Ia-IIIa) and crenarchaeol (IV).

substantial input of soil organic matter to the ocean. This is expressed with the Branched and Isoprenoid Tetraether (BIT) index (Hopmans et al., 2004), which is a helpful tool to decide where the MBT'/CBT proxy can be applied or not. Initially, a value of the BIT index of 1 was thought to indicate an environmental sample only containing soil organic matter, while a value of 0 was thought to reflect only aquatic organic matter. However, crenarchaeol is also produced in soils which can lead to a value of the BIT index of <1.0 (Weijers et al., 2006b; Kim et al., 2010c; Peterse et al., 2010; Yang et al., 2011). The BIT index is also influenced by the amount of crenarchaeol produced in the marine environment (e.g. Fietz et al., 2011; Smith et al., 2012; Wu et al., 2013) and by degradation processes (Huguet et al., 2008, 2009). This shows that also for the BIT index further investigation is needed to understand how it can be used in river systems to trace the transport of soil organic matter and if it can be used to indicate if and where the MBT'/CBT can be used.

We performed a proxy validation study in the Tagus River system. Compared to the river systems which have been studied previously, like Amazon (Bendel et al., 2010, Zell et al., 2013a,b), Congo (Weijers et al., 2007a), Yangtze (Zhu et al., 2011, Yang et al., 2013), and Yenisei (De Jonge et al., 2014), the Tagus River system is smaller and located in a much dryer climate zone. We traced the transport of brGDGTs from source to sink via rivers, identified the source of brGDGTs in marine sediments, and assessed the applicability of the MBT'/CBT proxy in the coastal ocean of the Portuguese margin. We analyzed brGDGTs and crenarchaeol in soils, in river suspended particulate matter (SPM) over a whole year, and in riverbank sediments collected in the Tagus River basin. In addition, marine SPM and surface sediments were analyzed along a transect from close to the Tagus estuary to the deep sea Setúbal canyon. Core lipid (CL) and intact polar lipid (IPL) derived GDGTs were analyzed, in order to distinguish recently produced (IPL-derived) GDGTs from older (CL) GDGTs.

6.2 STUDY AREA

The Tagus River is the longest river of the Iberian Peninsula, with a length of ca. 1000 km and a watershed of ca. 80.600 km^2 (Fig. 6.2). Mean annual precipitation (MAP) in the catchment area varies between <500 mm yr^{-1} and around 900 mm yr^{-1} and MAAT is from about 7°C in the mountain areas to 17°C along the Atlantic coast (Atlas Nacional de España, 1993; Ninyerola et al., 2005). River water discharge shows large seasonal variations: the mean annual water discharge of the Tagus River is 360 $m^3 s^{-1}$, but ranges between 80 and 720 $m^3 s^{-1}$. In addition, there are pronounced dry and wet seasons, monthly average discharges can vary between 1 and 2200 $m^3 s^{-1}$ (Lourairo et al, 1979, Loureiro & Macedo, 1986). The Tagus River is characterized by one of the largest European estuaries with an area of roughly 320 km^2 formed by several channels and islands (Vale et al., 1998) being connected to the sea by a relatively narrow channel (ca. 2 km).

An estimated amount of 0.4-1 million tons of suspended material is exported to the adjacent continental shelf annually (Jouanneau et al., 1998). The suspended matter carried by the Tagus River outflow forms a nepheloid layer that is subject to seasonal variations. During summer the surface nepheloid layer is more pronounced and extends up to 14 km offshore, while during winter the bottom nepheloid layer is more pronounced and stretches over the shelf brake (Jouanneau et al., 1998).

The Portuguese continental shelf ranges from 20 to 34 km in width. The shelf break varies between 130 and 150 m water depth, where several canyons intersect the outer shelf (Mougenot, 1988). The inner shelf is characterized by sands representing the river delta front, with bottom currents strong enough to avoid the deposition of fine-grained particles (Paiva et al., 1997). The decrease of velocity, together with increasing water depths unaffected by waves and storms, allow the deposition of fine particles forming a large muddy shelf sediment body (i.e. the Tagus mud belt) between 50 and 130 m water depths (Jouanneau et al., 1998). The suspended matter carried by the Tagus River outflow can be transported as far as the Lisbon Canyon (Jouanneau et al., 1998).

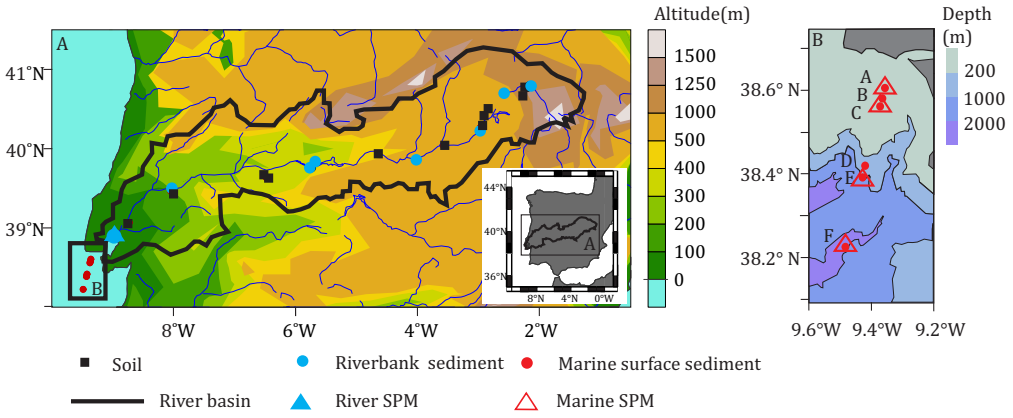

Fig. 6.2 (A) Overview of the study area with the sampling sites of soils, riverbank sediments, and river SPM and (B) detailed sampling locations of marine SPM and surface sediments.

6.3 MATERIAL AND METHODS

6.3.1 Sample collection

Surface soils and riverbank sediments (collected in areas that are strongly influenced by the river but not always covered by water) were sampled from the source to the mouth of the Tagus River in 2012 (Fig. 6.2, Table 6.1). Tagus River SPM samples were collected close to the river mouth, each month for one year from July 2011 until June 2012, except for August 2011 (Fig. 6.2). 1 to 7 L of river water were filtered on ashed

glass-fiber filters (Whatman GF-F, 0.7 µm pore size, 142 mm diameter) for lipid analysis. For organic carbon (OC) and stable carbon isotope analysis of the river SPM, 0.07-0.5 L waters were separately filtered on ashed GF-F filters (Whatman GF-F, 0.7 µm pore size, 47 mm diameter). Marine SPM and surface sediments were collected during the PACE-MAKER 64PE332 cruise with the R/V Pelagia between 14 and 29 March 2011. Marine SPM samples were collected at four stations along the Tagus transect from the Tagus estuary mouth towards the deep sea canyon and at 2-5 different water depths (Fig. 6.2B, Table 6.1). 64 to 240 L of seawater were filtered over ashed GF-F filters (Whatman GF-F, 0.7 µm pore size, 142 mm diameter) with a McLane in-situpump system (WTS, McLane Labs, Falmouth, MA). For the OC and stable carbon isotope analysis, about 8 L of seawater were separately filtered on GF-F filters (0.7 µm pore size, 47 mm diameter). Marine sediment cores were retrieved at 6 stations using a multicorer developed by Oktopus GmbH. In this study the surface sediments (top 0.5 cm of the multicores) were used. All samples were frozen immediately after sampling and freeze-dried before analysis.

6.3.2 Environmental parameters and bulk geochemical analysis

The pH of the Tagus River water was measured with a pH analyzer (Metrohm pH-meter 744 and combined pH-Electrode LL-Solitrode Pt1000, pH range 0-14, T range -130-200C° stored in 3 mol L^{-1} KCl). The electrode was calibrated with CertiPUR buffer solutions (pH 7.00 and 9.00); quality control was assured using CertiPUR buffer solutions with pH 6.00 and 8.00 analyzed in parallel with each batch of samples. The measurements were performed in the laboratory within 1 h after collection. The pH of the soil and riverbank sediment samples was measured in a mixture with distilled water 1:3.5 (v:v). This mixture was stirred vigorously and left to settle down for 20 min. For the pH measurements a pH analyzer (Wissenschaftlich-Technische Werkstätten pH 315i/SET and probe pH-Electrode SenTix 41, pH range 0-14, T range 0-80°C, stored in 3 mol L^{-1} KCl) was calibrated with CertiPUR buffer solutions with pH 4.01, 7.00, and 10.00.

For the OC and stable carbon isotope analysis, the riverine and marine SPM filters were decarbonated with HCl vapor as described by Lorrain et al. (2003). Soils, riverbank sediments, and marine surface sediments were decarbonated with 2 mol L^{-1} HCl (overnight at 50°C). All samples were analyzed with a Thermo Flash EA 1112 Elemental Analyzer interfaced with a Thermo Finnigan DeltaPlus mass spectrometer. OC is expressed as the weight percentage of dry sediment (wt. %). The analyses were determined in duplicate and the analytical error was on average better than 0.1 wt. % for the OC content. Isotope values were calibrated to a benzoic acid standard ($\delta^{13}C_{OC}$ = -27.8 ‰ with respect to Vienna Pee Dee Belemnite (VPDB) calibrated on NBS-22) and corrected for blank contribution. The analytical error was usually smaller than ±0.1 ‰ for $\delta^{13}C_{OC}$.

6.3.3 Lipid extraction and analysis

The soils and riverbank sediments were extracted using an accelerated solvent extraction (ASE) technique due to the fact that the Bligh and Dyer (BD) method is very time consuming. For the ASE extraction, 2–10 g freeze dried soils and riverbank sediments were extracted 3 times using a mixture of dichloromethane (DCM):methanol (MeOH) (9:1, v:v) at a temperature of 100˚C and a pressure of 1500 psi for 5 min with 60 % flush and purge 60 s. The extract was collected in a vial and solvents were removed using Caliper Turbovab®LV. The total extracts were taken up in DCM, dried over anhydrous Na_2SO_4, and blown down under a stream of nitrogen. For GDGT quantification, 0.1 µg of an internal standard (C_{46} GDGT; Huguet et al., 2006) was added to the total extracts. The total extracts were separated over an Al_2O_3 column (activated for 2 h at 150˚C) into two fractions using hexane:DCM (1:1, v:v), and DCM:MeOH (1:1, v:v), respectively.

In order to analyze both CL and IPL-derived GDGTs, a second extraction method was used, i.e. a modified BD technique (Pitcher et al., 2009). 4 soils, 4 riverbank sediments, and all the river and marine SPM samples and marine surface sediments were extracted with this BD method. The Bligh and Dyer extracts (BDE) were separated into a CL fraction and an IPL fraction over a silica gel (activated overnight) column with n-hexane:ethyl acetate (1:1, v:v) and MeOH as eluents, respectively (Pitcher et al., 2009). For the GDGT quantification, 0.01 µg of C_{46} GDGT internal standard was added to each fraction. The CL fractions of the BDEs were separated into three fractions over an Al_2O_3 column (activated for 2 h at 150˚C) using hexane:DCM (9:1, v:v), hexane:DCM (1:1, v:v), and DCM:MeOH (1:1, v:v), respectively. Part of the IPL fraction was hydrolyzed to obtain IPL-derived CLs. The CL polar fractions, the hydrolyzed IPL fractions, and the non-hydrolyzed IPL fractions were analyzed for CL GDGTs. The non-hydrolyzed IPL fractions were also analyzed, because it was reported by Pitcher et al. (2009) that during the separation of CL and IPL fractions a small amount of the CL GDGTs were carried over into the IPL fraction. Therefore, it was necessary to implement a correction to more accurately calculate the amounts of CL and IPL-derived GDGTs as described by Weijers et al. (2011).

All samples were analyzed using a high performance liquid chromatography–atmospheric pressure positive ion chemical ionization–mass spectrometry (HPLC-APCI-MS) with an Agilent 1100 series LC-MSD SL. The GDGTs were separated on an Alltech Prevail Cyano column (150 mm x 2.1 mm; 3 µm) using the method described by Schouten et al. (2007) and modified by Peterse et al. (2012). The compounds were eluted isocratically with 90 % A and 10 % B for 5 min at a flow rate of 0.2 ml min^{-1}, and then with a linear gradient to 16 % B for 34 min, where A = hexane and B = hexane:isopropanol (9:1, v:v). The injection volume was 10 µl per sample. Selective ion monitoring of the $[M+H]^+$ of the different brGDGTs and crenarchaeol was used to detect and quantify them. Quantification was achieved by calculating the area of the corresponding peak in the chromatogram and comparing it with the peak area of the internal standard and correcting for the different response factors (Huguet et al., 2006). The analytical error was determined

by duplicate measurements of 12 CL GDGTS and 7 IPL derived brGDGTs fractions. For the concentration of the sum of brGDGTs, the analytical error was 11 % for the CL GDGTs and 6 % for the IPL-derived GDGTs. Crenarchaeol concentrations had a standard deviation of 17 % for the CL GDGTs and 10 % for the IPL-derived GDGTs.

6.3.4 Calculation of GDGT-based indices

The numerals refer to the GDGTs depicted in Fig. 6.1. The BIT index (Hopmans et al., 2004), the MBT' (Peterse et al., 2012) and CBT indices (Weijers et al., 2007c), and the degree of cyclization (DC, Sinninghe Damsté et al., 2009) were calculated as follows:

$$\text{BIT index} = ([I]+[II]+[III])/([I]+[II]+[III]+[IV]) \quad (1)$$

$$\text{MBT'} = ([I]+[Ib]+[Ic])/([I]+[Ib]+[Ic]+[II]+[IIb]+[IIc]+[III]) \quad (2)$$

$$\text{CBT} = -\log(([Ib]+[IIb])/([I]+[II])) \quad (3)$$

$$\text{DC} = ([Ib]+[IIb])/([I]+[Ib]+[II]+[IIb]) \quad (4)$$

The average standard deviation for the BIT index was 0.01 (CL) and 0.03 (IPL-derived) and for the MBT' 0.01 (CL) and 0.06 (IPL-derived), and for the DC 0.01 (CL) and 0.05 (IPL-derived). For the calculation of pH and MAAT from the brGDGT distribution of soils, sediments, and SPM samples, the global soil calibrations (Peterse et al., 2012) were used:

$$\text{pH} = 7.90 - 1.97 \times \text{CBT} \quad (r^2 = 0.70) \quad (5)$$

$$\text{MAAT} = 0.81 - 5.67 \times \text{CBT} + 31{:}0 \times \text{MBT'} \quad (r^2 = 0.59) \quad (6)$$

6.3.5 Statistical analysis

To evaluate the differences in mean values between different groups the non-parametric Mann-Whitney U-test was used. Groups that showed significant differences ($p < 0.05$) were assigned different letters. The statistical test was performed with Sigma Plot.

Table 6.1 Environmental and bulk geochemical data of soils and riverbank sediments collected in the Tagus River basin.

Sample name	Sampling date (dd/mm/yyyy)	Long.	Lat.	Altitude (m)	Measured pH	$\delta^{13}C_{OC}$ (‰ VPDB)	OC (wt. %)	MAAT* (˚C)	MAP* (mm)
Tagus soils									
TRS-3	03/06/2012	-5.72	39.77	249	6.7	-29.0	0.7	17	664
TRS-4	03/06/2012	-6.51	39.68	278	6.7	-28.7	0.7	16	619
TRS-5	03/06/2012	-6.48	39.63	344	7.2	-28.4	2.2	16	579
TRS-7	06/06/2012	-8.73	39.07	29	5.5	-27.5	5.0	17	697
TRS-8b	06/06/2012	-8.04	39.47	28	6.7	-27.8	3.0	17	913
TRS-9	06/06/2012	-8.00	39.46	102	5.7	-27.2	0.5	16	903
TRS-10	06/06/2012	-4.65	39.94	380	7.8	-28.5	1.5	16	504
TRS-12	07/06/2012	-3.57	40.04	496	7.4	-25.1	0.2	14	508
TRS-13	07/06/2012	-2.96	40.27	581	7.8	-27.0	6.9	14	475
TRS-14b	07/06/2012	-2.97	40.26	580	8.3	-25.3	0.8	14	465
TRS-15	07/06/2012	-2.91	40.42	678	8.4	-25.7	0.9	13	517
TRS-16	07/06/2012	-2.84	40.51	768	7.8	-24.8	0.1	14	491
TRS-18	07/06/2012	-2.59	40.70	729	8.6	-23.4	0.1	13	595
TRS-19	07/06/2012	-2.28	40.67	1217	8.5	-25.7	0.1	10	710
TRS-20	07/06/2012	-2.20	40.78	1100	8.4	-26.1	0.1	11	671
TRS-21	07/06/2012	-2.16	40.79	931	7.6	-26.8	5.8	13	557
Tagus riverbank sediments									
TRS-1a	03/06/2012	-5.68	39.84	268	6.9	-26.9	0.9	16	758
TRS-1b	03/06/2012	-5.68	39.84	268	8.2	-27.6	1.5	16	758
TRS-2a	03/06/2012	-5.74	39.76	242	7.8	-23.6	3.3	16	858
TRS-2b	03/06/2012	-5.74	39.76	242	7.7	-25.1	0.5	17	656
TRS-6	06/06/2012	-8.98	38.95	0	7.9	-26.3	1.7	17	677
TRS-8a	06/06/2012	-8.04	39.47	23	7.1	-26.5	0.2	17	913
TRS-11	07/06/2012	-4.02	39.86	493	7.7	-27.0	1.3	15	386
TRS-14a	07/06/2012	-2.97	40.26	580	7.4	-27.1	3.0	14	465
TRS-17	07/06/2012	-2.59	40.70	717	7.8	-29.6	3.7	13	545
TRS-22	07/06/2012	-2.16	40.80	901	8.0	-29.8	0.6	12	946

*Data from Ninyerola et al. (2005)

Table 6.1 (continuation) Environmental and bulk geochemical data of soils and river-bank sediments collected in the Tagus River basin.

Sample name	Station	Sampling date (dd/mm/yyyy)	Long.	Lat.	Water depth (m)	Measured pH	$\delta^{13}C_{OC}$ (‰ VPDB)	OC (wt. %)	SPM (mg L^{-1})
Tagus River SPM									
TR 2 Sup	TR	12/07/2011	-8.99	38.95	0	8.1	-29.2	2.6	74
TR 3#1 Sup	TR	16/09/2011	-8.99	38.95	0	7.9	-28.4	1.8	165
TR 4#1 Sup	TR	18/10/2011	-8.99	38.95	0	7.4	-30.9	2.5	62
TR 5#1 Sup	TR	22/11/2011	-8.99	38.95	0	7.6	-28.9	1.3	63
TR 6#1 Sup	TR	16/12/2011	-8.99	38.95	0	8.0	-29.4	2.4	35
TR 7#1 Sup	TR	16/01/2012	-8.99	38.95	0	7.9	-29.8	2.4	28
TR 8#1 Sup	TR	17/02/2012	-8.99	38.95	0	8.0	-29.4	1.0	45
TR 9#1 Sup	TR	16/03/2012	-8.99	38.95	0	8.1	-29.0	2.2	20
TR 10#1 Sup	TR	12/04/2012	-8.99	38.95	0	8.1	-28.5	1.9	112
TR 11#1 Sup	TR	24/05/2012	-8.99	38.95	0	7.9	-28.5	1.7	121
TR 12#1 Sup	TR	24/06/2012	-8.99	38.95	0	8.0	-27.8	1.3	34
Marine SPM									
64PE332-27-1-1m	A	24/03/2011	-9.36	38.61	1	-	-24.6	3.6	2.3
64PE332-27-1-19m	A	24/03/2011	-9.36	38.61	19	-	-25.0	2.9	2.3
64PE332-28-3-1m	C	24/03/2011	-9.37	38.56	1	-	-24.2	9.8	0.6
64PE332-28-3-20m	C	24/03/2011	-9.37	38.56	20	-	-23.8	6.8	0.9
64PE332-28-3-50m	C	24/03/2011	-9.37	38.56	50	-	-23.9	5.3	0.6
64PE332-28-3-93m	C	24/03/2011	-9.37	38.56	93	-	-24.6	3.2	1.0
64PE332-32-1-1m	E	25/03/2011	-9.43	38.39	1	-	-25.8	9.6	0.5
64PE332-32-1-50m	E	25/03/2011	-9.43	38.39	50	-	-24.6	10.0	0.4
64PE332-32-1-200m	E	25/03/2011	-9.43	38.39	200	-	-26.0	2.5	0.8
64PE332-32-1-500m	E	25/03/2011	-9.43	38.39	500	-	-26.2	3.4	0.4
64PE332-32-1-1051m	E	25/03/2011	-9.43	38.39	1051	-	-26.9	3.0	0.7
64PE332-36-4-1m	F	27/03/2011	-9.48	38.23	1	-	-24.1	9.2	0.4
64PE332-36-4-50m	F	27/03/2011	-9.48	38.23	50	-	-25.1	6.9	0.4
64PE332-36-4-200m	F	27/03/2011	-9.48	38.23	200	-	-25.1	6.9	0.8
64PE332-36-4-1000m	F	27/03/2011	-9.48	38.23	1000	-	-26.1	1.6	1.0
64PE332-36-4-2431m	F	27/03/2011	-9.48	38.23	2431	-	-26.3	2.5	0.6
Marine surface sediments									
64PE332-27-3	A	24/03/2011	-9.36	38.61	20	-	-24.4	0.2	-
64PE332-29-2	B	25/03/2011	-9.35	38.58	48	-	-23.3	0.1	-
64PE332-28-1	C	24/03/2011	-9.37	38.56	94	-	-24.9	1.7	-
64PE332-31-2	D	25/03/2011	-9.42	38.42	478	-	-21.9	1.4	-
64PE332-33-1	E	26/03/2011	-9.43	38.39	1052	-	-22.2	1.3	-
64PE332-36-3	F	27/03/2011	-9.48	38.23	2432	-	-22.2	0.9	-

'-' = no data

6.4 RESULTS

6.4.1 Tagus soils

16 soil samples that were collected along the Tagus River (Fig. 6.2) were analyzed. The OC content ranged from 0.1 to 5.9 wt. %, the $\delta^{13}C_{OC}$ was -26.7±1.6 ‰ (average±standard deviation [1σ]) (Table 6.1). Soil pH was on average 7.4±1.0 (Table 6.1). CL brGDGTs were found in all soils with an average concentration of 3.2±3.4 μg g_{OC}^{-1} (Fig. 6.3A). Of the 4 soils for which IPL-derived brGDGTs were measured 7±2 % of the total brGDGTs amount was IPL-derived (Fig. 6.3B). The distribution of CL brGDGTs strongly varied between the soils, but brGDGT IIa (53±10 %) and Ia (24±15 %) were in general the most abundant compound (Fig. 6.4A). The BIT index was 0.62±0.28 in the CL GDGTs and 0.50±0.38 in the IPL-derived GDGTs (Fig. 6.3E-F). The CL MBT' was 0.30±0.13 and the CL DC 0.16±0.13 (Fig. 6.3G). The MBT' of IPL-derived brGDGTs was 0.41±0.11 (Fig. 6.3H). Only in soil TRS19 the concentration of IPL-brGDGTs was sufficiently high to calculate the DC, which was 0.39 (Figs. 6.3G-J). CL crenarchaeol concentration in soils was on average 1.1±0.8 μg g_{OC}^{-1} and a substantial amount (53±36 %) of the total crenarchaeol amount was IPL-derived (Figs. 6.3C-D).

The CL brGDGT and CL crenarchaeol concentrations obtained by ASE extraction were on average 4.6 μg g_{OC}^{-1} and 1.5 μg g_{OC}^{-1}, respectively, higher than with the BD method. Furthermore, the BIT index was on average 0.08 lower, the MBT' 0.01 higher, and the DC 0.02 higher in ASE extracted samples compared to BD extracted samples. This shows that the CL fractions extracted by BD and the GDGTs extracted by ASE give similar results, which is why they were treated as comparable results in the discussion.

6.4.2 Tagus River SPM

The pH of the river water was relatively constant at 7.4±0.1 over the annual cycle and the amount of SPM in the river water ranged from 28 to 165 mg L^{-1} (Fig. 6.5B; Table 6.1). The OC content of SPM varied between 1.0 and 2.6 wt. % and the $\delta^{13}C_{OC}$ was -29.1±0.8 ‰ (Table 6.1). The average CL brGDGT concentration was 43±16 μg g_{OC}^{-1} and the percentage of IPL-derived brGDGTs was 12±8 (Figs. 6.3A-B). The CL brGDGT distribution in river SPM was more uniform compared to those of the soils and the riverbank sediments (Fig. 6.4B). The most abundant CL brGDGTs were brGDGT IIa (39±5 %) and Ia (24±3 %) but with more abundant brGDGT IIIa (10±10 %) than in the soils. The crenarchaeol concentration was on average 13±6 μg g_{OC}^{-1} and the percentage of IPL-derived crenarchaeol was 23±13 (Fig. 6.3C-D). This resulted in a BIT index of 0.71±0.08 in the CL fractions and of 0.56±0.13 in the IPL-derived fractions (Fig. 6.3E-F). The average CL MBT' and DC values were 0.35±0.04 and 0.28±0.02, respectively, while the average IPL-derived MBT' and DC values were 0.40±0.05 and 0.27±0.04, respectively (Figs. 6.3G-J). The brGDGT and crenarchaeol concentrations in the Tagus River SPM fluctuated over the year; the highest concentrations (in ng L^{-1}) were seen in September and May (Fig.

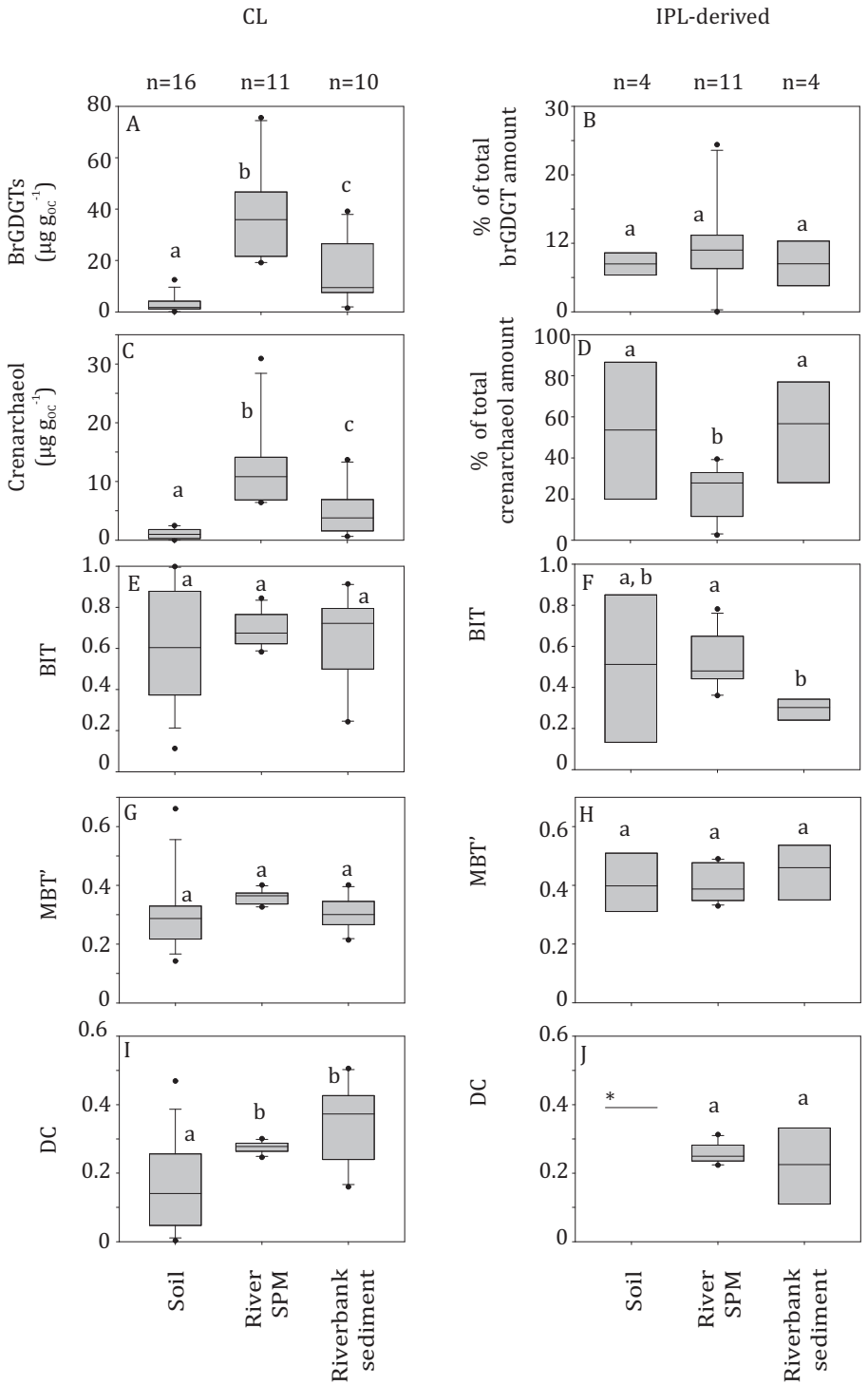

Fig. 6.3 Boxplots of (A-D) the CL brGDGT and CL crenarchaeol concentrations and the percentage of IPL-derived brGDGTs and crenarchaeol and (E-J) BIT, MBT', and DC of CL and IPL-derived GDGTs in soils, river SPM, and riverbank sediments, * indicates that the data was available only for one sample.

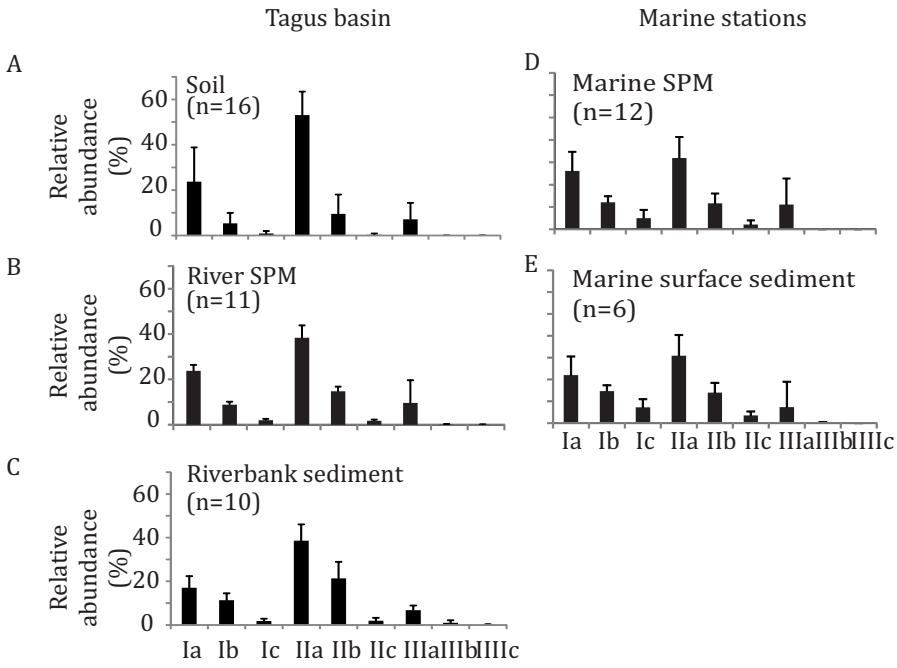

Fig. 6.4 Average CL brGDGT distribution of (A) Tagus soils, (B) Tagus River SPM, (C) riverbank sediments, (D) marine SPM, and (E) marine surface sediments.

6.6A). The brGDGT concentrations normalized on OC were highest in November and December, while crenarchaeol concentrations normalized on OC were highest in February-June (Fig. 6.6B). The highest percentage of IPL-derived brGDGTs was found in March and that for crenarchaeol in January and February (Fig. 6.6C). The CL BIT increased in November, while the CL MBT' and DC decreased in November (Fig. 6.7). IPL-derived BIT MBT' and DC all increased in March and April.

6.4.3 Tagus riverbank sediments

Ten riverbank sediments were analyzed. The OC content ranged from 0.2 to 3.7 wt. %, the $\delta^{13}C_{OC}$ from -23.6 to -28.6 ‰, and the pH from 6.9 to 8.2 (Table 6.1). CL brGDGTs were present with an average concentration of 15.2±11.9 μg g_{OC}^{-1} (Fig. 6.3A). For four riverbank sediments the IPL-derived brGDGTs were also measured: 7±3 % of the total brGDGTs amount were IPL-derived (Fig. 6.3B). The average distribution of CL brGDGTs (Fig. 6.4C) revealed that brGDGT IIa (39±7 %) and Ia (17±5 %) were the most abundant compounds. CL crenarchaeol concentration in riverbank sediments was on average 4.7±4.7 μg g_{OC}^{-1} and 54±26 % of the total crenarchaeol amount was IPL-derived (Figs. 6.3C-D). The BIT index was 0.65±0.23 in the CL GDGTs and 0.30±0.05 in the IPL-derived GDGTs (Figs. 6.3E-F). The CL MBT' was 0.31±0.05 and the CL DC 0.37±0.11. The MBT' and DC of IPL-derived brGDGTs were on average 0.45±0.10 and 0.22±0.12, respectively (Fig. 6.3G-J).

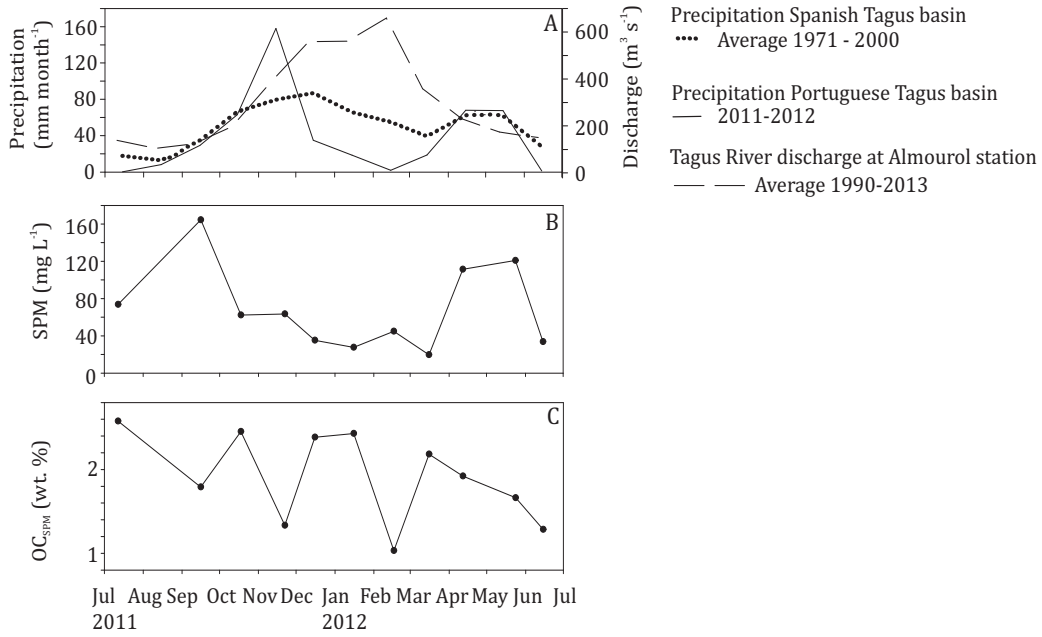

Fig. 6.5 (A) Mean monthly precipitation in the Portuguese and Spanish parts of the Tagus River basin and Tagus River discharge at Almourol station (data source: Sistema Nacional de Informaçião de Recursos Hídricos), (B) SPM concentration at the Tagus River station, and (C) amount of OC in the SPM (wt. %) of the Tagus River.

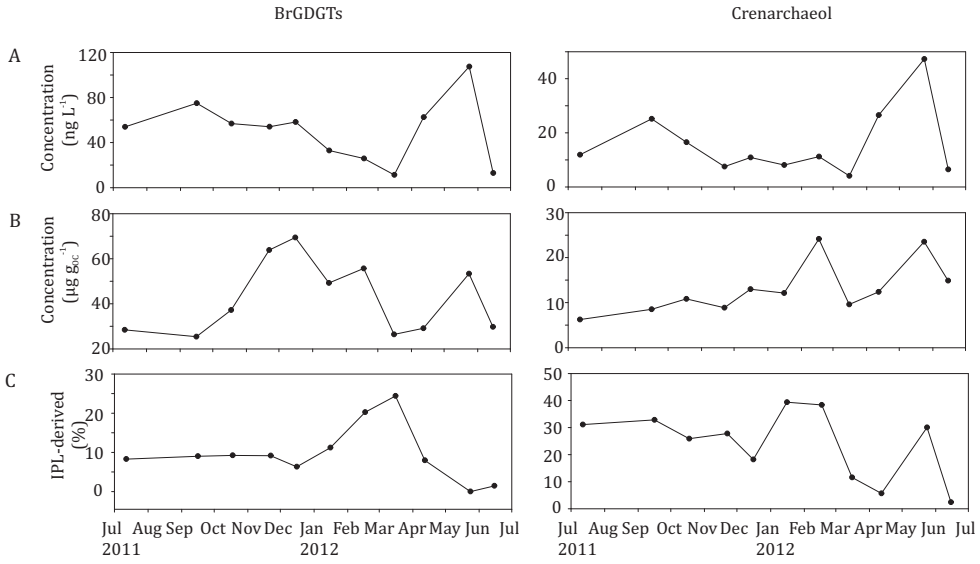

Fig. 6.6 Variations in CL brGDGT and CL crenarchaeol concentrations and the percentage of IPL-derived brGDGTs and crenarchaeol in Tagus SPM over one year (2011-2012).

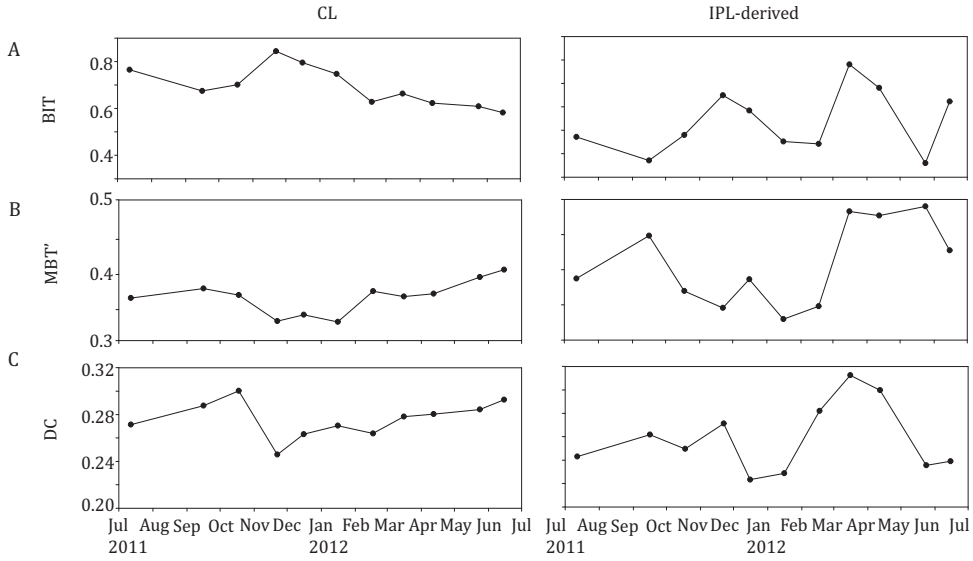

Fig. 6.7 Variations in CL and IPL-derived BIT, MBT' and DC in Tagus SPM over one year (2011-2012).

6.4.4 Marine SPM

The amount of SPM in marine water varied between 0.6 and 2.3 mg L^{-1} with the higher values closest to the estuary mouth (Table 6.1). The OC content of the SPM ranged from 1.6 to 10 wt. % and the $\delta^{13}C_{OC}$ from -24.1 to -26.9 ‰ (Table 6.1). In general, the OC content of SPM was higher in surface than in bottom waters (Fig. 6.8A) and $\delta^{13}C_{OC}$ was more enriched in surface waters compared to bottom waters (Fig. 6.8B). The CL brGDGT concentrations varied widely between 0.06 and 31 µg g_{OC}^{-1} with an average amount of 4±9 µg g_{OC}^{-1}. The percentage of IPL-derived brGDGTs of the total amount of brGDGTs was 15±13. CL brGDGT concentrations decreased from the estuary mouth towards the deep sea canyon (Fig 6.8C). The highest concentration was found in the surface water at the shallowest station A (31 µg g_{OC}^{-1}). The CL brGDGTs were not detectable in the surface water of the canyon station furthest away from the estuary mouth (station F). In all stations but the one closest to the estuary mouth higher brGDGT concentrations were found in the bottom than in surface waters (Fig. 6.8C). The most abundant CL brGDGTs were IIa (32±10 %) and Ia (26±9 %) (Fig. 6.4D). CL crenarchaeol concentrations varied between 82 and 242 µg g_{OC}^{-1} (Fig. 6.8D). The percentage of IPL-derived crenarchaeol was 20±10. The BIT index ranged between <0.01 and 0.18 with an average CL BIT of 0.03±0.06 and IPL derived BIT 0.02±0.03. The highest BIT values were measured closest to the estuary mouth (Fig. 6.9A-B).

Due to low CL and IPL-derived brGDGT concentrations, MBT' and DC could not be calculated for all SPM samples because not all of the necessary brGDGTs were detected. The MBT' and DC of CL brGDGTs were 0.49±0.06 and 0.26±0.14, respectively. For IPL-derived brGDGTs the MBT' and DC were 0.54±0.14 and 0.13±0.13, respectively (Fig. 6.9C-F).

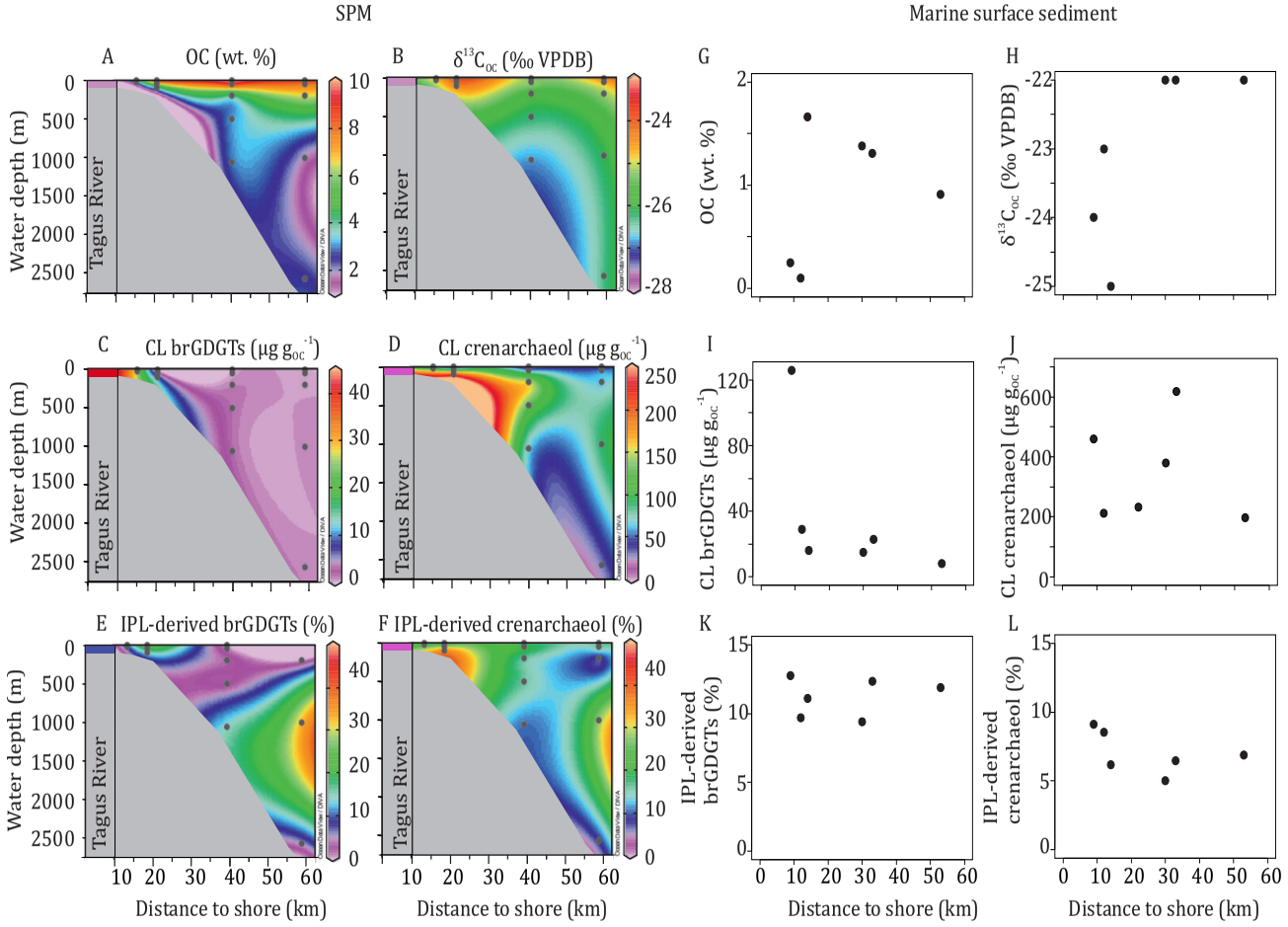

Fig. 6.8 OC content, $\delta^{13}C_{OC}$, CL brGDGT and CL crenarchaeol concentrations, and the percentage of IPL-derived brGDGTs and crenarchaeol (A-F) for marine SPM and (G-L) for marine surface sediments. The average values of the Tagus River SPM were also shown.

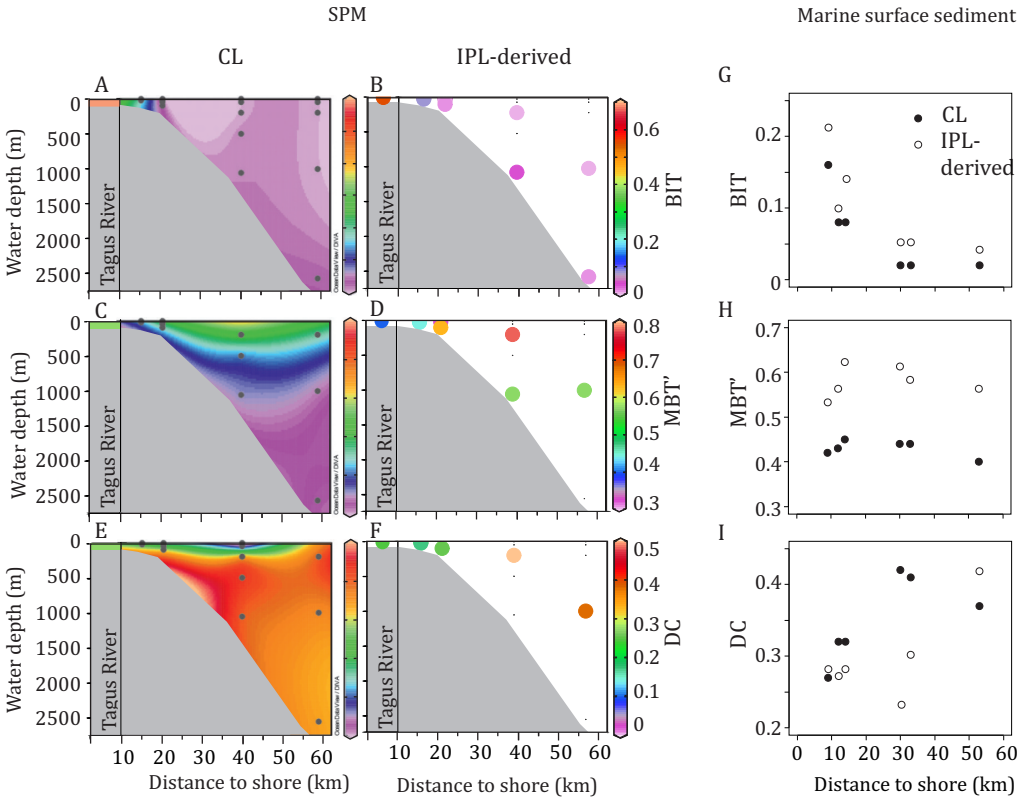

Fig. 6.9 BIT, MBT' and DC of CL and IPL-derived GDGTs (A-F) for marine SPM and (G-I) for marine surface sediments. The average values of the Tagus River SPM were also shown.

6.4.5 Marine surface sediments

The marine surface sediments had the average OC content between 0.01 and 1.7 wt. % and the $\delta^{13}C_{OC}$ values varied between -21.9 and -24.4 ‰ (Table 6.1; Figs. 6.8G-H). The CL brGDGT concentrations (Fig. 6.8I) were higher at stations closed to the estuary mouth (stations A-C) with values declining from 130 to 16 μg g_{OC}^{-1}. The surface sediments from the off-shore stations D-F had lower concentrations (between 23-7 μg g_{OC}^{-1}). The percentage of IPL-derived brGDGTs was on average 11±1. The most abundant brGDGTs were IIa (31±5%) and Ia (22±3 %) (Fig. 6.4E). The crenarchaeol concentrations varied between 120 and 600 μg g_{OC}^{-1} (Fig. 6.8J). The percentage of IPL-derived crenarchaeol was 7±2 (Fig. 6.8L). The BIT index varied between 0.16 and 0.02 in the CL fractions and 0.21 and 0.04 in the IPL-derived fractions, with a clear decreasing trend towards the deep sea canyon station (Fig. 6.9G). The average CL MBT' was 0.43±0.02 and the CL DC was 0.35±0.06. The MBT' of the IPL-derived brGDGTs was on average 0.58±0.03 and the DC 0.30±0.06. For both CL and IPL fractions, MBT' did not show a trend with increasing distance from the coast (Fig. 6.9H), whereas DC showed a trend toward higher values (Fig. 6.9I).

6.5 DISCUSSION

6.5.1 Characteristics of the bulk organic matter

The organic matter content of soil in dry and warm climates is usually low (Jobbágy and Jackson, 2000), which is also observed in the Tagus basin (on average 1.8±2.2 wt. %, Table 6.1). In river SPM, the OC content was similar to that of soil and relatively constant around the year (on average 1.9±0.5 wt. %) (Fig. 6.5C, Table 6.1). The $\delta^{13}C_{OC}$ values of soils, riverbank sediments, and river SPM showed an average value of -27.5±2 ‰, which is a typical C^3 higher plant signal (e.g. Fry and Sherr, 1984). In contrast, in marine SPM and surface sediments, the $\delta^{13}C_{OC}$ values (on average -25.1±2 ‰ and -23.1±2 ‰, respectively) were higher in comparison to those of the Tagus basin samples and increased from inshore to offshore (Figs. 6.8A and 8H). This suggests that the proportion of marine-derived OC to the total OC pool increased from close to the Tagus estuary to the deep sea canyon site. In addition, a higher OC content of SPM was recorded in the upper water layers where marine primary production takes place.

In the marine sediment sampled close to the river estuary the OC content was lower than in the open ocean (Fig. 6.8G). Jouanneau et al. (1998), who studied the OC contents in marine sediments of this area in more detail, also showed that the OC content was low close to the river estuary. This is because the OC content was closely related to the sediment grain size and the average grain size of the surface sediments was larger close to the river estuary. Therefore, the OC content of surface sediments increased towards the mud belt at 100 m water depth. The OC content may also increase at greater water depth due to marine production. Our $\delta^{13}C_{OC}$ data from the marine surface sediments indicate that the majority of the OC on the Portuguese shelf is of marine origin. Already in the estuary, only 50 to 65 % of OC content is estimated to be of terrestrial origin (Alt-Epping et al., 2007). The Tagus River acts mainly as a supplier of terrigenous lithogenic particles to the coastal ocean, while the majority of the terrestrial organic matter is retained inside the estuary (Jouanneau et al., 1998).

6.5.2 GDGTs in soils of the Tagus drainage basin.

BrGDGTs and crenarchaeol were found in all Tagus soils. The relative amount of brGDGTs to crenarchaeol, which is defined in the BIT index, was relatively low (BIT=0.7±0.2) compared to soils in general (cf. Schouten et al., 2013a for an overview). It has been reported in several studies that the BIT decreases with increasing soil pH and is lower and more variable above a pH of 5.5 (Kim et al., 2010c; Peterse et al., 2010; Yang et al., 2011). Indeed the pH of all but one of the soils studied was above 5.5. Recently, reduced values of the BIT index in soils have also been attributed to a dry climate (Xie et al., 2012; Dirghangi et al., 2013; Menges et al., 2013). The reason for the low BIT could be that in dry soils, oxygen can penetrate further into the soil (Cleveland et al., 2010). Xie et al. (2012) suggested that oxic conditions might be unfavorable for the facultative anaerobic brGDGT producing bacteria, but may be beneficial for nitrifying (i.e. requiring

oxygen) Thaumarchaeota, increasing crenarchaeol productions in soils.

The distribution of the brGDGTs varied strongly in the Tagus basin soils (Fig. 6.4), which led to highly variable MBT' and DC (or CBT) values (Fig. 6.10A). The variability in MBT' values is unexpected since in a global soil dataset (Peterse et al., 2012) they are related to MAAT and MAAT does not vary substantially (i.e. 10-17°C, see Table 6.1) for the Tagus basin. However, it has been previously described that the MBT' shows a less strong relationship with MAAT in dry areas (mean annual precipitation (MAP) <700-800 mm yr^{-1}) than in other climate regions (Peterse et al., 2012; Xie, 2012; Dirghangi et al., 2013). The MAP at the sampling sites is indeed low at 450-910 mm yr^{-1} (Table 6.1). A recent study of 23 Iberian soils (Menges et al. 2013) has revealed similar variable MBT' and DC (or CBT) values as we report here. In that study it is suggested that the MBT' is primarily related with the MAP and soil aridity. In our dataset the soils from >900 m altitude showed a higher DC (i.e. >0.3) compared to the rest of the soils, while those collected <200 m altitude showed a relatively low DC (i.e. <0.15) and a higher MBT' (i.e. >0.4) (Fig. 6.10A). However, we did not observe a clear correlation of the DC and MBT' with altitude. The brGDGT composition in soils of the Tagus River watershed was thus quite variable. Soils are notoriously heterogeneous in composition (e.g. Williams et al., 2002) and the fact that the Tagus River basin is in an arid climate zone may further contribute to this poor correlation. Despite the variability of brGDGT distributions in Iberian soils, we will compare them with those in the river system to test if they are an important source for riverine brGDGTs.

6.5.3 Sources of GDGTs in Tagus River SPM and riverbank sediments

Compared to soils, significantly higher concentrations (normalized to OC to account for differences in grain size) of both CL brGDGTs and CL crenarchaeol were found in river SPM (Figs. 6.3A and 6.3C). Higher crenarchaeol concentrations are expected since crenarchaeol is usually produced in higher amounts relative to brGDGTs in aquatic environments (Herfort et al. 2006; Kim et al. 2010). For rivrine brGDGTs it is originally assumed that they originate from surrounding soils (Hopmans et al., 2004). Consequently, it would be expected that riverine brGDGTs have similar concentrations and distributions as the soils in the watershed of the river. The significantly higher CL brGDGT concentration in river SPM than in soils thus suggests that brGDGTs were also produced in-situ in the Tagus River. This could be revealed by a relatively high amount of brGDGTs with polar head groups (cf. Peterse et al., 2011a). The percentage of IPL-derived brGDGTs in river SPM was not significantly higher than in soils (Fig. 6.3B). However, if riverine brGDGTs would only derive from soil erosion, one would expect this number to drop since labile IPL brGDGTs would be preferentially broken down during transport.

A third line of evidence for in-situ production in the river comes from the distribution of brGDGTs (Fig. 6.4). If riverine brGDGTs are derived from two different sources, this can also often be detected in the brGDGT distribution. We compared the brGDGT distribution with the help of the MBT' and DC (Fig. 6.10A). In order to examine what

MBT' and DC values a mixture of the brGDGTs from the drainage basin soils would theoretically have, we calculated a brGDGT concentration-weighted MBT' and DC. This is based on the assumption that soils that contain a higher concentration of brGDGTs will contribute more to the brGDGTs in the river. The weighted CL MBT' and CL DC values were 0.36 and 0.10, respectively (Fig. 6.10A). These values are substantially influenced by soil samples 7 and 8b (both from <200 m altitude), because they have high brGDGT concentrations compared to all other soils. If low-altitude soils are not considered, the weighted average (MBT'=0.18, DC=0.11) falls in the cloud of the majority of the soils (Fig. 6.10A). Irrespective of which average is used, Fig. 6.10A shows that the average DC in river SPM is substantially higher (i.e. 0.28 versus 0.10), which again supports that brGDGTs are produced in the river.

In a study of brGDGTs in SPM of the Amazon River (Brazil), it is shown that the brGDGT concentration and distribution can be influenced by hydrological changes, meaning that during times of increased precipitation higher amounts of brGDGTs are washed into the river from soils (Zell et al., 2013b). This influences the brGDGT distribution in rivers because it affects the amount of soil-derived relative to in-situ-produced brGDGTs in the river. In addition, the brGDGTs produced in the river might reflect environmental conditions in the river that change over the annual cycle. We evaluated temporal variations in the brGDGT composition of the SPM (sampled close to the river mouth) to shed further light on the potential origins of brGDGTs. The Iberian Peninsula is typically characterized by a period of higher precipitation from October to March and thus higher Tagus River discharge (Fig. 6.5A). However, during the SPM sampling period (2011-2012) the Iberian Peninsula experienced a relatively dry winter (Trigo et al., 2012). A profound increase in precipitation is evident for October and November, but December-March were unusually dry (Fig. 6.5A). This precipitation pattern does not show a clear relationship with the SPM concentration profile (Fig. 6.5B) and the concentration of brGDGTs (Figs. 6A-B), as would be expected if increased precipitation would result in increased soil erosion and subsequent input in the river system, although it should be noted that we did not measure the SPM and brGDGT fluxes. A further complication is that the Tagus River is strongly regulated with dams that are used to provide drinking water and water for agricultural purposes to Spain and Portugal and also to generate hydroelectricity. Therefore, the flow through the river is not only influenced by precipitation. In terms of compositional changes in SPM, it is noteworthy that at the peak of maximum precipitation in November 2011, the BIT index is at a maximum (0.84) and the DC of the brGDGT shows the lowest value (0.25). This could be interpreted as an increased contribution of soil-derived brGDGTs, although the value for the DC is still far away from the average for soils in the watershed (0.10-0.11; Fig 6.10C). With respect to the temporal changes in the MBT', the lowest values are recorded for November-March (Figs. 6.10B) with the largest changes observed for the IPL-derived brGDGTs. MBT' (and MBT) are also related to temperature in aquatic systems (Tierney et al., 2010; Zink et al., 2010; Pearson et al., 2011; Sun et al., 2011). Hence, MBT' could be used as evidence for in-situ production of

brGDGTs in the river as MBT' would then follow the changes in temperature over the annual cycle, whereas in case of a dominant soil origin for the brGDGTs, this would not be expected because of their residence time in soils (Weijers et al., 2011a). Our data show that seasonal hydrological changes may have an influence on the brGDGT distribution in the Tagus River, but these changes are not evident enough to make an estimate of the contributions of the two sources for brGDGTs in this river system.

Compared to the SPM, which was only sampled close to the river mouth, riverbank sediments were sampled at several stations along the river. In most of the riverbank sediment the DC was higher than in river SPM. However, the MBT' and DC of the riverbank sediment close to the river mouth (samples 6 and 8a) were similar to those of the river SPM, which was also collected close to the river mouth. This shows that the DC of brGDGTs most likely varies along the river. Numerous dams in the Tagus River hold back the sediment from the upstream parts and, thereby, they might decrease the influence of brGDGTs from the upstream drainage basin on the downstream river.

6.5.4 Sources of GDGTs in marine SPM and surface sediments

It should be considered that the results from the marine SPM only give a "snap shot" at the moment of sampling (i.e. March 2011, chosen to reflect the end of the season with highest amount of rainfall) and should, thus, be interpreted cautiously. The crenarchaeol concentrations were higher in marine SPM and surface sediments than in river SPM, which shows that marine Thaumarchaeota were the predominant source of crenarchaeol in the marine environment. In SPM IPL-derived crenarchaeol was higher than in sediments (Figs. 6.8F and 6.8L), suggesting that crenarchaeol production takes place predominantly in the water column. In the marine sediment the crenarchaeol concentration showed no clear trend from land to ocean (Fig. 6.8J). At the time of sampling the input of brGDGTs from the river into the marine system was evident. Higher CL brGDGT concentrations were detected at the stations (A-C) close to the river estuary but these concentrations were already lower than those in river SPM (Fig. 6.8C). Higher CL brGDGT concentrations were also found in the bottom water SPM as compared to shallow water SPM (Fig. 6.8C). This may indicate that the brGDGT in river SPM are (partially) transported by a bottom nepheloid layer. This terrestrial input to the bottom nepheloid layer is also clearly indicated by the lower $\delta^{13}C_{OC}$ values in the bottom SPM (Fig. 6.8B). IPL-derived brGDGTs in marine SPM show a completely different pattern (Fig. 8E) and do not seem to be transported from the Tagus River into the ocean.

A further clue towards potential sources of brGDGTs in the marine system can be obtained by comparing their distributions. Fig. 6.4 shows that marine SPM is on average less dominated by brGDGT IIa than river SPM. Furthermore, the MBT' and DC values of brGDGTs in marine SPM varied more than those of Tagus River SPM (Fig. 6.10A). The spatial distribution of CL MBT' (Fig. 6.9C) and DC values (Fig. 6.9E) showed lower MBT' and higher DC values in the deeper water layers than in surface waters. This trend was

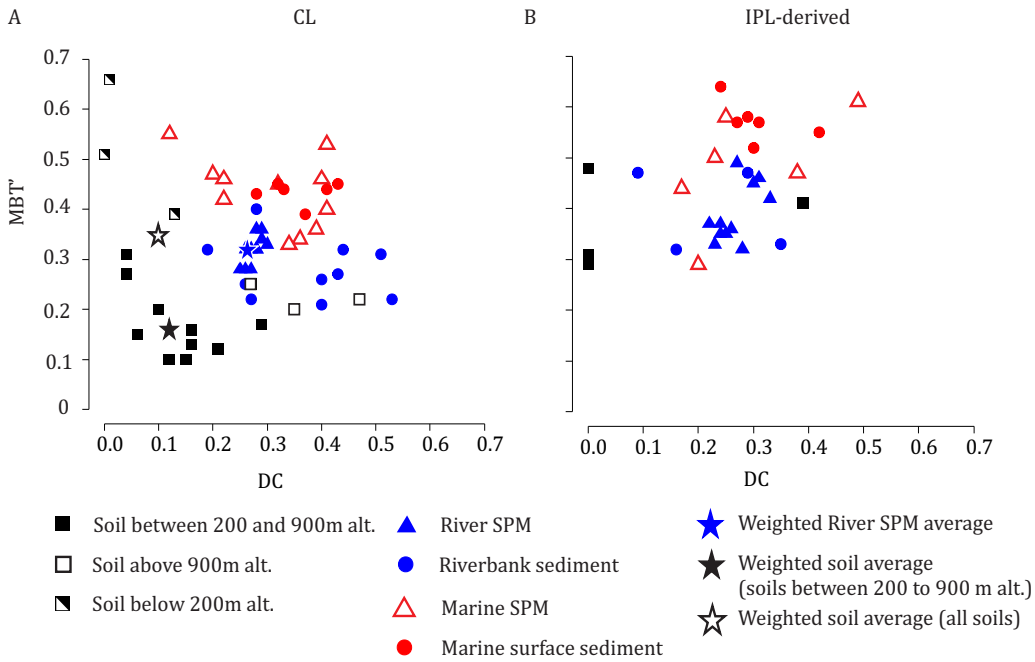

Fig. 6.10 Scatter plots of MBT' vs. DC for (A) CL and (B) IPL-derived brGDGTs in all sample types. The weighted average values of the Tagus basin samples were also shown.

also apparent in the MBT' and DC values of IPL brGDGTs (Figs. 6.9B and 6.9D), although less data could be obtained. The input of brGDGTs in river SPM is still clear from these plots since MBT' and DC values of the coastal stations (A-C) are comparable to those in river SPM. Further away from the river estuary, brGDGTs in marine SPM do not only show a substantially lower concentration but the changing DC and MBT' values also reveal a different distribution (Fig. 6.9C-F). This can only be explained by a rapid dilution of the river SPM with in-situ production of brGDGTs in the marine water column (albeit at much lower levels than in the river). This is consistent with expected alterations in brGDGTs since the higher pH of sea water and lower temperatures in deeper waters would give rise to the observed spatial patterns (i.e. higher DC and lower MBT' values).

The brGDGT composition of marine surface sediments, in contrast to that of marine SPM, may provide a signature that is averaged over seasons and years. However, it may be affected by in-situ production in the sediment (cf. Peterse et al., 2009a). As was seen for marine SPM (Fig. 6.8C), the CL brGDGT concentrations normalized per gOC in the marine sediments was highest at the station (A) closest to the estuary with a markedly declining trend with further distance from the river estuary (Fig. 6.8I). Surprisingly, the CL brGDGT concentration at station A was even higher than that in the Tagus River SPM (Fig. 6.8G). This might be caused by faster degradation of other riverine organic matter, while CL brGDGTs were more stable and consequently slightly increased in concentration (normalized on OC) (cf. Huguet et al., 2008). Overall, the concentration trend

is in line with rapid dilution of brGDGTs delivered from the river to the ocean.

A next step is to consider the brGDGT distribution of the marine sediments. The MBT' of CL brGDGTs was slightly higher than that of the Tagus River SPM (Fig. 6.10A) and showed no spatial variation (Fig. 6.9H). The DC in the coastal station A was similar to that of river SPM (Fig 6.10A), but it showed a clear increase from the coast to the ocean (Fig. 6.9I), consistent with the trend in marine SPM (Fig. 6.9E). IPL-derived brGDGT had a constant MBT' but it was higher than that of CL GDGTs. The DC of IPL-derived brGDGTs in marine sediment showed a similar increase with increasing distance offshore as for CL brGDGTs, although the trend was more scattered (Fig. 6.9I). Overall, these observed distributional changes are in line with an increasingly important contribution of marine in-situ production of brGDGTs with increasing distance from the river estuary.

If the MBT' and DC would in general change in the same way from river to ocean it would help to make predictions on how the MBT'/CBT proxy in marine sediments should be interpreted. Similar studies have been carried out in other locations. An increase of the DC from soil to the marine environment has been described so far in all studied locations [Yangtze River (Zhu et al., 2011), Pearl River (Zhang et al., 2012), a Norwegian fjord (Peterse et al., 2009a) and the Amazon River (Zell et al. submitted)]. This increase of the DC was assumed to be due to in-situ production of brGDGTs in the marine environment, since the pH in the marine environment (pH≈8) is usually higher compared to that of soils and river water. In contrast changes in MBT' in transects from land to ocean are different in different locations. On the Portuguese coast and on the East China Sea shelf (Zhu et al., 2011), the MBT' increased, but it remained unchanged on the South China Sea shelf (Zhang et al., 2012) and for the Amazon shelf it strongly decreased in both the CL and IPL-derived fraction (Zell et al., submitted). This might be depended on the marine water temperature compared to the continental air temperature. Further research is needed to understand the influences on the distribution of brGDGTs that were produced in the marine environment.

6.5.5 Implications for the use of GDGT-based proxies in marine sediments

6.5.5.1 BIT index

The BIT index was originally used to trace terrestrial OC input from land to ocean (Hopmans et al., 2004). Subsequently, since brGDGTs occur ubiquitously in soils (Weijers et al., 2006b) and because brGDGTs are not associated with fresh higher plant debris (Walsh et al., 2008), it is interpreted as a tracer of soil OC (e.g. Huguet et al., 2007; Weijers et al., 2009b). In the case of the Tagus River basin, we found that the brGDGTs in the river are not only derived from soils but also produced in-situ, in line with other recent studies of river systems (Zell et al., 2013a,b; De Jonge et al., 2014). Therefore, the BIT index should be considered as an indicator for continental OC rather than for soil OC. In the marine environment, the BIT decreases strongly with increasing distance from the river mouth. This can be seen clearly in both SPM and marine surface sediments (Fig. 6.9A, G). This trend in BIT from high values in the terrestrial environment

to low values in the marine environment is still in agreement with the first observation for the Congo River system (Hopmans et al., 2004). However, follow-up studies have suggested that changes in BIT in marine systems are predominantly due to changes in the crenarchaeol concentration (Castañeda et al., 2010; Schmidt et al., 2010; Fietz et al., 2011; Smith et al., 2012). Our data also show high crenarchaeol concentrations close to the shore (Fig. 6.8D, J) but they also reveal that by far the highest brGDGT concentrations are found close to the river estuary. This indicates that, at least for the Tagus River system, brGDGT concentrations are also important in determining the BIT index and that, in fact, the declining brGDGT concentrations with increasing distance from the river estuary are the key factor in the declining BIT values. Therefore, despite the mixed origin of the brGDGTs in the river (i.e. soil-derived and aquatic), the BIT in the Tagus River system works as a tracer for continental OC. Nevertheless, in future studies it remains recommendable to survey the concentrations of brGDGTs and crenarchaeol in addition to determining the BIT index.

6.5.5.2 Implications for the MBT'/CBT proxy

The MBT'/CBT proxy has been used to reconstruct MAAT and soil pH of the river basin by determining brGDGT distributions in marine sediments deposited in the vicinity of a river outflow (e.g. Weijers et al., 2007a). Subsequently, various problems with this approach have been reported, i.e., the potentially increased input of brGDGTs from a region that is not representative for the whole basin, for example from colder mountain regions (Bendle et al. 2010), production of brGDGTs in the river (Zell et al., 2013a,b, De Jonge et al., 2014), and production of brGDGTs in the marine environment (Peterse et al., 2009; Zell et al., submitted). Here, we followed in detail the transport of brGDGTs in the Tagus River system from source to sink and are able to evaluate potential difficulties with this approach.

In the case of the Tagus River basin we encountered various problems. Firstly, the MAAT cannot be accurately reconstructed using the brGDGT distribution of the soils. Reconstructed temperatures using a global soil calibration (Peterse et al., 2012) are between 0 and 10°C, while the actual MAAT of the soil sampling sites is substantially higher, i.e. between 10 and 17°C (Table 6.1). As discussed previously, caution has to be taken when the MBT'/CBT is used for MAAT reconstructions in dry environments (Peterse et al., 2012; Dirghani et al, 2013; Menge et al. 2013) and, clearly, this applies to the Tagus River basin. Secondly, due to the much higher concentrations of brGDGTs in the Tagus River SPM compared to the soils and their different brGDGT distributions, it is likely that the brGDGTs in the Tagus River are predominantly produced in the river. This means that the brGDGTs in the river do not represent the brGDGT distribution of the soils, which makes it impossible to reconstruct river basin soil conditions using brGDGTs transported by the Tagus River. Thirdly, from the river estuary to the open marine environment brGDGT distributions (and consequently MBT' and CBT values) changed again, due to the increasing influence of in-situ produced marine brGDGTs. This shows

that at least for the Tagus River system, but probably more generally, brGDGTs in marine sediments cannot directly be used to reconstruct soil pH and MAAT of the river basin.

Since the majority of the brGDGTs in the Tagus River are likely produced in the river, it might be possible to reconstruct the environmental conditions in the river instead of those of the river basin soils. It is well known that brGDGT soil calibrations differ from those reported for aquatic environments (Tierney et al., 2010; Zink et la., 2010; Pearson et al., 2011; Sun et al., 2011). However, calibrations for river water have not yet been reported. Therefore, for the reconstruction of the river pH and temperature the application of a lake calibration is currently used (cf. De Jonge et al., 2014). A number of calibrations have been reported for the MBT/CBT, but so far no lake calibrations for the MBT'/CBT exist to the best of our knowledge. Furthermore, river water temperatures were not measured when river SPM was collected and we were not successful to obtain Tagus River temperature data from the existing database neither. Therefore, we are for the moment unable to test if climate reconstructions using Tagus River-derived brGDGTs should, in principle, be possible.

In order to prevent strong influence of marine in-situ produced brGDGTs, it is recommendable to use cores that were taken close to the river mouth. How far away from the river the brGDGTs from the river are still dominant over the ones produced in the marine environment can be influenced by several factors, for example the degradation processes in the estuary, sedimentation rates and the ocean currents. The BIT index might be a good indicator for high river influence. In general the higher the BIT the more likely it is that there is more river input and thus a more similar MBT' and DC that is most similar to that of the river SPM. From our data we can see that at a BIT <0.05, especially the DC was quite different. Therefore, we recommend certainly not to apply the MBT'/CBT in sediment records with a BIT <0.05. Further studies are needed to understand what influences the MBT' and DC in brGDGTs that are produced in the marine environment. In general this study shows that there are many factors that can complicate the use of the MBT'/CBT to reconstruct river basin temperature and soil pH from marine sediment cores. Therefore, it is absolutely necessary to investigate the basin soils, river SPM and marine surface sediments before interpreting the MBT'/CBT records from a marine sediment core. This severely complicates paleostudies going back further in time.

6.6 CONCLUSION

Our study shows that in the case of the Tagus River system there are several problems concerning the use of the MBT'/CBT to reconstruct river basin MAAT and soil pH. Firstly, soil brGDGTs in dry environment do not accurately predict the MAAT and soil pH, secondly, brGDGTs in the river SPM are mainly produced in-situ, and thirdly MBT' and DC values in marine sediments are further influenced by brGDGTs produced in the marine environment. Since the majority of brGDGTs seem to be produced in the aquatic environment, it is probably possible to use a lake (or river) calibration to reconstruct the environmental conditions of the river itself. This indicates that in order to decide whether the MBT'/CBT can be used to reconstruct the terrestrial paleoenvironmental changes from marine sediment cores, it is essential to test the MBT'/CBT of drainage basin soils and river SPM. If it is decided that the MBT'/CBT can be used for environmental reconstructions, the core should be taken as close to the river as possible to minimize the influence of brGDGTs produced in the marine environment.

Acknowledgments
The research leading to these results has received funding from the European Research Council (ERC) under the European Union's Seventh Framework Program (FP7/2007-2013) ERC grant agreement [226600]. We thank Jérôme Bonnin for Tagus soil sampling, Pierre-Antoine Dessandier for the elemental analysis, and Henko de Stigter and Silvia Nave for the help of the cruise preparation. We also thank the captain and crew of the R/V Pelagia for their excellent services during the PACEMAKER cruise.

Picture by Maianne Baas

Chapter 7

Influence of rivers on the sources and distributions of branched tetraether lipids along the Portuguese continental margin

Claudia Zell, Jung-Hyun Kim, Denise Dorhout, Marianne Baas, and Jaap S. Sinninghe Damsté

Submitted to Marine Chemistry

Abstract

The branched vs. isoprenoid tetraethers (BIT) index, which is based on the relative abundance of non-isoprenoidal, so-called branched glycerol dialkyl glycerol tetraethers (brGDGTs) versus a structurally related isoprenoid GDGT "crenarchaeol", is used to trace continental organic carbon (OC) from land to the ocean. However, it has been reported that the BIT index is primarily influenced by crenarchaeol concentrations rather than by soil-derived brGDGT concentrations. This may hamper the application of this proxy as an indicator for the input of continental OC. Here we examined the concentration and distribution of brGDGTs as well as variations in the BIT index in marine surface sediments from five transects (Douro, Mondego, Estremadura, Tagus, and Sado) along the southern Portuguese continental margin and in marine suspended particulate matter (SPM) from the Douro and Tagus transects. Higher BIT values and brGDGT concentrations (normalized on OC content) were found close to the rivers and on the shelf than in deep offshore sites. This clearly indicated the continental input of brGDGTs and revealed that, at least in this setting, the BIT index was primarily influenced by the delivery of brGDGTs from the rivers. However, the BIT index was also, to a minor extent, influenced by crenarchaeol concentrations. This shows that the brGDGT concentration may provide a more straightforward indication of continental OC input than the BIT index. BrGDGT concentrations and distributions in sediments and SPM close to the rivers were similar to those of SPM in the Tagus River. This indicates that degradation processes in the estuaries had no significant effect on the riverine brGDGTs. Therefore, brGDGTs should be a good indicator for the rigid OC fraction transported from the continent to the ocean. Our results also indicate that there are multiple sources of brGDGTs in the marine environment, which complicates the use of the brGDGT distribution as an indicator for terrestrial vs. marine produced brGDGTs.

7.1 INTRODUCTION

Branched glycerol dialkyl glycerol tetraethers (brGDGTs) are most likely membrane-spanning lipids of anaerobic (Weijers et al., 2006a,b), heterotrophic (e.g. Oppermann et al., 2010; Pancost and Sinninghe Damsté, 2003; Weijers et al., 2010) bacteria. They have been used to trace continental organic carbon (OC) to the ocean, since brGDGTs are produced in higher concentrations in the continental environment than in the marine environment (e.g. Hopmans et al., 2004). Originally it was thought that brGDGTs were only produced in the terrestrial environment because high concentrations of brGDGTs were found in peats (Weijers et al., 2006a) and soils (Weijers et al., 2007). However, brGDGTs have subsequently been shown to also be produced in lakes (Bechtel et al., 2010; Loomis et al., 2011; Sinninghe Damsté et al., 2009; Tierney and Russell, 2009; Tierney et al., 2010, 2012; Zink et al., 2010) and rivers (De Jonge et al., 2014; Kim et al., 2012; Yang et al., 2013; Zell et al., 2013a,b; Zhang et al., 2012; Zhu et al., 2011), which is

why brGDGTs cannot only be related to soil OC. Recent studies provide increasing evidence that brGDGTs can also be produced in the marine environment, but the concentrations are much lower than in the continental environment (Hu et al., 2012; Peterse et al., 2009; Wu et al., 2014; Zhu et al., 2011). Higher brGDGTs in coastal areas, therefore, still likely indicate the input of continental OC from land, for example close to rivers, to the marine environment.

The branched vs. isoprenoid tetraethers (BIT) index has often been used to trace the transport of continental OC to the marine environment. The BIT index is a ratio of brGDGTs and crenarchaeol (Fig. 1). It is based on the generally higher abundance of crenarchaeol compared to brGDGTs in the marine environment (Hopmans et al., 2004). Initially, it was thought that the BIT index equaled 0 in the marine environment and 1 in the terrestrial environment (Hopmans et al., 2004). However, this is often not the case, since brGDGTs can also be produced in the marine environment (e.g. Hu et al., 2012; Peterse et al., 2009; Zhu et al., 2011) and crenarchaeol also occurs in soils (e.g. Weijers et al., 2006b). Especially in alkaline soils crenarchaeol concentrations are high, which leads to lower BIT values (e.g. Kim et al., 2010; Weijers et al., 2007; Xie et al., 2012; Yang et al., 2011). Furthermore, crenarchaeol is also produced in rivers, e.g. in the case of the Amazon River a BIT index as low as 0.4 was reported for suspended particulate matter (SPM) (Zell et al., 2013a). In addition, the BIT index can be influenced by variations in the crenarchaeol concentration in the marine environment (e.g. Castañeda et al., 2010; Fietz et al., 2011; Schmidt et al., 2010; Smith et al., 2012). Hence the BIT index can be influenced by many factors, which complicates its application. The measurement of absolute brGDGT concentrations might, therefore, be a more straightforward indication for continental OC input. This has also been proposed for other study sites, e.g. the southern North Sea (Herfort et al., 2006).

Here, we studied the input of brGDGTs along the Portuguese coast. An earlier study (Schmidt et al., 2010) revealed that values of the BIT index in surface sediments of the northern Portuguese shelf were always relatively low (≤0.1) and concluded that the BIT index, in comparison with other proxies such as lignin derived markers, was a less efficient marker for the transport of continental OC. We examined the concentration and distribution of brGDGTs in five transects along the southern Portuguese continental margin (Fig. 2). Transects I and IV start close to the river mouth of the Douro River and the Tagus River, respectively. It is therefore expected that the input of brGDGTs from the rivers can be seen in the concentration and distribution of brGDGTs. Transects II and V start close to the mouth of substantially smaller rivers, the Mondego River and the Sado River, respectively, while transect III does not receive any direct input from a river. Transect III is, therefore, thought to be less influenced by the terrestrial environment. It is known that organic matter transported by rivers is often strongly degraded in the estuary. This degradation processes might also influence the amounts of brGDGTs that are delivered by the rivers. The Douro and Tagus river systems have different types of estuaries. The Tagus River has a large estuary (the largest in Western Europe) and it

has been reported that its estuary retains the majority of the terrestrial organic matter transported by the river (Jouanneau et al., 1998). By contrast, the Douro estuary is smaller and has a higher discharge rate, thus the riverine organic matter has a relatively short residence time in this estuary (a few days) (Abril et al., 2002). Consequently, by measuring brGDGTs and crenarchaeol in surface sediments from the five transects and in SPM from the Tagus and Douro transects, our study sheds light on the application of brGDGTs as a tracer for continental OC.

7.2 STUDY AREA

The Portuguese continental shelf ranges from 20 to 34 km in width. The shelf break varies between 130 and 150 m water depth. Several canyons (e.g. Nazaré, Cascais, and Setúbal–Lisbon canyons) intersect the shelf (e.g. Vanney and Mougenot, 1981). In summer (May to September), the Azores high pressure system is driven closer to the coast, which together with the associated northerly winds makes the colder, less salty and nutrient enriched subsurface water (from 60 to 120 m depth) rise to the surface along the Iberian margin (Fiúza, 1983). This upwelling leads to increased productivity in summer along a ca. 50 km wide zone. In winter, the Azores high moves south which results in southerly winds and downwelling conditions. The down welling conditions lead to deposition of sediment on the shelf (Frouin et al., 1990). Winter storms can remobilize sediment and transport it northward by bottom currents (Dias et al., 2002; Vitorino et al., 2002) and eventually deposit it in the mid-shelf mudbelt (between 50 and 130 m water depths) (Vitorino et al., 2002). Hence, the upper 10 to 15 cm of sediment on the inner shelf (above 100 m water depth) represent a mixing layer which decreases in mixing frequency and depth towards the ocean (Jouanneau et al., 2002). Although the Portugal coastal counter current hinders material export from the shelf to the ocean in general, a transport of fine material occurs during storm events from the mid-shelf area that is subsequently eroded due to the northward slope current on the outer shelf (Vitorino et al., 2002).

The shelf is also influenced by the input of various rivers, delivering nutrients and terrestrial material. The Douro and Tagus Rivers are the two largest rivers on the Iberian Peninsula (Fig. 2). The Douro River is located in the north of the Iberian Peninsula, which has a drainage basin of 95,700 km^2 and an annual mean water discharge of 500 $m^3 s^{-1}$ (Van der Leeden, 1975). The Tagus River is located in the central part of the Peninsula, its watershed is about 80,600 km^2 and its annual mean water discharge is 360 $m^3 s^{-1}$ (Jouanneau et al., 1998). The Tagus River has a big mesotidal estuary with an area of 340 km^2 (Vale and Sundby., 1985). Both rivers have strong seasonal changes in discharge. There are also smaller rivers that enter the ocean along the Portuguese coast. Two of them, relevant for this study (Fig. 2), are the Sado

River, which has a mean annual discharge of <10 m^3 s^{-1} (Loureiro et al., 1986), and the Mondego River, which has a mean annual discharge of 82 m^3 s^{-1} (Van der Leeden, 1975).

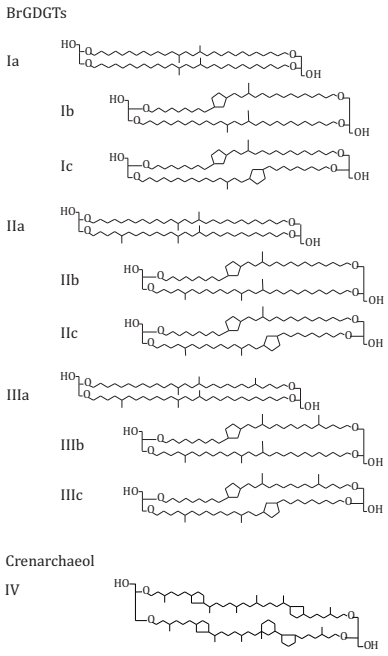

Fig. 7.1 Chemical structure of brGDGTs (Ia-IIIa) and crenarchaeol (IV).

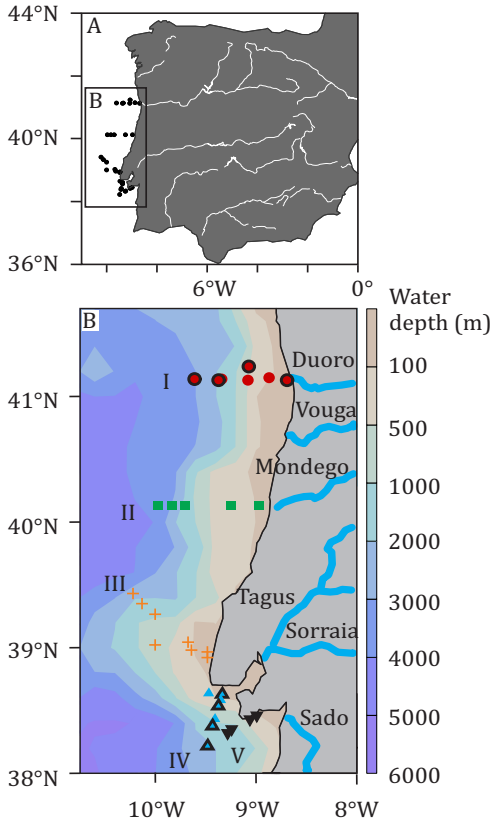

Fig. 7.2 (A) Overview of the study area with the sampling sites of surface sediments and (B) detailed sampling locations of surface sediments along the five (I: Douro, II: Mondego, III: Estremadura, IV: Tagus, and V: Sado) transects. Symbols with a black outline indicate the sites at which SPM samples were also taken.

7.3 MATERIALS AND METHODS

7.3.1 Sample collection

Marine SPM and sediments were taken during the 64PE332 cruise with the R/V Pelagia between 14th and 29th March 2011 (Table 1 and 2). Marine SPM was collected at three stations along the Douro transect and at four stations along the Tagus transect at 2-5 different water depths (Fig. 2; Table 1). Between 60 and 240 L of seawater were filtered over ashed glass-fiber filters (Whatman GF-F, 0.7 µm pore size, 142 mm diameter) with a McLane in-situ pump system (WTS, McLane Labs, Falmouth, MA). For the OC and stable carbon isotope ($\delta^{13}C_{OC}$) analysis, about 8 L of seawater were filtered on a separate filter (Whatman GF-F, 0.7 µm pore size, 47 mm diameter). Marine sediment cores were retrieved at 31 stations at transects I-V (Fig. 2, Table 2) using a multicorer

developed by Oktopus GmbH. The top 0.5 cm of the multi-cores was used in this study. All samples were frozen immediately after sampling and freeze-dried before analysis.

7.3.2 Bulk geochemical analysis

For the OC and $\delta^{13}C_{OC}$ analysis, the SPM filters were decarbonated with HCl vapor as described by Lorrain et al. (2003). Surface sediments were decarbonated with 2 mol L^{-1} HCl (overnight at 50°C). All samples were analyzed with a Thermo Finnigan Flash 1112 series Elemental Analyzer interfaced with a Thermo Finnigan DeltaPlus mass spectrometer. OC is expressed as the weight percentage of dry sediment or SPM (wt. %). The $\delta^{13}C_{OC}$ values are reported in the standard delta notation relative to Vienna Pee Dee Belemnite standard (VPDB). A laboratory acetanilide standard with $\delta^{13}C_{OC}$ value calibrated against NBS-22 oil and a known OC content was used for calibration. The analyses were determined at least in duplicate and the analytical error was on average better than 0.1 wt. % for the OC content and smaller than ±0.1 ‰ for the $\delta^{13}C_{OC}$.

7.3.3 Lipid extraction and analysis

SPM filters and surface sediment of transects I and IV were extracted with a modified Bligh and Dyer (BD) technique (Pitcher et al., 2009). The Bligh and Dyer extracts (BDE) were separated into a CL fraction and an IPL fraction on activated silica using n-hexane:ethyl acetate (1:1, v:v) as eluent for the CL fraction and methanol for the IPL fraction (Oba et al., 2006; Pitcher et al., 2009). For GDGT quantification, 0.01 µg C46 GDGT internal standard was added into the CL as well as into the IPL fractions (Huguet et al., 2006). The CL fractions were separated into two fractions, with hexane:DCM (1:1, v:v) and DCM:MeOH, (1:1, v:v) over an Al2O3 column (activated for 2 h at 150˚C). Of the IPL fraction 2/3 was hydrolyzed to obtain IPL-derived CLs (Weijers et al., 2011). The DCM:MeOH fraction from the original CL fraction contains the CL brGDGTs and is from now on referred to as CL fraction. The CL fractions, the hydrolyzed IPL fractions (IPL-derived fraction), and the non-hydrolyzed IPL fractions were analyzed for CL GDGTs. The non-hydrolyzed IPL fractions were analyzed, because it was reported by Pitcher et al. (2009) that during the separation of CL and IPL fraction a small amount of the CL GDGTs is carried over into the IPL fraction. Therefore, it was necessary to implement a correction to more accurately calculate the amounts of CL and IPL-derived GDGTs as described by Weijers et al. (2011).

All surface sediments (between 0.3–3 g) were extracted with an Accelerated Solvent Extractor (ASE). A mixture of DCM:MeOH (9:1, v:v) was used at a temperature of 100˚C and a pressure of 1500psi, for 5 min with 60% flush and purge 60s (3x). The extracts were dried with a Caliper Turbovab®LV and then taken up in DCM and dried over anhydrous Na2SO4. The internal standard C46 GDGT (0.1 µg) was added to the total extracts. Then, the ASE extracts were separated into two fractions over an Al2O3 column (activated for 2 h at 150˚C) using hexane:DCM (1:1, v:v), and DCM:MeOH (1:1, v:v), respectively.

The GDGTs were analyzed using a high performance liquid chromatography–atmospheric pressure positive ion chemical ionization–mass spectrometry (HPLC-APCI-MS) with an Agilent 1100 series LC/MSD SL. They were separated on an Alltech Prevail Cyano column (150 mm x 2.1 mm; 3 µm) using the method described by Schouten et al. (2007) and modified by Peterse et al. (2012). The injection volume was 10 µl per sample. The compounds were eluted isocratically with 90 % hexane and 10 % hexane:isopropanol (9:1, v:v) for 5 min at a flow rate of 0.2 ml min^{-1}, and then with a linear gradient to 16 % hexane:isopropanol (9:1, v:v) for 34 min. Selective ion monitoring of the $[M+H]^+$ of the different brGDGTs and crenarchaeol was used to detect and quantify them. Quantification was achieved by calculating the area of its corresponding peak in the chromatogram and comparing it with the peak area of the internal standard and correcting for the different response factors (Huguet et al., 2006). The analytical error was determined by duplicate measurements of 6 samples. For the concentration of the sum of brGDGTs, the analytical error was 9 % for the brGDGTs and 15 % of crenarchaeol.

Table 7.1 SPM sampling stations and bulk geochemical data.

Station	Long.	Lat.	Sampling water depth (m)	Sampling date (dd/mm/yyyy)	SPM (mg L^{-1})	OC of SPM (wt. %)	$\delta^{13}C_{OC}$ (‰ VPDB)
I. Douro transect							
1	-8.69	41.13	1	14/03/2011	11.9	2.7	-26.7
			14	14/03/2011	9.6	4.0	-24.1
4	-9.08	41.13	1	17/03/2011	1.9	7.7	-21.7
			20	17/03/2011	0.8	11.3	-22.6
			50	17/03/2011	1.0	5.9	-23.3
			109	17/03/2011	1.4	7.7	-23.6
6	-9.37	41.13	1	16/03/2011	0.6	11.2	-23.9
			200	16/03/2011	1.0	3.5	-25.9
			1006	16/03/2011	0.2	8.3	-29.8
7	-9.61	41.14	1	15-16/03/2011	0.6	22.5	-25.0
			200	15-16/03/2011	0.3	8.9	-27.9
			1988	15-16/03/2011	0.8	2.1	-29.1
IV. Tagus transect*							
1	-9.36	38.61	1	24/03/2011	2.3	3.6	-24.6
			19	24/03/2011	2.3	2.9	-25.0
4	-9.37	38.56	1	24/03/2011	0.6	9.8	-24.2
			20	24/03/2011	0.9	6.8	-23.8
			50	24/03/2011	0.6	5.3	-23.9
			93	24/03/2011	1.0	3.2	-24.6
5	-9.43	38.39	1	25/03/2011	0.5	9.6	-25.8
			50	25/03/2011	0.4	10.0	-24.6
			200	25/03/2011	0.8	2.5	-26.0
			500	25/03/2011	0.4	3.4	-26.2
			1051	25/03/2011	0.7	3.0	-26.9
7	-9.48	38.23	1	27/03/2011	0.4	9.2	-24.1
			50	27/03/2011	0.4	6.9	-25.1
			200	27/03/2011	0.8	6.9	-25.1
			1000	27/03/2011	1.0	1.6	-26.1
			2431	27/03/2011	0.6	2.5	-26.3

*The data from the IV Tagus transect are from Zell et al. (in prep.).

Table 7.2 Sampling stations of marine surface sediments and bulk geochemical data.

Transect	Station	Long.	Lat.	Water depth (m)	Sampling date (dd/mm/yyyy)	OC of sediment (wt. %)	$\delta^{13}C_{OC}$ (‰ VPDB)
I. Douro transect	1	-8.69	41.13	15	14/03/2011	0.1	-22.8
	2	-8.87	41.15	51	17/03/2011	0.1	-22.1
	3	-9.07	41.24	104	18/03/2011	1.4	-24.6
	4	-9.08	41.13	110	17/03/2011	1.2	-24.1
	5	-9.34	41.14	506	17/03/2011	0.2	-20.6
	6	-9.37	41.13	1007	16/03/2011	0.9	-22.3
	7	-9.61	41.14	1989	16/03/2011	1.0	-22.1
II. Mondego transect	1	-8.97	40.13	28	19/03/2011	0.1	-22.1
	2	-9.25	40.13	108	19/03/2011	0.3	-22.2
	3	-9.70	40.13	505	19/03/2011	0.1	-22.1
	4	-9.83	40.13	981	19/03/2011	0.6	-22.6
	5	-9.97	40.13	1808	20/03/2011	0.9	-22.4
III. Estremadura transect	1	-9.47	38.95	41	23/03/2011	0.1	-20.6
	2	-9.48	38.93	48	21/03/2011	0.1	-21.4
	3	-9.67	39.03	116	21/03/2011	1.4	-22.2
	4	-9.64	38.97	119	23/03/2011	1.2	-22.1
	5	-10.00	39.01	259	23/03/2011	0.1	-21.6
	6	-10.00	39.26	308	21/03/2011	0.2	-22.2
	7	-10.13	39.34	1100	22/03/2011	0.6	-22.3
	8	-10.22	39.42	1980	22/03/2011	0.5	-22.3
IV. Tagus transect*	1	-9.36	38.61	20	24/03/2011	0.2	-24.4
	2	-9.36	38.58	48	25/03/2011	0.1	-23.3
	3	-9.47	38.65	81	25/03/2011	1.5	-23.6
	4	-9.37	38.56	94	24/03/2011	1.7	-24.9
	5	-9.42	38.42	478	25/03/2011	1.4	-21.9
	6	-9.43	38.39	1052	26/03/2011	1.3	-22.2
	7	-9.48	38.23	2432	27/03/2011	0.9	-22.2
V. Sado transect	1	-8.99	38.45	48	26/03/2011	1.8	-21.4
	2	-9.06	38.42	98	28/03/2011	0.8	-21.7
	3	-9.24	38.34	516	28/03/2011	1.3	-23.1
	4	-9.26	38.33	979	28/03/2011	1.3	-22.4

*The data from the IV Tagus transect are from Zell et al. (in prep.).

7.3.4 Calculation of GDGT-based indices

The numerals refer to the GDGTs indicated in Fig. 7.1. The BIT index (Hopmans et al., 2004), the MBT' (Peterse et al., 2012), and the degree of cyclization (DC, Sinninghe Damsté et al., 2009) were calculated as follows:

$$\text{BIT index} = ([Ia]+[IIa]+[IIIa])/([Ia]+[IIa]+[IIIa]+[IV]) \quad (1)$$

$$\text{MBT'} = ([Ia]+[Ib]+[Ic])/([Ia]+[Ib]+[Ic]+[IIa]+[IIb]+[IIc]+[IIIa]) \quad (2)$$

$$\text{DC} = ([Ib]+[IIb])/([Ia]+[Ib]+[IIa]+[IIb]) \quad (3)$$

The average standard deviation of the BIT index was 0.01, the MBT' 0.01 and the DC 0.003.

7.4 RESULTS

7.4.1 Bulk organic geochemical data

The amount of OC in SPM varied between 2 and 23 wt. % (Table 1). Higher contents were found in the surface waters (Fig. 3A, G). The $\delta^{13}C_{OC}$ ranged from -22 to -30 ‰ (Table 1). In both transects a decrease of $\delta^{13}C_{OC}$ values was seen in deeper water depths (Fig. 3B, H).

In the surface sediment the OC content varied between 0.1 and 1.7 wt. %. The $\delta^{13}C_{OC}$ varied between -20 and -25 ‰ (Table 2). In most transects the OC content was low close to the continent, increased in the mid shelf and then decreased again. Lower $\delta^{13}C_{OC}$ values were found close to the Douro and Tagus Rivers in transects I and IV (Fig. 4B).

7.4.2 GDGTs in SPM

The concentration of summed brGDGTs in SPM varied from not detectable concentrations to 30 μg g_{OC}^{-1}. Input of brGDGTs from the rivers is clearly visible by the highest concentrations of brGDGTs closest to the Douro and Tagus Rivers (Fig. 3C, I). The percentage of IPL-derived brGDGTs relative to the total brGDGTs was 19±17 (Fig. 3E). Crenarchaeol concentrations were higher (from 3 to 300 μg g_{OC}^{-1}) than brGDGT concentrations (Fig. 3D, J). The IPL-derived crenarchaeol of the total crenarchaeol represented 18±9 % (Fig. 3F). Due to the much higher crenarchaeol concentrations compared to the brGDGT concentrations, values of the BIT index were relatively low in all samples (0 to 0.26 for CL GDGTs and 0 to 0.28 for IPL-derived GDGTs). The highest values were found closest to the rivers (Fig. 5A, B, G, H). The MBT' of the CL brGDGTs ranged from 0.37 to 0.66 (Fig. 5C, H). The MBT' of the IPL-derived brGDGTs was slightly higher (from 0.34 to 0.88) (Fig. 5D, I) and for the Douro transect it could only be determined in surface waters. The DC generally increased from close to the rivers towards the ocean (CL 0.12 to 0.41, IPL-derived 0.17 to 0.5) (Fig. 5E-L) although this trend was not as evident for CL brGDGTs of the Douro transect.

7.4.3 GDGTs in surface sediment

The CL crenarchaeol concentrations obtained by BD extraction were on average 14 % lower than those extracted with the ASE method, while the CL brGDGT concentration was on average 8 % higher. The BIT index was on average 0.004, the MBT' 0.002 and the DC 0.002 higher in BD extracted samples compared to those extracted with the ASE method. This shows that the CL fractions extracted by BD and the GDGTs extracted by ASE give comparable results, which is why they were treated as comparable results in

Table 7.3 GDGT concentrations in BDEs of transect I and IV SPM and sediments

		Sampling	CL (µg g_{oc}^{-1})											IPL-derived (µg g_{oc}^{-1})										
Transect	Station	water depth (m)	Cren.	Ia	Ib	Ic	IIa	IIb	IIc	IIIa	IIIb	IIIc	Summed brGDGTs	Cren.	Ia	Ib	Ic	IIa	IIb	IIc	IIIa	IIIb	IIIc	Summed brGDGTs
SPM																								
I. Douro transect	1	1	70.7	8.6	1.9	0.5	12.5	2.2	0.2	3.8	-	-	29.7	3.9	0.5	-	-	0.9	-	-	0.1	-	-	1.5
	1	14	296.1	7.3	3.1	0.4	10.6	3.0	0.5	0.1	-	-	25.1	13.0	2.7	0.6	-	0.6	-	-	0.2	-	-	4.1
	4	1	89.5	0.1	-	-	0.1	-	-	0.0	-	-	0.2	10.0	0.1	0.0	-	-	-	-	0.0	-	-	0.1
	4	20	116.9	0.2	0.1	0.1	0.2	0.0	-	0.1	-	-	0.6	25.6	-	-	-	-	-	-	-	-	-	-
	4	50	55.4	0.1	0.1	0.0	0.1	0.1	-	-	-	-	0.3	17.1	0.2	-	-	-	-	-	-	-	-	0.2
	4	109	34.7	0.1	-	-	0.1	-	-	0.0	-	-	0.1	9.3	0.1	0.0	-	-	-	-	-	-	-	0.1
	6	1	78.3	0.1	-	-	0.1	-	-	-	-	-	0.2	16.3	0.3	-	-	-	-	-	-	-	-	0.3
	6	200	304.6	1.5	0.6	0.3	1.3	0.7	0.2	-	-	-	4.6	69.4	-	-	-	-	-	-	-	-	-	-
	6	1006	32.6	0.5	0.1	-	0.8	0.2	-	0.2	-	-	1.9	19.6	0.4	0.0	-	0.3	-	-	-	-	-	0.7
	7	1	147.6	0.6	0.2	0.1	0.5	0.2	0.0	0.1	-	-	1.6	29.5	0.4	0.1	0.0	0.0	0.1	-	0.0	-	-	0.6
	7	200	229.4	0.9	0.3	0.1	0.4	0.1	-	0.2	-	-	2.0	35.2	-	-	0.1	0.2	-	-	-	-	-	0.2
	7	1988	191.1	1.1	0.8	0.4	1.4	0.6	0.2	0.4	-	-	4.8	26.7	0.3	0.0	0.0	0.0	-	0.0	0.1	-	-	0.4
IV. Tagus transect*	1	1	104.1	9.1	3.0	1.1	12.5	2.9	0.4	2.5	-	-	31.2	38.1	1.1	0.3	0.1	1.0	0.3	-	0.2	-	-	3.0
	1	19	81.9	6.3	2.2	0.8	8.7	2.2	0.3	1.8	-	-	22.2	18.0	0.7	0.1	0.1	0.7	0.1	-	0.3	-	-	1.9
	4	1	13.7	0.1	0.0	-	0.1	-	-	-	-	-	0.3	3.02	0.1	-	-	-	-	-	-	-	-	0.1
	4	20	21.0	0.1	0.0	-	0.1	0.0	-	-	-	-	0.3	4.7	0.1	-	-	0.1	-	-	0.1	-	-	0.2
	4	59	145.6	0.4	0.1	-	0.5	0.1	-	-	-	-	1.1	78.2	0.1	-	-	-	-	-	-	-	-	0.1
	4	93	242.0	3.0	1.9	0.9	4.2	1.6	0.3	0.8	-	-	12.6	159.8	0.9	0.3	0.1	0.5	0.3	-	-	-	-	2.1
	5	1	18.3	0.1	-	-	-	-	-	-	-	-	0.1	3.3	-	-	-	-	-	-	-	-	-	-
	5	50	55.3	0.0	-	-	-	-	-	0.0	-	-	0.1	19.3	-	-	-	-	-	-	-	-	-	-
	5	200	177.8	0.2	0.2	0.1	0.3	0.2	0.0	-	-	-	0.9	25.5	0.0	0.0	-	-	0.0	-	-	-	-	0.0
	5	500	88.8	0.2	0.1	0.1	0.2	0.1	0.0	-	-	-	0.7	17.9	-	-	-	-	-	-	-	-	-	-
	5	1051	75.2	0.3	0.2	0.1	0.3	0.2	0.1	-	-	-	1.1	7.5	0.1	-	-	0.1	-	0.0	-	-	-	0.2
	7	1	17.3	-	-	-	-	-	-	-	-	-	-	2.1	-	-	-	-	-	-	-	-	-	-
	7	50	82.7	-	-	-	-	-	-	-	-	-	-	27.7	-	-	-	-	-	-	-	-	-	-
	7	200	53.9	0.1	0.0	0.0	0.1	0.0	0.0	0.0	-	-	0.3	1.4	-	-	-	-	-	-	-	-	-	-
	7	1000	92.4	0.1	0.1	0.0	0.2	0.1	0.0	-	-	-	0.5	38.9	0.1	0.0	0.0	0.1	0.0	-	-	-	-	0.2
	7	2431	30.9	0.1	0.1	0.0	0.1	0.1	0.0	-	-	-	0.5	2.7	0.0	-	-	-	-	-	-	-	-	-	-
Surface sediment																								
I. Douro transect	1		174.1	8.2	4.0	1.9	12.8	5.2	1.5	3.7	0.2	-	37.5	19.9	1.9	0.5	0.3	1.3	0.7	0.3	0.2	-	-	5.3
	2		320.7	6.6	3.8	1.8	10.6	4.0	1.02	3.0	-	-	30.8	19.5	0.6	0.0	0.1	0.3	0.2	0.1	0.1	-	-	1.4
	3		203.8	2.6	1.7	0.9	4.3	2.0	0.6	1.1	0.1	0.0	13.4	10.3	0.7	0.2	0.1	0.4	0.6	0.1	0.1	-	-	2.2
	4		217.1	2.7	2.0	1.1	4.5	2.4	0.7	1.2	0.1	-	14.6	7.9	0.6	0.1	0.1	0.5	0.3	0.1	0.1	-	-	1.7
	5		219.3	1.1	0.8	0.4	1.4	1.2	0.4	0.6	-	-	5.8	16.9	0.3	0.1	0.1	0.2	0.2	0.1	0.1	-	-	1.2
	6		131.7	0.8	0.5	0.3	0.9	0.8	0.3	0.3	0.0	-	3.9	9.0	0.2	0.1	0.0	0.2	0.1	0.0	0.0	-	-	0.6
	7		259.0	1.0	0.5	0.3	1.1	0.6	0.1	0.0	-	-	3.5	12.8	0.1	0.0	0.0	0.1	0.1	0.1	0.0	-	-	0.4
IV. Tagus transect*	1		459.1	31.3	15.5	6.0	46.5	13.8	2.5	9.4	0.1	-	125.8	46.0	6.1	2.6	1.0	5.4	2.0	0.5	0.8	-	-	18.4
	2		211.1	6.5	4.3	1.9	10.2	3.6	0.7	2.1	0.1	-	29.5	19.7	1.3	0.3	0.1	0.7	0.4	0.1	0.2	-	-	3.2
	3		232.3	5.1	3.1	1. 5	7.9	2.87	0.6	1.6	0.1	0.0	22.7	20.7	1.5	0.3	0.2	0.7	0.2	0.1	0.1	-	-	3.0
	4		124.4	3.7	2.3	1.1	5.5	2.0	0.4	1.0	0.1	-	16.1	8.2	0.9	0.2	0.1	0.5	0.3	0.1	0.0	-	-	2.0
	5		38.0	0.3	0.3	0.2	0.4	0.3	0.1	0.1	0.0	-	1.6	2.0	0.1	0.0	0.0	0.0	0.0	0.0	0.0	-	-	0.2
	6		61.9	0.5	0.3	0.2	0.6	0.4	0.1	0.2	-	-	2.3	4.3	0.2	0.0	0.0	0.1	0.1	0.0	0.0	-	-	0.3
	7		196.4	1.9	0.7	0.4	1.9	1.6	0.6	0.5	-	0.1	7.7	14.5	0.4	0.2	0.0	0.2	0.2	0.0	0.0	-	-	1.0

*The data from the IV Tagus transect are from Zell et al. (in prep.).

Table 7.4 GDGT concentrations of surface sediments (as determined by ASE).

		GDGTs (μg g_{oc}^{-1})										
Transect	**Station**	**Cren.**	**Ia**	**Ib**	**Ic**	**IIa**	**IIb**	**IIc**	**IIIa**	**IIIb**	**IIIc**	**Summed brGDGTs**
I. Douro transect	1	176.0	8.5	4.1	2.0	13.0	5.4	1.7	3.9	-	-	38.5
	2	478.4	8.3	4.7	2.2	13.6	5.0	1.4	3.9	-	-	39.1
	3	261.3	3.2	2.1	1.1	5.0	2.5	0.7	1.2	-	-	15.8
	4	322.2	3.4	2.5	1.3	5.7	3.1	0.9	1.4	-	-	18.2
	5	364.3	1.6	1.1	0.6	2.2	1.7	0.6	1.0	-	-	8.9
	6	232.7	1.4	0.8	0.5	1.5	1.2	0.4	0.5	-	-	6.0
	7	281.5	1.1	0.5	0.3	1.2	0.7	-	-	-	-	3.8
II. Mondego transect	1	461.6	7.0	4.2	2.1	10.8	4.4	1.3	3.1	-	-	32.9
	2	718.5	4.7	4.3	2.7	7.3	5.3	2.1	1.9	-	-	28.1
	3	669.3	2.5	1.9	1.1	3.8	2.9	1.1	2.4	-	-	15.7
	4	229.9	0.8	0.5	0.3	1.0	0.7	0.2	0.3	-	-	3.8
	5	425.1	1.6	0.8	0.5	1.4	1.1	0.3	0.5	-	-	6.6
III. Estremadura transect	1	703.4	5.4	4.1	2.0	9.1	4.9	1.5	1.9	-	-	28.9
	2	761.7	5.6	4.2	2.2	9.6	4.8	1.3	2.4	-	-	30.1
	3	576.1	2.7	2.6	1.6	4.4	2.7	0.9	1.1	0.1	0.1	16.2
	4	571.8	3.7	3.4	2.1	6.5	4.0	1.3	1.7	-	-	22.7
	5	1232.5	4.3	3.9	2.5	6.5	5.3	2.9	2.4	-	-	27.2
	6	396.2	1.6	1.1	0.7	2.2	1.5	0.6	1.0	-	-	8.7
	7	335.0	1.2	0.7	0.4	0.8	0.9	0.3	0.0	-	-	4.2
	8	312.5	1.5	0.7	0.4	1.6	0.9	0.3	0.0	-	-	5.2
IV. Tagus transect	1	171.7	10.8	5.3	2.1	16.5	4.5	0.9	3.3	0.2	-	43.7
	2	358.8	10.1	6.3	2.8	15.8	5.6	1.3	3.3	-	-	45.0
	3	319.7	5.9	3.6	1.7	9.1	3.2	0.7	1.7	0.2	0.1	26.2
	4	181.9	4.6	2.8	1.3	7.0	2.4	0.5	1.3	0.1	-	19.9
	5	504.8	3.5	2.9	1.7	5.2	3.1	0.9	1.3	0.2	0.1	18.8
	6	414.0	2.8	2.0	1.2	3.3	2.4	0.8	1.0	0.1	-	13.8
	7	272.1	2.4	1.2	0.5	2.4	1.9	0.7	0.7	0.1	-	9.9
V. Sado transect	1	154.2	5.1	4.0	1.7	4.2	2.5	0.6	1.5	-	-	19.6
	2	525.4	6.5	5.9	3.1	11.3	5.2	1.4	2.4	0.2	0.1	36.1
	3	327.7	2.3	1.8	1.1	3.2	2.2	0.8	1.0	0.1	-	12.5
	4	369.4	2.2	1.6	1.0	2.9	2.0	0.7	1.0	0.1	-	11.5

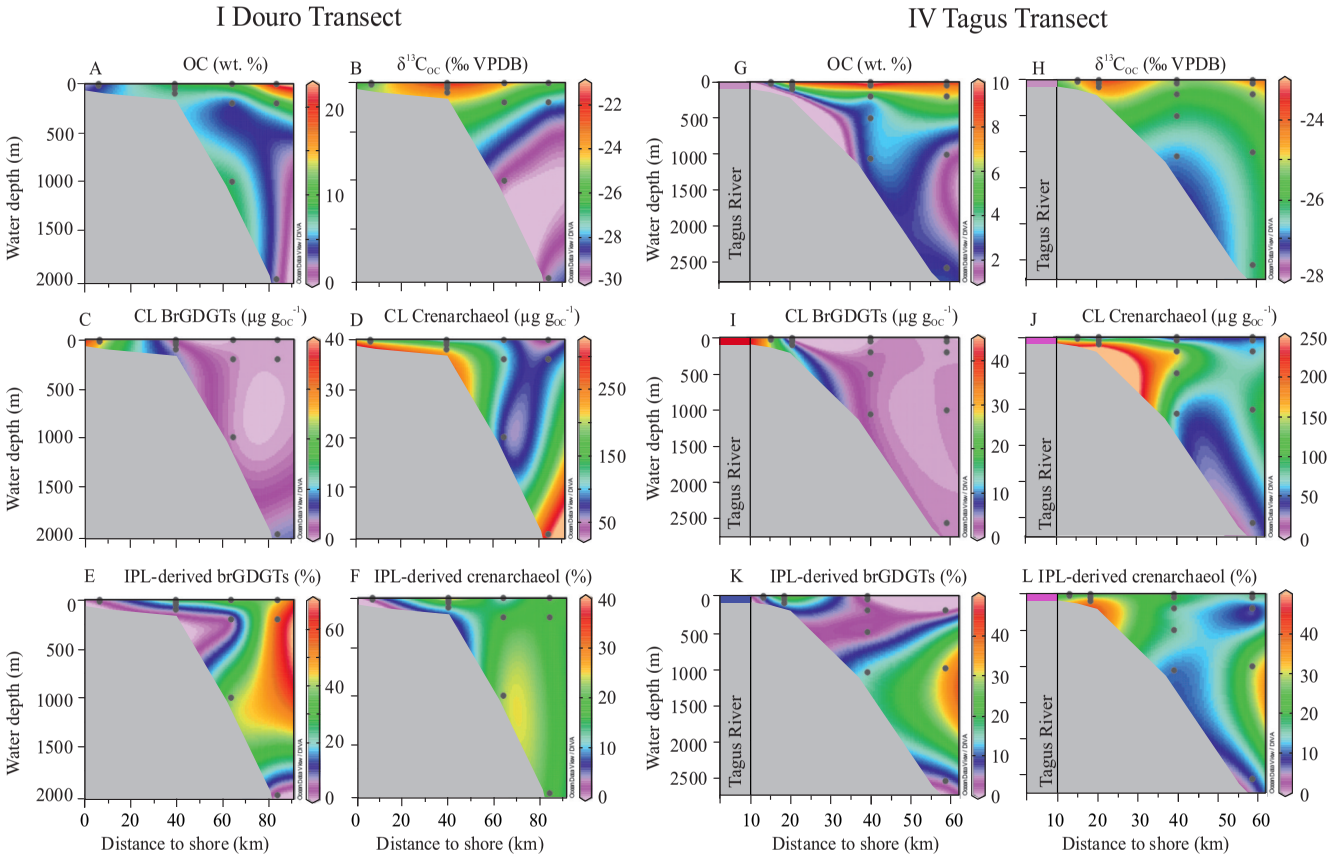

Fig. 7.3 Comparison of OC contents, $\delta^{13}C_{OC,}$ CL brGDGT and CL crenarchaeol concentrations, and the percentage of IPL-derived brGDGTs and crenarchaeol between (A-F) Douro and (G-L) Tagus SPM samples. The data of the Tagus transect are from Zell et al. (2014).

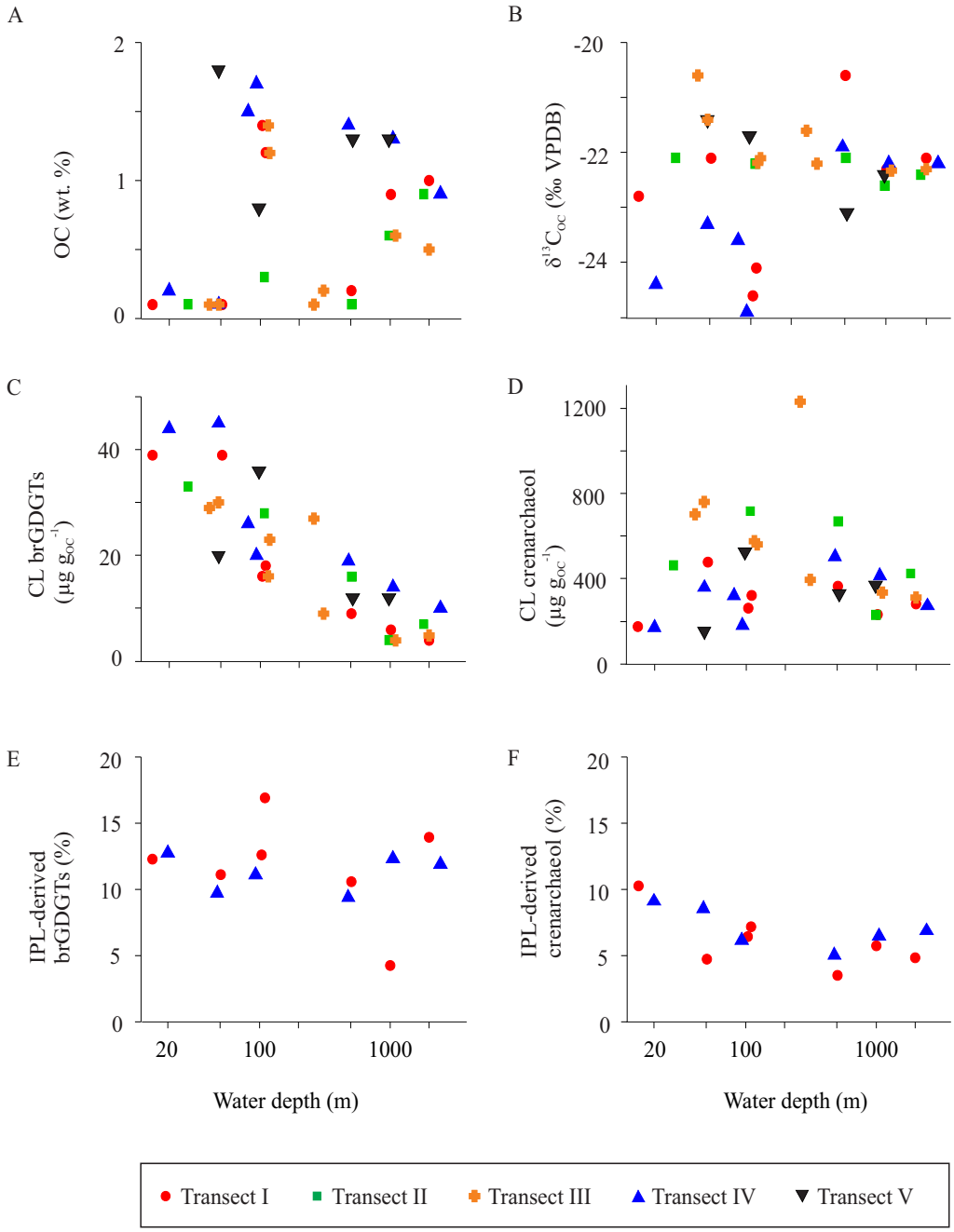

Fig. 7.4 Scatter plots between water depth and (A) OC contents, (B) $\delta^{13}C_{OC}$, (C-D) CL brGDGT and CL crenarchaeol concentrations, and (E-F) the percentage of IPL-derived brGDGTs and crenarchaeol of surface sediments. Note that the x axes are logarithmic scales.

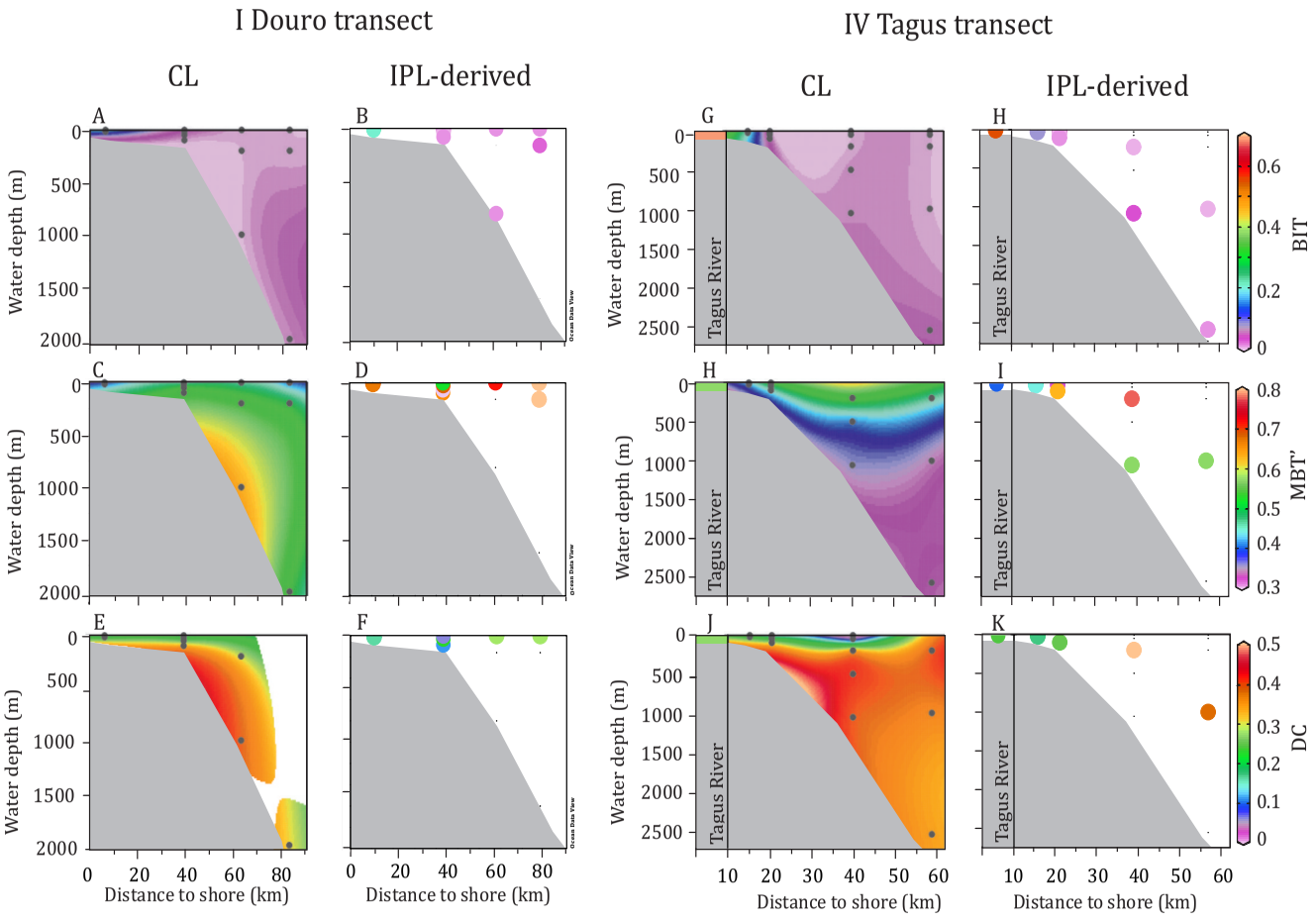

Fig. 7.5 Comparison of BIT, MBT' and DC of CL and IPL-derived GDGTs between (A-F) Douro and (G-L) Tagus SPM samples. The data of the Tagus transect are from Zell et al. (2014).

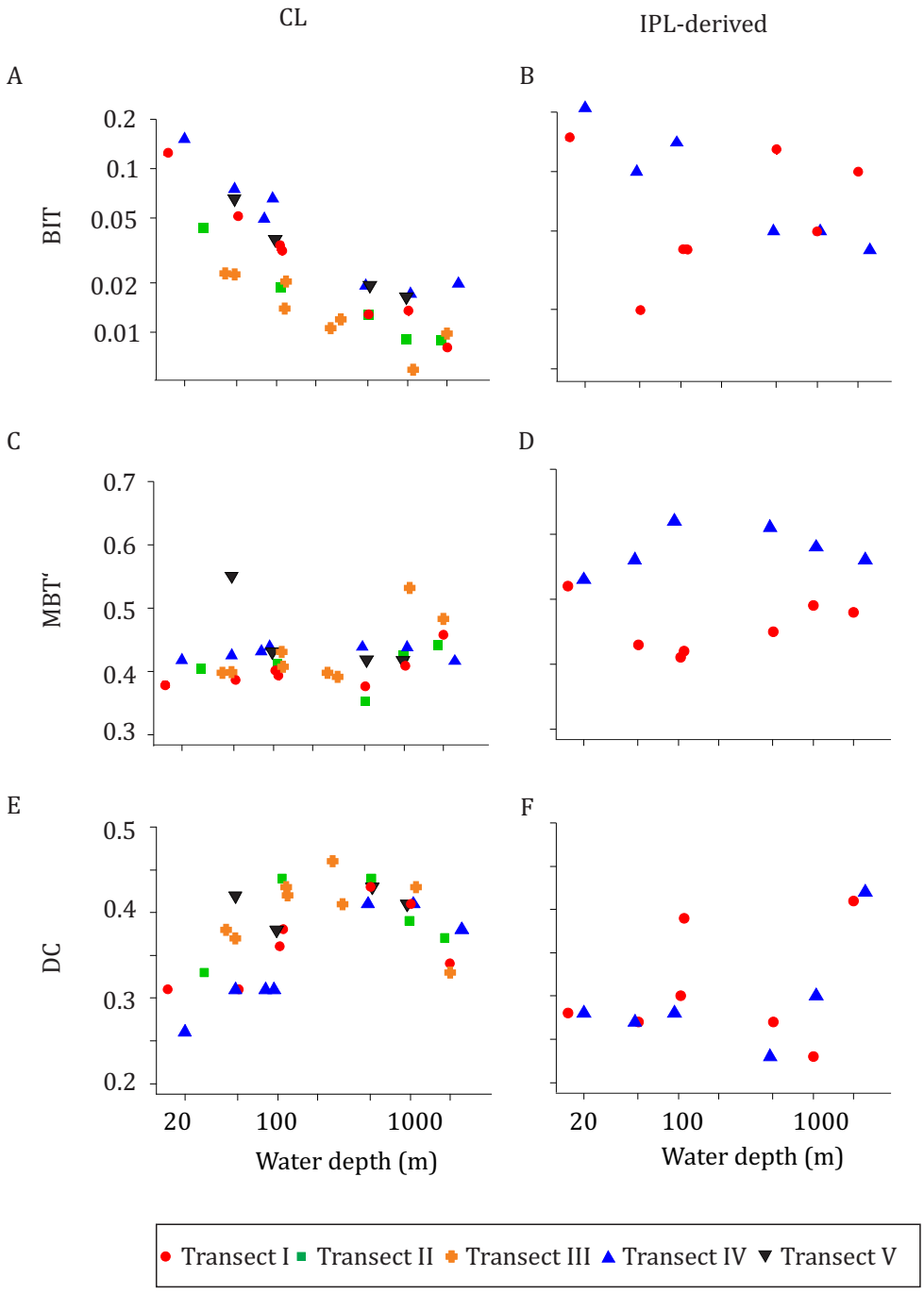

Fig. 7.6 Scatter plots between water depth and (A) BIT, (B) MBT', and (C) DC of surface sediments for CL and IPL-derived GDGTs. Note that all the x axes and y axes for the BIT index are logarithmic scales.

the discussion.

The summed brGDGT concentrations varied between 4 and 45 μg g_{OC}^{-1}. All transects showed a steep decrease of the CL brGDGT concentration from the continent towards the open ocean (Fig. 4C). CL brGDGT concentrations in front of major rivers (transects I and IV, and to a lesser extent, transect II) were slightly higher than those transects that received a less dominant river input. The percentage of IPL-derived brGDGTs in transects I and IV was 11±3 (Fig. 4E). Crenarchaeol concentrations were always higher than brGDGT concentrations (200 to 1200 μg g_{OC}^{-1}; Fig. 4D) and did not show a clear trend with water depth. The percentage of IPL-derived crenarchaeol in transects I and IV was 6±1 (Fig. 4F). The CL BIT values varied between 0.01 and 0.15. Highest CL BIT values were found close to the rivers and decreased rapidly with water depth in all transects (Fig. 6A). In transect III which was not directly influenced by a river the decline was less steep since the BIT index of shallow sediments was lower (Fig. 6A). The IPL-derived BIT values varied between 0.02 and 0.21. For the Tagus transect a clear decrease of the BIT with water depth was seen, but not for the Douro transect (Fig. 6B).

The MBT' of the CL brGDGTs was ca. 0.40 with a few exceptions. No clear land to ocean trend was observed (Fig. 6C). An obvious difference was seen between the MBT' of the IPL-derived brGDGTs of transects I and IV, which was higher (0.60 vs. 0.48) in transect IV compared to transect I (Fig. 6D). For both transects no trend with water depth was apparent. The DC of the CL brGDGTs varied between 0.31 and 0.46 (Fig. 6E) and the IPL-derived DC between 0.27 and 0.42 (Fig. 6F), with a tendency of higher DC values at greater water depth.

7.5 DISCUSSION

7.5.1 Tracing continental OC: BIT vs. brGDGT concentration

Schmidt et al. (2010) studied the sources and transport of terrestrial OC at the Portuguese margin north of our study area. In that study they also tested the BIT index as an indicator for soil OC transport. It was concluded that based on the BIT index, the contribution of soil OC to the sedimentary OC appeared to be small, because the BIT decreased rapidly from 0.72-0.96 in riverbank sediment to 0.04-0.1 on the shelf. However, the lignin based 3,5-Bd/V ratio indicated high input of soil OC to the surface sediment of the shelf. Based on this observation, it is concluded that the BIT index is a less sensitive indicator than the other molecular indicators. However, a sharp decrease of BIT values to below 0.1 is commonly found in coastal areas (e.g. Herfort et al., 2006; Hopmans et al., 2004b; Kim et al., 2006; Zhu et al., 2011). Logically, in regions with high crenarchaeol production, the BIT index would drop more abruptly than in regions with low crenarchaeol production. This means that the BIT index cannot be used as an absolute measure for the amount of continental OC input, but rather as an indicator for its relative input (cf. Weijers et al., 2009).

In the present study the BIT values as well as brGDGT and crenarchaeol concen-

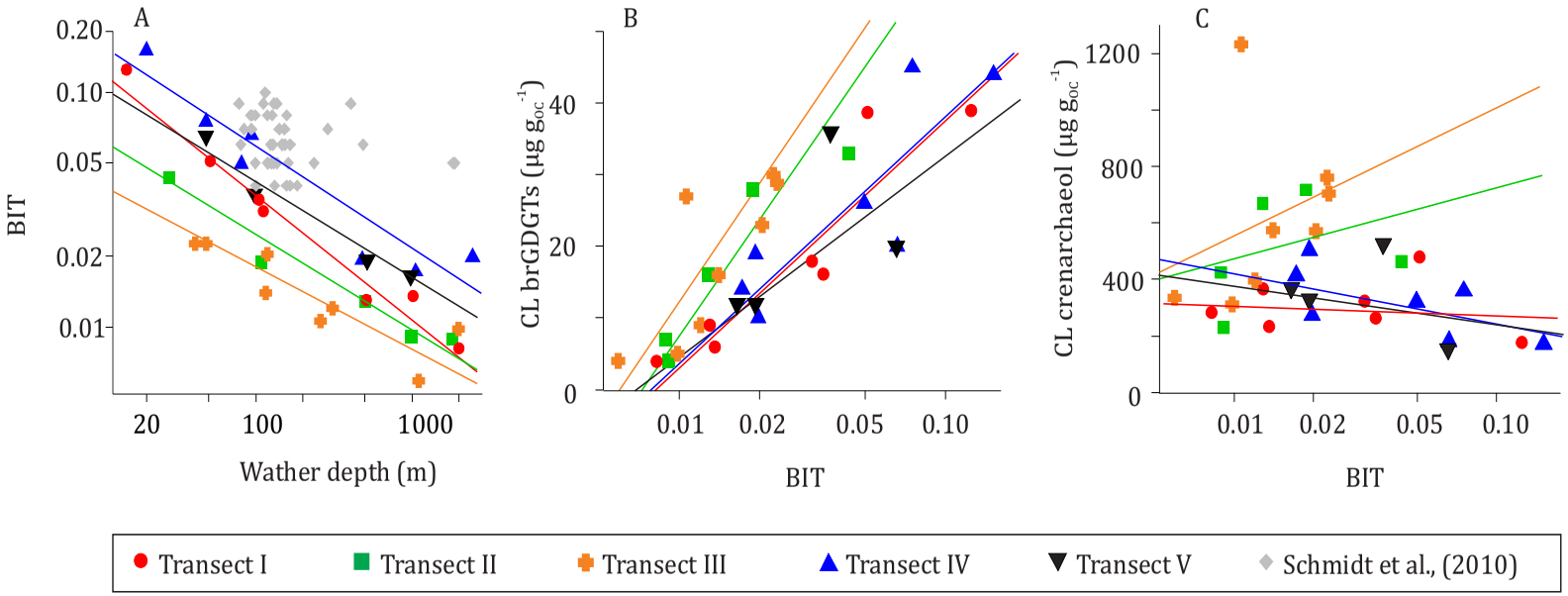

Fig. 7.7 (A) Correlation between BIT and water depth (note that X and Y axes are logarithmic scales.) as well as between BIT and concentrations of (B) CL brGDGTs and (C) CL crenarchaeol (note that X axes are logarithmic scales.).

trations in SPM and sediment in five transects along a stretch of the Portuguese coast were investigated in order to understand what influences the BIT index and if it can be used to trace continental OC input along the Portuguese coast. Compared to the study by Schmidt et al. (2010) which mainly analyzed shelf surface sediments, we analyzed SPM as well as surface sediments. In addition the investigated transects were much longer: they started on the shelf (two of them close to major Iberian rivers) and ended at a water depth of about 2500 m on the continental slope. Hence, a larger range of BIT values was expected. Our data showed, both in the SPM (Fig. 5A, G) and the surface sediments (Figs. 6A and 7A), that BIT values rapidly declined from the coast to the open ocean. The highest BIT values were found close to the major rivers in transects I and IV. Inter-laboratory studies have shown that the BIT values from different laboratories cannot directly be compared (Schouten et al., 2009, 2014). However, most of the data from the shelf of both studies are in a similar range, but in the data of Schmidt et al. (2010) no trend towards deeper water depth was seen. This might be due to the smaller depth range in the dataset of Schmidt et al. (2010) (Fig. 7A) and the lack of data from sediments collected close to a large river system.

When the brGDGT and crenarchaeol concentrations are plotted against the BIT index, it can be observed that the brGDGT concentration positively correlated with the BIT index (Fig. 7B, Table 3), while the crenarchaeol concentration did not significantly correlate with the BIT index for most transects (Fig. 7C, Table 3). This clearly shows that for the Portuguese continental margin the BIT index is mainly influenced by the brGDGT concentrations. This is not the case in all locations, as it has been shown in previous studies. For example it has been shown that in regions which are poor in soil and peat like the Vancouver fjords (Walsh et al., 2008) no trend of the BIT index from the coast to the open ocean is found. Furthermore it is assumed that in regions with high primary productivity for example due to high nutrient input from a river; variations in the crenarchaeol concentration dominate the BIT index (Casañeda et al., 2010; Fietz et al., 2011; Smith et al., 2012).

In the present data set it can be seen that the crenarchaeol concentration also influences the BIT index to a minor extent. Optimally the crenarchaeol concentrations in the marine environment would remain constant. However, in transects II and III higher crenarchaeol concentrations along the coast led to lower BIT values (Fig. 4C). On the other hand in transects IV and V the crenarchaeol concentration slightly increased towards the ocean which led to lower BIT values offshore (Fig. 6A). This shows that the BIT index can give an indication for continental OC, but is also influenced by the crenarchaeol concentrations. Therefore, the brGDGT concentrations probably give a more accurate indication of continental OC input.

BrGDGT concentrations seem to be mostly related to the rivers, since the highest values were found closest to the rivers. However, in all transects including transect III, which is not close to a river, the highest brGDGT concentrations were found in sediments on the shelf. The brGDGTs might be transported along the shelf with the northwards

current (Dias et al., 2002; Vitorino et al., 2002) or eroded from coastal soils. Similar brGDGT concentrations were found in the Tagus River SPM (Zell et al., 2014) as in marine sediment and SPM closest to the river. No comparable sample from the Douro River was analyzed, but since the delivery time of water in the Douro basin is very short (Abril et al., 2002), it is unlikely that degradation processes influence the brGDGT concentration in the Douro estuary. Thus, the estuary type does not seem to affect the brGDGT concentration at our study sites. This might indicate that brGDGTs mainly represent the rigid fraction of continental OC. However, this is in contrast to the findings in the Yangtze estuary (Zhu et al., 2011) that indicate a strong degradation of the brGDGT in the estuary. More research needs to be done to understand why brGDGT degradation is different in the estuaries in distinct river systems.

7.5.2 Provenance of brGDGTs: terrestrial vs. marine

BrGDGTs can also be produced in small concentrations in the marine environment (BrGDGTs can also be produced in small concentrations in the marine environment (e.g. Hu et al., 2012; Peterse et al., 2009; Wu et al., 2014; Zhu et al., 2011). If the distribution of brGDGTs produced in the marine environment is different to that of the brGDGTs coming from the continent, the distribution of the brGDGTs can give an indication about the source of the brGDGTs in the marine environment (Zell et al., 2014). We use the MBT' and DC to compare the brGDGT distribution in the different environments. The CL MBT' and DC of soils in the Tagus River basin (Zell et al., 2014) and also in the whole Iberian Peninsula (Menges et al., 2013) possesses a wide range. Compared to the average of the Tagus basin soils the CL MBT' and DC in the Tagus River were higher, this is why it is assumed that brGDGTs are mainly produced in the Tagus River itself and do not derive from soil erosion (Zell et al., 2014) (Fig. 8). When the CL MBT' and DC of Tagus River SPM are compared with those of marine SPM an increase of the CL MBT' is seen, while CL DC values were either higher or lower. The difference between the brGDGT distributions of the riverine and marine SPM might indicate marine in situ production of brGDGTs (Zell et al., 2014).

Differences in the brGDGT distribution were also seen between brGDGTs in the surface and deeper water depths. Towards the deeper water depths, the MBT' decreased but the DC increased (Fig. 5C-K). A higher MBT' was found both in CL and IPL-derived brGDGTs of transect I compared to transect IV. Interestingly, the reverse was seen in the sediment where a lower MBT' was found in transect I compared to transect IV (Fig. 6C, D). This could indicate that the brGDGTs produced in the SPM and those produced in the surface sediment are different. The difference between the two transects for the CL brGDGTs was not as big as for the IPL-derived brGDGTs. This most likely indicates a mixed origin of the CL brGDGTs. The data of the five sediment transects showed little variation in the CL MBT' (Fig. 6C), while the DC of the CL brGDGTs increased until around 500 m depth and then slightly decreased again (Fig. 6E). Most of the sediment showed lower IPL-derived DC values. This indicates that the increase of the CL DC is not due to brGDGT

production in the sediment, but rather due to brGDGT production in the water column.

In the SPM and sediment on the Portuguese shelf, where the highest brGDGT concentrations were found, the brGDGT distributions were most similar to those found in the river. If brGDGTs were produced in the marine environment, an increasing influ-

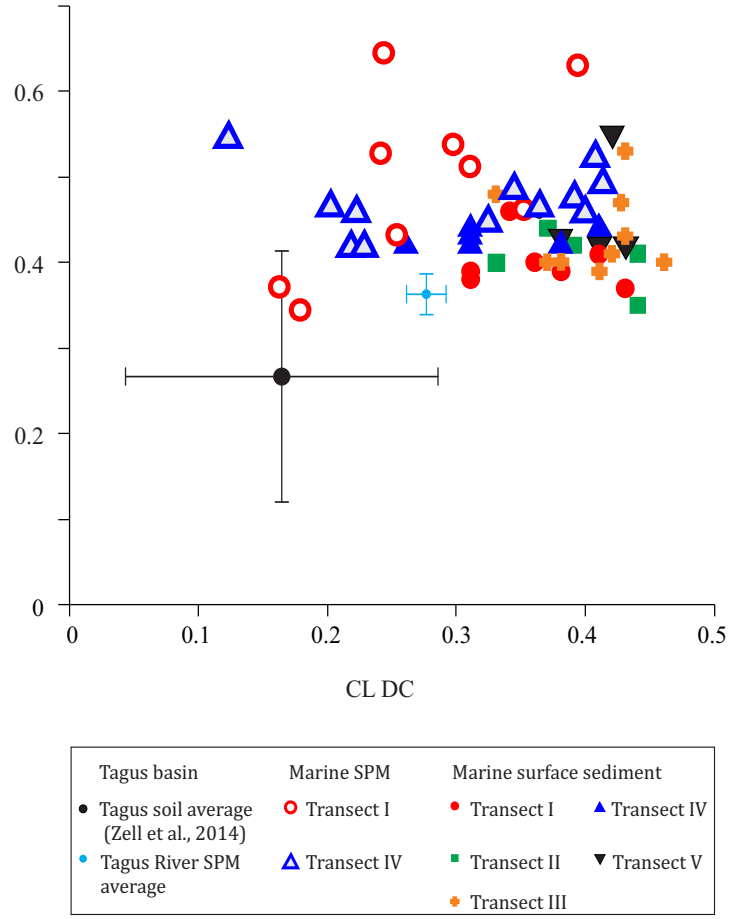

Fig. 7.8 Comparison of MBT' and DC of CL GDGTs in Tagus basin soil, river SPM, marine SPM and marine sediment.

Table 7.5 Results of the linear regression analyses between the BIT inex and water depth as well as between the BIT index and the concentrations of CL brGDGTs and CL crenarchaeol. The correlation is based on the non-transformed data.

	Water depth vs. BIT		Crenarchaeol vs. BIT		BrGDGTs vs. BIT	
Transect	**R^2**	**p**	**R^2**	**p**	**R^2**	**p**
I Douro transect	-0.33	0.18	0.11	0.47	0.70	0.02
II Mondego transect	-0.48	0.20	0.02	0.83	0.73	0.06
III Estremadura transect	-0.42	0.08	-0.09	0.48	0.65	0.02
IV Tagus transect	-0.33	0.18	-0.46	0.09	0.68	0.02
V Sado transect	-0.66	0.19	-0.30	0.45	0.15	0.61

p <0.05 significance level

ence of the marine produced brGDGTs would be expected with increasing distance to the continent. We observe that the change of the brGDGT distribution from the shelf to the deepest water depth was not linear. The DC increased along the shelf break and then decreased again. This might again indicate various sources of brGDGTs. Our results show that there seem to be differences in the brGDGT distribution produced in marine SPM and those produced in marine sediment and along the shelf break compared to the shelf and the deep water basin. The multiple marine sources complicate the use of the brGDGTs distribution to distinguish between brGDGTs of terrestrial and marine origin.

7.6 CONCLUSION

We investigated marine surface sediments from five (Douro, Mondego, Estremadura, Tagus, and Sado) transects and marine SPM from the Douro and Tagus transects to assess the application of the BIT index as an indicator for the input of continental OC along the Portuguese continental margin. Our results show that the BIT index gives a clear decreasing trend from the coast to the open ocean and is predominantly influenced by brGDGTs transported from the rivers. However, crenarchaeol concentrations also have a minor influence on the BIT index. This suggests that the brGDGT concentrations give a more straightforward indication of continental OC input to the ocean than the BIT index. Therefore, we recommend to measure brGDGT and crenarchaeol concentrations when the BIT index is applied. Degradation of brGDGTs in the estuaries of the Tagus and Douro Rivers does not seem to have a substantial influence on brGDGT concentration and distribution, which indicates that brGDGTs can be a good indicator of the rigid continental OC fraction to the ocean, at least at our study sites. Our results also show that the use of the brGDGT distribution to distinguish between terrestrial and marine produced brGDGTs is more complicated than expected since there seem to be multiple sources of brGDGTs in the marine environment.

Acknowledgments

The research leading to these results has received funding from the European Research Council (ERC) under the European Union's Seventh Framework Program (FP7/2007-2013) ERC grant agreement [226600]. We thank Pierre-Antoine Dessandier for the organic carbon analysis, and Henko de Stigter at NIOZ and Silvia Nave at LNEG for the help of the cruise preparation. We also thank to the crew of the R/V Pelagia during the PACEMAKER cruise for their excellent services.

References

Abril, G., Nogueira, M., Etcheber, H., Cabeçadas, G., Lemaire, E., Brogueira, M.., (2002). Behaviour of organic carbon in nine contrasting European estuaries. Estuar. Coast. Shelf Sci. 54, 241–262.

Arbuszewski, J., de Menocal, P., Kaplan, A., Farmer, E.C. (2010). On the fidelity of shell-derived δ18O seawater estimates. Earth Planet. Sci. Lett. 300, 185–196.

Aller R. C., Blair N. E., Xia Q. and Rude P. D. (1996) Remineralization rates, recycling, and storage of carbon in Amazon shelf sediments. Cont. Shelf Res. 16, 753–786.

Alt-Epping, U., Mil-Homens, M., Hebbeln, D., Abrantes, F., Schneider, R. R. (2007). Provenance of organic matter and nutrient conditions on a river- and upwelling influenced shelf: A case study from the Portuguese Margin, Mar. Geol. 243, 169–179, doi:10.1016/j.margeo.2007.04.016.

Antonov J. I., Seidov D., Boyer T. P., Locarnini R. A., Mishonov A. V., Garcia H. E., Baranova O. K., Zweng M. M. and Johnson D. R. (2010) World Ocean Atlas 2009, volume 2: salinity. In Levitus S. (Ed.), NOAA Atlas NESDIS 69, U. S. Government Printing Office, Washington, D. C., 184 pp.

Araújo-Lima, C. A. R. M., Forsberg, B. R., Victoria R. and Martinelli L. (1986). Energy sources for detrivorous fishes in the Amazon. Science 234, 1256–1258.

Ayari, A., Yang, H., Xie, S. (2013). Flooding impact on the distribution of microbial tetraether lipids in paddy rice soil in China. Front. Earth Sci. 7, 384–394.

Bailey, I.W., Sinnott, E.W. (1915). A botanical index of Cretaceaous and Tertiary climates. Science 41, 831–834.

Ballantyne, A. P., Greenwood, D. R., Sinninghe Damsté, J. S., Csank, A. Z., Eberle, J. J., Rybczynski, N. (2010). Significantly warmer Arctic surface temperatures during the Pliocene indicated by multiple independent proxies. Geology 38, 603–606. doi: 10.1130/G30815.1

Batjes, N., Dijkshoorn, J. (1999). Carbon and nitrogen stocks in the soils of the Amazon Region. Geoderma 89, 273–286. doi: 10.1016/S0016-7061(98)00086-X

Batjes, N. H. (2005). SOTER-based Soil Parameter Estimates for Latin America and the Caribbean (ver. 1.0). Wageningen: ISRIC World Soil Information

Bechtel, A., Smittenberg, R. H., Bernasconi, S. M. and Schubert, C. J. (2010). Distribution of branched and isoprenoid tetraether lipids in an oligotrophic and a eutrophic Swiss lake: insights into sources and GDGT-based proxies. Org. Geochem. 41, 822–832.

Beman, J. M., Chow, C.-E., King, A. L., Feng, Y., Fuhrman, J. A., Andersson, A., Bates, N. R., Popp, B. N., and Hutchins, D. A. (2010). Global declines in oceanic nitrification rates as a consequence of ocean acidification, Proc. Natl. Acad. Sci. 108, 208–213, doi:10.1073/pnas.1011053108

Bendle, J.A., Weijers, J.W.H., Maslin, M.A., Sinninghe Damsté, J.S., Schouten, S., Hopmans, E.C., Boot, C.S., Pancost, R.D. (2010). Major changes in glacial and Holocene terrestrial temperatures and sources of organic carbon recorded in the Amazon fan by tetraether lipids. Geochem. Geophys. Geosystems 11, Q12007. Doi:10.1029/2010GC003308

Bird M. I., Giresse P., Ngos, S. (1998). A seasonal cycle in the carbon-isotopic composition of organic carbon in the Sanaga River. Cameroon. Limnol. Oceanogr. 43, 143–146.

Blaga, C.I., Reichart, G.-J., Heiri, O., Sinninghe Damsté, J.S. (2009). Tetraether membrane lipid distributions in water-column particulate matter and sediments: a study of 47 European lakes along a north-south transect. J. Paleolimnol. 41, 523–540. doi: 10.1007/s10933-008-9242-2

Blaga, C.I., Reichart, G.-J., Schouten, S., Lotter, A.F., Werne, J.P., Kosten, S., Mazzeo, N., Lacerot, G., Sinninghe Damsté, J.S. (2010). Branched glycerol dialkyl glycerol tetraethers in lake sediments: Can they be used as temperature and pH proxies? Org. Geochem. 41, 1225–1234.

Bligh, E.G. and Dyer, W.J. (1959). A rapid method of total lipid extraction and purification. Can. J. Biochem. Physiol. 37, 911– 917.

Bonnet, M.P., Barroux, G., Martinez, J.M., Seyler, F., Moreira-Turcq, P., Cochonneau, G., et al. (2008). Floodplain hydrology in an Amazon floodplain lake (Lago Grande de Curuaí). J. Hydrol. 349, 18–30. doi: 10.1016/j.jhydrol.2007.10.055

Bradley, R.S. and Jonest, P.D. (1993). "Little Ice Age" summer temperature variations: their nature and relevance to recent global warming trends. The Holocene 3, 367–376.

Brassell, S.C., Eglinton, G., Marlowe, I.T., Pflaumann, U., Sarnthein, M. (1986). Molecular stratigraphy: a new tool for climatic assessment. Nature 320, 129–133.

Brochier-Armanet, C., Boussau, B., Gribaldo, S., and Forterre, P. (2008). Mesophilic crenarchaeota: proposal for a third archaeal phy-

lum, the Thaumarchaeota. Nat. Rev. Microbiol. 6, 245–252. doi: 10.1038/nrmicro1852

Bustillo V., Victoria R. L., de Moura J. M. S., de Castro Victoria D., Toledo A. M. A. and Collicchio E. (2011). Factors driving the biogeochemical budget of the Amazon River and its statistical modelling. Comptes Rendus Geosci. 343, 261–277

Callède, J., Kosuth, P., Loup, J.-L., and Guimarães, V. S. (2000). Discharge determination by acoustic Doppler current profilers (ADCP): a moving bottom error correction method and its application on the River Amazon at Óbidos. Hydrol. Sci. J. 45, 911–924. doi:10.1080/02626660009492392

CallèdeJ., Kosuth, P., Oliveira, E. (2001). Etablissement de la relation hauteur-débit de l'Amazone à Óbidos: méthode de la dénivelée normale à géométrie variable. Hydrol. Sci. J. 46, 451– 463.

Castañeda, I.S., Schefuß, E., Pätzold, J., Sinninghe Damsté, J.S., Weldeab, S., Schouten, S. (2010). Millennial-scale sea surface temperature changes in the eastern Mediterranean (Nile River Delta region) over the last 27,000 years. Paleoceanography 25. doi:10.1029/2009PA001740.

Colinvaux, P.A., De Oliveira, P.E., Moreno, J.E., Miller, M.C., Bush, M.B. (1996). A long pollen record from Lowland Amazonia: Forest and cooling in glacial times. Science 274, 85–88.

Conte, M.H., Thompson, A., Lesley, D., Harris, R.P., (1998). Genetic and physiological influences on the alkenone/alkenoate versus growth temperature relationship in Emiliania huxleyi and Gephyrocapsa oceanica. Geochim. Cosmochim. Acta 62, 51–68.

Crump, B.C. and Baross, J.A. (2000). Archaeaplankton in the Columbia River, its estuary and the adjacent coastal ocean, USA. FEMS Microbiol. Ecol. 31, 231–239.

Crutzen, P.J., Stoermer, E.F., 2000. The "Anthropocene". IGBP Newsletter 41, 17–18.

De Jonge, C., Hopmans, E.C., Stadnitskaia, A., Rijpstra, W.I.C., Hofland, R., Tegelaar, E., Sinninghe Damsté, J.S. (2013). Identification of novel penta- and hexamethylated branched glycerol dialkyl glycerol tetraethers in peat using HPLC–MS2, GC–MS and GC–SMB-MS. Org. Geochem. 54, 78–82.

De Jonge, C., Stadnitskaia, A., Hopmans, E.C., Cherkashov, G., Fedotov, A., Sinninghe Damsté, J.S. (2014). In situ produced branched glycerol dialkyl glycerol tetraethers in suspended particulate matter from the Yenisei River, Eastern Siberia. Geochim. Cosmochim. Acta 125, 476–491.

De Villiers, S., Shen, G.T., Nelson, B.K. (1994). The Sr/Ca-temperature relationship in coralline aragonite: Influence of variability in and skeletal growth parameters. Geochim. Cosmochim. Acta 58, 197–208.

Degens ,E. T., Kempe, S. and Richey, J.E. (1991). Chapter 15, summary: biogeochemistry of major world rivers. In: Biogeochemistry of major world river (eds. E. T. Degens, S. Kempe and J. E. Richey). Scope 42, Wiley, New York. pp. 323–344.

Devol, A.H. and Hedges, J.I. (2001). Organic matter and nutrients in the mainstem Amazon River. In The Biogeochemistry of the Amazon Basin (eds. M. E. McClain, R. L. Victoria and J. E. Richey). Oxford University Press, Oxford, pp. 275–306.

Dias, J.M., Jouanneau, J., Gonzalez, R., Araújo, M., Drago, T., Garcia, C., Oliveira, A., Rodrigues, A., Vitorino, J., Weber, O. (2002). Present day sedimentary processes on the northern Iberian shelf. Prog. Oceanogr. 52, 249–259.

Donders, T.H., Weijers, J.W.H., Munsterman, D.K., Kloosterboer-van Hoeve, M.L., Buckles, L.K., Pancost, Schouten, S., Sinninghe Damsté, J. S., Brinkhuis, H. (2009). Strong climate coupling of terrestrial and marine environments in the Miocene of northwest Europe. Earth Planet. Sci. Lett. 281, 215–225. doi: 10.1016/j.epsl.2009.02.034

Duncan, W.P., and M.N. Fernandes (2010). Physicochemical characterization of the white, black, and clearwater rivers of the Amazon Basin and its implications on the distribution of freshwater stingrays (Chondrichthyes, Potamotrygonidae). Pan-Am. J. Aquat. Sci. 5: 454–464.

Dunne, T., Mertes L.A.K., Meade, R.H., Richey, J.E., Forsberg B.R. (1998). Exchanges of sediment between the flood plain and channel of the Amazon River in Brazil. Geol. Soc. Am. Bull. 110, 450–467.

Elderfield, H., Cooper, M., Ganssen, G. (2000). Sr/Ca in multiple species of planktonic foraminifera: Implications for reconstructions of seawater Sr/Ca. Geochem. Geophys. Geosystems 1. doi: 10.1029/2001GC000194.

Elderfield, H. and Ganssen, G., (2000). Past temperature and δ18O of surface ocean waters inferred from foraminiferal Mg/Ca ratios. Nature 442–445.

Epstein, S., Buchsbaum, R., Lowenstam, H.A., Urey, H.C. (1953). Revised carbonate-water isotopic temperature scale. Geol. Soc. Am. Bull. 64, 1315.

Ernst, N., Peterse, F., Breitenbach, S.F.M., Syiemlieh, H.J., Eglinton, T.I. (2013). Biomarkers record environmental changes along an altitudinal transect in the wettest place on Earth.

Org. Geochem. 60, 93–99.

Ertel J.R., Hedges J.I., Devol A.H., Richey J.E. and Ribeiro M. (1986). Dissolved humic substances of the Amazon River system. Limnol. Oceanogr. 31, 739–754.

Fawcett, P.J., Werne, J.P., Anderson, R.S., Heikoop, J.M., Brown, E.T., Berke, M.A., Smith, S. J., Goff, F., Donohoo-Hurley, L., Cisneros-Dozal, L. M., Schouten, S., Sinninghe Damsté, J. S., Huang, Y., Toney, J., Fessenden, J., Wolde, G., Atudorei, V., Geissman, J. W., Allen, C. D. (2011). Extended megadroughts in the southwestern United States during Pleistocene interglacials. Nature 470, 518–521. doi: 10.1038/nature09839

Fietz, S., Martínez-Garcia, A., Huguet, C., Rueda, G., Rosell-Melé, A. (2011). Constraints in the application of the Branched and Isoprenoid Tetraether index as a terrestrial input proxy. J. Geophys. Res. 116. doi:10.1029/2011JC007062

Filizola, N. and Guyot, J. L. (2004). The use of Doppler technology for suspended sediment discharge determinations in the River Amazon. Hydrol. Sci. J. 49, 143–153. doi: 10.1623/hysj.49.1.143.53990

Fiúza, A. (1983). Upwelling patterns off Portugal. In: Suess, E., Thide, J. (Eds.) Coastal upwelling, its sediment record: Responses of sedimentary regime to present coastal upwelling. Nato Conference Series 10B, Springer, pp. 58–89.

Fricke, H.C., Clyde, W.C., O'Neil, J.R., Gingerich, P.D. (1998). Evidence for rapid climate change in North America during the latest Paleocene thermal maximum: Oxygen isotope compositions of biogenic phosphate from the Bighorn Basin (Wyoming). Earth Planet. Sci. Lett. 160, 193–208.

Frouin, R., Fiúza, A.F.G., Ambar, I., Boyd, T.J. (1990). Observations of a poleward surface current off the coasts of Portugal and Spain during winter. J. Geophys. Res. 95, 679–69.

Gaillardet, J., Durpe, B., Allegre, C. J., Négrel, P. (1997). Chemical and physical denudation in the Amazon River Basin. Chem. Geol. 142: 141–173, doi:10.1016/S0009-2541(97)00074-0

Gao, L., Nie, J., Clemens, S., Liu, W., Sun, J., Zech, R., Huang, Y. (2012). The importance of solar insolation on the temperature variations for the past 110 kyr on the Chinese Loess Plateau. Palaeogeogr. Palaeoclimatol. Palaeoecol. 317-318, 128–133.

Gibbs R.J. (1967a). Amazon River system: environmental factors that control its dissolved and suspended load. Science 156, 1734–1737. doi: 10.1126/science.156.3783.1734

Gibbs, R.J. (1967b). Geochemistry of Amazon River system: Part I. Factors that control salinity and composition and concentration of suspended solids. Geol. Soc. Am. Bull. 78: 1203–1232, doi:10.1130/0016-7606(1967)78[1203:TGOTAR]2.0.CO;2

Gibbs R.J. (1982). Currents on the shelf of northeastern South America. Coast. Shelf Sci. 14, 283–299.

Gliozzi, A., Paoli, G., Derosa, M., Gambacorta, A., (1983). Effect of isoprenoid cyclization on the transition temperature of lipids in thermophilic archaebacteria. Biochim. Biophys. Acta BBA - Biomembr. 735, 234–242.

Goulding, M., Barthem R., Ferreira, E. (2003). The Smithsonian Atlas of the Amazon. Smithsonian Institution Press, Washington, D.C., USA.

Greenwood, D.R., Wilf, P., Wing, S.L., Christophel, D.C. (2004). Paleotemperature estimation using leaf-margin analysis: Is Australia different? Palaois 19, 129–142.

Harvey, H.R., Fallon, R.D., Patton, J.S. (1986). The effect of organic-matter and oxygen on the degradation of bacterial-membrane lipids in marine-sediments. Geochim. Cosmochim. Acta 50, 795–804. doi: 10.1126/science.156.3783.1734

Hedges, J.I., Clark, W.A., Quay, P.D., Richey, J.E., Devol, A.H. and Santos U.M. (1986a). Composition and fluxes of organic matter in the Amazon River. Limnol. Oceanogr. 31, 717–738.

Hedges, J.I., Quay, P.D., Grootes, P.M., Richey, J.E., Devol, A.H., Farwell, G.W., Schmidt, F.W., Salati, E. (1986b) Organic carbon-14 in the Amazon River system. Science 231, 1129– 1131.

Hedges, JI., Hatcher, P.G., Ertel, J.R., Meyers-Schulte, K.J. (1992). A comparison of dissolved humic substances from seawater with Amazon River counterparts by 13C-NMR spectrometry. Geochim. Cosmochim. Acta 56, 1753–1757.

Herfort, L., Schouten, S., Boon, J.P., Woltering, M., Baas, M., Weijers J.W.H. and Sinninghe Damsté J.S. (2006). Characterization of transport and deposition of terrestrial organic matter in the southern North Sea using the BIT index. Limnol. Oceanogr. 51, 2196–2205. doi: 10.4319/lo.2006.51.5.2196

Herfort, L., Kim, J.-H., Abbas, B., Schouten, S., Coolen, M.J.L., Herndl, G.J., Sinninghe Damsté J.S. (2009). Diversity of Archaea and potential for crenarchaeotal nitrification of group 1.1a in the rivers Rhine and Têt. Aquat. Microbial Ecol. 55, 189–201.

Hopmans, E.C., Schouten, S., Pancost, R.D., van der Meer, M.T.J., Sinninghe Damsté, J.S. (2000). Analysis of intact tetraether lipids in archaeal cell material and sediments by high performance liquid chromatography/atmospheric pressure chemical ionization mass spectrom-

etry. Rapid Commun. Mass Spectrom. 14, 585–589.

Hopmans, E. C., Weijers J. W. H., Schefuß, E., Herfort L., Sinninghe Damsté, J. S., Schouten S. (2004). A novel proxyfor terrestrial organic matter in sediments based on branched and isoprenoidtetraether lipids. Earth Plan. Sci. Lett. 224, 107– 116. doi: 10.1016/j.epsl.2004.05.012

Hren, M.T., Pagani, M., Erwin, D.M., Brandon, M. (2010). Biomarker reconstruction of the early Eocene paleotopography and paleoclimate of the northern Sierra Nevada. Geology 38, 7–10.

Hu, J., Meyers, P.A., Chen, G., Peng, P., Yang, Q. (2012). Archaeal and bacterial glycerol dialkyl glycerol tetraethers in sediments from the Eastern Lau Spreading Center, South Pacific Ocean. Org. Geochem. 43, 162–167.

Huguet C., Hopmans E.C., Febo-Ayala W., Thompson D.H., Sinninghe Damsté J.S., Schouten S. (2006). An improved method to determine the absolute abundance of glycerol dibiphytanyl glycerol tetraether lipids. Org. Geochem. 37, 1036–1041. doi:10.1016/j.orggeochem.2006.05.008

Huguet, C., Smittenberg, R.H., Boer, W., Sinninghe Damsté, J.S., Schouten, S. (2007). Twentieth century proxy records of temperature and soil organic matter input in the Drammensfjord, southern Norway. Org. Geochem. 38, 1838–1849. doi:10.1016/j.orggeochem.2007.06.015

Huguet, C., de Lange, G.J., Gustafsson, O., Middelburg, J.J., Sinninghe Damsté, J.S., Schouten, S. (2008). Selective preservation of soil organic matter in oxidized marine sediments (Madeira Abyssal Plain). Geochim. Cosmochim. Acta 72, 6061–6068.

Huguet, A., Fosse C., Metzger, P., Fritsch, E., Derenne, S. (2010). Occurrence and distribution of extractable glycerol dialkyl glycerol tetraethers in podzols. Org. Geochem. 41, 291–301. doi: 10.1016/j.orggeochem.2010.02.015

IPCC (2013). Working Group I Contribution to the IPCC Fifth Assessment Report Climate Change 2013: The Physical Science Basis Summary for Policymakers.

Ittekkot, V. (1988). Global trends in the nature of organic matter in river suspensions. Nature 332, 436–438.

Ittekkot, V., Haake, B. (1990). The terrestrial link in the removal of organic carbon in Facets of Modern Biogeochemistry. (eds. V. Ittekkot et al.). Springer, New York. pp. 319–325.

Jaccon, G. (1987). Jaugeage de l'Amazone à Óbidos par les méthodes du bateau mobile et des grands fleuves. Hydrologie Continentale 2, 117–126.

Jones, P.D., Briffa, K.R., Barnett, T.P., Tett, S.F.B. (1998). High-resolution palaeoclimatic records for the last millennium: interpretation, integration and comparison with General Circulation Model control-run temperatures. The Holocene 8, 455–471.

Jones, R.T., Robeson, M.S., Lauber, C.L., Hamady, M., Knight, R., Fierer, N. (2009). A comprehensive survey of soil acidobacterial diversity using pyrosequencing and clone library analyses. ISME J. 3, 442–453.

Jordan, G.J. (1997). Uncertainty in palaeoclimatic reconstructions based on leaf physiognomy. Aust. J. Bot. 45, 527.

Jouanneau, J.M., Garcia, C., Oliveira, A., Rodrigues, A., Dias, J.A., Weber, O. (1998). Dispersal and deposition of suspended sediment on the shelf off the Tagus and Sado estuaries, S.W. Portugal. Prog. Oceanogr. 42, 233–257.

Jouanneau, J.M., Weber, O., Drago, T., Rodrigues, A., Oliveira, A., Dias, J.M.A., Garcia, C., Schmidt, S., Reyss, J.L. (2002). Recent sedimentation and sedimentary budgets on the western Iberian shelf. Prog. Oceanogr. 52, 261–275.

Jouzel, J., Lorius, C., Petit, J.R., Genthon, C., Barkov, N.I., Kotlyakov, V.M., Petrov, V.M. (1987). Vostok ice core: a continuous isotope temperature record over the last climatic cycle (160,000 years). Nature 329, 403–408.

Jouzel, J., Alley, R.B., Cuffey, K.M., Dansgaard, W., Grootes, P., Hoffmann, G., Johnsen, S.J., Koster, R.D., Peel, D., Shuman, C.A., Stievenard, M., Stuiver, M., White, J. (1997). Validity of the temperature reconstruction from water isotopes in ice cores. J. Geophys. Res. 102, 26471.

Junk, W. J. (1997) General aspects of floodplain ecology with special reference to Amazonian floodplains. In The Central-Amazonian Floodplain: Ecology of a Pulsing System, Ecological Studies (ed. W. J. Junk). Springer Verlag, Heidelberg, Berlin, New York, pp. 3–22.

Karner, M.B., DeLong, E.F., Karl, D.M. (2001). Archaeal dominance in the mesopelagic zone of the Pacific Ocean. Nature 409, 507–510.

Kennett, J.P. and Stott, L.D. (1991). Abrupt deep-sea warming, palaeoceanographic changes and benthic extinctions at the end of the Palaeocene. Nature 353, 225–229.

Kim, J.-H., Schouten S., Buscail, R., Ludwig, W., Bonnin, J., Sinninghe Damsté, J. S., Bourrin, F. (2006). Origin and distribution of terrestrial organic matter in the NW Mediterranean (Gulf of Lions): application of the newly developed BIT index. Geochem. Geophys. Geosyst. 7, Q11017. http:// dx.doi.org/10.1029/2006GC001306.

Kim, J.-H., Ludwig W., Schouten, S., Kerhervé, P., Herfort, L., Bonnin, J., Sinninghe Damsté, J.S. (2007) Impact of flood events on the transport of terrestrial organic matter to the ocean: a study of the Têt River (SW France) using the BIT index. Org. Geochem. 38, 1593–1606 doi: 10.1016/j. orggeochem.2007.06.010

Kim, J.-H., Buscail, R., Bourrin, F., Palanques, A., Sinninghe Damsté, J. S., Bonnin, J., Schouten S. (2009). Transport and depositional process of soil organic matter during wet and dry storms on the Têt inner shelf (NW Mediterranean). Paleogeogr. Paleoclimatol. Paleoecol. 273, 228–238.

Kim, J.-H., van der Meer, J., Schouten, S., Helmke, P., Willmott, V., Sangiorgi, F., Koc, N., Hopmans, E.C., Sinninghe Damsté, J.S. (2010a). New indices and calibrations derived from the distribution of crenarchaeal isoprenoid tetraether lipids: Implications for past sea surface temperature reconstructions. Geochim. Cosmochim. Acta 74, 4639–4654. doi: 10.1016/j. gca.2010.05.027

Kim, J.-H., Zarzycka, B., Buscail, R., Peterse, F., Bonnin, J., Ludwig, W., Schouten, S., Sinninghe Damsté, J.S. (2010b). Contribution of river-borne soil organic carbon to the Gulf of Lions (NW Mediterranean). Limnol. Oceanogr. 55, 507–518.

Kim, J.-H., Zarzycka, B., Buscail, R., Peters, F., Bonnin, J., Ludwig, W., Schouten, S., Sinninghe Damsté, J. S. (2010c). Factors controlling the Branched Isoprenoid Tetraether (BIT) Contribution of river-borne soil organic carbon to the Gulf of Lions (NW Mediterranean). Limnol. Oceanogr. 55, 507–518.

Kim, J.-H., Zell, C., Moreira-Turcq, P., Pérez, M.A.P., Abril, G., Mortillaro, J.-M., et al. (2012). Tracing soil organic carbon in the lower Amazon River and its tributaries using GDGT distributions and bulk organic matter properties. Geochim. Cosmochim. Acta 90, 163–180. doi: 10.1016/j.gca.2012.05.014

Koga, Y., Kyuragi, T., Nishihara, M., Sone, N. (1998). Did archaeal and bacterial cells arise independently from noncellular precursors? A hypothesis stating that the advent of membrane phospholipid with enantiomeric glycerophosphate backbones caused the separation of the two lines of descent. J. Mol. Evol. 46, 54–63.

Kohn, M.J., Law, J.M. (2006). Stable isotope chemistry of fossil bone as a new paleoclimate indicator. Geochim. Cosmochim. Acta 70, 931–946.

Kohnhauser, K.O., Fyfe, W.S., Kronberg, B.I. (1994). Multielement chemistry of some Amazonian waters and soils. Chem. Geol. 111: 155–175, doi:10.1016/0009-2541(94)90088-4

Lal, R. (2003) Soil erosion and the global carbon budget. Environ. Int. 29, 437–450.

Langworthy, T.A., Holzer, G., Zeikus, J.G., Tornabene, T.G., (1983). Iso- and anteiso-branched glycerol diethers of the thermophilic anaerobe Thermodesulfotobacterium commune. Syst. Appl. Microbiol. 4, 1–17.

LaZerte, B.D. (1983). Stable carbon isotope ratios: implications for the source sediment carbon and for phytoplankton carbon assimilation in Lake Memphremagog, Quebec. Can. J. Fish. Aquat. Sci. 40, 1658–1666.

Lea, D.W. (2003). Elemental and isotopic proxies of past ocean temperatures, in: Holland, D.H. and Turekian K.K (Eds.), The Ocean and Marine Geochemistry. Treatise on Geochemistry. Elsevier-Pergamon, Oxford, pp. 365–390.

Lee, S. and Furhman, J.D. (1987). Relationships between biovolume and biomass of naturally derived marine bacterioplankton. Appl. Environ. Microbiol. 53, 1298–1303.

Leng, M.J., Marshall, J.D. (2004). Palaeoclimate interpretation of stable isotope data from lake sediment archives. Quat. Sci. Rev. 23, 811–831.

Lengger, S. K., Hopmans, E. C., Reichart, G.-J., Nierop, K. G. J., Sinninghe Damsté, J. S., Schouten, S. (2012a). Intact polar and core glycerol dibiphytanyl glycerol tetraether lipids in the Arabian Sea oxygen minimum zone: Part II. Selective preservation and degradation in sediments and consequences for the TEX86. Geochim. Cosmochim. Acta, 98: 224–258, doi:10.1016/j.gca.2012.05.003

Lengger, S. K., Hopmans, E. C., Sinninghe Damsté, J. S., Schouten, S. (2012b). Comparison of extraction and work up techniques for analysis of core and intact polar tetraether lipids from sedimentary environments. Org. Geochem. 47, 34–40.

Likens, G. E., Mackenzie, F. T., Richey, J. E., Sedell, J. R. and Turekian, K. K. (1981). Flux of organic carbon by rivers to the ocean. U S Dept Energy, NRC-C0NF-8009140, Washington, DC. p. 397.

Lipp, J. S., and Hinrichs, K.-U. (2009). Structural diversity and fate of intact polar lipids in marine sediments. Geochim. Cosmochim. Acta 73: 6816–6833, doi:10.1016/j. gca.2009.08.003

Liu, X.-L., Leider, A., Gillerspie, A., Gröger, J. , Versteegh, G. J. M., Hinrichs, K.-U. (2010). Identification of polar lipid precursors of the ubiquitous branched GDGT orphanlipids in a peat bog in Northern Germany. Org. Geo-

chem. 41: 653–660, doi:10.1016/j.orggeochem.2010.04.004

Liu, W., Wang, H., Zhang, C.L., Liu, Z., He, Y. (2013). Distribution of glycerol dialkyl glycerol tetraether lipids along an altitudinal transect on Mt. Xiangpi, NE Qinghai-Tibetan Plateau, China. Org. Geochem. 57, 76–83.

Logemann, J., Graue, J., Köster, J., Engelen, B., Rullkötter, J., Cypionka, H. (2011). A laboratory experiment of intact polar lipid degradation in sandy sediments. Biogeosciences 8, 2547–2560.

Loomis, S.E., Russell James, M. Sinninghe Damsté, J. S. (2011). Distributions of branched GDGTs in soils and lake sediments from western Uganda: implications for a lacustrine paleothermometer. Org. Geochem. 42, 739–751.

Lorrain, A., Savoye, N., Chauvaud, L., Paulet, Y.-M., Naulet, N. (2003). Decarbonation and preservation method for the analysis of organic C and N contents and stable isotope ratios of low-carbonated suspended particulate material. Anal. Chim. Acta 491, 125–133.

Loureiro, J.J., Machado, M.L., Macedo, M.E., Nunes, M.N., Botelho, O.F., Sousa, M.L., Almeida, M.C., Martins, J.C. (1986). Direcção Geral dos Serviços Hidraulicos. Monografias hidrológicas dos principais cursos de água de Portugal Continental., Lisboa, p. 569.

Ludwig, W., Probst J.-L. and Kempe S. (1996). Predicting the oceanic input of organic carbon by continental erosion. Global. Biogeothem. Cycles 10, 23–42.

Mann, M.E., Bradley, R.S., Hughes, M.K. (1998). Global-scale temperature patterns and climate forcing over the past six centuries. Nature 329, 779–787.

Marengo, J.A., Liebmann, B., Kousky, V.E., Filizola, N.P., Wainer, C. (2001). Onset and end of the rainy season in the Brazilian Amazon Basin. J. Clim. 14, 833–852.

Mariotti, A., Gadel, F., Giresse, P., Mouzeo, K. (1991). Carbon isotope composition and geochemistry of particulate organic matter in the Congo River (Central Africa): application to the study of Quaternary sediments off the mouth of the river. Chem. Geol. 86, 345–357.

Marlowe, I.T., Green, J.C., Neal, A.C., Brassell, S.C., Eglinton, G., Course, P.A. (1984). Long chain (n-C37 –C39) alkenones in the Prymnesiophyceae. Distribution of alkenones and other lipids and their taxonomic significance. Br. Phycol. J. 19, 203–216.

Martinelli, L.A., Victoria, R.L., Forsberg, B.R., Richey, J.E. (1994). Isotopic composition of major carbon reservoirs in the Amazon floodplain. Int. J. Ecol. Environ. Sci. 20, 31–46.

Martinelli, L.A., Victoria, R.L., de Camargo, P.B., de Cassia Piccolo, M., Mertes, L., Richey, J.E., Devol, A.H., Forsberg, B.R. (2003). Inland variability of carbon–nitrogen concentrations and δ13C in Amazon floodplain (várzea) vegetation and sediment. Hydrol. Process. 17, 1419–1430.

Martinez, J.M., Le Toan, T. (2007). Mapping of flood dynamics and spatial distribution of vegetation in the Amazon floodplain using multitemporal SAR data. Remote Sens. Environ. 108, 209–223. doi:10.1016/j.rse.2006.11.012

Martinez, J.M., Guyot, J.L., Filizola, N., Sondag F. (2009). Increase in suspended sediment discharge of the Amazon River assessed by monitoring network and satellite data. Catena 79, 257–264. doi: 10.1016/j.catena.2009.05.011

Mayorga, E., Aufdenkampe, A.K., Masiello, C.A., Krusche, A.V., Hedges, J.I., Quay, P.D., Richey, J.E., Brown, T. A. (2005). Young organic matter as a source of carbon dioxide outgassing from Amazonian rivers. Nature 436, 538–541.

McDermott, F. (2004). Palaeo-climate reconstruction from stable isotope variations in speleothems: A review. Quat. Sci. Rev. 23, 901–918.

Meade, R.H., Nordin, C.F., Curtis, W.F., Costa Rodrigues, F.M., Do Vale, C.M., Edmond, J.M. (1979). Sediment loads in the Amazon River. Nature 278, 161–163. doi: 10.1038/278161a0

Meade, R. H., Dunne, T., Richey, J. E., Santos, U. M., Salati E. (1985). Storage and remobilization of suspended sediment in the lower Amazon River of Brazil. Science 228, 488–490. doi: 10.1126/science.228.4698.488

Medlin, L.K., Sáez, A.G., Young, J.R. (2008). A molecular clock for coccolithophores and implications for selectivity of phytoplankton extinctions across the K/T boundary. Mar. Micropaleontol. 67, 69–86.

Melack, J.M., and Hess, L.L. (2010). Remote sensing of the distribution and extent of wetlands in the Amazon Basin, p. 43–59. In Junk, W. J., Piedade, M.T.F., Wittmann, F., Schöngart, J., Parolin, P. [eds.], Amazonian floodplain forests: Ecophysiology, biodiversity, and sustainable management. Springer Ecological Studies.

Menges, J., Huguet, C., Alcañiz, J.M., Fietz, S., Sachse, D., Rosell-Melé, A. (2013). Water availability determines branched glycerol dialkyl glycerol tetraether distributions in soils of the Iberian Peninsula. Biogeosciences Discuss. 10, 9043–9068.

Ménot, G., Bard, E., Rostek, F., Weijers, J.W.H., Hopmans, E.C., Schouten, S., Sinninghe Damsté, J.S. (2006). Early reactivation of European rivers during the last deglaciation. Science 313, 1623–1625. doi: 10.1126/science.1130511

Meybeck, M. (1982) Carbon, nitrogen, and phosphorus transport by world rivers. Am. J. Sci. 282, 401–450.

Meyers, P. A. (1994) Preservation of elemental and isotopic source identification of sedimentary organic matter. Chem. Geol. 114, 289–302.

Molinier, M., Guyot, J. L., Oliveira, E. and Guimaraes, V. (1996). Les regimes hydrologiques de l'Amazone et de ses affluents. In L'hydrologie tropicale: geoscience et outil pour le developpement (eds. P. Chevallier and B. Pouyaud). AIHS, Paris, pp. 209–222.

Moreira-Turcq, P., Seyler, P., Guyot, J. L., Etcheber, H. (2003). Exportation of organic carbon from the Amazon River and its main tributaries. Hydrol. Process. 17, 1329–1344.

Moreira-Turcq, P., Bonnet, M.-P., Amorim, M., Bernardes, M., Lagane, C., Maurice, L., et al. (2013). Seasonal variability in concentration, composition, age, and fluxes of particulate organic carbon exchanged between the floodplain and Amazon River. Global Biogechem. Cycl. 27, 119–130. doi: 10.1002/gbc.20022

Mortillaro, J. M., Abril, G., Moreira-Turcq, P., Sobrinho, R. L., Perez, M., Meziane, T. (2011) Fatty acid and stable isotope (δ13C, δ15N) signatures of particulate organic matter in the Lower Amazon River: seasonal contrasts and connectivity between floodplain lakes and the mainstem. Org. Geochem. 42, 1159–1168.

Mounier S., Braucher, R., Benaim, J. Y. (1998). Differentiation of organic matter's properties of the Rio Negro basin by cross flow ultrafiltration and UV-spectrofluorescence. Water Res. 33, 2363–2373.

Müller, P.J., Kirst, G., Ruhland, G., von Storch, I., Rosell-Melé, A. (1998). Calibration of the alkenone paleotemperature index UK'37 based on core-tops from the eastern South Atlantic and the global ocean (60°N-60°S). Geochim. Cosmochim. Acta 62, 1757–1772.

New, M., Lister, D., Hulme, M., Makin, I. (2002). A high resolution data set of surface climate over global land areas. Clim. Res. 21, 1–25. doi: 10.3354/cr021001

Niemann, H., Stadnitskaia, A., Wirth, S.B., Gilli, A., Anselmetti, F.S., Sinninghe Damsté, J.S., Schouten, S., Hopmans, E.C., Lehmann, M.F. (2012). Bacterial GDGTs in Holocene sediments and catchment soils of a high Alpine lake: application of the MBT/CBT-paleothermometer. Clim. Past 8, 889–906.

Nores, M. (2011). The western Amazonian boundary for avifauna determined by species distribution patterns and geographical and ecological features. Int. J. Ecol. 2011. http://dx.doi.org/10.1155/2011/958684.

Nunes, F., Norris, R.D. (2006). Abrupt reversal in ocean overturning during the Palaeocene/Eocene warm period. Nature 439, 60–63.

Nürnberg, D., Bijma, J., Hemleben, C. (1996). Assessing the reliability of magnesium in foraminiferal calcite as a proxy for water mass temperatures. Geochim. Cosmochim. Acta 60, 803–814.

Oba, M., Sakata, S., Tsunogai, U. (2006). Polar and neutral isopranyl glycerol ether lipids as biomarkers of archaea in near-surface sediments from the Nankai. Org. Geochem. 37, 1643–1654. doi:10.1016/j.orggeochem.2006.09.002

Oppermann, B. I., Michaelis, W., Blumenberg, M., Frerichs, J., Schulz, H. M., Schippers, A., Beaubien, S. E., Krüger, M. (2010). Soil microbial community changes as a result of longterm exposure to a natural CO2 vent. Geochim. Cosmochim. Acta 74, 2697–2716. doi: 10.1016/j.gca.2010.02.006

Pancost, R. D. and Sinninghe Damsté, J. S. (2003). Carbon isotopic compositions of prokaryotic lipids as tracers of carbon cycling in diverse settings. Chem. Geol. 195, 29–58. 10.1016/S0009-2541(02) 00387-X

Patterson, B. D., Stotz, D. F., Solari, S., Fitzpatrick, J. W., Pacheco, V. (1998). Contrasting patterns of elevational zonation for birds and mammals in the Andes of southeastern Peru. J. Biogeography 25, 593–607.

Pearson, E.J., Juggins, S., Talbot, H.M., Weckström, J., Rosén, P., Ryves, D.B., Roberts, S.J., Schmidt, R. (2011). A lacustrine GDGT-temperature calibration from the Scandinavian Arctic to Antarctic: Renewed potential for the application of GDGT-paleothermometry in lakes. Geochim. Cosmochim. Acta 75, 6225–6238.

Peterse, F., Kim, J.-H., Schouten, S., Klitgaard Kristensen, D., Koç, N., Sinninghe Damsté, J.S. (2009a). Constraints on the application of the MBT/CBT palaeothermometer at high latitude environments (Svalbard, Norway). Org. Geochem. 40, 692–699.

Peterse, F., Schouten, S., van der Meer, M.T.J., Sinninghe Damsté, J.S. (2009b). Distribution of branched tetraether lipids in geothermally heated soils: Implications for the MBT/CBT temperature proxy. Org. Geochem. 40, 201–205.

Peterse, F., van der Meer, M.T.J., Schouten, S., Jia, G., Ossebaar, J., Blokker, J., Sinninghe Damsté, J.S. (2009c). Assessment of soil n-alkane δD and branched tetraether membrane lipid distributions as tools for paleoelevation reconstruction. Biogeosciences 6, 2799–2807.

Peterse, F., Nicol, G.W., Schouten, S., Sinninghe Damsté, J.S. (2010). Influence of soil pH on

the abundance and distribution of core and intact polar lipid-derived branched GDGTs in soil. Org. Geochem. 41, 1171–1175.

Peterse, F., Hopmans, E.C., Schouten, S., Mets, A., Rijpstra, W.I.C., Sinninghe Damsté, J.S., (2011a). Identification and distribution of intact polar branched tetraether lipids in peat and soil. Org. Geochem. 42, 1007–1015. doi:10.1016/ j.orggeochem.2011.07.006

Peterse, F., Prins, M.A., Beets, C.J., Troelstra, S.R., Zheng, H., Gu, Z., Schouten, S., Sinninghe Damsté, J.S., (2011b). Decoupled warming and monsoon precipitation in East Asia over the last deglaciation. Earth Planet. Sci. Lett. 301, 256–264. doi: 10.1016/j.epsl.2010.11.010

Peterse, F., van der Meer, J., Schouten, S., Weijers, J.W.H., Fierer, N., Jackson, R.B., Kim, J.-H., Sinninghe Damsté, J.S. (2012). Revised calibration of the MBT–CBT paleotemperature proxy based on branched tetraether membrane lipids in surface soils. Geochim. Cosmochim. Acta 96, 215–229. doi: 10.1016/j.gca.2012.08.011

Pitcher, A., Hopmans, E.C., Schouten, S., Sinninghe Damsté, J.S. (2009). Separation of core and intact polar archaeal tetraether lipids using silica columns: Insights into living and fossil biomass contributions. Org. Geochem. 40, 12–19. doi:10.1016/j.orggeochem.2008.09.008

Pitcher, A., Hopmans E. C., Mosier A. C., Park S.-J., Rhee S.-K., Francis C. A., Schouten S. and Sinninghe Damsté J. S. (2011a). Core and intact polar glycerol dibiphytanyl glycerol tetraether lipids of ammonia-oxidizing archaea enriched from marine and mstuarine sediments. Appl. Environ. Microbiol. 77, 3468–3477.

Pitcher, A., Villanueva, L., Hopmans, E. C., Schouten, S., Reichart, G.-J., Sinninghe Damsté, J. S. (2011b). Niche segregation of ammonia-oxidizing archaea and anammox bacteria in the Arabian Sea oxygen minimum zone. ISME J. 5: 1896–1904, doi:10.1038/ismej.2011.60

Powers, L.A., Werne, J.P., Johnson, T.C., Hopmans, E.C., Sinninghe Damsté, J.S., Schouten, S. (2004). Crenarchaeotal membrane lipids in lake sediments: A new paleotemperature proxy for continental paleoclimate reconstruction? Geology 32, 613-616

Powers, L.A. (2005). Large temperature variability in the southern African tropics since the Last Glacial Maximum. Geophys. Res. Lett. 32. Doi: 10.1029/2004GL022014

Powers, L., Werne, J.P., Vanderwoude, A.J., Sinninghe Damsté, J.S., Hopmans, E.C., Schouten, S., (2010). Applicability and calibration of the TEX86 paleothermometer in lakes. Org. Geochem. 41, 404–413. doi: 10.1016/j.orggeochem.2009.11.009

Prahl, F.G., Wakeham, S.G., (1987). Calibration of unsaturation patterns in long-chain ketone compositions for palaeotemperature assessment. Nature 330, 367–369.

Prahl, F.G., Muehlhausen, L.A., Zahnle, D.L. (1988). Further evaluation of long-chain alkenones as indicators of paleoceanographic conditions. Geochim. Cosmochim. Acta 52, 2303–2310.

Pross, J., Contreras, L., Bijl, P.K., Greenwood, D.R., Bohaty, S.M., Schouten, S., Bendle, J.A., Röhl, U., Tauxe, L., Raine, J.I., Huck, C.E., van de Flierdt, T., Jamieson, S.S.R., Stickley, C.E., van de Schootbrugge, B., Escutia, C., Brinkhuis, H., Brinkhuis, H., Escutia Dotti, C., Klaus, A., Fehr, A., Williams, T., Bendle, J.A.P., Bijl, P.K., Bohaty, S.M., Carr, S.A., Dunbar, R.B., Gonzàlez, J.J., Hayden, T.G., Iwai, M., Jimenez-Espejo, F.J., Katsuki, K., Soo Kong, G., McKay, R.M., Nakai, M., Olney, M.P., Passchier, S., Pekar, S.F., Pross, J., Riesselman, C.R., Röhl, U., Sakai, T., Shrivastava, P.K., Stickley, C.E., Sugisaki, S., Tauxe, L., Tuo, S., van de Flierdt, T., Welsh, K., Yamane, M. (2012). Persistent near-tropical warmth on the Antarctic continent during the early Eocene epoch. Nature 488, 73–77.

Quay, P. D., Wilbur, D. O., Richey, J. E., Hedges, J. I., Devol, A. H. (1992). Carbon cycling in the Amazon River: implications from the 13C composition of particulate and dissolved carbon. Limnol. Oceanogr. 37, 857–871.

Quesada, C.A., Lloyd, J., Anderson, L.O., Fyllas, N.M., Schwarz, M., Czimnczik, C.I. (2009). Soils of Amazonia with particular reference to the RAINFOR sites. Biogeosciences 8: 1415–1440, doi:10.5194/bg-8-1415-2011

Rampen, S.W., Willmott, V., Kim, J.-H., Uliana, E., Mollenhauer, G., Schefuß, E., Sinninghe Damsté, J.S., Schouten, S. (2012). Long chain 1,13- and 1,15-diols as a potential proxy for palaeotemperature reconstruction. Geochim. Cosmochim. Acta 84, 204–216.

Raymond P.A. and Bauer J.E. (2001) Riverine export of aged terrestrial organic matter to the North Atlantic Ocean. Nature 409, 497–500.

Robinson, W.J., Cook, E., Pilcher, J.R., Eckstein, D., Kairiukstis, L., Shiyatov, S., Norton, D.A. (1990). Some historical background on dendrochronology, in: Cook, E.R., Kairiukstis, L.A. (Eds.) Methods of Dendrochronology. Kluwer Academic Publishers, Dordrecht, The Netherlands, pp. 1–21.

Rontani, J.-F., Beker, B., Volkman, J.K. (2004). Long-chain alkenones and related compounds in the benthic haptophyte Chrysotila lamellosa Anand HAP 17. Phytochemistry 65, 117–126.

Rosenthal, Y., Lohmann, G.P., Lohmann, K.C., Sherrell, R.M. (2000). Incorporation and preserva-

tion of Mg in Globigerinoides sacculifer: implications for reconstructing the temperature and 18O/16O of seawater. Paleoceanography 15, 135–145.

Ruddiman, W.F. (2008). Earth's climate: past and future, 2nd revised edition. W.H. Freeman and Company.

Rueda, G., Rosell-Melé, A., Escala, M., Gyllencreutz, R., Backman, J. (2009). Comparison of instrumental and GDGT-based estimates of sea surface and air temperatures from the Skagerrak. Org. Geochem. 40, 287–291 doi: 10.1016/j.orggeochem.2008.10.012

Salati, E., Dall'Olio, A., Matsui, E., Gat, J. R. (1979). Recycling of water in the Amazon Basin: an isotopic study. Water Resour. Res. 15, 1250. doi: 10.1029/WR015i005p01250

Schlesinger, W.H. and Melack, J.M. (1981). Transport of organic carbon in the world's rivers. Tellus 33, 172–187.

Schmidt, F., Hinrichs, K.-U., Elvert, M. (2010). Sources, transport, and partitioning of organic matter at a highly dynamic continental margin. Mar. Chem. 118, 37–55.

Schoon, P. L., de Kluijver, A., Middelburg, J. J., Downing, J. A., Sinninghe Damsté, J. S., and Schouten, S. (2013). Influence of lake water pH and alkalinity on the distribution of core and intact polar branched glycerol dialkyl glycerol tetraethers (GDGTs) in lakes, Org. Geochem. 60, 72–82, doi:10.1016/j.orggeochem.2013.04.015.

Schouten, S., Hopmans, E.C., Pancost, R.D., Sinninghe Damsté, J.S., (2000). Widespread occurrence of structurally diverse tetraether membrane lipids: Evidence for the ubiquitous presence of low-temperature relatives of hyperthermophiles. Proc. Natl. Acad. Sci. USA 97, 14421–14426.

Schouten, S., Hopmans, E.C., Schefuß, E., Sinninghe Damsté, J.S. (2002). Distributional variations in marine crenarchaeotal membrane lipids: a new tool for reconstructing ancient sea water temperatures? Earth Planet. Sci. Lett. 204, 265–274doi: 10.1016/S0012-821X(02)00979-2

Schouten, S., Hopmans, E.C., Sinninghe Damsté, J.S. (2004). The effect of maturity and depositional redox conditions on archaeal tetraether lipid palaeothermometry. Org. Geochem. 35, 567–571.

Schouten, S., Huguet C., Hopmans, E.C., Kienhuis, M., Sinninghe Damsté, J.S. (2007). Analytical methodology for TEX86 paleothermometry by high-performance liquid chromatography/atmospheric pressure chemical ionization-mass spectrometry. Anal. Chem. 79, 2940–2944 doi: 10.1021/ac062339v

Schouten S., Baas M., Hopmans E. C. and Sinninghe Damsté J. S. (2008a). An unusual isoprenoid tetraether lipid in marine and lacustrine sediments. Org. Geochem. 39, 1033–1038.

Schouten, S., Eldrett, J., Greenwood, D. R., Harding, I., Baas, M., Sinninghe Damsté, J.S. (2008b). Onset of long-term cooling of Greenland near the Eocene-Oligocene boundary as revealed by branched tetraether lipids. Geology 36, 147-150.

Schouten, S., Hopmans, E. C., Baas, M., Boumann H., Standfest, S., Könneke, M., Stahl. D. A., Sinninghe Damsté, J. S. (2008c). Intact membrane lipids of 'Candidatus Nitrosopumilus maritimus', a cultivated representative of the cosmopolitan mesophilic group I crenarchaeota. Appl. Environ. Microbiol. 74: 2433–2440, doi:10.1128/AEM.01709-07

Schouten, S., Hopmans, E. C., van der Meer, J., Mets, A., Bard, E., Bianchi, T. S., Diefendorf, A., Escala, M., Freeman, K. H., Furukawa, Y., Huguet, C., Ingalls, A., Ménot-Combes, G., Nederbragt, A.J., Oba, M., Pearson, A., Pearson, E.J., Rosell-Mel, A., Schaeffer, P., Shah, S.R., Shanahan, T.M., Smith, R.W., Smittenberg, R., Talbot, H.M., Uchida, M., van Mooy, B.A.S., Yamamoto, M., Zhang, Z., Sinninghe Damsté, J.S. (2009). An interlaboratory study of TEX86 and BIT analysis using high-performance liquid chromatography-mass spectrometry. Geochem. Geophys. Geosyst. 10, 1–13.

Schouten, S., Middelburg, J.J., Hopmans, E.C., Sinninghe Damsté, J.S. (2010). Fossilization and degradation of intact polar lipids in deep subsurface sediments: A theoretical approach. Geochim. Cosmochim. Acta 74: 3806–3814, doi:10.1016/j.gca.2010.03.029

Schouten, S., Hopmans, E.C., Rosell-Melé, A., Pearson, A., Adam, P., Bauersachs, T., Bard, E., Bernasconi, S.M., Bianchi, T.S., Brocks, J.J., Carlson, L.T., Castañeda, I.S., Derenne, S., Selver, A.D., Dutta, K., Eglinton, T., Fosse, C., Galy, V., Grice, K., Hinrichs, K.-U., Huang, Y., Huguet, A., Huguet, C., Hurley, S., Ingalls, A., Jia, G., Keely, B., Knappy, C., Kondo, M., Krishnan, S., Lincoln, S., Lipp, J., Mangelsdorf, K., Martínez-García, A., Ménot, G., Mets, A., Mollenhauer, G., Ohkouchi, N., Ossebaar, J., Pagani, M., Pancost, R.D., Pearson, E.J., Peterse, F., Reichart, G.-J., Schaeffer, P., Schmitt, G., Schwark, L., Shah, S.R., Smith, R.W., Smittenberg, R.H., Summons, R.E., Takano, Y., Talbot, H.M., Taylor, K.W.R., Tarozo, R., Uchida, M., van Dongen, B.E., Van Mooy, B.A.S., Wang, J., Warren, C., Weijers, J.W.H., Werne, J.P., Woltering, M., Xie, S., Yamamoto, M., Yang, H., Zhang, C.L., Zhang, Y., Zhao, M., Sinninghe Damsté, J.S. (2013a). An interlaboratory study of TEX86 and BIT analysis of sediments, extracts and

standard mixtures. Geochem. Geophys. Geosyst., doi:10.1002/2013GC004904.

Schouten, S., Hopmans, E.C., Sinninghe Damsté, J.S. (2013b). The organic geochemistry of glycerol dialkyl glycerol tetraether lipids: A review. Org. Geochem. 54, 19–61.

Silva, T.S.F., Costa, M.P.F., Melack, J.M. (2009). Annual net primary production of macrophytes in the eastern Amazon floodplain. Wetlands 29, 747–775.

Sinninghe Damsté, J. S., Hopmans, E. C., Pancost, R. D., Schouten S., Geenevasen, J.A.J. (2000). Newly discovered nonisoprenoid glycerol dialkyl glycerol tetraether lipids in sediments. Chem. Comm. 17, 1683–1684. doi: 10.1039/b004517i

Sinninghe Damsté, J.S., Hopmans, E.C., Schouten, S., Van Duin, A.C.T., Geenevasen, J.A.J. (2002) Crenarchaeol: the characteristic core glycerol dibiphytanyl glycerol tetraether membrane lipid of cosmopolitan pelagic crenarchaeota. J. Lipid Res. 43, 1641–1651. doi:10.1194/jlr.M200148-JLR200

Sinninghe Damsté, J.S., Ossebaar, J., Schouten, S., Verschuren, D. (2008). Altitudinal shifts in the branched tetraether lipid distribution in soil from Mt. Kilimanjaro (Tanzania): Implications for the MBT/CBT continental palaeothermometer. Org. Geochem. 39, 1072–1076.

Sinninghe Damsté, J.S., Ossebaar, J., Abbas, B., Schouten, S., Verschuren, D. (2009). Fluxes and distribution of tetraether lipids in an equatorial African lake: constraints on the application of the TEX86 palaeothermometer and BIT index in lacustrine settings. Geochim. Cosmochim. Acta 73, 4232– 4249 doi: 10.1016/j.gca.2009.04.022

Sinninghe Damsté, J.S., Rijpstra, W.I.C., Hopmans, E.C., Weijers, J.W.H., Foesel, B.U., Overmann, J., Dedysh, S.N. (2011). 13,16-Dimethyl Octacosanedioic Acid (iso-Diabolic Acid), a common membrane-spanning lipid of Acidobacteria subdivisions 1 and 3. Appl. Environ. Microbiol. 77, 4147–4154. doi:10.1128/AEM.00466-11

Sioli, H. (1984). The Amazon. Limnology and landscape ecology of a mighty tropical river and its basin. W. Junk.

Sioli H. (1950). Das Wasser in Amazonasgebiet. Forsch. Fortsch. 26, 274–280.

Sluijs, A., Schouten, S., Pagani, M., Woltering, M., Brinkhuis, H., Sinninghe Damsté, J.S., Dickens, G.R., Huber, M., Reichart, G.-J., Stein, R., Matthiessen, J., Lourens, L.J., Pedentchouk, N., Backman, J., Moran, K., the Expedition 302 Scientists (2006). Subtropical Arctic Ocean temperatures during the Palaeocene/Eocene thermal maximum. Nature 441, 610–613.

Sluijs, A., Brinkhuis, H., Crouch, E.M., John, C.M., Handley, L., Munsterman, D., Bohaty, S.M., Zachos, J.C., Reichart, G.-J., Schouten, S., Pancost, R.D., Sinninghe Damsté, J.S., Welters, N.L.D., Lotter, A.F., Dickens, G.R. (2008). Eustatic variations during the Paleocene-Eocene greenhouse world: Paleoceanography 23. doi: 10.1029/2008PA001615.

Smith, R.W., Bianchi, T.S., Li, X. (2012). A re-evaluation of the use of branched GDGTs as terrestrial biomarkers: Implications for the BIT Index. Geochim. Cosmochim. Acta 80, 14–29.

Smittenberg, R.H., Baas, M., Green, M.J., Hopmans, E.C., Schouten, S., Sinninghe Damsté, J.S. (2005). Pre- and post-industrial environmental changes as revealed by the biogeochemical sedimentary record of Drammensfjord, Norway. Mar. Geol. 214, 177–200.

Spang, A., Hatzenpichler, R., Brochier-Armanet, C., Rattei, T., Tischler, P., Spieck, E., Streit, W., Stahl, D.A., Wagner, M., Schleper, C. (2010). Distinct gene set in two different lineages of ammonia-oxidizing archaea supports the phylum Thaumarchaeota. Trends Microbiol. 18, 331–340. doi: 10.1016/j.tim.2010.06.003

Spero, H.J., Bijma, J., Lea, D.W., Russell, A.D. (1999). Deconvolving glacial ocean carbonate chemistry from the planktonic foraminifera carbon isotope record In: Abrantes F., Mix A.C. (Eds.) Reconstruction ocean history: A window into the future. Springer US, Boston, MA.

Spitzy, A. and Ittekkot, V. (1991). Dissolved and particulate organic matter in rivers. In Ocean Margin in Global Change (eds. R. F. C. Mantoura, J. M. Martin and R. Wollast). John Wiley and Sons, New York, pp. 5–17.

Street-Perrott, F.A., Huang, Y., Perrott, R.A., Eglinton, G., Barker P., Khelifa L.B., Harkness, D., Olago, D.O. (1997). Impact of lower atmospheric carbon dioxide on tropical mountain ecosystems. Science 278, 1422–1426.

Strong, D.J., Flecker, R., Valdes, P.J., Wilkinson, I.P., Rees, J.G., Zong, Y.Q., Lloyd, J.M., Garrett, E., Pancost, R.D. (2012). Organic matter distribution in the modern sediments of the Pearl River Estuary. Org. Geochem. 49, 68–82.

Sturt, H.F., Summons, R.E., Smith, K., Elvert, M., Hinrichs, K.U. (2004). Intact polar membrane lipids in prokaryotes and sediments deciphered by high-performance liquid chromatography/electrospray ionization multistage mass spectrometry—new biomarkers for biogeochemistry and microbial ecology. Rapid Commun. Mass Spectrom. 18: 617–628.

Sun, Q., Chu, G.Q., Liu, M.M., Xie, M.M., Li, S.Q., Ling, Y.A., Wang, X.H., Shi, L.M., Jia, G.D., Lu, H.Y. (2011). Distributions and temperature dependence of branched glycerol

dialkyl glycerol tetraethers in recent lacustrine sediments from China and Nepal. J. Geophys. Res.-Biogeo. 116. G01008. doi: 10.1029/2010JG001365

Tierney, J. E. and Russell, J. M. (2009). Distributions of branched GDGTs in a tropical lake system: implications for lacustrine application of the MBT/CBT paleoproxy. Org. Geochem. 40, 1032–1036. doi:10.1016/j.orggeochem.2009. 04.014

Tierney, J.E., Russell, J.M., Eggermont, H., Hopmans, E.C., Verschuren, D. and Sinninghe Damsté J.S. (2010) Environmental controls on branched tetraether lipid distributions in tropical East African lake sediments. Geochim. Cosmochim. Acta 74, 4902–4918. doi:10.1016/j.gca.2010.06.002

Tierney, J.E., Schouten, S., Pitcher, A., Hopmans, E.C., Sinninghe Damsté, J.S., (2012). Core and intact polar glycerol dialkyl glycerol tetraethers (GDGTs) in Sand Pond, Warwick, Rhode Island (USA): Insights into the origin of lacustrine GDGTs. Geochim. Cosmochim. Acta 77, 561–581. doi:10.1016/j.gca.2011.10.018.

Tripati, A., (2005). Deep-sea temperature and circulation changes at the Paleocene-Eocene Thermal Maximum. Science 308, 1894–1898.

Tyler, J.J., Nederbragt, A.J., Jones, V.J., and Thurow, J.W. (2010). Assessing past temperature and soil pH estimates from bacterial tetraether membrane lipids: evidence from the recent lake sediments of Lochnagar, Scotland. J. Geophys. Res. 115, G01015, doi: 10.1029/2009JG001109

Uda, I., Sugai, A., Itoh, Y.H., Itoh, T. (2001). Variation in molecular species of polar lipids from thermoplasma acidophilum depends on growth temperature. Lipids 36, 103–105.

Urey, H.C. (1947). The thermodynamic properties of isotopic substances. J. Chem. Soc. 562-681.

Vale, C., Sundby, B. (1987). Suspended sediment fluctuations in the Tagus estuary on semidiurnal and fortnightly time scales. Estuar. Coast. Shelf Sci. 25, 495–508.

Van der Leeden, F. (1975). Water resources of the world: selected statistics. Water Information Center, Port Washington, N.Y., p. 808.

Vanney, J.R. and Mougenot, D. (1981). La plateforme continentale de Portugal et les provinces adjacentes: Analyse geomorphologique. Memoriás dos Serviçios Geológicos de Portugal 28, p. 86.

Verschuren, D., Sinninghe Damsté, J.S., Moernaut, J., Kristen, I., Blaauw, M., Fagot, M., et al. (2009). Half-precessional dynamics of monsoon rainfall near the East African equator. Nature 462, 637–641. doi: 10.1038/nature08520

Versteegh, G.J., Riegman, R., de Leeuw, J.W., Jansen, J.H.F., (2001). UK'37values for Isochrysis galbana as a function of culture temperature, light intensity and nutrient concentrations. Org. Geochem. 32, 785–794.

Vitorino, J., Oliveira, A., Jouanneau, J.M., Drago, T. (2002). Winter dynamics on the northern Portuguese shelf. Part 2: Bottom boundary layers and sediment dispersal. Prog. Oceanogr. 52, 155–170.

Volkman, J.K., Eglinton, G., Corner, E.D.S., Sargent, J.R. (1980). Novel unsaturated straight-chain C37–C39 methyl and ethyl ketones in marine sediments and a coccolithophorid Emiliania huxleyi. In: Douglas, A.G., Maxwell, J.R. (Eds.), Advances in Organic Geochemistry. Pergamon, New York, pp. 219–227.

Volkman, J.K., Barrett, S.M., Dunstan, G.A., Jeffrey, S.W. (1992). C30-C32 alkyl diols and unsaturated alcohols in microalgae of the class Eustigmatophyceae. Org. Geochem. 18, 131–138.

Volkman, J.K., Barrerr, S.M., Blackburn, S.I., Sikes, E.L. (1995). Alkenones in Gephyrocapsa oceanica: Implications for studies of paleoclimate. Geochim. Cosmochim. Acta 59, 513–520.

Volkoff, B. and Cerri, C.C. (1987). Carbon isotopic fractionation in subtropical Brazilian grassland soils: comparison with tropical forest soils. Plant and Soil 102, 27–31.

Walsh, E. M., Ingalls, A. E., Keil, R. G. (2008). Sources and transport of terrestrial organic matter in Vancouver Island fjords and the Vancouver-Washington Margin: a multiproxy approach using δ13Corg, lignin phenols, and the ether lipid BIT index. Limnol. Oceanogr. 53, 1054–1063. doi:10.4319/lo.2008.53.3.1054

Weber, J.N. (1973). Incorporation of strontium into reef coral skeletal carbonate. Geochim. Cosmochim. Acta 37, 2173–2190.

Wefer, G., Berger, W.H., Bijma, J., Fischer, G. (1999). Clues to ocean history: A brief overview of proxies, in: Use of proxies in paleoceanography: Examples from the South Atlantic. Springer, Berlin, Heidelberg, pp. 1–68.

Weijers, J.W.H., Schouten, S., van der Linden, M., van Geel, B., Sinninghe Damsté, J. S. (2004) Water table related variations in the abundance of intact archaeal membrane lipids in a Swedish peat bog. FEMS Microbiol. Lett. 239, 51–56.

Weijers, J.W.H., Schouten, S., Hopmans, E.C., Geenevasen, J.A.J., David, O.R.P., Coleman, J.M., Pancost, R.D., Sinninghe Damsté, J.S. (2006a). Membrane lipids of mesophilic anaerobic bacteria thriving in peats have typical ar-

chaeal traits. Environ. Microbiol. 8, 648–657. doi: 10.1111/j.1462-2920.2005.00941.x

Weijers, J.W.H., Schouten, S., Spaargaren, O., Sinninghe Damsté, J. S. (2006b) Occurrence and distribution of tetraether membrane lipids in soils: implications for the use of the TEX86 proxy and the BIT index. Org. Geochem. 37, 1680–1693. doi: 10.1016/j. orggeochem.2006.07.018

Weijers, J.W.H., Schefuß, E., Schouten, S., Sinninghe Damsté, J.S. (2007a). Coupled thermal and hydrological evolution of tropical Africa over the last deglaciation. Science 315, 1701–1704. doi: 10.1126/science. 1138131

Weijers, J.W.H., Schouten, S., Sluijs, A., Brinkhuis, H., Sinninghe Damsté, J.S. (2007b). Warm arctic continents during the Palaeocene-Eocene thermal maximum. Earth Planet. Sci. Lett. 261, 230–238.

Weijers, J.W.H., Schouten, S., van den Donker, J. C., Hopmans, E.C., Sinninghe Damsté, J. S. (2007c). Environmental controls on bacterial tetraether membrane lipid distribution in soils. Geochim. Cosmochim. Acta 71, 703–713. doi: 10.1016/j.gca.2006. 10.003

Weijers, J.W.H., Panoto, E., van Bleijswijk, J., Schouten, S., Rijpstra, W.I.C., Balk, M., Stams, A.J.M. Sinninghe Damsté, J. S. (2009a). Constraints on the biological source(s) of the orphan branched tetraether membrane lipids. Geomicrobiol. J. 26, 402– 414. doi: 10.1080/01490450902937293

Weijers, J.W.H., Schouten, S., Schefuß, E., Schneider, R. R., Sinninghe Damsté, J. S. (2009b). Disentangling marine, soil and plant organic carbon contributions to continental margin sediments: a multi-proxy approach in a 20,000 year sediment record from the Congo deep-sea fan. Geochim. Cosmochim. Acta 73, 119–132.

Weijers, J.W.H., Wiesenberg, G.L.B., Bol, R., Hopmans, E. C., Pancost, R. D. (2010). Carbon isotopic composition of branched tetraether membrane lipids in soils suggests a rapid turnover and a heterotrophic life style of their source organism(s). Biogeosciences 7, 2959–2973.

Weijers, J.W.H., Bernhardt, B., Peterse, F., Werne, J.P., Dungait, J.A.J., Schouten, S., Sinninghe Damsté, J.S. (2011a). Absence of seasonal patterns in MBT-CBT indices in mid-latitude soils. Geochim. Cosmochim. Acta 75, 3179–3190. doi: 10.1080/01490450902937293

Weijers, J.W.H., Steinmann, P., Hopmans, E.C., Schouten, S., Sinninghe Damsté, J.S. (2011b). Bacterial tetraether membrane lipids in peat and coal: Testing the MBT-CBT temperature proxy for climate reconstruction. Org. Geochem. 42, 477–486.

White, D.C., Davis, W.M., Nickels, J.S., King, J.D., Bobbie, R.J. (1979). Determination of the sedimentary microbial biomass by extractable lipid phosphate. Oecologia 40, 51–62. doi:10.1007/BF00388810

Wing, S.L. (2005). Transient floral change and rapid global warming at the Paleocene-Eocene Boundary. Science 310, 993–996.

Wolfe, J.A. (1971). Tertiary climatic fluctuations and methods of analysis of tertiary floras. Palaeogeogr. Palaeoclimatol. Palaeoecol. 9, 27–57.

Wu, W., Ruan, J., Ding, S., Zhao, L., Xu, Y., Yang, H., Ding, W., Pei, Y., 2014. Source and distribution of glycerol dialkyl glycerol tetraethers along lower Yellow River-estuary–coast transect. Mar. Chem. 158, 17–26. doi:10.1016/j. marchem.2013.11.006

Wuchter, C., Schouten, S., Coolen, M.J.L., Sinninghe Damsté, J.S. (2004). Temperature-dependent variation in the distribution of tetraether membrane lipids of marine Crenarchaeota: Implications for TEX86 paleothermometry. Paleoceanography 19, 4. Doi.10.1029/2004PA001041.

Xie, S., Pancost, R.D., Chen, L., Evershed, R.P., Yang, H., Zhang, K., Huang, J., Xu, Y. (2012). Microbial lipid records of highly alkaline deposits and enhanced aridity associated with significant uplift of the Tibetan Plateau in the Late Miocene. Geology 40, 291–294.

Yang, H., Ding, W., Wang, J., Jin, C., He, G., Qin, Y., Xie, S. (2011). Soil pH impact on microbial tetraether lipids and terrestrial input index (BIT) in China. Sci. China Earth Sci. 55, 236–245.

Yang, G., Zhang, C.L., Xie, S., Chen, Z., Gao, M., Ge, Z., Yang, Z. (2013). Microbial glycerol dialkyl glycerol tetraethers from river water and soil near the Three Gorges Dam on the Yangtze River. Org. Geochem. 56, 40–50. doi:10.1016/j.orggeochem.2012. 11.014

Young, K. R. and Blanca, L. (1999). Peru's humid eastern montane forests: An overview of their physical settings, biological diversity, human use and settlement, and conservation needs. DIVA Technical Report 5, Kalø, Denmark, Centre for Research on Cultural and Biological Diversity of Andean Rainforests (DIVA), 97 p.

Zachos, J.C. (2005). Rapid acidification of the ocean during the Paleocene-Eocene Thermal Maximum. Science 308, 1611–1615.

Zachos, J.C., Dickens, G.R., Zeebe, R.E. (2008). An early Cenozoic perspective on greenhouse warming and carbon-cycle dynamics. Nature 451, 279–283.

Zell, C., Kim, J.-H., Abril, G., Sobrinho, R.L., Dorhout, D., Moreira-Turcq, P., Sinninghe Damsté, J.S. (2013a). Impact of seasonal hydrological variation on the distributions of tetraether lipids along the Amazon River in the central Amazon basin: implications for the MBT/CBT paleothermometer and the BIT index. Front. Microbiol. 4, doi:10.3389/fmicb.2013.00228.

Zell, C., Kim, J.-H., Moreira-Turcq, P., Abril, G., Hopmans, E.C., Bonnet, M.-P., Lima Sobrinho, R., Sinninghe Damsté, J.S. (2013b). Disentangling the origins of branched tetraether lipids and crenarchaeol in the lower Amazon River: Implications for GDGT-based proxies. Limnol. Oceanogr. 58, 343–353.

Zell, C., Kim, J.-H., Balsinha, M., Dorhout, D., Fernandes, C., Baas, M., Sinninghe Damsté, J. S. (2014). Transport of branched tetraether lipids from the Tagus River basin to the coastal ocean of the Portuguese margin: consequences for the interpretation of the MBT'/CBT paleothermometer. Biogeosciences Discuss. 11, 1–46, doi:10.5194/bgd-11-1-2014-

Zhang, C.L., Wang, J., Wei, Y., Zhu, C., Huang, L., Dong, H. (2012). Production of branched tetraether lipids in the lower Pearl River and estuary: effects of extraction methods and impact on bGDGT proxies. Front. Microbiol. 2, doi:10.3389/fmicb.2011.00274.

Zhou, H., Hu, J., Ming, L., Peng, P., Zhang, G. (2011). Branched glycerol dialkyl glycerol tetraethers and paleoenvironmental reconstruction in Zoigê peat sediments during the last 150 years. Chin. Sci. Bull. 56, 2456–2463.

Zhu C., Weijers, J.W.H., Wagner, T., Pan, J.-M., Chen, J.-F., Pancost, R.D. (2011). Sources and distributions of tetraether lipids in surface sediments across a large river-dominated continental margin. Org. Geochem. 42, 376–386. doi: 10.1016/j.orggeochem.2011. 02.002

Zink, K.G., Vandergoes, M.J., Mangelsdorf, K., Dieffenbacher- Krall, A. C., Schwark, L. (2010). Application of bacterial glycerol dialkyl glycerol tetraethers (GDGTs) to develop modern and past temperature estimates from New Zealand lakes. Org. Geochem. 41, 1060–1066. doi: 10.1016/j.orggeochem.2010. 03.004

Zocatelli R.O. (2010) Reconstrução paleoclimática do Lago Santa Ninha e Lago Boqueirão. Ph.D. Thesis, Departamento de Geoquímica, Universidade Federal Fluminense, Niteroi, Brasil.

Summary

Branched glycerol dialkyl glycerol tetraethers (brGDGTs) are membrane-spanning lipids most likely of anaerobic and heterotrophic bacteria ubiquitously occurring in soils, peat bogs, and lake and coastal marine sediments. In soil the number of methyl groups of the alkyl chains in brGDGTs correlates with the mean annual air temperature (MAAT) and soil pH, while the number of cyclopentane moieties correlates with soil pH. Based on this observation, the methylation index of branched tetraethers (MBT) and the cyclisation index of branched tetraethers (CBT) were introduced to reconstruct MAAT and soil pH. Since brGDGTs are found in large quantities in soil and peat, it was assumed that they are mainly produced on land and are washed into small streams and rivers by erosion and further transported to the ocean. Hence, the study of changes in the brGDGT composition using the MBT/CBT proxy can also be used in river influenced marine settings to reconstruct past MAAT and soil pH of the drainage basin of a river system.The MBT/CBT proxy has been successfully used in past continental climate reconstruction in the drainage area of theCongo river and of the Arctic and Greenland regions, but for the Amazon basin this method did not generate realistic results. Therefore, it still remains uncertain how well the MBT/CBT proxy reconstructs an integrated average MAAT and soil pH of the drainage basin of a river based on marine brGDGT records. Hence, it is important to further assess the applicability of the MBT/CBT proxy in diverse river systems, tracing the initial soil signal through its transport pathway from source to sink.

In the frame work of this thesis, detailed studies were carried out in two river systems, the Amazon River and the Tagus River that are different in terms of river size and climate setting. The Amazon River forms the largest drainage system in the world in terms of water discharge and catchment area and is located in tropical climate. In contrast, the Tagus River is much smaller and located in the dry climate of the Iberian Peninsula. In order to understand the origin of brGDGTs in the drainage basin, soils and river suspended particulate matter (SPM) were analyzed. In addition, marine SPM and surface sediments were examined by comparing the brGDGT concentrations (normalized on organic carbon) and distributions with those of soil and riverine SPM. Core lipid (CL) and intact polar lipid (IPL)-derived brGDGTs were analyzed, in order to distinguish recently produced (IPL-derived) GDGTs from older (CL) GDGTs. In this way, potential sources of brGDGTs in the river basin, including in-situ production of brGDGTs in the river, the transport of brGDGTs from the river basin to the marine environment, and marine in-situ production of brGDGTs were investigated.

In the Amazon basin, it was found that 70-80 % of the particulate organic carbon (OC) pool in the river was derived of soil OC but the high mountainous Andes were not a major source of particulate OC and thus brGDGTs in the Amazon River. The composition of brGDGTs in lowland Amazon soils was remarkably similar over a large area of the basin. Interestingly, the distribution of both CL and IPL-derived brGDGTs in lowland Amazon soils was slightly different compared to that of SPM in the Amazon River

mainstem, indicating in-situ production of brGDGTs in the river itself. In the Amazon River main stem a small, but significant influence of the seasonal water level variation on the brGDGT concentration and distribution was detected. The highest concentration of CL brGDGTs was found during the high water season. During this season the MBT and CBT values in the Amazon River mainstem were also most similar to those of lowland Amazon soils, indicating that the highest input of soil-derived brGDGTs occurred due to increased water runoff. During the other seasons, the MBT and CBT indices indicated an increased influence of in-situ production of brGDGTs even though soils remained the main source of brGDGTs. In the Amazon shelf and fan, the delivery of brGDGTs from the Amazon River was evident from the elevated CL brGDGT concentrations in marine SPM and surface sediments close to the river mouth. However, further away from the river, the distributions of CL brGDGTs in marine SPM and sediments varied widely, generally showing a higher relative abundance of methylated and cyclic brGDGTs than those in the river. Since this difference in brGDGT distribution was also found in IPL-derived brGDGTs, the change in the marine brGDGT distribution was most likely due to marine in-situ production.

In the Tagus River drainage basin, the brGDGT distributions in soils were very variable and did not reflect the MAAT and soil pH, as has been noted before in soils in an arid climate. The concentrations of brGDGTs in river SPM were substantially higher and their distributions were different compared to those of the drainage basin soils. This indicates that brGDGTs are mainly produced in the river itself. Monthly analysis of brGDGTs in the Tagus River showed changes of brGDGT concentrations and distributions; however compared to the differences between the soil samples the brGDGT concentration and distribution in the river were remarkably stable. Since the brGDGTs seem to be mainly produced in the river the MAAT and soil pH cannot be reconstructed with the commonly used soil calibrations. However, it might be possible to use an aquatic calibration to reconstruct the temperature and pH of the river. In marine surface sediments along the Portuguese margin, brGDGT concentrations were high at locations where rivers enter the ocean, indicating the significance of riverine brGDGT input. BrGDGT concentrations rapidly decreased with increasing distance from the shore. At the same time, the brGDGT distributions in marine SPM and surface sediments changed, indicating that marine in-situ production also takes place.

In conclusion, the work presented in this thesis shows the complexity of processes that influence the brGDGT distribution during the transport from land to ocean as well as during the sedimentation and deposition in marine settings. Various problems that complicate the use of the MBT/CBT proxy for paleoreconstructions using coastal marine sediments in the vicinity of a river were identified. Hence, this thesis emphasizes the importance of a detailed study about the source of brGDGTs in a river basin an adjacent marine setting, before using the MBT/CBT records for paleoclimatic reconstructions. If the majority of brGDGTs is soil derived, it should be possible to reconstruct the temperature and soil pH changes of the river basin. However, if the majority of brGDGTs

are produced in the river, it might be possible to reconstruct the environmental (temperature and pH) conditions of the river water using an appropriate aquatic calibration that needs to be developed. In general, it is recommendable to apply the MBT/CBT proxy only to marine sediments collected at sites under strong river influence.

Samenvatting

Vertakte glycerol dialkyl glycerol tetraethers (vGDGTs) zijn membraanlipiden, waarschijnlijk afkomstig van anaerobe en heterotrofe bacteriën, die wijdverspreid voorkomen in bodems, veen, en sedimenten van meren en kustzeeën. Uit onderzoek van bodems is gebleken dat het aantal methylgroepen van vGDGTs correleert met de jaargemiddelde luchttemperatuur (MAT), terwijl het aantal cyclopentaan groepen afhankelijk is van de pH. Gebaseerd op deze waarnemingen zijn de 'Methylation of Branched Tetraethers' (MBT) index en de 'Cyclisation of Branched Tetraethers' (CBT) index geïntroduceerd om MAT en bodem pH te reconstrueren. Omdat vGDGTs in grote hoeveelheden worden aangetroffen in de bodem en in veen is aangenomen dat vGDGTs vooral op het land geproduceerd worden en door erosie via rivieren naar zee getransporteerd worden, waar ze worden afgezet in het kustgebied. Bestudering van veranderingen in de samenstelling van vertakte GDGTs m.b.v. de MBT-CBT proxy in een afzetting van kustsedimenten kan dus ook worden toegepast om een reconstructie van veranderingen in MAT en bodem pH in het stroomgebied van de rivier in het verleden te maken. Succesvolle toepassingen zijn gerapporteerd voor de reconstructie van het continentale klimaat van het stroomgebied van de Congo en voor Groenland en het Arctisch gebied maar voor het stroomgebied van de Amazone werkte de methode niet goed. Het is daarom de vraag hoe goed de MBT-CBT proxy in staat is om een reconstructie van de geïntegreerde MAT en bodem pH van een rivier te maken op basis van in mariene sedimenten gepreserveerde vGDGTs. Het is daarom van belang de toepasbaarheid van de MBT-CBT proxy te testen in diverse riviersystemen, waarbij bestudeerd moet worden of de oorspronkelijke vGDGT samenstelling in de bodem onveranderd blijft gedurende het transport en afzetting in kustzeeën.

Het onderzoek beschreven in dit proefschrift bestudeerd twee riviersystemen, de Amazone en de Taag. Zij verschillen in grootte en heersende klimaatcondities. De Amazone vormt het grootste riviersysteem ter wereld, zowel m.b.t. waterafvoer als grootte van het stroomgebied, dat gekenmerkt wordt door een tropisch klimaat. De Taag daarentegen is veel kleiner en haar stroomgebied ligt in de droge klimaatzone van het Iberisch schiereiland. Om de herkomst van vGDGTs te bestuderen, werden bodemmonsters en gesuspendeerd particulair materiaal (GPM) van de rivier geanalyseerd. De concentratie (genormaliseerd op organisch koolstofgehalte) en distributie van vGDGTs in dit materiaal werd vergeleken met die van marien GPM en mariene oppervlaktesedimenten. Zowel de core tetraethers (CLs) alsmede de intacte polaire tetraethers (IPLs),

waar nog een polaire groep aan de kop van de tetraether vast zit, werden bestudeerd om onderscheid te kunnen maken tussen recent geproduceerde (i.e. IPLs) en fossiele (i.e. CLs) vGDGTs. Op deze manier zijn de mogelijke bronnen van vGDGTs, waaronder in-situ productie in de rivier, in het stroomgebied, het transport van vGDGTs van het stroomgebied naar het mariene milieu, en mariene in-situ productie van vGDGTs bestudeerd.

In het geval van de Amazone bleek dat 70-80% van het particulair organisch koolstof in de rivier afkomstig was van organisch koolstof van de bodem terwijl de hoge Andes geen belangrijke bron voor particulair organisch koolstof en dus voor vGDGTs in de rivier was. De samenstelling van vGDGTs in bodems van de laagvlakte was opmerkelijk constant over een groot gebied. De vGDGT distributie van zowel CL- als IPL-vGDGTs in bodems van de laagvlakte verschilde enigszins van die van het GPM van de rivier. Dit wordt toegeschreven aan in-situ productie in de rivier. De concentratie en distributie van vGDGTs in het GPM in de rivier bleek kleine maar significante verschillen te vertonen gedurende het seizoen. De hoogste vGDGT concentraties werden gevonden tijdens de hoogste waterstand. In dit seizoen waren de MBT en CBT waarden in het GPM van de Amazone ook het meest vergelijkbaar met die van de bodems, hetgeen aangeeft dat in perioden van veel neerslag en hoge bodemerosie een grote aanvoer van vGDGTs uit de bodem optreedt. Gedurende de andere seizoenen gaven de MBT en CBT waarden een verhoogde bijdrage van vGDGTs afkomstig van in-situ productie aan, hoewel ook tijdens deze perioden bodems de belangrijkste bron van vGDGTs in de rivier bleven. Uit de vGDGT samenstelling van mariene oppervlaktesedimenten en GPM van de waterkolom van locaties in de Zuid Atlantische Oceaan voor de monding van de Amazone bleek de invloed van de rivier als bron voor vGDGTs; locaties die dichtbij de monding lagen hadden de hoogste CL-vGDGT concentraties. Veder weg van de riviermonding werden de distributies van CL-GDGTs echter gekenmerkt door een grotere relatieve bijdrage van meer vertakte en gecycliseerde vGDGTs dan die in de rivier. Omdat dit verschil in distributie ook gevonden werd voor IPL-vGDGTs, is het meest aannemelijk dat dit veroorzaakt wordt door mariene in-situ productie.

In het stroomgebied van de Taag bleek de vGDGT distributie in de bodem uiterst variabel en bleek de MAT en bodem pH niet te reflecteren, een observatie die al eerder voor bodems uit een droog klimaat gemaakt is. De vGDGT concentraties in het GPM van de rivier was aanzienlijk hoger en de distributies verschillend van die gevonden in de bodem. Dit gaf aan dat de vGDGTs voornamelijk in de rivier zelf geproduceerd worden. Analyse van maandelijks genomen GPM monsters lieten kleine veranderingen in vGDGT concentratie en distributie zien; in vergelijking tot de variatie die in de bodemmonsters aangetroffen werd waren deze veranderingen klein. Omdat de vGDGTs voornamelijk in-situ geproduceerd in de rivier kunnen MAT en pH niet via een bodem kalibratie bepaald worden; mogelijk dat een aquatische kalibratie uitkomst kan bieden. Mariene sedimenten afgezet langs de kust van Portugal hebben een hogere concentratie aan vGDGTs wanneer zij dicht bij de monding van een rivier liggen. Dit geeft aan dat rivieren een belangrijke bron van vGDGTs kunnen zijn. Met toenemende afstand tot de kust nam de

vGDGT concentratie snel af, terwijl ook de vGDGT distributie in zowel GPM als oppervlakte sedimenten veranderde. Dit duidt op marine in-situ productie van vGDGTs.

Samenvattend toont dit proefschrift de complexiteit van de processen die de vGDGT distributie beïnvloeden tijdens het transport van het continent naar de oceaan en de afzetting in mariene sedimenten aan. Verschillende problemen compliceren de toepassing van de MBT-CBT proxy voor reconstructie van het continentale klimaat gebruikmakend van mariene sedimenten afgezet in de nabijheid van een rivier. Het is daarom van belang om voor een specifiek riviersysteem een gedetailleerde studie te maken van de herkomst van vGDGTs in mariene sedimenten alvorens de MBT-CBT proxy aan te wenden voor palaeoklimaatreconstructie. Wanneer de vGDGTs voornamelijk afkomstig zijn van geërodeerd bodemmateriaal moet het mogelijk zijn een reconstructie van MAT en bodem van het stroomgebied in het verleden te maken. Wanneer de vGDGTs voornamelijk afkomstig zijn productie in de rivier zal een aquatische kalibratie (die nog ontwikkeld moet worden) mogelijk uitkomst bieden. In zijn algemeenheid is het duidelijk geworden dat de MBT-CBT proxy allen toegepast kan worden in mariene sedimenten wanneer die dicht bij de monding van een rivier liggen.

Zusammenfassung

Verzweigte Glyzerol-dialkyl-glyzerol-tetraether (vGDGTs) sind Membranlipide, wahrscheinlich von anaeroben heterotrophen Bakterien, die weitverbreitet in Böden, Torf, Seesedimenten und Küstensedimenten vorkommen. In Böden korreliert die Anzahl der Methylgruppen der Alkylketten in den vGDGTs mit der durchschnittlichen Jahres-Lufttemperaturen (dJLT) und mit dem Boden pH-Wert, während die Anzahl der Cyclopentan Einheiten nur mit dem Boden pH-Wert korreliert. Basierend auf diesen Beobachtungen wurde der 'Methylation of Branched Tetraethers' -(MBT) und 'Cyclisation of Branched Tetraethers'- (CBT) Index entwickelt, mit dem die dJLT rekonstruiert werden kann. Da vGDGTs in größeren Mengen im Boden und in Torf gefunden wurden, wurde angenommen, dass sie hauptsächlich auf dem Land produziert werden und durch Bodenerosion in kleine Bäche und Flüsse eingetragen werden, die sie dann weiter in den Ozean transportieren. Die Beobachtung der vGDGT Komposition mit Hilfe des MBT/CBT proxy in von Flüssen beeinflusstem marinem Sediment kann also auch dazu benutzt werden, Veränderungen der dJLT und des Boden pH-Wertes des Flussbeckens in der Vergangenheit zu rekonstruieren. Das MBT/CBT proxy wurde bereits erfolgreich für kontinentale Klimarekonstruktionen vom Flussbecken, des Kongos von Grönland und von der arktischen Region angewandt, aber für das Amazonasbecken hat diese Methode keine realistischen Ergebnisse geliefert. Darum bleibt es noch ungewiss, wie gut das MBT/CBT proxy in marinem Sediment die dJLT und den Boden pH eines Flussbecken wiedergeben kann. Folglich ist es wichtig, die Anwendbarkeit des MBT/CBT proxies in diversen Flusssystemen weiter zu untersuchen, indem das Signal der vGDGTs von sei-

nem Ursprungsort, dem Boden, bis zum Ablagerungsort verfolgt wird.

Im Rahmen der vorliegenden Doktorarbeit wurden detaillierte Studien über zwei Flusssysteme, die sich in Bezug auf ihre Größe und Klimazone unterscheiden, ausgeführt: dem Amazonas und dem Tajo. Der Amazonas hat das größte Flussbecken der Welt in Bezug auf den Wasserabfluss und das Wassereinzugsgebiet und er befindet sich in tropischem Klima. Der Tajo ist im Vergleich viel kleiner und befindet sich in dem trockenen Klima der Iberischen Halbinsel. Um die Herkunft der vGDGTs in den Flüssen zu verstehen, wurden Bodenproben der Flussbecken und Schwebstoffe aus den Flüssen untersucht. Des Weiteren wurden die vGDGT Konzentrationen (auf den organischen Kohlenstoffgehalt normalisiert) und Verteilung in marinen Schwebstoffen und Sedimenten mit denen im Boden und im Fluss verglichen. Sowohl Core-Lipide (CLs) vGDGTs als auch von intakten polaren Lipiden (IPLs) stammende vGDGTs wurden analysiert, um zwischen kürzlich produzierten (IPLs) vGDGT und älteren (CLs) vGDGTs zu unterscheiden. So konnten die potentiellen Ursprünge (inklusive in-situ Produktion), der Transport von vGDGTs in den Flüssen, der Transport von den Flussbecken ins Meer und die marine in-situ vGDGT Produktion untersucht werden.

Es wurde festgestellt, dass 70 bis 80% des partikulären organischen Kohlenstoffes im Amazonas aus Böden stammt, aber dass die hohen Anden keine wichtige Rolle für den Eintrag von partikulärem organischen Kohlenstoff im Amazonas spielen. Darum können sie auch nicht der Hauptursprungsort der vGDGTs sein. Die Zusammensetzung der vGDGTs im Amazonas Tiefland war über eine beträchtliche Fläche des Flussbeckens erstaunlich ähnlich. Interessanterweise, war die Verteilung von CL und von IPL abstammenden vGDGTs in den Schwebstoffen des Amazons-Hauptstammes etwas anders als im Boden, was auf in-situ Produktion von vGDGTs im Amazons hindeutet. Im Amazons-Hauptstamm wurde ein kleiner, aber signifikanter Unterschied zwischen den saisonalen Wasserstands-Variationen auf die vGDGT Konzentration und Verteilung festgestellt. Die höchste Konzentration von CL vGDGTs wurde während des höchsten Wasserstandes gefunden. Während dieser Zeit wurden auch MBT- und CBT-Werte gefunden, die der des Tieflandbodens am ähnlichsten waren. Das deutet drauf hin, dass der höchste Eintrag von Boden-vGDGTs während dieser Jahreszeit stattfindet. In den anderen Jahreszeiten weisen MBT und CBT auf einen erhöhten Einfluss der in-situ Produktion hin. Auf dem Amazonas-Schelf war der Eintrag von vGDGTs vom Amazonas deutlich sichtbar durch die hohen CL vGDGT Konzentrationen in den marinen Schwebstoffen und im Oberflächensediment in der Nähe der Flussmündung. Weiter entfernt vom Fluss variiert die Distribution vom CL vGDGTs allerdings stark. Im Allgemeinen ist die Methylierung und die Anzahl von Cyclopentan-Gruppen in den vGDGTs im Meer höher, als die der vGDGTs im Fluss. Da der Unterschied in der vGDGT Verteilung auch in den von IPLs stammenden vGDGTs gefunden wurde, ist es wahrscheinlich, dass die Veränderung der Verteilung auf mariner in-situ Produktion basiert.

Die vGDGT Verteilung in Bodenproben des Tajobeckens waren sehr variabel und reflektierten nicht die dJLT und den Boden pH-Wert. Eine Beobachtung, die auch

schon in früheren Arbeiten über Böden aus trockenem Klima beschrieben wurde. Die Konzentration der vGDGTs in den Schwebstoffen des Flusses war wesentlich höher und ihre Verteilung war anders als die der Böden. Das weist darauf hin, dass die vGDGTs hauptsächlich im Fluss selbst produziert wurden. Monatliche Analysen der vGDGT im Tajo zeigten Unterschiede bezüglich der Konzentration und Verteilung; allerding waren die Unterschiede in Konzentration und Verteilung unbedeutend im Vergleich zu den Unterschieden, in den Böden. Da die vGDGTs anscheinend hauptsächlich im Fluss produziert werden, ist es nicht möglich die Lufttemperatur und den Boden pH-Wert mit der normalerweise verwendeten Boden-Kalibrierung zu rekonstruieren. Allerdings könnte es möglich sein, eine aquatische Kalibrierung zu verwenden, um die Temperatur und den pH-Wert des Flusses zu rekonstruieren. In marinen Sedimenten entlang der portugiesischen Küste war die vGDGT Konzentration am höchsten, wo Flüsse ins Meer münden, was den Eintrag von vGDGTs durch die Flüsse deutlich macht. Die vGDGT Konzentration nimmt allerdings mit steigender Distanz zur Küste schnell ab. Zur gleichen Zeit verändert sich die vGDGT Verteilung in marinen Schwebstoffen und Oberflächensedimenten mit steigender Distanz zum Kontinent, was darauf hinweist, dass auch in-situ Produktion stattfindet.

Zusammenfassend, zeigt die Doktorarbeit die Komplexität der Prozesse, die, die vGDGT Verteilung während des Transportes vom Land zum Meer, wie während der Sedimentierung und Deposition beeinflussen. Diverse Probleme verkomplizieren den Gebrauch des MBT/CBT proxies für Paleorekonstruktionen in marinen Sedimentkernen in der Nähre von Flussmündungen. Es ist darum wichtig, eine detaillierte Studie über die Herkunft der vGDGTs im Fluss und in der angrenzenden marinen Umgebung durchzuführen, bevor das MBT/CBT proxy für Paleorekonstruktionen angewandt wird. Falls die meisten vGDGTs aus erodierten Böden des Flussbeckens stammen, sollte es möglich sein, Unterschiede der Lufttemperatur und des Boden pH-Wertes des Flussbeckens zu rekonstruieren. Wenn die meisten vGDGT allerdings im Fluss produziert werden, sollte es möglich sein, die Umweltbedingungen (Wassertemperatur und pH-Wert) des Flusses mit Hilfe einer passenden aquatischen Kalibrierung (die noch entwickelt werden muss) zu rekonstruieren. Generell ist es empfehlenswert, das MBT/CBT proxy nur in marinen Sedimenten anzuwenden, die unter starkem Einfluss des Flusses standen.

Sumário

Os glicerol dialquil glicerol tetraéteres ramificados (brGDGTs) são lipídeos de membrana característicos de bactérias anaeróbicas e heterotróficas ocorrendo ubiquamente em solos, turfeiras e sedimentos lacustres e marinhos. No solo, o número de grupos metil das cadeias alquil em brGDGTs correlacionam-se com a temperatura atmosférica anual média (TAAM) e com o pH do solo, enquanto que o número de anéis ciclopentanos correlacionam-se com o pH do solo. Baseado nesta observação, o índice

de metilação de tetraéteres ramificados (MBT) e o índice de ciclização de tetréteres ramificados (CBT) foram introduzidos para reconstruir a TAAM e o pH do solo. Uma vez que os brGDGTs são encontrados em grandes quantidades em solos e turfas, supõem-se que eles sejam produzidos principalmente em terra e são transferidos para pequenos córregos e rios por erosão e posteriosmente transportados para o oceano. Portanto, o estudo das mudanças na composição de brGDGTs utilizando o "proxy" MBT/CBT pode também ser usado em regiões marinhas influenciadas por rios. Para reconstruir a TAAM e o pH do solo passados da bacia de drenagem de um sistema ripário o proxy MBT/CBT vem sendo usado em reconstruções paleoclimáticas na área de drenagem do rio Congo e nas regiões do Ártico e Groelândia, mas para a bacia Amazônica este método não gerou resultados realistas. Sendo assim, ainda permanence incerto o quão bem o proxy MBT/CBT reconstrói uma média integrada da TAAM e do pH do solo da bacia de drenagem em ambientes marinhos. Portanto, é importante investigar a aplicabilidade do proxy MBT/CBT em diversos sitemas ripários, traçando o sinal inicial do solo e sua via de transporte da fonte à deposição.

Na composição desta tese, estudos detalhados foram realizados em dois sistemas ripários, o rio Amazonas e o rio Tagus, os quais são diferentes em termos de tamanho e configuração climática. O rio Amazonas forma o maior sistema de drenagem no mundo, em termos de descarga e área de drenagem e é localizado em clima tropical. Em contrapartida, o rio Tagus é muito menor e localizado no clima seco da Península Hibérica. A fim de entender a origem dos brGDGTs na bacia de drenagem, solos e material particulado em suspensão (MPS) do rio foram analizados. Somado à isso, MPS marinho e sedimentos superficiais foram examinados comparando as concentrações de brGDGTs (normalizados por CO) e as distribuições daqueles de origem no solo e no MPS ripário. Foram analizados brGDGTs derivados da fração polar intacta (IPL) e da fração apolar, contendo apenas sua parte central (CL) para distinguir os GDGTs produzidos recentemente (derivados-IPL) daqueles mais velhos (CL). Neste sentido, possíveis fontes de brGDGTs na bacia de drenagem, incluindo a produção in situ de brGDGTs no rio e o transporte de brGDGTs do rio para o ambiente marinho e a produção marinha in situ foram investigados.

Na bacia Amazônica foi relatado que 70-80% do carbono orgânico (CO) particulado dos rios era derivado do CO do solo, entretanto o alto relevo Andino não é uma fonte majoritária de CO particulado e portanto, de brGDGTs para o rio Amazonas. A composição de brGDGTs nos solos da planície Amazônica foi notavelmente similar sobre uma ampla área da bacia. Curiosamente, a distribuição brGDGTs de ambas as frações CL e IPL nos solos da planície Amazônica foi levemente diferente se comparados ao MPS do canal do rio Amazonas, indicando produção in situ de brGDGTs no próprio rio. No canal central do rio Amazonas, uma pequena, porém significante, influência da variação sazonal do nível de água na concentração e distribuição de brGDGTs foi detectada. A maior concentração de brGDGTs foi encontrada durante o príodo de águas altas. Nesta estação os valores de MBT e CBT no rio Amazonas foram também similares àqueles dos

solos da planície Amazônica, indicando que a maior entrada de brGDTs derivados do solo ocorreu devido ao aumento no escoamento da água. Durante as outras estações, os índices MBT e CBT indicaram aumento na influência da produção in situ de brGDGTs, mesmo que os solos tenham permanecido sua principal fonte. Na plataforma continental e no leque aluvial Amazônico a transferência de brGDGTs advindo do rio Amazonas foi evidente à partir das elevadas concentrações de CL brGDGTs no MPS marinho e sedimento superficial próximo a desembocadura do rio. Entretanto, mais distante do rio, a distribuição de CL brGDGTs no MPS marinho e no sedimento superficial variou amplamente, geralmente mostrando uma maior abundância relativa de brGDGTs metilados ou cíclicos em comparação àqueles encontrados no rio. Como esta mesma diferença foi também observada nos derivados-IPL de brGDGTs, as mudanças na distribuições do brGDGTs marinho ocorreu provelmente devido a produção marinha in-situ.

Na bacia de drenagem do rio Tagus, as distribuições de brGDGTs nos solos foram bastante variáveis e não refletiram a TAAM e o pH do solo, como foi notado anteriormente em solos de clima árido. As concentrações de brGDGTs no MPS do rio foram substancialmente altas e suas distribuições foram diferentes se comparadas àquelas dos solos da bacia de drenagem. Isto indica que os brGDGTs são pricipalmente produzidos no próprio rio. Análises mensais de brGDGTs no rio Tagus mostraram mudanças nas concentrações e distribuições de brGDGTs; entretanto comparado às diferenças entre as amostras de solo, as concentrações e as distribuições de brGDGTs no rio foram notavelmente estáveis. Uma vez que os brGDGTs parecem ser produzidos principalmente no rio, a TAAM e o pH do solo não podem ser reconstruídas com as calibrações comumente utilizadas nos solos. Entretanto, poderia ser possível utilizar uma calibração aquática para reconstrutir a temperatura e o pH do rio. Nos sedimentos superficiais marinhos, ao longo da costa portuguesa, as concentrações de brGDGTs foram altas próximas à desembocadura do rio, indicando a significância da entrada de brGDGTs ripário. Entretanto, as concentrações de brGDGTs decaem rapidamente com o aumento da distância à costa. Ao mesmo tempo, as distribuições de brGDGTs no MPS marinho e sedimentos superficiais mudaram, indicando que a produção marinha in situ também ocorre.

Como conclusão, o trabalho apresentado nesta tese mostra a complexidade de processos que influenciam a distribuição de brGDGTs durante seu transporte da terra para o oceano, assim como sua sedimentação e deposição em ambientes marinhos. Vários problemas que complicam o uso do proxy MBT/CBT para reconstruções paleoclimáticas usando sedimentos marinhos costeiros nas proximidades de um rio foram identificadas. Portanto, esta tese enfatiza a importância de um estudo detalhado de uma bacia hidrográfica para interpretar o MBT/CBT em testemunhos para recontruções paleoclimáticas em uma região marinha adjacente. Se os brGDGTs são majoritariamente derivados do solo, seria possível reconstruir as mudanças na temperatura e no pH do solo da bacia de drenagem. Entretanto, se os brGDGTs forem majoritariamente produzidos no rio, poderia ser possível reconstruir as condições ambientais (temperatura e pH) da água do rio, usando uma calibração apropriada que precisa ser desenvolvida. Em

geral, é recomendado aplicar o "proxy" MBT/CBT apenas em sedimentos marinhos coletados em locais sob forte influência do rio.

Acknowledgements

First of all I want to thank Jaap. His admirable overview and ability to put things in to the right way has helped me many times, when I didn't know how to continue my work. Thank you for helping me, especially in the last period of my PhD. In addition, the excellent way to lead the BGC group together with Stefan, provides the basis for all of us to do good work. Second I want to thank Kim, for always helping me out and always being reachable, wherever she was. Thanks also for involving me in the unforgettable field work in Brazil and in Portugal. Further I want to thank the technicians (Anchelique, Danielle, Ellen, Irene, Jort, Jord, Kevin, Monique, Marianne) in our group. I am looking slightly worried into the future, how it will be to work in a lab without all of you. I want to especially thank Denise who analyzed many of my samples and Marianne who has been a great help during the cruise preparation and also during our cruise to Portugal on the Pelagia (often in the middle of the night).

Throughout my whole PhD I shared an office with Nicole, the best office mate ever, as she is the most caring and helpful person. Thank you for organizing so many fun social activities. I really can't imagine our group without you. Thanks a lot also to the "branched GDGT girls" Cindy and Lisa, the science talks with you were very helpful (sorry to everyone who had to listen). Thanks also to all the other wonderful colleagues of the BGC department, for the good atmosphere in the lab, at lunch, at coffee and during numerous parties: Alina, Angela, Cecile, Cindy (I will never forget how you came running with the flowers for my wedding, that was amazing thank you so much), Daniela, Darci, David, Dorien, Eli & Lisa, Elisabeth, Els, Evgenia, Francien, Isla, Kees, Laura, Loes, Luke, Marc, Marcel, Marta, Martina, Nicole, Petra (thanks for the music time and for beeing a patient Dutch teacher), Raquel, Rob, Ronald, Rodrigo, Sabine, Sandra, Sebastian, Sebastiaan, Thorsten, Yvonne. Further there were many nice guests in our department for example Argiroooo (I am sure we will meet in many more places of the world), Carmina, Elisabeth, Frederike, Kasia, Laura, Lennart, Luciane, Marlen, Marita, Marishka, Mireira, Wilhelmijn …… also thanks to the many people who I got to meet during the three cruises and who have always been very helpful: Gwenael, Patricia, Felipie, Sonia, Luciane,Marcela, Jean-Michel, Laura, David Hollander, Paul Baker, Enrique, Kara, Carlie, Magali, Maria, Anna, Anna, Jerome ….. and many more.

In addition I got to meet many other people from the NIOZ and from Texel who made life on Texel a lot of fun: Andreas, Anja, Arno, Bart, Catarina, Catarina, Christina, Craig and Julie, Els and Wilhelm, Jenny, John, Juliane, Jan-Berend (& family), Lennart, Marina, my piano teacher Margot, Santiago, Yvo, …….Many thanks also to the numerous house mates that I had during the 4 years in Herenstraat 11. Maarten, Richard, Cindy, Kasia, Catarina, Catarina and David. It is so important to live in a place where you feel at home, which I did thanks to you all. Thank you to everyone for sharing many good moments, but also the less happy moments during the last four and a half years you made life on Texel very pleasant.

Last but not least I want to thank my family. Mama, Papa thank you for your support, thank you for always being there for me. Santi, thanks for taking care of me when I was writing this thesis, I would have starved without you. Thank you for sharing your life with me, life with you is much more fun than it was before, may it never be boring!

Picture by Magali Schweizer

About the author

Claudia Zell was born in 1985 in Cologne, Gemany. After a training as biological technical Assistant she studied Applied Biology. As she found out to be very interested in the interaction of Microbes with the environment she continued with a Master in Microbiology at the Institute for Chemistry and Biology of the Sea (ICBM) of the Carl von Ossietzky University Oldenburg. After recieving her Master she started to work on the present PhD thesis in the Organic Biogeochemistry department of the Royal Netherlands Institute for Sea Research (NIOZ) under the supervision of Prof. Jaap Sinninghe Damsté and Dr. Jung-Hyun Kim. She will move on to a Post-Doc position in the Biogeosciences group at the ETH in Zürich.